City Research Online

City, University of London Institutional Repository

020220975

THE SOLITARY WAVE AND THE FORCES IT IMPOSES
ON A SUBMERGED HORIZONTAL CIRCULAR CYLINDER

AN ANALYTICAL AND EXPERIMENTAL STUDY

BY

P.O.SIBLEY, B.Sc, C.Eng, MICE, ABIM.

Thesis submitted to The City University for the
Degree of Doctor of Philosophy in the Department of
Civil Engineering.

September, 1991.

020220975

To my family and friends.

SYNOPSIS

A study has been made of the forces generated on a submerged horizontal cylinder, held remote from the channel bed, due to the passage of a solitary wave.

The horizontal cylinder was positioned with its major axis parallel to the direction of the wave crest. The vertical and in-line forces were measured using a force balance. The horizontal fluid velocities were measured using a Hot Film Anemometer (HFA).

The drag and inertia components of the force are separated in the analysis by three different methods and correlated with Reynolds, Keulegan & Carpenter and Inverson's numbers.

This study investigates a basic wave/ structure interaction using Morison's equation. This supposes that the total force on a submerged object is the simple superposition of two well established force components, namely the drag and inertia components.

History effects are removed by using the fluid environment generated by the solitary wave, which is unidirectional accelerated motion in still water.

Measurement and validation of the fluid flow characteristics are made, to ensure a high degree of certainty for the results.

The objective is to establish a relation by which the coefficients used in Morison's equation can be accurately determined from basic wave characteristics.

ACKNOWLEDGEMENTS

CONTENTS

CHAPTER 3   THEORETICAL CONSIDERATIONS

CHAPTER 4   APPARATUS & EXP'TAL TECHNIQUE

CHAPTER 5   ANALYSIS OF RESULTS

CHAPTER 6   EXPERIMENTAL RESULTS

CHAPTER 7   DISCUSSION

CHAPTER 8   SUMMARY & CONCLUSIONS

LIST OF FIGURES

LIST OF TABLES

CHAPTER 1 INTRODUCTION

1.1 Background

The past thirty years have seen a rapid development of offshore engineering, principally in the gas and oil industries, but also in the generation of electricity, harnessing either wind or water energy.

These industries require ever more detailed information on the mechanisms and loads to which structures and pipelines in the sea are subjected.

The majority of effort has been directed towards providing the engineer with such information and to obtain a deeper understanding of the fluid mechanics of the oceans. In particular, the interaction of structures and pipelines with waves has attracted much attention. To date this work has given a range of often conflicting conclusions for what is a complicated and multi-variable problem.

Much of the effort has been directed towards the calculation of force coefficients used in Morison's equation. Though empirically determined, Morison's equation has gained a wide degree of acceptance because of its practical use and simplicity, but has been much criticised because of the lack of a term which takes into account "history" effects. These effects are important in oscillatory flows, and are often blamed for the lack of correlation of Morison's coefficients.

A preliminary investigation was carried out as a final year undergraduate project. This formed the basis of this study. The findings were published and are included as Appendix C and D.

The aim of the present study is to reduce the number of variables to achieve a deeper understanding of the hydrodynamics, force generation and analytical procedure that the engineer may adopt to design economic and efficient structures.

Consequently a flow environment was chosen that had no history effects due to flow reversal and was unique in form. The solitary wave was chosen because of its unique shape, stability and uni-directional flow environment generated as the wave passes.

This research with the solitary wave is set against work performed by many eminent researchers including Scott Russell (1834), Boussinesq(1871), Morison (1950), Longuet-Higgins (1970's), Daily and Stephen (1951), McCowan (1891) and more recently Naheer (1978) all of which are widely respected and referenced.

Of these Scott Russell, Daily & Stephan and Naheer restricted themselves to an experimental investigation of the solitary wave and its characteristics; Boussinesq and McCowan looked at the theoretical aspects of the solitary wave whereas Longuet-Higgins looked at both.

On the other hand Morison was concerned with the force generated on vertical surface piercing cylinders.

However, none have attempted such a comprehensive experimental investigation as attempted here with the modern techniques available.

1.2 Scope of Present Work

The initial objective of this study was to find a relationship between forces on a submerged cylinder and wave characteristics, such as Nkc and Re. However since no exact correlation has been determined, it was necessary to confirm the component steps in the study. This has led to considerable work in a number of related areas to confirm the measurements in each step. Details are given in figure 1.1.

Most importantly this study has investigated the loads on smooth horizontal right circular cylinders lying parallel to the crest of a two dimensional solitary wave. The experiments include the case where the cylinder was close to the channel bed as well as in the body of the fluid. The cylinders sizes were varied, within limits so as not to affect the shape of the incident waves. The investigation may be regarded as one of loads induced in an unidirectional accelerating flow field.

The author attempts to correlate Morison force coefficients with parameters characterising the ambient flow and suggest physical explanations for their occurrence. Attention has been paid to the forces perpendicular to the direction of wave since these have to date attracted little attention for horizontal cylinders.

The horizontal cylinder was chosen for this study because of the spanwise correlation. Integrating the force along the cylinder leads to a greater sensitivity in the measurements.

| Wave probe calib. HFA calibration Force calib. | ← Test | Set up experiment and test procedure. |

| Compare with wave profile theories. Wave attentn. Wave reflection. Max. amplitude Wave distortion. Wave celerity. | ← Test | Meas. wave profile |

| Comparison with theory. | ← Test | Meas. vel. & accel. | Meas. forces |

Analyse forces using Morison's eqn.

Separate Morison's coefficients. (3 methods)

| Phys. signif Agreement Limitations | ← Test | Correlation with Nkc / Correlation with Re / Correlation with fluid profile.(ut/D) | Cd,Cm |

Total force coefficient

| Phys. signif. Agreement Limitations | ← Test | Correlation with fluid profile.(ut/D) |

Figure 1.1 - Scope of thesis

- 4 -

Fluid velocities and wave profiles are measured and compared with theory. Recommendations are made as to which should be used to obtain a 'best fit'. Inconsistencies in a theory's validity are highlighted and where possible explanations proposed. Measured velocities are used to calculate forces and compute the parameters used to compare loading conditions.

A full analytical approach is not presented in this study since it would involve a mathematical model to take into account boundary layer development and separation over a wide range of Reynolds numbers in accelerating flow conditions. An accelerating flow field was chosen of a form that would remove 'history' effects from the flow since its direction does not reverse periodically.

This thesis attempts to identify parameters and theories from an extensive literature survey that require further investigation. The survey also established the accuracy and scope of the experimental investigation to follow.

In a series of experiments described here basic wave and force data are determined by measurement. The analysis of this data is presented for a range of wave/structure configurations.

1.3 Summary of findings

A comparison of the derived quantities first identified in the literature survey are evaluated and results contrasted with previous investigations. Explanations of any differences identified are offered where possible.

This investigation has confirmed close agreement between Boussinesq's theory and measured wave profiles. It has also confirmed the findings of Daily and Stephen (1952) that celerity of the solitary wave is given by Russell's (1838) expression.

However results for fluid velocities show good correlation with the theory of McCowan.

In assessing the validity of Morison's equation, the choice of coefficient to be used has demanded much attention. This research has demonstrated a correlation between Morison's coefficients and Reynolds numbers, also between Morison's coefficients and the Keulegan Carpenter number (Section 6.5.10). Limits are established on the validity of the correlation (Section 5.46).

A relationship is identified that links the instantaneous total force coefficient with Iverson's number.

Several areas are identified which require further research to establish the limits of the validity.

1.4 Introduction of nomenclature

To aid discussion of previous studies in this field the nomenclature to be adopted throughout this thesis is introduced here.

Figure 1.1 shows the system used to define the geometry of the experimental arrangement. The cylinder of diameter D lies beneath waves of amplitude, a in water depth , y_o. The coordinate axes run along the mean water level (y=0) and through the centre of the cylinder (x=0). The cylinder centre lies at a depth $y=z_c-y_o$ below the still water level or $z=z_c$ (after McCowan) above the channel bed. For the case of a cylinder in close proximity to the bed, the clearance between the cylinder and channel bed is e.

Figure 1.2 - Wave Geometry
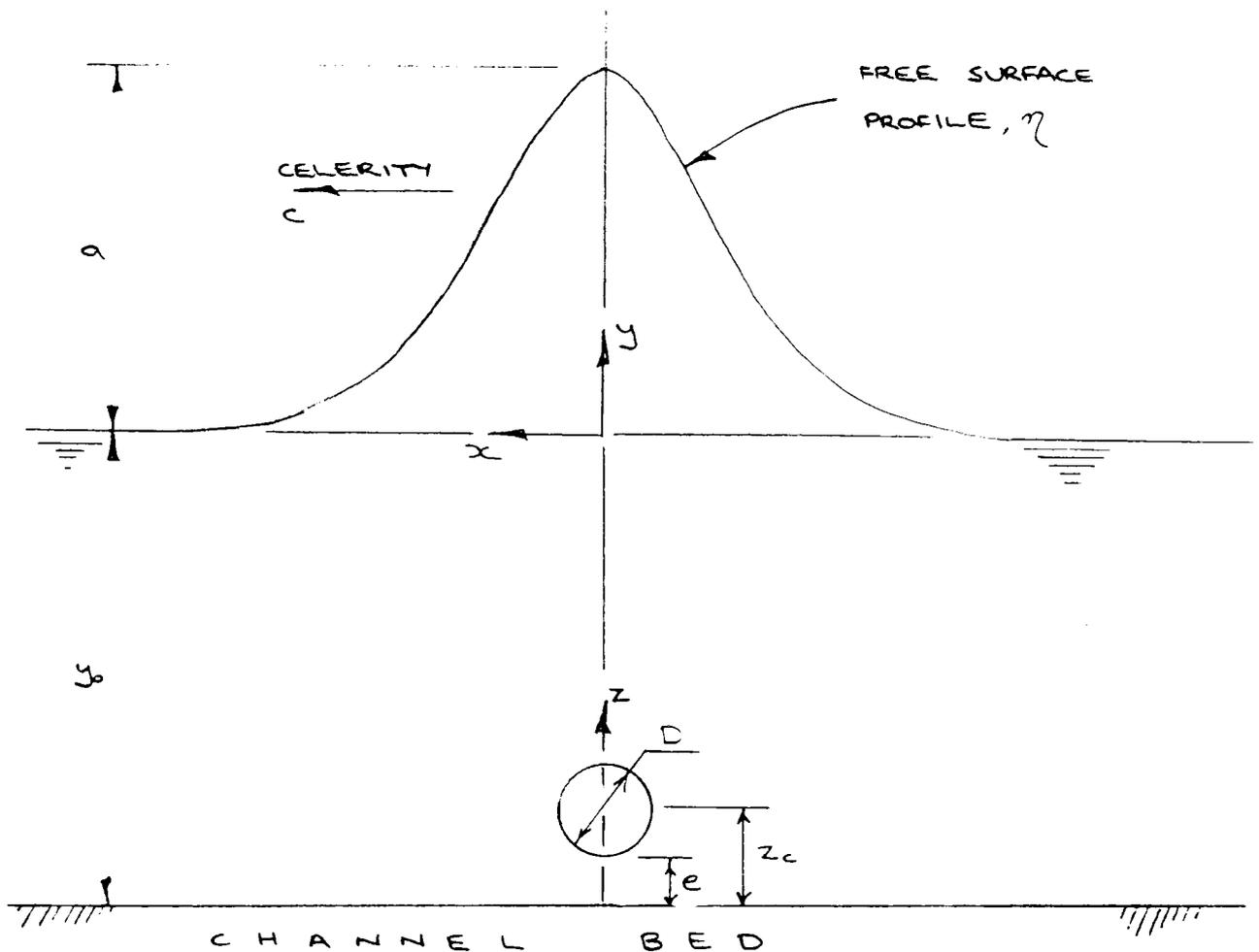
CHAPTER 2   LITERATURE SURVEY

2.1 Historical Note

John Scott Russell discovered and named the solitary wave in 1834. The results of his experimental investigation (1834,1835) were reported to the British Association in 1837 and 1844.

Russell described how the wave was formed from a disturbance generated by a canal vessel which was suddenly stopped. The disturbance formed a solitary elevation which continued along the channel with no apparent change of form or celerity, its height gradually diminishing with distance and its energy being dissipated by friction (figure 2.1)

The description of the wave as a solitary elevation of finite amplitude and permanent form stimulated considerable interest, not least since it appeared to contradict Airy's (shallow water wave theory) prediction that a wave of finite amplitude cannot propagate without change of form.

Russell generated solitary waves in the laboratory by releasing an impounded elevation of water or simply dropping a rectangular weight into the water at one end of the channel. From these experiments it was found that the volume of the wave was equal to the initial displacement and that the wave advanced with a celerity, c, such that (figure 2.1)

$$c^2 = g(y_o + a) \qquad\qquad 2.1$$

Russell also observed that breaking would occur with the wave amplitude approximately equal to the undisturbed water depth

though Bazin (1865), repeating Russell's experiments and confirming equation 2.1, concluded that breaking occurs with the wave height somewhat less than the undisturbed water depth. Rayleigh (1876) argued that fluid velocities could never exceed the wave speed, hence confirming Bazin's findings.

Russell did not determine an explicit relation between the height and characteristic length of a solitary wave but from close inspection of his results it can be seen that an initial elevation might evolve into a pure solitary wave with residual wave train.

The conflict between Russell's observations and Airy's shallow water theory was resolved by Boussinesq (1871) and Rayleigh (1876) quite independently of each other.
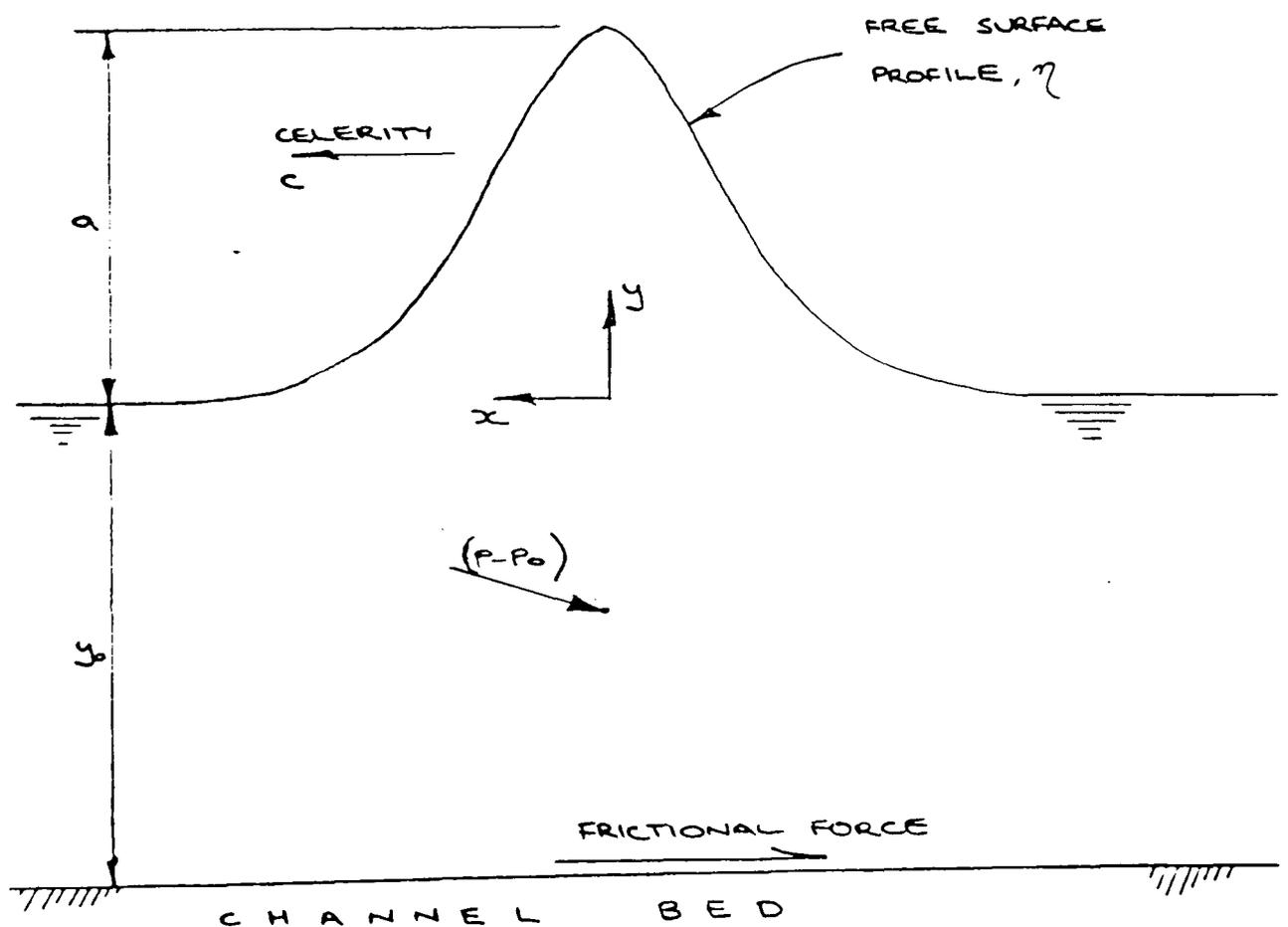
Figure 2.1 - Wave characteristics

Airy (Lamb ß 169) proposed that a progressive wave of small amplitude may travel with no change of form over the water surface since the vertical acceleration of the fluid particles may be neglected i.e. the pressure at any point in the fluid is equal to the static pressure due to the depth below the free surface, (figure 2.1)

$$p - p_o = g \ (y_o + \eta - y) \hspace{3cm} 2.2$$

A wave of finite height whose length is great compared with the depth of water must inevitably suffer a continual change of form as it advances (Lamb ß 175), these changes becoming more rapid the greater the elevation above the undisturbed water level. It follows from equation 2.2 that the horizontal velocity is uniform over the depth of the channel, though Rayleigh points out that this is impossible in a frictionless fluid which was initially at rest, since to satisfy Laplace's equation

$$\delta^2 \Phi / \delta x^2 + \delta^2 \Phi / \delta y^2 = 0 \hspace{3cm} 2.3$$

Φ must be a function of both x and y.

A "wavelength" cannot be defined for the solitary wave due to the asymtotic nature of the profile, but the effective length of the wave is normally taken as the distance between points on the surface which are some arbitrary fraction of the wave amplitude, say 10%, as proposed by Rayleigh. Table 2.1 gives the "length" of the solitary wave corresponding to its height using the "10%" criteria.

This table demonstrates that the longer the solitary wave the smaller the amplitude, and the more closely it approaches the character of a "long" wave. It can be argued that the solitary wave exists as a balance between non-linear effects, tending to steepen the wave front as a consequence of increasing wave speed with amplitude, and dispersion tending to flatten the wave front. A measure of the balance between these two effects was given by Ursell (1953) in his dimensionless parameter

$$U = a\lambda^2/y_o^3 \qquad\qquad 2.4$$

Ursell showed that Airy's conclusion that long waves cannot travel without change of form is valid if this parameter is large, whereas it is taken as unity for the solitary wave.

a/y_o	λ/y_o
0.1	14.6
0.2	10.3
0.3	8.4
0.4	7.3
0.5	6.5
0.6	6.0

Table 2.1 - Length of Solitary
wave with a/y_o
(calc. from eqns. 3.24, 3.25)

- 11 -

2.2 Characteristics of the Solitary wave

2.2.1 Experimental investigations

One of the most important pieces of work on the solitary wave since Russell's investigations was by Daily and Stephan (1952). In two papers the generally accepted essential characteristics of the wave were systematically investigated. Waves with an amplitude to depth ratio of less than 0.1 were not tested because of the difficulty of generating such waves without trailing disturbances. An upper wave height restriction was imposed $(a/y_o=0.61)$ which kept the channel width to water depth ratio low, of the order of 1:3, and ensured two dimensional motion.

2.2.1.1 Free Surface Profile

It was shown by Daily and Stephan and confirmed in this investigation that Boussinesq's theory best described the free surface profile of the solitary wave, this being primarily due to the square of the hyperbolic secant term in his expansion.

$$\eta = a.\operatorname{sech}^2 x/y_o \sqrt{(3a/4y_o)} \qquad 2.5$$

The differences between theoretical and experimental values were not consistent with changing a/y_o. For high waves the experimental profile had a sharper crest with more gentle side slopes and a broader base than given by theory. Whereas at low a/y_o the exact opposite was observed. Boussinesq's expression is in agreement with experimental results since it's dependance upon a/y_o is an average of those found by experiment.

Benjamin (1961) considered a solitary wave propagated in either direction on a horizontal stream with an arbitrary velocity distribution.

This contrasts to previous investigations where the solitary wave was propagated in a homogeneous fluid assuming irrotational motion. Analyses on this basis may apply to a solitary wave advancing in still water as in this thesis, because of the effect of viscosity on the fluid motion may be confined to thin boundary layers on the channel bottom and sides.

However for waves passing over a submerged cylinder the assumption of irrotational motion may be somewhat artificial. The waves generated are of the same form as the true solitary wave, but contain an accumulated vorticity which will only become apparent when considering the flow field.

From Benjamin's investigation a form of profile including the square of the hyperbolic secant may be determined, though in a considerably more complicated expression than in the irrotational case. This appears to add credence to Daily and Stephan's claim that it is the hyperbolic function which gives Boussinesq's expression for the solitary wave profile validity.

2.2.1.2 Fluid Velocity

Boussinesq's theory gives no variation of fluid velocity with depth. Clearly this is not the case in a real fluid and therefore his theory can only be considered as giving a rough approximation of the fluid particle kinematics in the wave. His expression for celerity, determined also by Rayleigh and empirically by Russell (equation 2.1) was shown by Daily and Stephan to be only 1% higher at low a/y_o and 2.5% higher at high a/y_o than those obtained in experiments.

Boussinesq's expression for fluid velocity is only an approximation to those measured. This loss of accuracy in the theory may be reconciled by the work of Benjamin (1962).

The situation considered by Benjamin might develop in a long channel when vorticity produced by frictional action at the boundary and at wave generation becomes diffused over the whole cross section or after the wave has passed over a submerged cylinder.

Benjamin's result also shows that the comparison of theoretical and experimental celerities is a poor basis for assessing the validity of a theory since it is insensitive to the internal motion of solitary waves. It seems that vorticity in the solitary wave has little effect on many of the wave characteristics, so that results from theory assuming irrotational motion often apply to a good degree of accuracy. Quite why this should be the case is unclear though it maybe a result of the stability (minimum energy) of the solitary wave form.

The characteristics considered by Benjamin are not a direct result of the flow field but a result of the method of generation. It is clear that fluid velocities would be affected by any diffused vorticity, and would therefore seem a better basis for comparing theory and experiment. The variability of fluid velocity for waves of similar height is demonstrated in this investigation.

It is important to discuss the accuracy of measurement required to effectively compare theoretical and experimental measurements for surface profile and wave celerity.

Daily and Stephan's results show considerable scatter at low a/y_0 and attribute this to low experimental accuracy in this range. They impose close tolerances on their experimental study and require profile measurements to +-0.15mm depth of water to differentiate between the two closest theories for wave profiles.

Since celerity measurements were made by timing the wave between two points, and since the wave is dispersive an average celerity was determined. To minimise errors Daily and Stephan timed to an accuracy of +-0.001secs. which is equivalent to approximately 3mm travel of the wave crest. The method used by Daily and Stephan to determine fluid velocities and celerities was based on photographic techniques.

Large experimental errors can result from using high speed film and scaling the wave profile from an imposed grid. Manual scaling is always inaccurate because errors are random and not consistent. Consequently the errors cannot be corrected in subsequent analysis. The large grain size used in High Speed film increases the errors in scaling, particularly if images are enlarged during analysis. Daily and Stephan describe some blurring with finite times of exposure and loss of resolution with photographic enlargement. Their results also show a change in slope of the wave as it progressed.

Clearly their results would be improved with more modern data gathering techniques which would reduce errors. Considering the large quantity of data requiring reduction and the required accuracy it is surprising that the scatter in both profile and celerity measurements is not greater.

Daily and Stephan determined fluid velocities by filming on 35mm film the motion of neutrally buoyant droplets. Horizontal and vertical components of mean fluid velocities were determined by measuring the position of droplets at interval of 0.055secs.. Droplet positions were determined to +-0.3mm giving a minimum error of +-2%, the error increasing the shorter the displacement in 0.055secs..

The results compare well with those of McCowan (1891) and show that at the tail of the wave, theoretical velocity is lower than that found in experiments; at the point of inflection the situation

reverses with the theoretical velocity becoming larger than found in experiments at the wave crest. These differences between the experimental and theoretical fluid velocities are consistent for the range of a/y_0 values investigated.

In summary, Daily and Stephan's free surface profile measurements most closely agree with the theory of Boussinesq; Whereas their measurements for fluid velocities show best agreement with the theory of McCowan.

Consequently from the measurements of Daily and Stephan, it is unlikely that there is a relation between surface profile and fluid velocity as was first suggested by Boussinesq. This is confirmed in results presented in this thesis.

After basic experimental work of Daily and Stephan of low or mid range waves much attention was directed to the shoaling and breaking of solitary waves on slopes. This was seen to exhibit characteristics similar to those of long period oscillatory waves approaching the surf zone. Ippen and Kulin (1954) investigated steep solitary waves on a sloping beach determining particle motion and surface deformation at breaking using high speed photography. Even the most sophisticated photographic equipment proved inadequate, since it was unable to prevent blurring with a finite exposure time, very much as Daily and Stephan discovered years earlier.

Naheer (1978) determined fluid velocities beneath a solitary wave using high speed photography. Naheer acknowledges two crucial points.

The first was that reasonable agreement between theoretical and measured free surface profiles and wave celerity was not adequate to conclude that the theory also describes well other parameters. Despite fluid velocities and pressures being low and

of short duration they must be measured as a prerequisite to the choice of a suitable wave theory.

Secondly, if work on the solitary wave was to be used to calculate forces on submerged bodies the velocity and pressure fields used to estimate hydrodynamic forces must have been accurately determined to avoid large errors.

As Daily and Stephan found 26 years earlier, with zero bed slope, measured free surface profiles closely agreed with those of Boussinesq and McCowan throughout the range of a/y_o investigated. With increasing a/y_o, differences with the theory of Laitone (1960) increased. (figure 2.2). At small a/y_o differences between theories were negligible, exactly the region of maximum error in surface profile measurements made by Daily and Stephan.

As the method of wave generation was less than ideal the wave would take time to adopt its final stable form. Consequently there was always some question as to whether the wave achieved a form postulated by theory on reaching the test section. As the wave approached its limiting condition the rate of deformation would slow and perhaps oscillate about a final form. Friction would cause continual attenuation and damp any oscillation. Disturbances are generated with all solitary waves though since this is a dispersive system, waves with large a/y_o leave the trailing waves further behind than do those with low a/y_o, hence the increased error for low waves. Unlike Daily and Stephan, Naheer used resistance type wave gauges reducing the errors in measurement and data reduction.
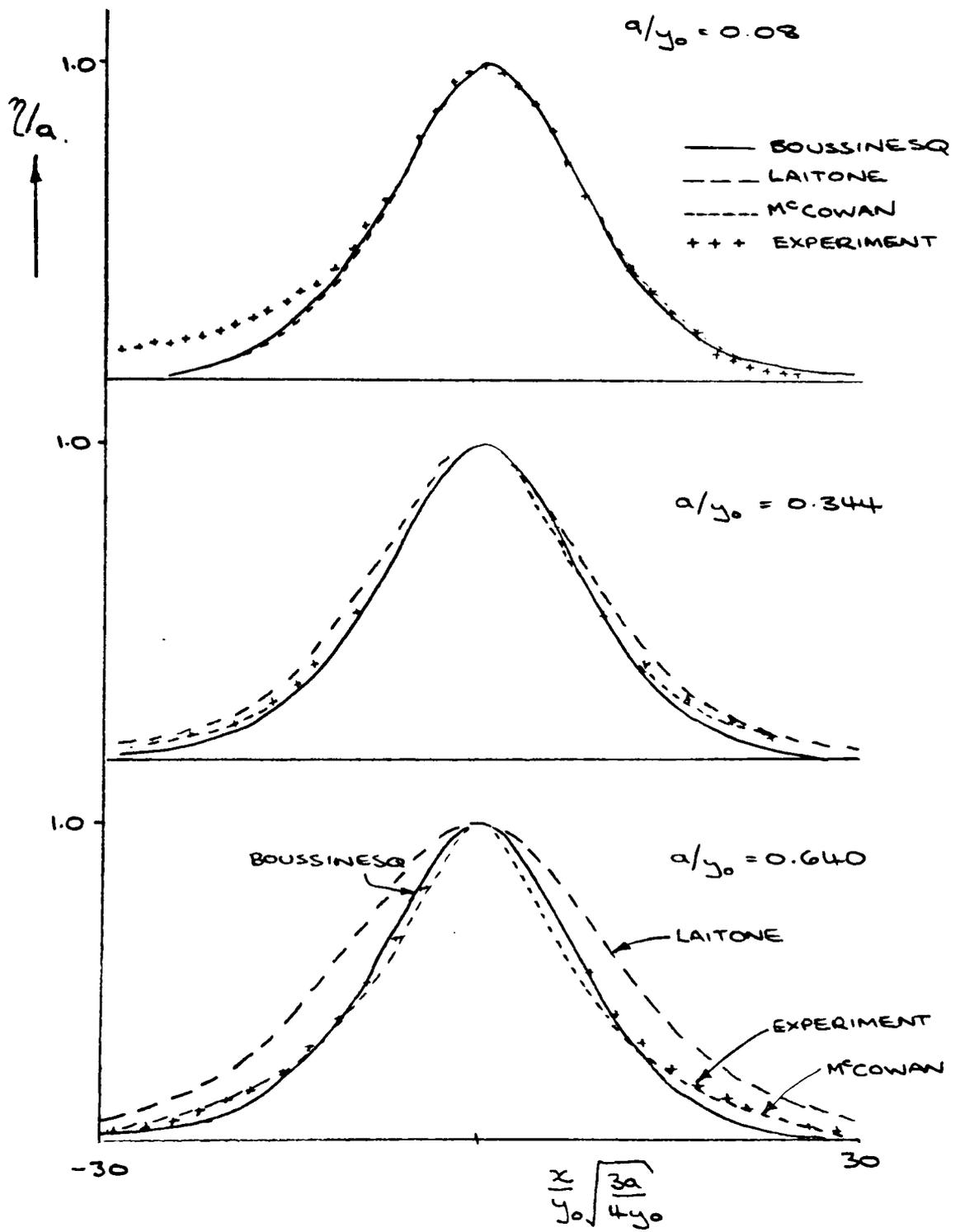
Figure 2.2 - Wave profile

(After Naheer)

Naheer showed that McCowan's theory did not give wave celerity as close to those measured as Laitone's (1960) and Boussinesq's (1871), the latter giving best agreement. Daily and Stephan's results more closely agree with those of Laitone than those of Boussinesq. (figure 2.3). Presumably the difference was a result of systematic errors, though the differences were of little practical significance or interest.

Unfortunately Naheer only measures fluid velocities over rough beds and consequently may not be meaningfully compared to those of Daily and Stephen. However from the work of Benjamin (1961) discussed previously the wave profile and celerity can be compared with that of Daily and Stephan.

Naheer's results for fluid velocity have a considerable scatter possibly due to an accumulated vorticity diffusing through the water. (figure 2.4) The results show a turbulence in the wave increasing towards its rear, and trailing disturbances. It has been shown previously that though vorticity may not affect wave profile or celerity, it will affect fluid velocities and therefore may not be compared with fluid velocities from a theory assuming irrotational fluid motion.

Messrs Lee, Skjelbreia and Raichlen (1982) performed the most significant experimental work on the solitary wave since Russell and Daily and Stephan (1951). They used Laser Doppler Velocimetry (L.D.V.) to measure fluid velocities both beneath and above the undisturbed water level as a solitary wave passed. LDV allowed them to use significantly improved data gathering techniques, obtaining results of greater accuracy. Wave profiles were measured using parallel wire resistance gauges of small diameter (0.25mm). Waves were reproduced with errors in wave amplitude of +-0.75%, despite admitting to an asymmetry of wave profile at the low values of a/y_o tested. (figure 2.5). The accuracy in reproducing waves
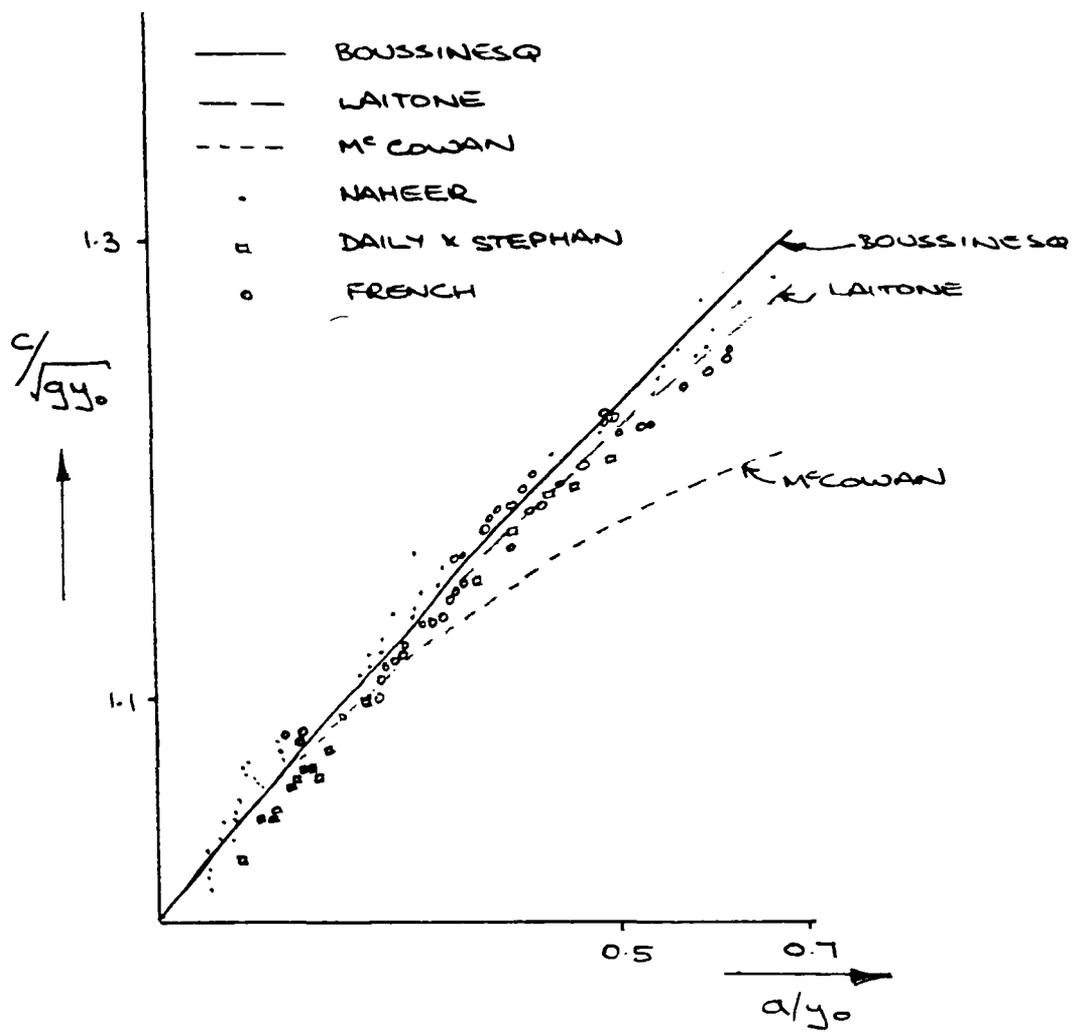
Figure 2.3 - Wave celerity

(After Naheer)
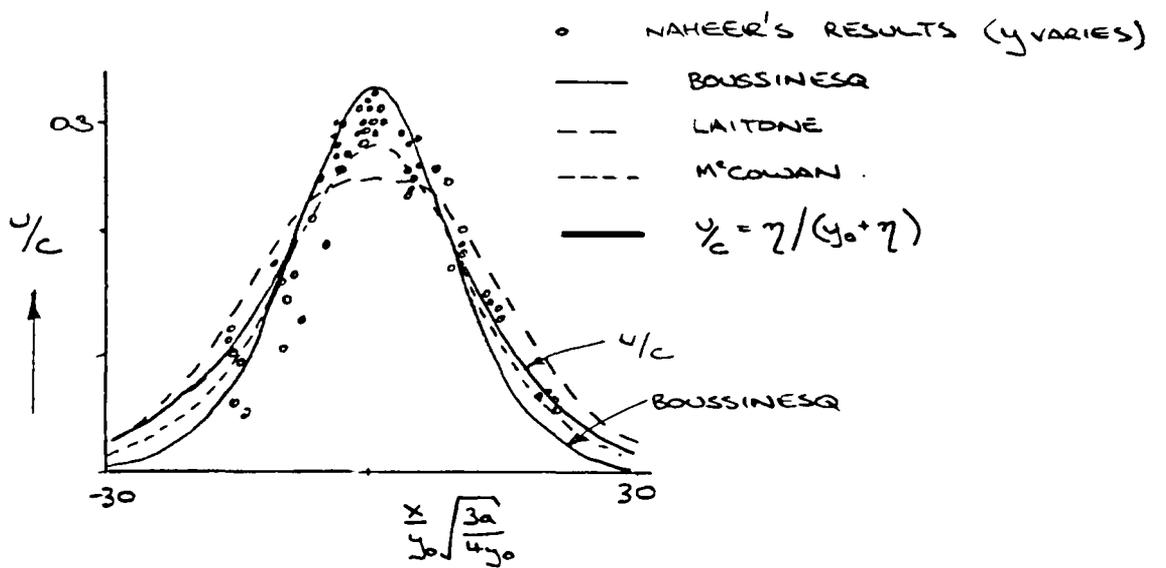
Figure 2.4 - Fluid velocities

(After Naheer)

in this way can be questioned since an asymmetry of wave profile is not only a product of friction but of the method of wave generation and therefore difficult to reproduce accurately.
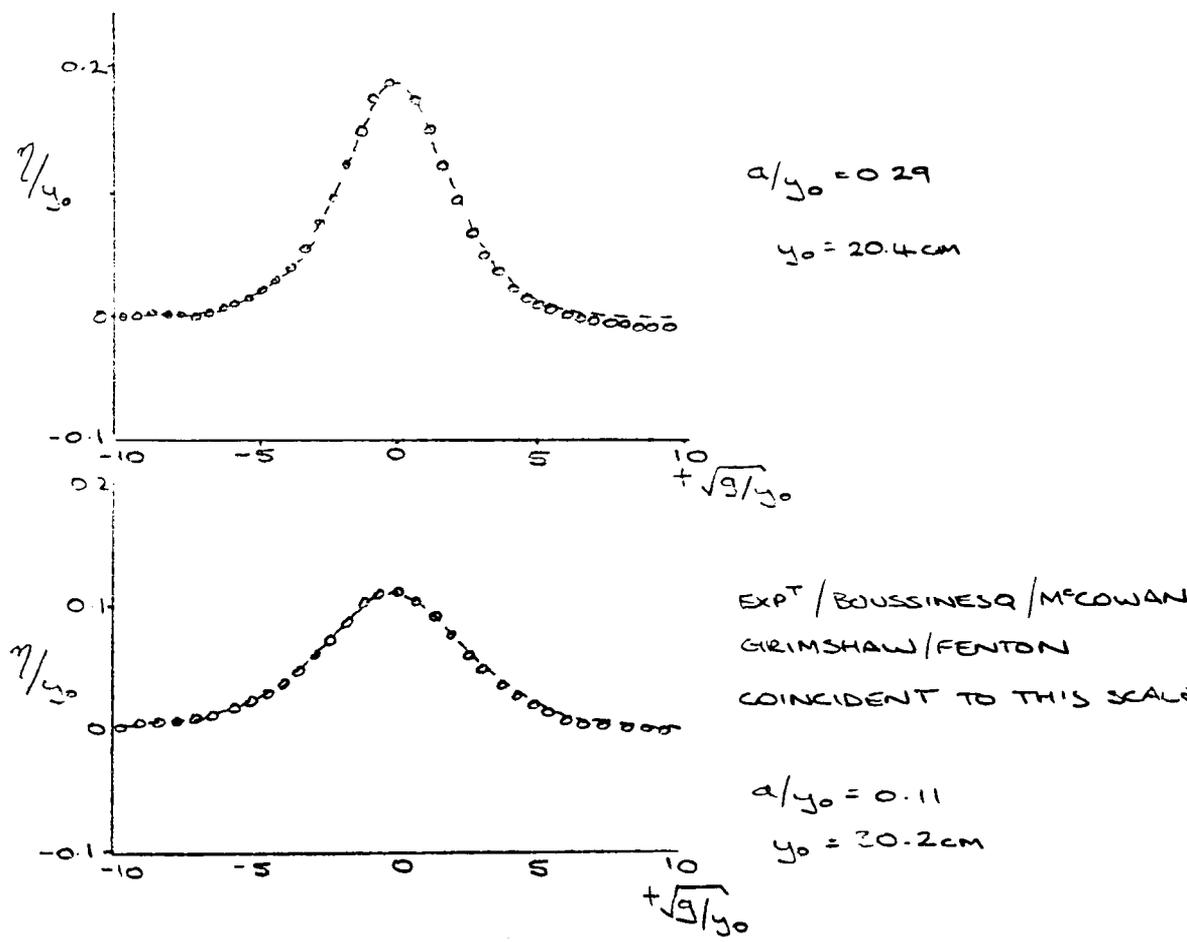
Figure 2.5 - Wave profile
(After Naheer)

Tuck (1974) discusses the uses of paddle or piston type wavemakers in shallow water to generate regular wave trains and shows that generated waves distort as they propagate. This is due to nonlinear free surface effects. Tuck claims that these should only become significant over distances of many wavelengths from the wave generator, but in practice require only 3-4 wavelengths to produce wave distortion. In addition the small gap present between the paddle and the bottom of the channel affects the efficiency and purity of the waves. For long waves a variable gap can seriously distort the wave.

Results for constant gap size indicate a significant lessening of wave generation efficiency if the gap is small. For example, for a wavelength of about 30 times the water depth, a gap of 1% of the water depth halves the generated wave amplitude relative to the zero gap case. (figure 2.6) since the gap between the wave generator and the channel wall changes for each test it is difficult to maintain an accurate repetition of the wave profile.

Lee et al. (1982) tested waves with $a/y_o \leq 0.29$. As Naheer showed, theories differ little in this low a/y_o region. Because of this Lee only compared theories close to breaking thus exaggerating any differences also concealing an inability to differentiate between theories in the region tested.

Work of Daily and Stephan and subsequently Naheer suggest that trailing disturbances would not have separated from the main wave before reaching the test section for the waves used by Lee et al. These disturbances would modify both the wave profile and fluid velocities through fluid turbulence. The experimental results presented by Lee et al. for fluid velocities are widely spaced through the wave
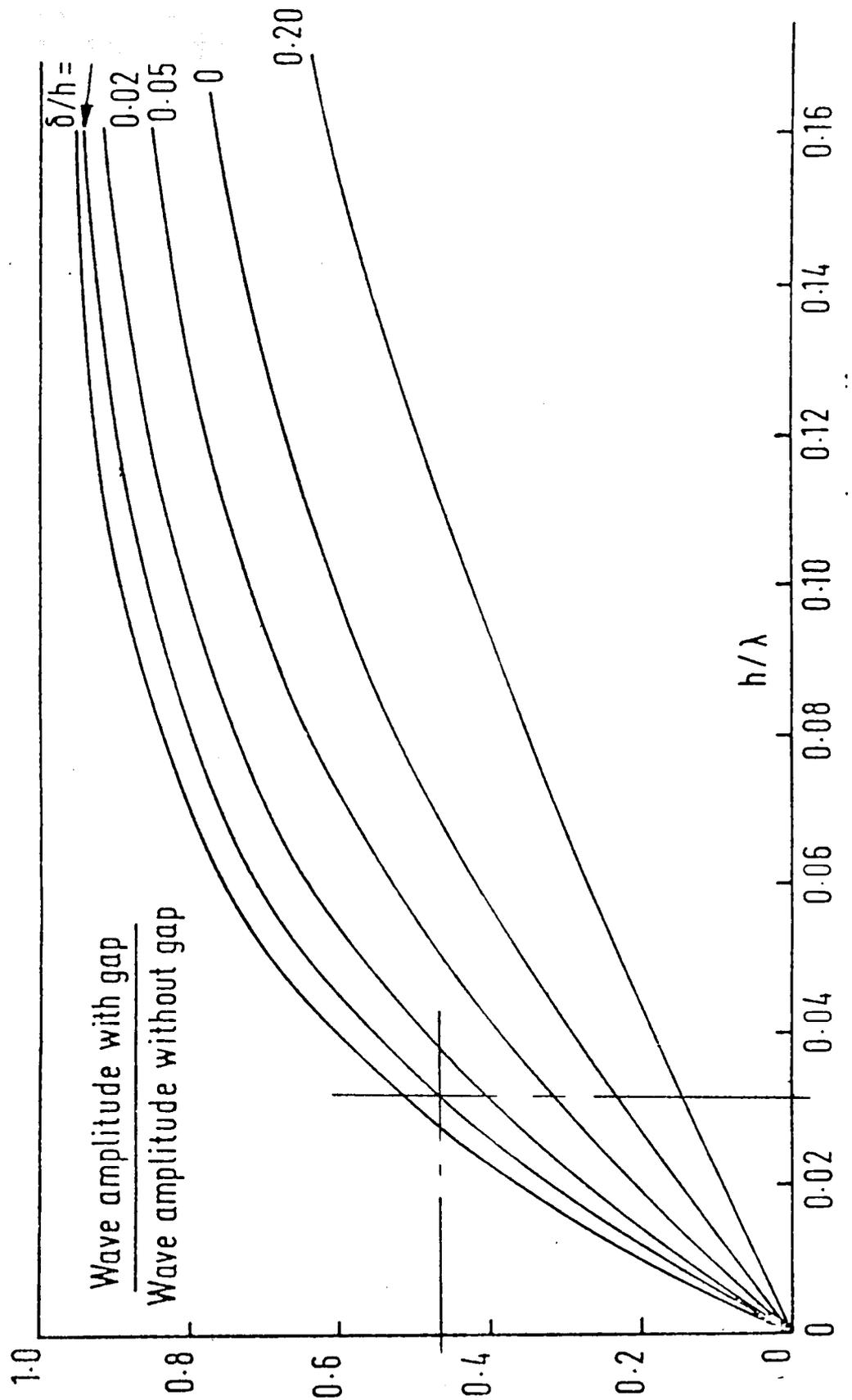
Figure 2.6 - Effects of gap size on wave amplitude

(After Tuck)

and may hide turbulence present. This time lag between velocity measurements is much greater than for surface profile measurements and is presumably a result of a poor signal to noise ratio for LDV. The results for fluid velocities are up to 6% different than theory predicts. (figure 2.7) The normalised velocity and profile measurements show good agreement with theory at the leading edge of the wave.
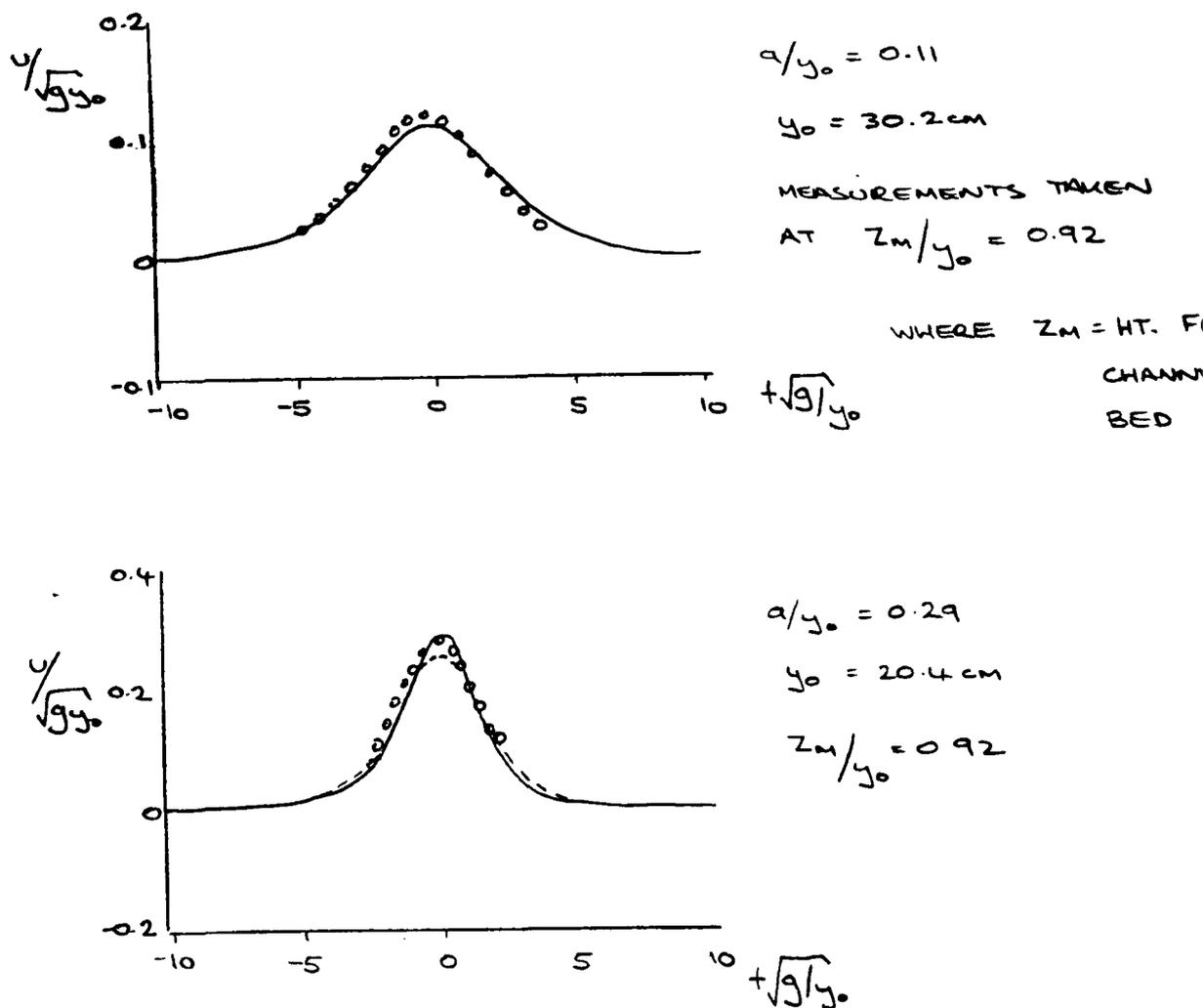
Figure 2.7 - Fluid Velocity Results
(After Naheer)

The poor agreement suggests the presence of trailing waves affecting both the waves profile and fluid velocities.

With the voltage threshold of the electronic equipment set high, the readings would not be taken that cover the low velocities of the disturbances in the solitary wave. Also only a few points would give sufficient output to be recorded, thereby increasing the spacing between measurements. A large spacing may hide points of interest. With a low voltage threshold the number of particles increase, as does the density and scatter of results. This may also have the effect of hiding points of interest.

Fluid velocities were also measured in the vertical direction by Lee et al.. They show good agreement with theory despite the velocities being, at most, one fifth of those in the horizontal direction. They exhibit a measure of asymmetry with the maximum negative velocity being generally greater than the maximum positive velocity. This is without doubt due to trailing waves referred to previously. Since the magnitude of the component of the turbulence in the vertical direction was likely to be of the same magnitude as that in the horizontal direction it may be expected to have a greater effect on the vertical velocities than the horizontal, explaining the asymmetry of the vertical velocity trace. (figure 2.8). It was more obvious in the vertical velocity trace than in the horizontal, because the magnitude of the turbulence was a larger percentage of the fluid velocities in this direction.

Longuet-Higgins (1981) examined fluid particle trajectories in otherwise stationary water as a solitary wave passed. He showed little improvement could be made over the Rayleigh-Boussinesq solution for wave speed, at least over the lower range of wave steepness.
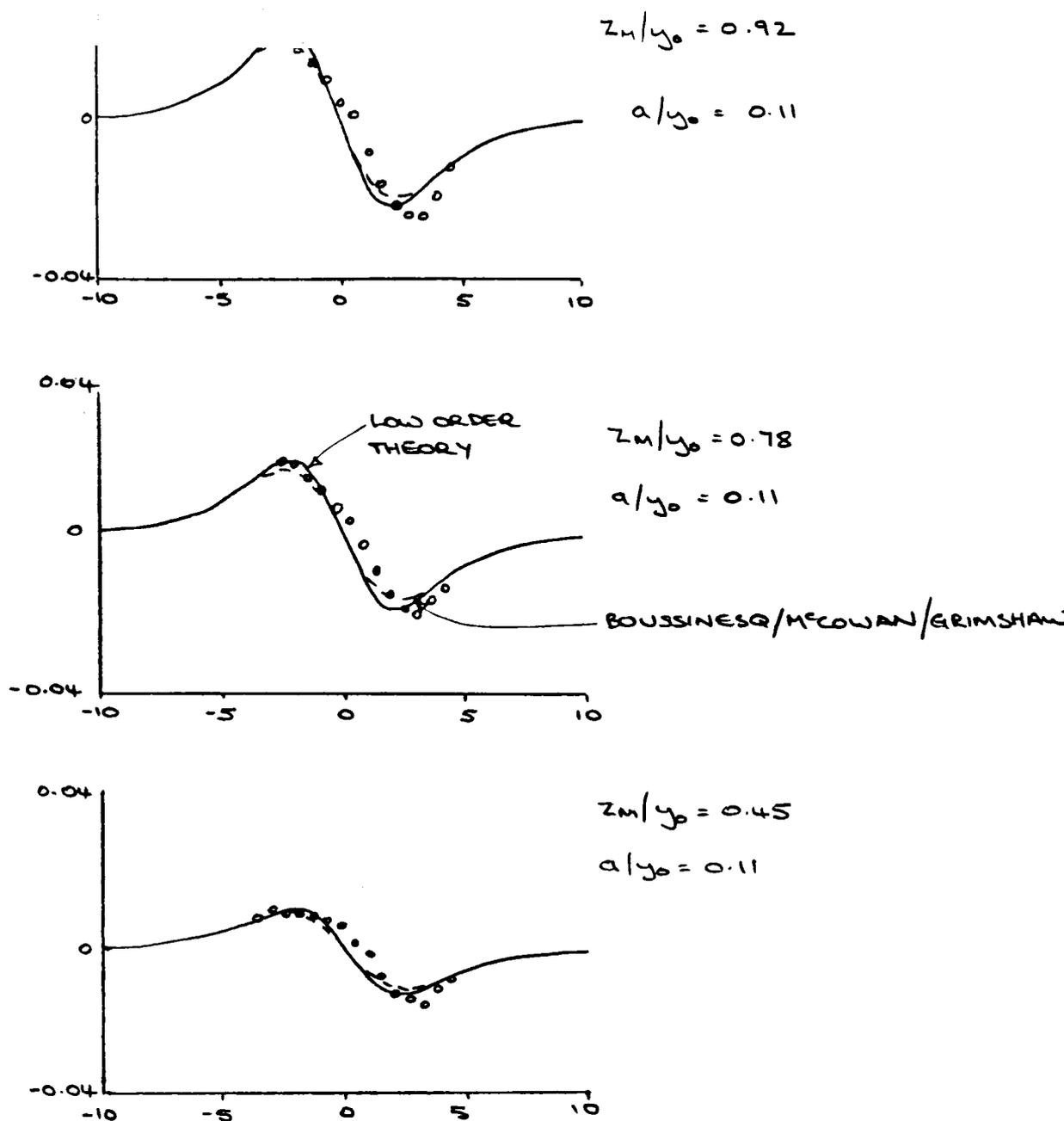
Figure 2.8 - Vertical fluid velocity
(After Naheer)

Longuet-Higgins discussed methods of generating solitary waves used by Russell and Daily and Stephan. He pointed out that these have been successful since the speed of the solitary wave increased as a function of amplitude, with the main disturbance tending to outrun any transient disturbances associated with its generation. This only holds for $0.1 <= a/y_0 <= 0.6$. Above this and certainly in the region of a/y_0 approximately equal to 0.75 the inability of experimenters to generate waves is possibly a result of a phenomena first discovered by Longuet-Higgins and Fenton (1974).

They found that the wave speed increased with amplitude to a certain value where it fell slightly. Consequently at the upper range of wave amplitudes two waves of different amplitude but with the same displaced mass exist. The fluid selects the wave of lower amplitude because of the stability of the corresponding motion. A wave generated higher than this critical value dissipates energy within the fluid and at the boundaries causing it to steepen and ultimately break. A wave initially of lower than critical height simply loses height with energy dissipation. Hence a very steep solitary wave is unlikely to be found in anything other than a transient state. This was observed by the author during laboratory tests close to the limiting height.

The method used by Longuet-Higgins to generate steep solitary waves was to allow them to run up a slope, then to test the properties in an elevated flat section of channel. This enabled Longuet-Higgins to reach the "stable" form of the solitary wave with $a/y_0 > 0.6$ without the possibility of generating a wave of the same displaced mass but with the higher wave speed. By allowing the wave to run up a gently sloping channel bed Longuet-Higgins was attempting to follow the energy curve in figure 2.9 to peak value. However by doing this Longuet-Higgins developed a wave with asymmetric free surface profile, fluid particle motions and velocities. In fact he found a large scatter of results for this very reason.
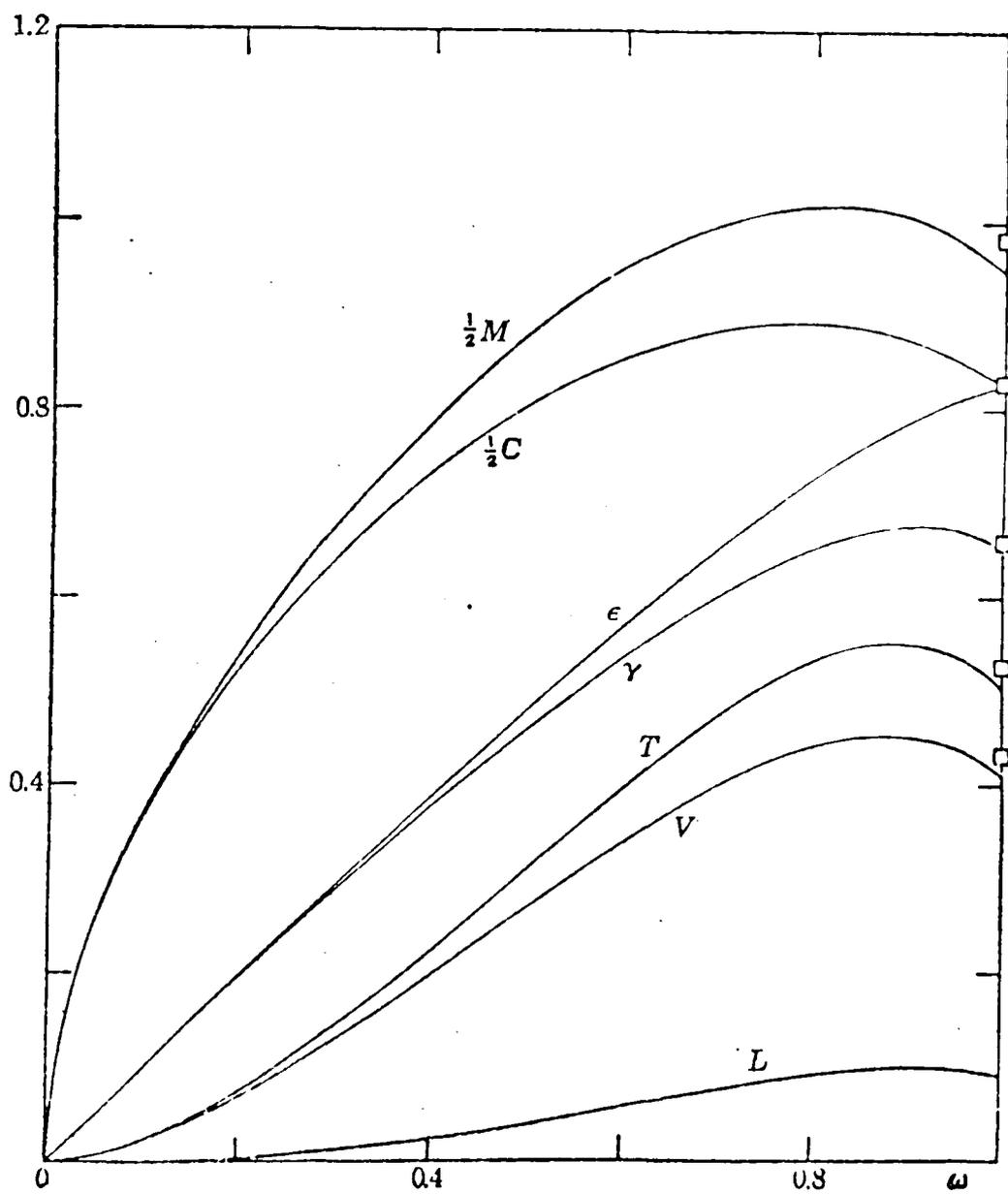
Figure 2.9 - Energy curves

(After Longuet-Higgins)

$$\omega = 1 - \frac{u^2}{gy_0}$$

$$\gamma = F^2 - 1$$

2.2.2 Theoretical Investigations

2.2.2.1 Solitary Wave of maximum amplitude

Yamada (1957), transformed the problem of the solitary wave of maximum amplitude into one of a holomorphic function describing the velocity field in a unit circle whose real and imaginary parts satisfy nonlinear surface conditions on the circumference of the circle. This is an almost identical formulation as that in deep water due to Levi-Civita (1925)

Yamada has shown that by employing a power series expansion the coefficients can be determined using Bernoulli's boundary condition where the free surface represents a streamline with constant atmospheric pressure all along its length. Direct solution complicated the expression therefore Yamada chose a numerical iteration method used by Levi-Civita. After a number of cycles Yamada was able to calculate the celerity, the wave height and the wave profile, in which

$$F=1.286$$

$$a/y_O=0.8266$$

where $F=c/\sqrt{(gy_O)}$. These are substantially different from the earlier results of McCowan who found that

$$F=1.25$$

$$a/y_O=0.78$$

McCowan's analytic approach gave a pressure distribution over the free surface and hence may have contributed to errors in his result for waves of maximum amplitude.

Yamada estimated the errors resulting from an expansion as a Fourier cosine series at generally 1% but up to 2.4% at the crest and wave extremes.

Yamada reduced the errors at these points using methods first adopted by Levi-Civita and obtained

$$F=1.287$$

$$a/y_o=0.8284$$

Later Yamada (1958) used the same method to calculate the celerity for a wave with $a/y_o=0.4808$.

His results for wave celerity did not compare well with those of Rayleigh (1876) and Boussinesq (1871) but since only two waves were calculated by Yamada comparisons were somewhat difficult. Generally Yamada's method is tediously long and complicated.

Laitone (1960) developed the expansion method of Friedrichs (1948) to the fourth order from shallow water theory for a channel with a flat horizontal bed, obtaining a complete second approximation for both cnoidal and solitary waves.

Friedrichs method stretches the vertical axis with respect to the horizontal axis using non-dimensional variables.

Equations of motion and continuity, potential and the boundary conditions at the free surface were transformed using the non-dimensional stretching parameter to give classical nonlinear shallow water equations.

Keller (1948) used Friedrichs expansion to obtain the first approximation to finite amplitude waves similar to the periodic cnoidal waves of Korteweg-deVries and the solitary wave of Boussinesq and Rayleigh. Laitone found that the solution was

identical to the solutions originally given by Korteweg-deVries. The pressure was still hydrostatic but the vertical velocity could not be neglected, it's variation being a linear function of the water depth.

Laitone calculated the second approximation to the cnoidal wave and showed that the $(a/y_O)^2$ term of the Korteweg-deVries equation was incorrect despite predicting nearly the same behaviour. For k=1, the solitary wave results were found to be in exact agreement.

The second approximation showed that the fluid velocities depend upon the undisturbed water depth, y_O. The vertical velocity variation was monotonic if a/y_O was sufficiently large and consequently may be reversed for all y near the wave crest. This reversal in the variation of the vertical velocity may be regarded as defining the limiting height of cnoidal waves, the maximum occurring when k=1, the solitary wave case giving

$$a/y_O = 8/11 = 0.727$$

$$F = 1.284$$

These values are in close agreement with results of Daily and Stephan (1952) and Ippen and Kulin (1955) who have shown that all steady state solitary waves have an $a/y_O < 0.72$ rather than 0.782 originally evaluated by McCowan or the 0.828 obtained by Yamada.

Laitone was the first to determine the limiting condition of a solitary wave from the vertical velocity variation. All others have been based upon the Stokes conjecture that the enclosed angle of the sharp peak formed at breaking would be 120 degrees and correspond to a relative local velocity of zero. Laitone pointed out that Korteweg-deVries proved that any finite amplitude shallow water profile not corresponding to the Korteweg-deVries

equation would not be steady in time. Consequently the sharp peak wave crest would be higher than the limiting value of $a/y_0=8/11$ since it would exceed breaking height. To the authors knowledge no experimenter has observed a breaking wave with a peaked wave crest. As this is an interesting and controversial point it will be discussed in relation to work of Longuet-Higgins whose most recent analysis casts doubt on this conjecture (Section 2.2.2.2).

Lenau (1966) determined the solitary wave of maximum amplitude assuming irrotational two dimensional motion and that the free surface at the wave crest becomes pointed.

Lenau approaches the problem of the solitary wave in a similar way to Yamada, by transforming the problem to a plane more easily solved, defining a function and expanding this as a power series. Using an iteration method Lenau determined the necessary coefficients to calculate the wave profile.

It is impossible to determine precisely the magnitude of the error in Lenau's analysis but is estimated to be of the order of +-0.01 in a/y_0.

Lenau estimated $a/y_0=0.8281$ and that F=1.285. This is in good agreement with Yamada's results who found $a/y_0=0.828$. This is to be expected since both methods are very similar.

This increased interest in the determination of the solitary wave of maximum amplitude prompted Yamada et al. (1968) to re-examine the approximations used in his original series of papers. At that time Yamada identified the main source of error as the Fourier series determination of the conjugate harmonic functions. In this paper of the "precise determination of the solitary wave" Yamada uses Villat's formula and obtains a result little different from that previously, $a/y_0=0.8262$ and F=1.2854

2.2.2.2 Solitary Wave of maximum amplitude: Stokes conjecture

Sasaki and Murakami (1973) also base their work on that of Yamada using his formulation but concentrating on determining the angle the free surface makes to the horizontal and not its profile. Though this seems a retrograde step, it is important to verify Stokes conjecture on which analytic theories are based.

Sasaki and Murakami show that for $u < c$ (i.e. the wave is physically possible) the crest angle is less than 120 degrees though this was obtained by extrapolation and consequently may not be accurate or indeed valid.

An assumption used in investigations of the solitary wave near maximum amplitude was first postulated by Rankine (1865) and further investigated by Stokes (1880). Rankine's investigation concluded that in the steepest possible oscillatory waves of the irrotational kind, the crest became a vertex infinitely curved so that a section of the crest in plane motion presents two branches of a curve which meet at a right angle.

To verify or otherwise, Stokes (1880) in his investigation assumed, in the first instance, that the steepness may be pushed to the limit of a finite curvature at a particular point. Secondly that the variations of the components of velocity in passing from crest to a point infinitely close to it may be obtained using Taylor series expansion of the variables.

Supposing wave motion to be propagated uniformly without change of form so that a sharp crest is formed by two branches of a curve which meet at a finite angle, it follows that a particle on the surface must momentarily be at rest on passing the crest. Thus Stokes found that the angle at the wave crest to be 120 degrees not 90 first supposed by Rankine.

Extensive computation of the solitary wave has been performed by many investigators. A strange scatter of results has been observed and to date has remained largely unexplained. In an attempt to explain the scatter Longuet-Higgins performed computer simulations of particle trajectories at maximum amplitude. These cast doubt on Stokes conjecture of a sharply peaked surface at maximum amplitude. Indeed it is likely that no such condition can ever be practically formed. Since where curvature is great or indeed infinite, surface tension becomes locally important producing an increase in normal stress. Showing a crest angle of 120 degrees does not prove that the disturbance can actually be generated with sharp edges. More likely there exists a limit for which the outline is still a smooth curve beyond which no waves of the oscillatory irrotational kind can be propagated without change of form, though Stokes found no evidence of this limit.

As a swell propagates towards a smooth, gently sloping shore, the height increases when the finiteness of depth begins to take effect. The limiting height of uniformly propagated irrotational waves is passed and the form of the wave changes independently of the change to diminishing depth. The tendency is for the higher parts to overtake the lower parts in front of them, becoming higher until the crest topples over and the waves breaks. This breaking is no doubt influenced by friction against the bottom. Stokes proposed that before the wave breaks the crest becomes thin and similar to that postulated previously. Consequently if the height of maximum amplitude is taken as that at breaking it represents an over estimate compared to that given by theory.

Work by Byatt-Smith (1970) determined the solitary wave in terms of the velocity potential and stream function. This was in preference to the more usual approach of determining the stream function and velocity potential and from these determine the

wave characteristics. He did not obtain an explicit solution but left it in the form of a first order differential equation that could be solved numerically.

Assuming the fluid is incompressible, inviscid, two dimensional, irrotational and steady a velocity potential and stream function exists such that $\psi + i\Phi$ is an analytic function of $x + iy$. Using a Fourier transform of y with respect to ψ Byatt-Smith obtained an integral equation for the free surface elevation. Byatt-Smith obtained solutions for large amplitude solitary waves and found that as F increased beyond 1.2 the number of iterations needed for convergence increased rapidly until it was necessary to take very small steps in F with a very accurate first guess. This was because as F increased a singularity in the integrand was approached with the amplitude equal to $\frac{1}{2}F^2$. No solution was explicitly determined at this critical value but by plotting F against amplitude an estimate of the critical value of F was found (figure 2.9).

Byatt-Smith's results for wave speeds compared well with those of Laitone and improved for higher order approximations for all values of amplitude. However the results show that Byatt-Smith's first approximation for the wave profile more closely agrees with those of Laitone and experimental results of Daily and Stephen (1953) than his second approximation. This is strange because the coefficient of the second order correction is small compared with the first order solution for all values of x.

As x increases towards infinity the solution of the exact equation tends to zero. Thus the accuracy falls for large wave amplitudes and has the effect of stretching the horizontal length scale. This gives surface profiles with smaller slopes on the leading and trailing edges of the wave than would be expected.

Through extrapolation Byatt-Smith obtained an estimate of the amplitude of the solitary wave of maximum height,

$$F=1.31$$

$$a/y_o=0.86$$

some 4% higher than the estimates of Lenau (1966) and Yamada (1951).

Fenton (1972) obtained an exact differential equation of finite order for the surface profile of steady water waves. A form of solution was assumed and coefficients to the ninth order were found numerically.

Fenton's work was based on that of Benjamin and Lighthill and described the free surface in terms of three basic parameters of flow, Q,R and S defined thus

volume flow rate per unit span, Q

$$Q=\int_o^\eta u\,dy \qquad\qquad 2.6.1$$

energy per unit mass, R

$$p/\rho+gy+0.5(u^2+v^2) \qquad\qquad 2.6.2$$

the force plus momentum flux divided by density per unit span, S

$$\int_o^\eta (p/\rho+u^2)\,dy \qquad\qquad 2.6.3$$

In a wave train without friction or other losses these three are constant.

Expanding his exact differential equation for the free surface and by calculating the corresponding three equations for the solitary wave case, Fenton showed that the first three terms agree with those of Laitone (1960) and Grimshaw (1970). Fenton

used this to justify expressing all solutions for the solitary wave profile in a series, each term being proportional to the product of some power of amplitude and some power of a hyperbolic secant of x.

Combining this expression of the exact differential equation with the series from Laitone and Grimshaw, Fenton obtains unknown coefficients to the ninth order.

Fenton found convergence slow to the ninth order and used a Shanks transform to make it more rapid. His results show that to the seventh order the transform did not adversely affect the results. Through extrapolation Fenton obtained

$$a/y_o = 0.85$$

$$F = 1.304$$

for the solitary wave of greatest height. This agrees well with results of Byatt-Smith who obtained

$$a/y_o = 0.86$$

As the curve of F has a maximum at

$$a/y_o = 0.85$$

Fenton claimed that this was due to a rounded crest 'snapping through' to become the cusped crest of the highest wave proposed by Stokes. Later Fenton reviewed this statement having investigated the phenomena with Longuet-Higgins. Together they argue that F must decrease slightly as maximum a/y_o is approached.

For a/y_o>0.752 differences between Fenton's profile and that of Byatt-Smith grow, with the profile at a/y_o=0.85 bearing no resemblance to the sharp crested wave proposed by Stokes.

Fenton's results rely upon Shanks transforms for convergence. He found that expressions for fluid velocities due to the passage of a solitary wave show "certain irregularities" which seem to invalidate the use of the transform. Consequently the validity of profile results using the transforms must be in doubt as are his results for fluid velocities. In both cases there is no physical reason for the transforms use and appear to be a numerical convenience.

Longuet-Higgins (1973) follows the same course as Fenton defining the excess mass of the wave

$$\int_{-\infty}^{\infty} \eta \, dx \qquad\qquad 2.7.1$$

the total momentum (or impulse),

$$M_h = \int_{-\infty}^{\infty}\int_{-y_o}^{\eta} u \, dy \, dx \qquad\qquad 2.7.2$$

the kinetic energy,

$$T_h = \int_{-\infty}^{\infty}\int_{-y_o}^{\eta} 0.5(u^2+v^2) \, dy \, dx \qquad\qquad 2.7.3$$

and the potential energy,

$$V_h = \int_{-\infty}^{\infty} 0.5g\eta^2 \, dx \qquad\qquad 2.7.4$$

and the total circulation of the wave,

$$C_h = \int_{-\infty}^{\infty} u \cdot ds = [\Phi]_{-\infty}^{\infty} \qquad\qquad 2.7.5$$

all equations being per unit span and mass.

Longuet-Higgins identified three equations by which these are related, due to Starr (1947) (eqns. 2.8.1, 2.8.3) and McCowan (1891) (eqn. 2.8.2).

$$I = cM_h \qquad\qquad 2.8.1$$

$$2T_h = c(I - y_o C_h) \qquad\qquad 2.8.2$$

$$3V_h = (c^2 - gy_o)M_h \qquad\qquad 2.8.3$$

Assuming Stokes's conjecture that at a sharp crest, the angle at the corner is 120 degrees and Lamb's approximation, that the solitary wave profile may be represented by a simple exponential

$$\eta = A_h e^{-\varepsilon|x|} \qquad\qquad 2.9$$

Longuet-Higgins obtained F=1.161. Since the single term of the expression for the surface profile only satisfies two conditions at the crest and at infinity, Longuet-Higgins introduces a second term thus

$$\eta = A_h e^{-\varepsilon|x|} + B_h e^{-2\varepsilon|x|} \qquad\qquad 2.10$$

giving F=1.290.

Longuet-Higgins compares his profile to that of Yamada, minimising differences to the order of 0.002 with

$$\eta = A_h e^{-\varepsilon|x|} + B_h e^{-2\tau|x|} \; (\tau > \varepsilon) \qquad 2.11$$

to determine the surface profile in terms of exponentials. This giving F=1.2881 and a/y_o=0.8296 both somewhat lower than results Fenton (1971) and Byatt-Smith (1970) though only marginally higher than Lenau (1966) and Yamada (1957).

Longuet-Higgins with Fenton (1974) published a second paper of the same title for waves of less than maximum amplitude.

Longuet-Higgins and Fenton took the original theory of Fenton and extended the series to the fifteenth power of a/y_o.

Beyond the ninth power the coefficients became irregular increasing rapidly and altering in sign. This was possibly why Fenton restricted his analysis to the ninth order. Using Longuet-Higgins's identities developed in the first paper, these irregularities are shown to be significant and due to rounding errors.

Changing the independent variable to (F^2-1) removed irregularities in the series for momentum and energy. These were due to a singular behaviour of a/y_o as a function of the independent variable near maximum a/y_o. This may have been a consequence of a sharp increase in wave height as the maximum amplitude approached with no corresponding increase in total mass, very much in line with Stokes's (1880) conjecture of a sharp crested wave. This would leave momentum and energy smooth functions of (F^2-1).

One difficulty of using either

$$(F2-1)$$

$$\text{or } a/y_o$$

as an expansion parameter was that the precise range of the variable was not well determined. Consequently Longuet-Higgins and Fenton introduce a third variable related to the particle speed at the wave crest.

$$1-u^2/gy_o \qquad\qquad 2.12$$

Series of M, T and V in powers of this variable initially appear less regular than previously. Using summation by Padé approximants leads to rapidly converging results. The validity of this technique applied to gravity waves has not been questioned though it has yet to be justified rigorously. However, using this technique F=1.285 was calculated from M and V thence the wave height, a/y_o=0.827.

The maximum height compared well with results of Yamada and Lenau determined by completely different methods discussed earlier.

Author	Date	a/y_o	F	Comment
Yamada	1957	0.8284	1.287	
McCowan	1891	0.78	1.25	
Laitone	1960	0.727	1.284	From vert Vel
Lenau	1966	0.8281	1.285	
Byatt-Smith	1970	0.86	1.31	Extrapolation
Fenton	1972	0.85	1.304	Extrapolation
Longuet-Higgins	1973	0.8296	1.2881	
L-H & Fenton	1974	0.827	1.285	

Calculations show that the wave speed F reached a maximum at a wave height less than maximum. (figure 2.9). From this Longuet-Higgins and Fenton concluded that there was a range of speeds near maximum where two distinct solitary waves can exist with the same wave speed.

This may explain why the maximum a/y_o proposed by Byatt-Smith (1970) and Fenton (1972) are substantially larger than the latest results. Both are based on extrapolation of the relation between a/y_o and F for waves of substantially less than maximum amplitude and do not take account of the sharp curvature now found to exist in the graph near maximum amplitude.

In discussion Longuet-Higgins and Fenton speculate regarding the physical interpretation of their results. With amplitudes less than maximum, the wave crest was rounded and the wave profile convex for a short length adjacent the wave crest. For the limiting height Longuet-Higgins suggested that the wave surface will be two concave arches falling away with horizontal distance from the crest. As the wave approached its limit, the crest would "flip up" locally. The limiting wave profile would then intersect the profile of a wave of slightly smaller amplitude, with a total volume of the limiting wave being slightly less. Since

both the kinematic and potential energies may be expressed as integrals over the volume of the wave, these may also reduce slightly for the same reason. As a/y_o increases, F also increases, and since F is related to the exponent (-2α) by an exact relation, at the extremes of the wave the total base width of the wave diminishes. This latter point is a widely accepted and experimentally verified characteristic of solitary waves. However in the final stages of growth as a/y_o tends to a maximum value Longuet-Higgins and Fenton suggest that a slightly wider base is required to support the wave and so F must finally decrease. In fact Longuet-Higgins and Fenton determine F from integral properties M, T and V finding that F reached a maximum before maximum a/y_o (figure 2.9). Assuming that the relation between a/y_o and base width is valid to maximum amplitude it of course follows that after attaining a minimum width the wave does in fact broaden at its base with decreasing F.

To clarify the situation it is helpful to plot the actual sequence of wave profiles to the highest wave.

Whereas at low amplitudes each profile would intersect the proceeding profile at only one point, the highest wave would intersect its neighbours at two points. (figure 2.10 Byatt-Smith and Longuet-Higgins, 1976).

Though the celerity and energy of the solitary wave both converge satisfactorily for all waves up to the highest, this was not the case with surface profiles. Neither the celerity nor the energy of the wave were determined instantaneously in experiments with waves of less than maximum amplitude, the celerity being an average value.
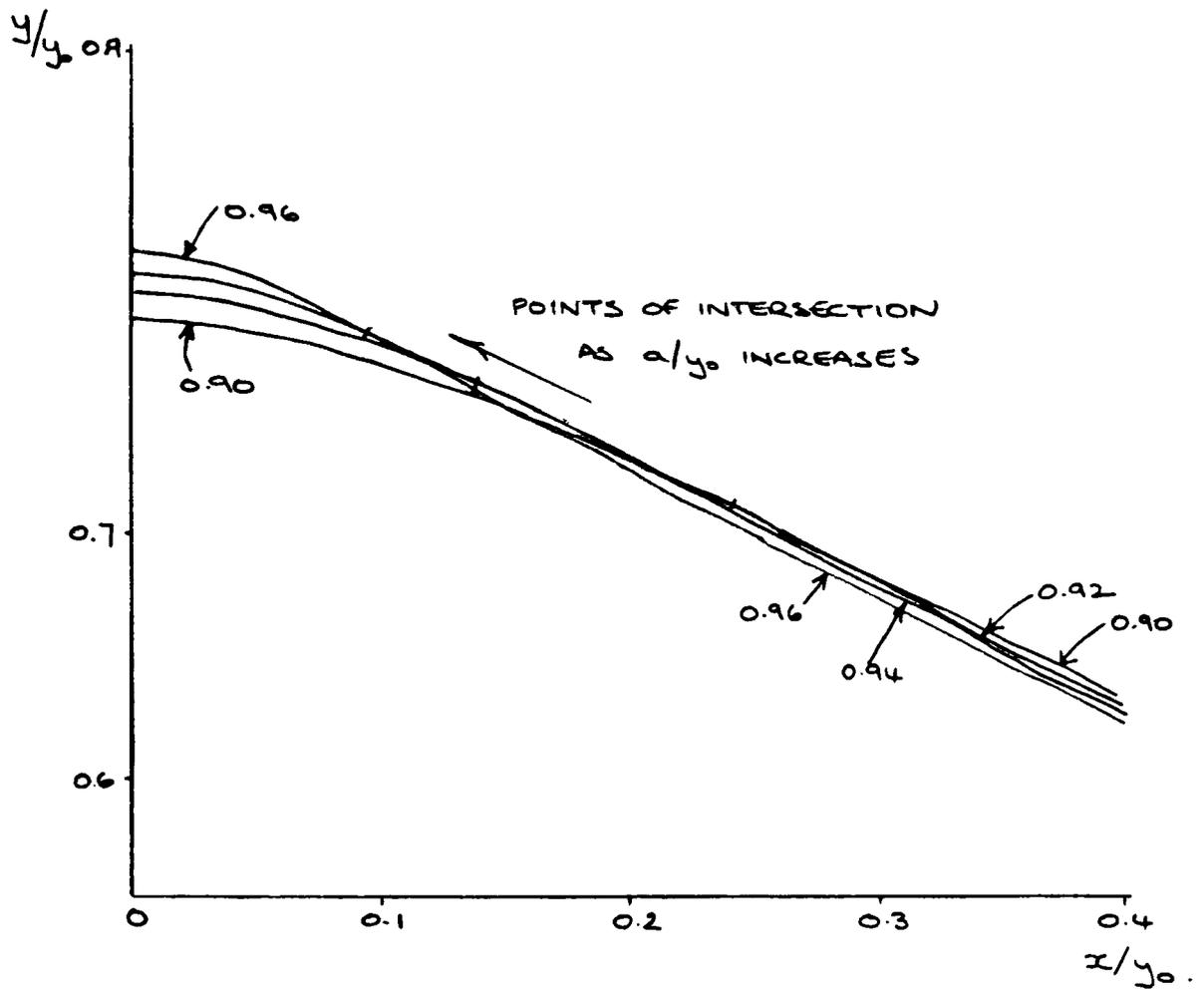
Figure 2.10 - Near maximum Solitary wave profile
(After Byatt-Smith and Longuet-Higgins)

A plot of Longuet-Higgins's and Fenton's results of F versus a/y_o shows closer agreement with those of Daily and Stephan, than with those of Rayleigh/ Boussinesq or McCowan's theory. (figure 2.11)

The observed wave height slightly exceeds the theoretical value for a given F, which is possibly due to the boundary effects of the channel bed.
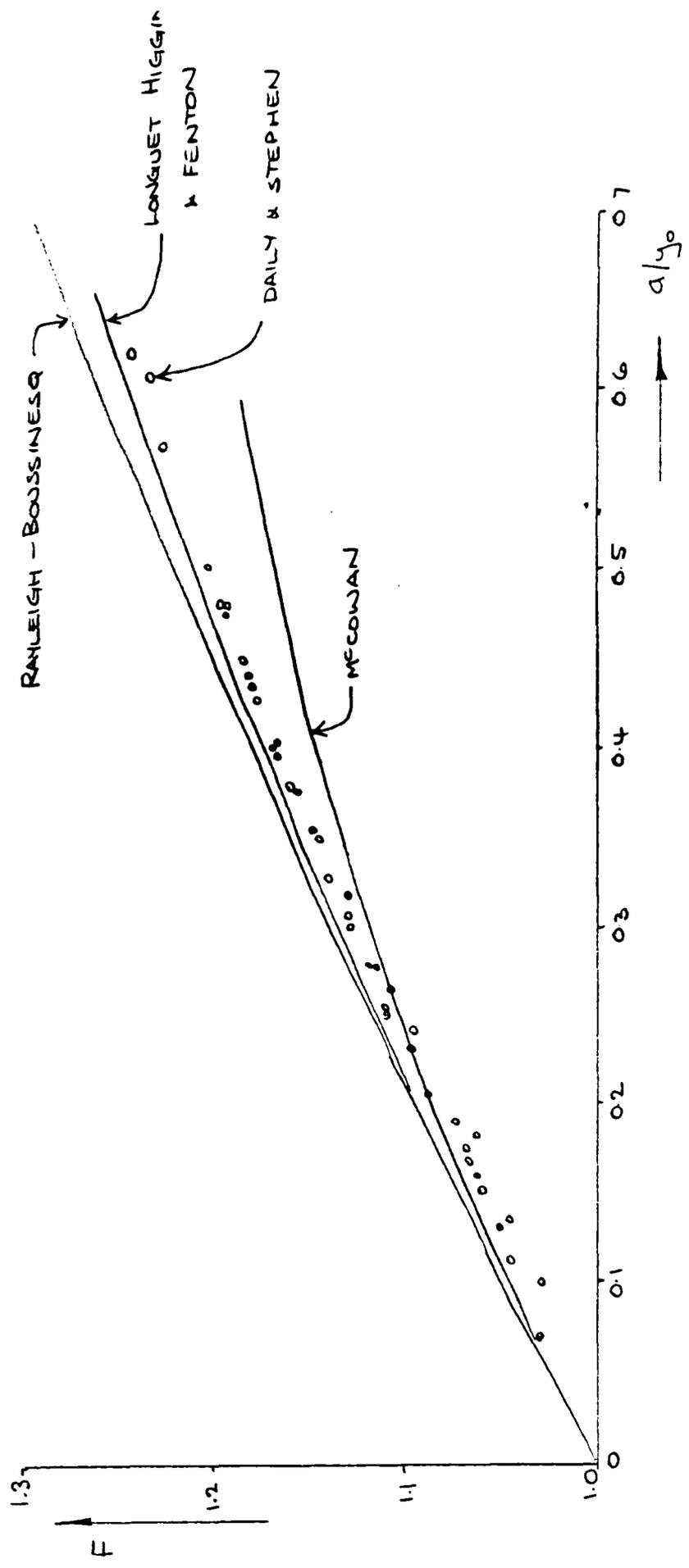
Figure 2.11 - Wave Celerity

(After Longuet-Higgins and Fenton)

Daily and Stephan were limited to waves with $a/y_o < 0.62$ because their method of generation determined only the mass and impulse of the wave. These properties are nearly stationary functions of a/y_o for high waves. Consequently waves were generated which were ill-defined since large changes in amplitude would result from only small changes in mass and impulse. In small scale experiments side walls can often give rise to appreciable losses and hence large changes in amplitude. Higher waves can only be produced by generating waves of moderate amplitude into a gradually narrowing channel or into water of gradually diminishing depth.

Longuet-Higgins followed up this work with experiments on particle trajectories beneath the solitary wave using such a method to generate higher waves. Naheer (1978) showed that with shoaling solitary waves the profile became steeper at its front and of shallower slope at its rear. Naturally this affected results obtained using this method of generation. Indeed a gradual narrowing of a channel can create a three dimensional flow which would not be modelled by theory and would affect results in an unknown way.

Longuet-Higgins continued work on the solitary wave with Byatt-Smith (1976) investigating the validity of Padé approximants applied to gravity waves.

They obtained the wave profile directly as the solution of a singular equation first proposed by Byatt-Smith (1970). Longuet-Higgins recast the solution of the integral equation in terms of a parameter which is monotonic throughout its entire range (eqn. 2.12) and was first proposed by Longuet-Higgins and Fenton.

With computations to

$$1-u^2/gy_o =0.96$$

the maximum value of F was 1.294 for

$$1-u^2/gy_o =0.917$$

This agreed well with calculations based on Padé approximants, justifying there use by Longuet-Higgins and Fenton.

The integral equation method used by Longuet-Higgins and Byatt-Smith gave the profile of the wave with considerable accuracy. Plots to maximum amplitude confirm that the profiles of high solitary waves intersect the more rounded profiles of lower waves at points not far from the wave crest. (figure 2.10). Thus the highest wave actually lies beneath the not so high waves over most of the wave profile. Byatt-Smith and Longuet-Higgins were unable to confirm that the crest became sharp with an internal angle of 120 degrees.

Stokes's conjecture was discussed further by Toland (1978).

Toland proved the existence of a wave of greatest height, and investigated the nature of the discontinuity at maximum amplitude.

This was not sufficient to determine the local behaviour of the wave of greatest height. For that, it must be determined whether there was a "jump" discontinuity as a/y_o increased as was proposed by Stokes.

Using Nekrasov's integral equation corresponding to the existence of a wave of greatest height and of permanent form moving on the surface of irrotational, infinitely deep flow Toland

proved the existence of a stagnation point at the wave crest but was not able to prove the shape of the wave crest at maximum amplitude.

In an attempt to verify or otherwise Stokes "corner flow" theory Longuet-Higgins analytically investigated the trajectories in the wave of maximum amplitude.

Longuet-Higgins results showed that each fluid particle moved as though it were under the action of a central force of constant strength directed away from the crest. The resulting trajectories could then be described by known functions in the form of an elliptic integral that could be evaluated using Simpsons rule. Longuet-Higgins found a discontinuity in the velocity for periodic waves. This gave an apparently smooth orbit, though the surface was discontinuous in slope. Either side of the origin the trajectories were parabolic with axes inclined at angles of +-30 degrees to the vertical.

For the solitary wave the maximum height of the trajectory equals the wave height $a/y_o=0.829$ and the particle translated $4.229y_o$ horizontally. Using Stokes relation Longuet-Higgins found that the internal angle was 120.26 degrees, not 120 degrees previously assumed.

Work with Cokelet (1977) followed the development of the surface of a wave numerically beyond the instant when the tangent first became vertical. Results show that the waves would not develop a sharp corner or singularity before the free surface becomes unstable and overturns. (figure 2.12). Further there is nothing to suggest that the flow does not remain smooth (neglecting surface tension and viscosity) up to the instant of impact. Longuet-Higgins proposed that Stokes conjecture was only valid for a highly singular form, intermediate between steady and symmetric plunging wave. This is highly unsatisfactory since it appears so highly singular that it may not be applied to any

situation of general interest. Clearly Longuet-Higgins's analysis to determine the mass momentum and energy of the solitary wave should be repeated in the light of his recent findings.
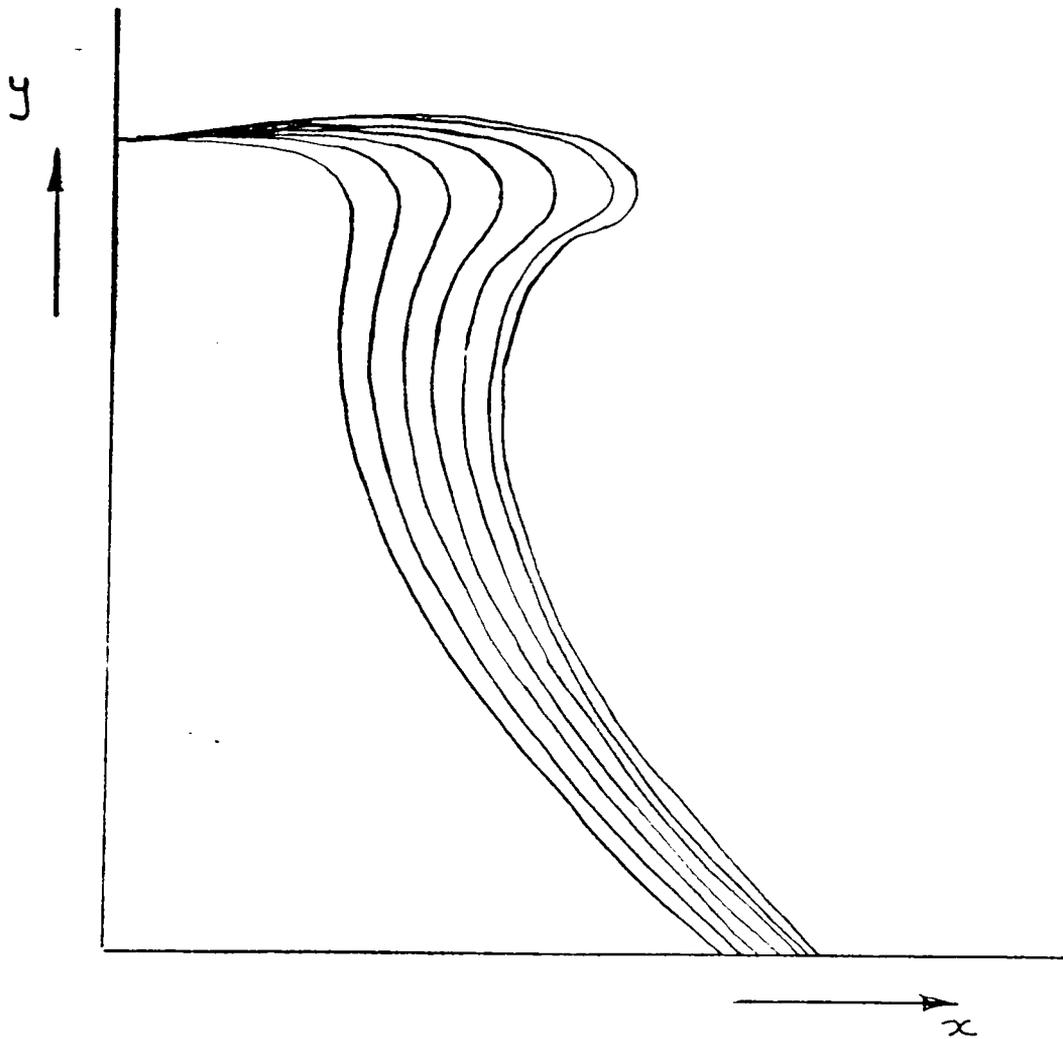
Figure 2.12 - Time variation of Wave profile
close to overturning (After Cokelet)

2.3 Forces on small structures

A small diameter cylinder subject to long wavelength oscillatory waves, will experience flow conditions not dissimilar from those of the same cylinder in steady flow. Morison et al. (1950) proposed that the force on a small vertical cylinder comprised of two parts, one analogous to the steady flow drag force and hence proportional to velocity squared, the second proportional to acceleration, both quantities being measured on the axis of the cylinder. In the disturbed flow, to allow for errors introduced by assuming the cylinder does not disturb the flow field a coefficient was assigned to both; Cd, the drag force coefficient and Cm the inertia force coefficient.

The equation known as Morison's equation is usually written

$$F = \tfrac{1}{2}\rho C d A u |u| + Cm \, \rho V_m \, du/dt \qquad\qquad 2.13$$

The choice of suitable coefficients, Cd and Cm, has proved to be the most complex problem in the use of Morison's equation.

Verley (1975) has shown that the calculation of forces on submerged structures may be segregated into regimes depending upon the relative sizes of structures and waves. Because of the complex nature of fluid structure interaction and the lack of general complete solution of the problem, simplifying assumptions can lead to useful rules and methods.

Hogben, Miller, Searle and Ward (1977) recognised the danger of simplifying assumptions and attempted to produce a critical working guide to methods and data available for estimating fluid loading on offshore structures.

The majority of their discussion is in relation to horizontal wave forces on vertical cylinders which are isolated and pierce the free surface.

The Keulegan Carpenter (Nkc) number represents the relative importance of drag over inertia forces and can be shown to be proportional to their ratio. In the form

$$Nkc = u_m T / D \qquad\qquad 2.14$$

it is strictly only applicable to simple harmonic flow.

Hogben et al. present wave force coefficients qualified with respect to both Reynolds and Keulegan Carpenter numbers. These two parameters were used on the basis of dynamic similarity and that they are widely referenced in available literature. They are considered the best available parameters which define the wave force coefficients for specified conditions. Clearly they are more applicable to laboratory experiments than to real sea experiments since they take no account of orbital motion of fluid particles and the irregularities of sea waves.

Reynolds and Keulegan and Carpenter numbers are based upon a representative fluid velocity which was usually calculated from a suitable wave theory. As no general complete solution has been determined the situation is further confused since different theories with differing accuracies are employed by investigators. The representative velocity is usually the amplitude of the orbital velocity normal to the axis of the cylinder. The calculated orbital velocity is dependent on the wave theory selected and the depth below the surface.

In steady flow, Reynolds number is well established as a correlation parameter for Cd and provides boundaries for fairly well defined regimes. Published Cd data for oscillatory flow shows trends with Reynolds number similar to that for steady

flow, though the boundaries are not so clearly established. As for steady flow three regimes are defined "sub-critical, critical and post critical", the latter embracing the super critical and post critical regimes of the steady flow case. This is done because for oscillatory flow there is a large scatter of results with a trend towards a constant mean, independent of Reynolds number.

Theory and experiment indicate that the drag force dominates in Morison's equation at high Keulegan Carpenter numbers and that the inertia force dominates at low Nkc. There are intermediate values at which the drag and inertia forces attain similar magnitude, the flow behaviour being complex in this region.

The accuracy of evaluation of wave force coefficients is dependent on the loading regime in which the experiment was conducted. Data obtained when drag forces predominate enables accurate evaluation of Cd but not Cm and vice versa. Dean (1976-Trondheim) presented a detailed analysis of the influence of loading regime on the uncertainties in Cd and Cm showing that the large scatter in published coefficients could, at least partially be due to the lack of determination in the selection of suitable data for each particular coefficient.

It is inadvisable for coefficients obtained in a study by particular methods of data analysis and using particular wave theories to be applied to another situation significantly different to that of the original experiment. This dilemma is yet to be solved and is largely unresearched.

2.3.1 Steady Flow

Practical work by Bishop and Hassan (1964) measuring lift forces on horizontal cylinders demonstrate lift and drag coefficients in steady flows (3600<Re<11000) are dependent on Reynolds number. Similar investigations showed that the Strouhal number (non

dimensional eddy shedding frequency parameter relating
frequency of vortex shedding with cylinder diameter and free
stream vorticity) in a steady flow is also a function of Reynolds
number, although the values of the Strouhal number remain
practically constant at about 0.2 (smooth cylinders) for a wide
range of Reynolds number (10^3- 10^5). Detachment of vortices is
associated with an unsteady lift force oscillating at a frequency
and a similar drag force at twice the shedding frequency.

2.3.2 Accelerated Flows

Sarpkaya and Garrison (1963) investigated a uniformly
accelerated flow on a submerged horizontal cylinder measuring
lift and drag forces, fluid velocities by photographic techniques
and accelerations through pressure measurements. With a
maximum Reynolds number of $5.2*10^5$, Cd (=1.2) reached a
maximum at a relative displacement, s/D=2.5. This compared well
with Cd obtained with an impulsively started flow for which
s/D=2.0.(figure 2.13).

The significance of s/D the relative displacement as a non
dimensional parameter is clear when one considers that during
the early stages of the fluid acceleration, the wake behind the
body is relatively under-developed compared with that formed in
a steady flow of the same Reynolds number.

Work by Sarpkaya and Shoaff (1979a & b) show that in an
impulsively-started flow, vorticity is slow to diffuse and
therefore accumulates rapidly in the close vicinity of the
cylinder. Sarpkaya found that the growing vortices soon reached
unstable proportions and separated from the cylinder. Their
growth was so rapid that the vortices became much larger than
their steady state counterparts, before separation.

Sarpkaya also found that as s/D increased Cd and Cm fluctuated

between limits with ever decreasing amplitude. For s/D>2.0
average values of Cd and Cm are 1.2 and 1.3 respectively
(figure 2.13).

Using the idealised flow values of Cm=2.0 and Cd=1.2 for model
tests at low Re, Morison's equation over-predicts the forces
early in the transition from laminar to turbulent boundary

<figure>
Graph with vertical axis ranging from 0.00 to 2.00 in increments of 0.25, and horizontal axis labeled s/D ranging from 0 to 5.

Dotted curve labeled C_m starts near 2.00, decreases to about 1.25 at s/D ≈ 2.5, rises to about 1.40 at s/D ≈ 3.5, then decreases again.

Solid curve labeled C_d starts near 0.00, rises to about 1.25 at s/D ≈ 2.5, then decreases to about 1.00.
</figure>
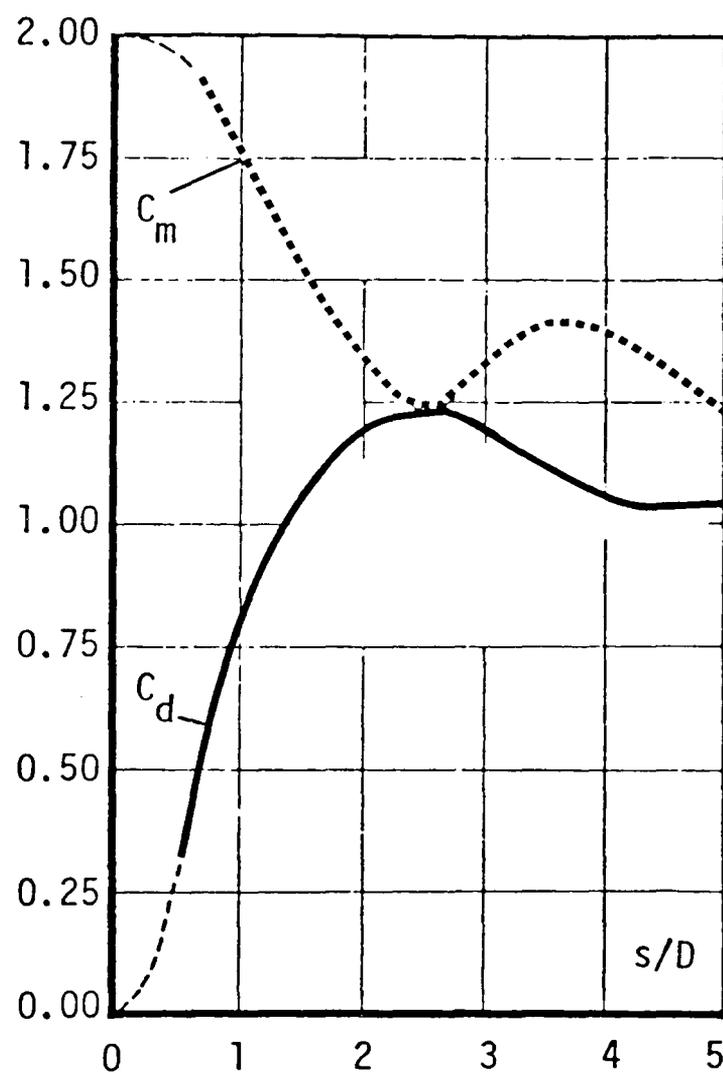
Figure 2.13 - Morison's coefficients with relative displacement
(After Sarpkaya and Garrison)

- 54 -

layer, under predicting later in this transition compared with those forces calculated using C defined by Sarpkaya and Garrison thus

$$C = Cm + 4/\pi \cdot s/D \cdot Cd \qquad\qquad 2.15$$

$$\text{or} \qquad C = F/\tfrac{1}{4}\pi\rho D^2 Cd$$

This is due to the presence of a "drag crisis" in accelerating flows.

The value of C, is derived from Morison's equation by non dimensionalising the force with $\tfrac{1}{4}\pi\rho D^2 \delta u/\delta t$ and taking $s = \tfrac{1}{2}\rho t^2 \delta u/\delta t$.

In this thesis the horizontal force was non dimensionalised with $\tfrac{1}{2}\rho D u^2$, since the level of confidence in u was greater than with $\delta u/\delta t$.

When Reynolds number lies between 1 and 50 the entire flow is steady and laminar. For 50<Re<200 the flow retains its laminar character but the near wake becomes unstable and oscillates periodically. At higher Re<1500, turbulence spreads downstream. For $1500 < Re < 2*10^5$ the transition and turbulence gradually move upstream along the free shear layers, the far wake becoming increasingly irregular.

In this thesis $2,800 \le Re \le 26,000$, taking the fluid/ structure interaction into a transition region between drag and inertia dominated regimes.

When transition coincides with the separation point (Re approximately $5*10^5$) the flow undergoes first a laminar separation, followed by a reattachment to the cylinder and then a turbulent separation to form a narrower wake. This causes a large fall in both lift and drag coefficient, termed the drag or resistance crisis.

Sarpkaya and Garrison obtained good correlation between C and s/D justifying there exclusion of Reynolds number from theoretical consideration for the range encountered. (figure 2.14).

$$C = 4F/(\rho \pi D^2 du/dt)$$
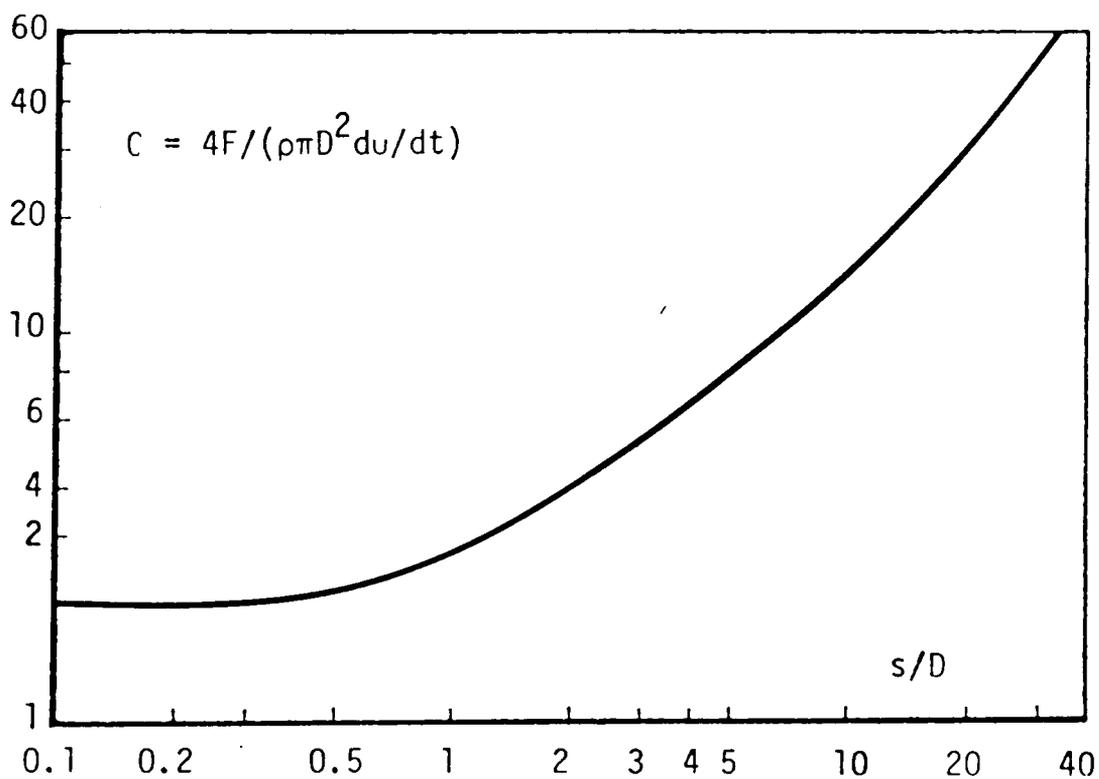
Figure 2.14 - Total force coefficient with relative displacement

(After Sarpkaya and Garrison)

The solitary wave may be characterised as an unsteady motion accelerated from rest.

Kulin (1958) carried out an experimental program investigating wave forces generated on submerged cylinders and plates subject to a solitary wave.

He concludes that in the case of an unsteady motion started from rest, the Reynolds number alone may be insufficient to describe the state of vortex development, at least during the first instants of motion. Enough motion must occur to supply the separated boundary layers which eventually form the vortices.

This leads to Kulin considering the relative displacement of the fluid past the cylinder, very much as Sarpkaya and Garrison (1963).

He reproduces pictures of flow around one of the larger cylinders he tested under a low wave and of a smaller cylinder subjected to a large wave.

Figure 2.15 shows that he found Cd rising to a peak value at s/D=2.5, the subsequent downward trend of the curve being associated with the substantial growth of a symmetrical pair of vortices.

At high s/D (>8), Cd appears to be somewhat greater than the usually accepted steady-state values at corresponding Reynolds number.

Kulin calculates Cd from simultaneous Morison's equations either side of the wave crest, such that Cd(x)=Cd(-x) and Cm(x)=Cm(-x). This method is discussed in this thesis (section 7.1.10 pp 282) and is generally discredited since there is no distinction between accelerating and decelerating flows. This is not discussed by Kulin.

Kulin concludes, somewhat speculatively, that Cd may be considered a constant provided that

- the total fluid motion is large with respect to the cylinder diameter i.e. drag dominated regime

- the extreme beginning and end regions of the wave motion are are excluded from consideration.
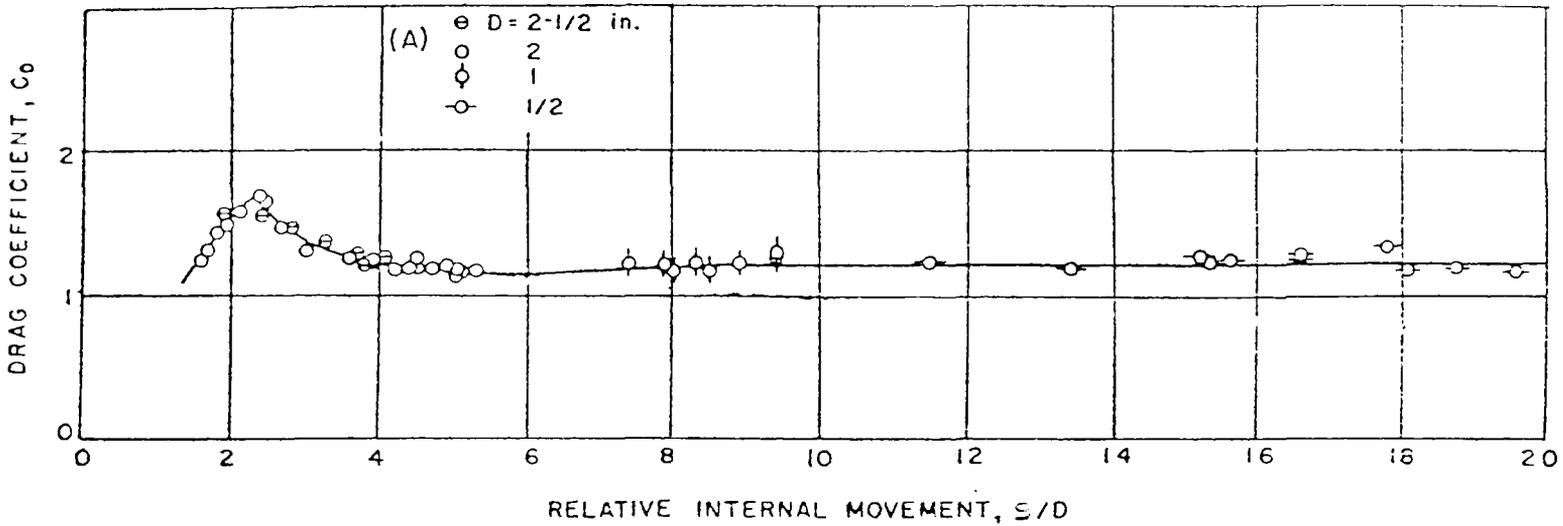
Figure 2.15 - Drag Coefficient with relative displacement
(After Kulin)

It would seem that Kulin, by excluding the extremes of wave motion, is attempting to reduce the solitary wave to a uni-directional flow whose solitary wave acceleration changes at a uniform rate.i.e between the peak and trough in the acceleration trace. This would minimise the effect of calculating the drag coefficient as $Cd(x)=Cd(-x)$.

2.3.3 Oscillating Flow

The natural extension to the study of forces in unidirectional accelerating flows is to examine those in periodic flows. In these the ambient fluid velocity continuously changes in magnitude and periodically reverse in direction.

The first work of significance is by Keulegan and Carpenter (1958). They performed tests using horizontal cylinders suspended, axis normal to the flow, under a node of a standing wave, halfway between the surface and wave tank bed. This arrangement provided a sinusoidally oscillating horizontal velocity and a small vertical component of fluid oscillation always less than 6% of the magnitude of the horizontal fluctuation. Measurement of the in-line forces on the cylinder for a variety of waves produced records of the oscillating force and observations of the flow structure around the body using dye yielding information on the wake.

Dimensionless analysis by Keulegan and Carpenter revealed three non dimensional groups which might correlate with the force coefficient.

$$F/_{\rho u^2_{max} D} = f(t/_T, u_{max}D/ , u_{max}T/_D) \qquad 2.16$$

The first term indicated the time dependance of the force; the second was Reynolds number based on maximum fluid velocity; the third was termed the period parameter discussed earlier.

For the restricted case of oscillatory flow it can be assumed that the force per unit length on a cylinder may be expressed as a Fourier series in terms of the phase angle. Comparing with Morison's equation showed that Cd and Cm may each be expressed as a series, the first term being a constant.

$$Cm(\Theta) = \frac{2u_m T}{\pi^2 D}[A1 + A3 + A5 + 2(A3+A5)\cos2\Theta + 2A5\cos4\Theta....] \qquad 2.17$$

$$Cd(\Theta) = 2B1' + 2/|\cos\Theta|[2(B3'+B5') + 4(B5'+B3')\cos3\Theta - 4B5'\cos4\Theta..]$$

By this method the non dimensional force is expressed as Morison's equation plus a remainder function. Analysis of this function allows the variation of Cd and Cm with phase to be calculated.

To examine the form of this remainder function Keulegan and Carpenter performed an experimental investigation described previously.

The variation of A3, A5, B3 and B5 with Nkc is by no means insignificant at low Nkc. At Nkc=15.6, Cd and Cm oscillate corresponding to the formation of a single eddy per half period, giving a substantial lift force. Detailed examination of Keulegan and Carpenter's results suggest that the most important contributing factor is that the peak drag force is out of phase with the peak velocity which leads it. This is because the eddy contributing to this force takes time to separate, this time being a significant proportion of the quarter period. The acceleration component falls through zero at peak velocity and is the only

available term to accommodate this phase lag. Consequently the instantaneous value of Cm is large and negative. Thus a suitable method of accommodating this phase lag may allow Cm to remain constant value 2.

The graphs of Cd and Cm against the Keulegan Carpenter number or period parameter, are shown in figure 2.16.

The smooth curve suggested by Keulegan and Carpenter may be replaced by a more realistic family of curves. Above Nkc=25 there remains a strong dependance on diameter. This may be non dimensionalized as ß=D²/T called the frequency parameter by Sarpkaya.

Cd depends both on Nkc and Re, and decreases with increasing Re for a given Nkc. Cm depends on both Nkc and Re for Nkc larger than approximately 15 and decreases with increasing Re.
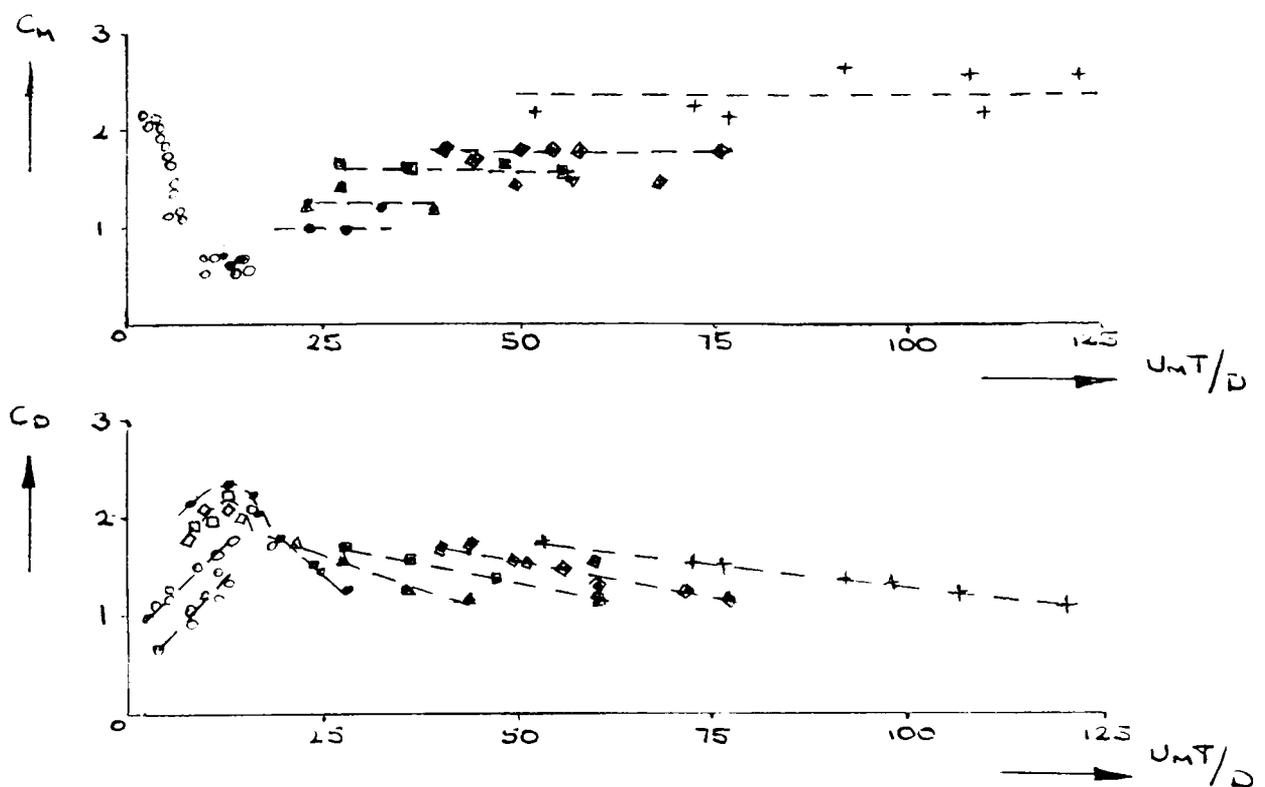
Figure 2.16 - Variation of Cd and Cm with Nkc

(After Keulegan and Carpenter)

A similar analysis of Sarpkaya's data (1975) also shows that Cd and Cm depend on both Re and Nkc and that Cm increases with increasing Re.

This inconsistency in results remains unexplained but may be due to the inability of the analyses to match the fluid structure interaction, forcing the coefficients to change accordingly.

In work by Bearman, Chaplin, Graham, Kostense, Hall and Klopman (1985) they find that Morison's equation fails to fit horizontal cylinder force data, primarily due to the presence of a strong vortex shedding component.

They carried out large scale tests and consequently achieved a maximum Reynolds number of about $5.5*10^5$ and a maximum Keulegan Carpenter number of about 20.

Drag and inertia coefficients were computed from the horizontal cylinder measurements on the basis of a vector form of Morison's equation. They were obtained by minimising the difference between the measured force vector and that derived from Morison's equation. The drag and inertia loads were considered to be in-line respectively with the instantaneous velocity and acceleration vectors. With a least squares analysis, summations were taken over all samples in a wave period. The absence of any representation of a periodic vortex shedding force in the method they used made the computed results less stable than the drag and inertia coefficients evaluated from in-line force measurements on vertical cylinders they tested.

Their results (figure 2.17) show considerable scatter arising from small changes in flow conditions. The drag coefficient has minimum values at Nkc=5.1 and Nkc=15, suggesting the influence of periodic vortex shedding at multiples of the wave frequency.

They conclude that the changes in Cd are influenced by the phase rather than the magnitude of the total force.
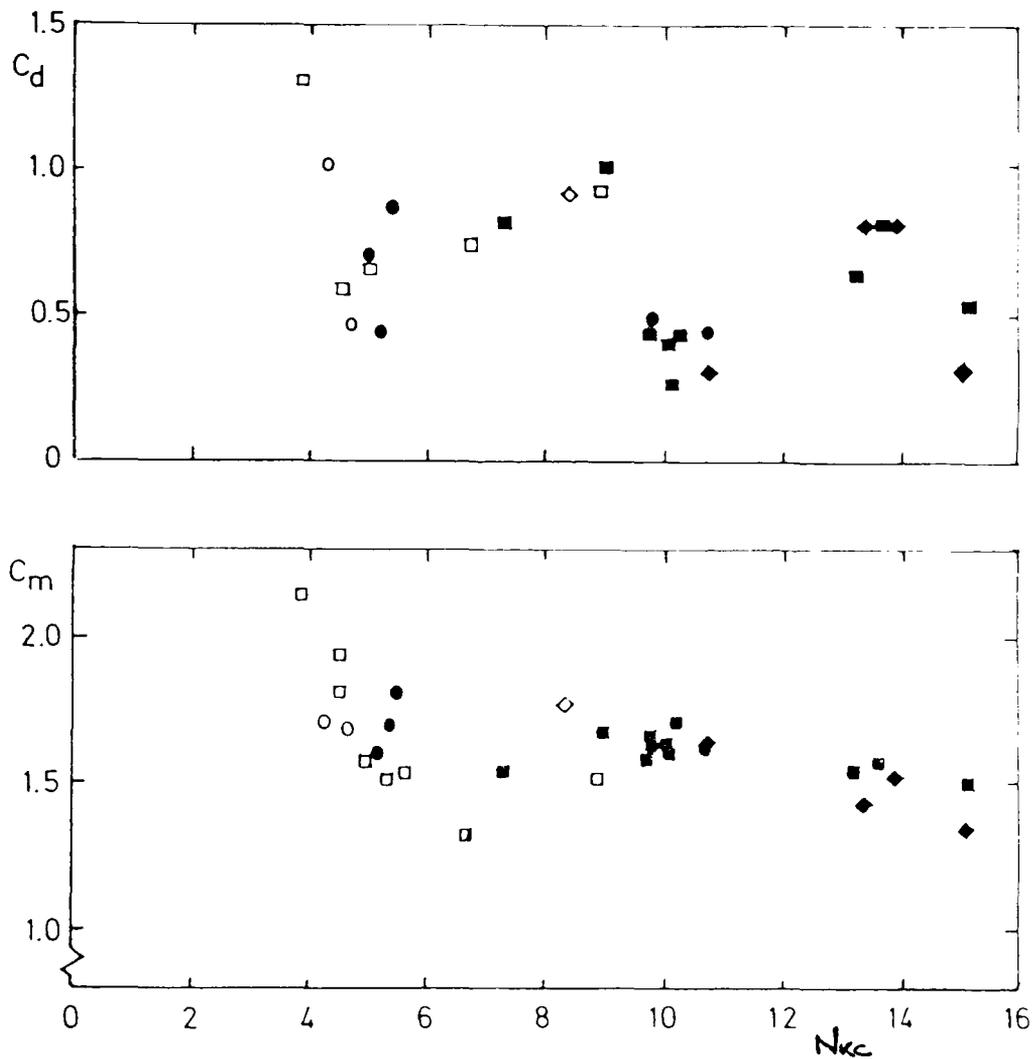
Figure 2.17 - Least squares drag and inertia coefficients in regular waves (After Bearman et.al.)

Teng & Nath (1985) carried out experiments on a horizontal cylinder in waves and under waves whilst being towed. They also reached Reynolds numbers of up to $5*10^5$. As Bearman et.al., Teng and Nath determined Cd and Cm using a least squares formulation minimising the error between measured and calculated forces from a vector form of Morison's equation.

Their results for Cd and Cm versus Reynolds number show some scatter. As Bearman, they conclude that this is primarily due to the absence of a term for the vortex shedding effect. However they also suggest that the actual particle kinematics were different from those predicted by the stream function analysis they used to determine velocities. This alone may cause considerable scatter of results as fluid velocities are squared in Morison's equation.

By comparing their results with those of other experimenters, they found that the presence of a vertical velocity component reduces the drag coefficient. Consequently the force coefficients, Cd and Cm, for a horizontal cylinder in waves are smaller than those for a vertical cylinder.

Chaplin (1984) measured forces on a submerged horizontal cylinder subjected to deep water waves. Experiments were performed for Nkc<3. Chaplin found that the oscillatory loading on the cylinder may be as much as 50% less than that predicted by linear theory. He puts this down a dominant nonlinear contribution to the loading being proportional to the cube of the Keulegan-Carpenter number.

He also finds that on passing over the cylinder, the waves underwent a phase shift and gained new frequency components.

A Fourier analysis of the wave records revealed higher frequency components generated by interaction with the cylinder. For steeper waves the component at frequency 2ω was about 5 times the value of the corresponding component of the incident waves.

2.3.4 Summary

The present study was undertaken as a continuation of the investigation of wave forces on submerged objects. This was by considering the effect of a single disturbance offering both accelerated and decelerated motion which was essentially uni-directional.

To this end, work summarised in this section (2.3) serve only as an indication of areas that may be usefully researched and factors that required consideration in the thesis.

CHAPTER 3   THEORETICAL CONSIDERATIONS

3.1 Introduction

Chapter two provides a critical description of previous studies both on the solitary wave and loads on cylinders. The chapter outlines the nature of loads on cylinders in flow that may be generally categorised as unsteady. These flows may be generated by the action of progressive surface waves, the oscillation of fluid in a "U" tube, or by some other means. The concept of drag and inertia force components has been introduced and the methods of evaluating empirical estimates of force coefficients have been demonstrated.

This chapter will synthesise the theories associated with the solitary wave as used in this investigation, so that they may be verified or otherwise by experiment. Analysis of the problem of wave loading on a cylinder orientated horizontally will be introduced. The chapter will also deal with the calculation of forces on structures. This involves two stages of analysis, firstly the analysis of the wave environment used to determine the velocities and accelerations. Secondly the relation of this wave environment to forces via Morison's equation. This procedure involves one very basic assumption, that the structure does not have any effect on the waves. This shall be discussed more fully later.

3.2 Solitary Wave Theory

Various theoretical analyses have been investigated in chapter two. Results from these have been compared for solitary waves up to breaking but none have been used as a basis for the calculation of forces on horizontal cylinders. The following

sub-sections verify the calculation of wave parameters so that they may be compared to those measured and subsequently used in the calculation of forces.

3.2.1 General Theory

It has been thought by some that the solitary wave is included in the general theory of long waves. This is only true to a very rough approximation. The celerity of the wave does not agree closely with that of long waves nor does the wave profile gradually increase in steepness at its front as the long wave does. The change which does take place in the profile of the solitary wave is simply a reduction of height and consequent increase in length such as might be caused by the dissipation of its energy by friction,etc..

3.2.2 Analysis by McCowan (1891)

It is assumed in general theory that the wave moves with constant amplitude, it not varying with distance and that the motion is 2-dimensional. Within the scope of the experiments performed, these assumptions are not unreasonable since the test section is short and the effects within the length will do little to change the wave characteristics. (Results given in chapter 6 verify this.) The fluid motion may be considered two dimensional since waves are propagated in a long smooth sided horizontal channel, the results showing no evidence of 3-dimensional flow.

The wave motion may be reduced to steady motion by impressing a velocity equal and opposite to that of the wave celerity, c, by assuming the wave does not vary with distance.

The motion is essentially irrotational the wave being propagated into incompressible liquid at rest.

Thus in complex form the stream function is

$$\psi + i\Phi \qquad\qquad 3.1$$

being a function of z+ix, where x=0 at $\eta = y_o + a$.

At a large distance from the wave crest the liquid will practically be at rest. Therefore in the corresponding steady motion it will be flowing uniformly, thus for the steady motion it is convenient to take

$$\psi + i\Phi = -c(z+ix) + f(z+ix) \qquad\qquad 3.2$$

The form of unknown function of x and z will be non periodic in x since the motion disappears with $x = +-\infty$. Also it must be finite and continuous in magnitude throughout the fluid, including along the boundary surfaces.

At large distance, practically infinity in both directions from the wave crest, motion must vanish or have a finite value independent of x or z.

Additionally, if the stream function is taken as zero at the bottom of the channel, it must be an odd function.

On this basis McCowan proposed a form of function to the first approximation

$$f(z+ix) = \sum_{i=0}^{i=\infty} a_{2i+1} \tan^{2i+1} \tfrac{1}{2}m(z+ix) \qquad 3.3$$

Expanding the function in terms of half angles, hyperbolic functions and after simplification this expression becomes

$$ca(\sin mz + i.\sinh mx)/(\cosh mx + \cos mz) \qquad 3.4$$

Thus equating terms of equation 3.2 the real part becomes

$$\psi = -cz + ca\sin mz/(\cosh mx + \cos mz) \qquad 3.5$$

the imaginary part

$$\Phi = -cx + ca\sinh mx/(\cosh mx + \cos mz) \qquad 3.6$$

with

$$u = -\delta\psi/\delta z = \delta\Phi/\delta x \qquad 3.7$$

the horizontal particle velocity

$$u=-c+cm\alpha(\cosh mx.\cos mz+1)/(\cosh mx+\cos mz)^2 \qquad 3.8$$

the vertical particle velocity

$$v=cm\alpha.\sinh mx.\sin mz/(\cos mx+\cos mz)^2 \qquad 3.9$$

As vector quantities the resultant velocity component of the fluid particles is

$$q^2=u^2+v^2 \qquad 3.10$$

giving after simplification

$$q^2=u^2\{1+(m^2\alpha^2-2m^2(1+\cos mz.\cosh mx))/(\cos mz+\cosh mx)^2\} \qquad 3.11$$

Expanding and substituting with equation 3.5 this becomes

$$q^2=u^2-2mc(\psi+cz)\cot mz+m^2(\psi+cz)^2(\text{cosec}^2mz-2/m\alpha) \qquad 3.12$$

At the free surface an infinite distance from the wave crest $\psi=-cy_0$, then $\psi+cy_0=c\zeta$.

As before when substituting in equation 3.5, the surface profile becomes

$$\eta = a.\sinh m(y_o + \eta) / (\cos m(y_o + \eta) + \cosh mx) \qquad 3.13$$

This reduces equation to

$$q^2 = c^2(1 - 2m\eta \cot m(y_o + \eta) + m^2\eta^2(\csc^2 m(y_o + \eta) - 2/ma) \qquad 3.14$$

Expanding using Taylor's series neglecting powers of η^3 and beyond

$$q^2 = c^2\{1 - 2m\eta \cot my_o + m^2\eta^2(3\csc^2 my_o - 2/ma)$$

$$-4m^3\eta^3 \csc^2 my_o . \cot my_o) \qquad 3.15$$

This maybe compared term for term with

$$q^2 = u^2 - 2g\eta \qquad 3.16$$

the dynamic free surface condition, giving a wave celerity

$$c^2 = g/m.\tan my_o \qquad 3.17$$

and

$$m\alpha = 2/3 . \sin \ m(y_o + 2a/3) \qquad 3.18$$

with equation

$$a = \alpha . \tan \ \tfrac{1}{2}m(y_o + a) \qquad 3.19$$

$m\alpha$ is essentially positive, which by equation 3.19 shows the wave consists solely of an elevation. There cannot be a wave of depression capable of propagating itself in accordance with the observations of Scott Russell.

An important aspect of the work of McCowan is that the approximation does not give constant pressure over the fluid surface.

The expression for the pressure is determined by substituting equation 3.18 into equation 3.14 giving

$$q^2 = u^2 - 2u^2 m\eta \ \cot my_o + 4u^2 m \ (a - \eta)\eta^2 \cot my_o \cosec^2 my_o \qquad 3.20$$

but for the free surface the condition to be satisfied is equation 3.16 then the pressure defect over the surface becomes

$$\delta p = -4u^2 m^3 (a - \eta)\eta^2 \ \cot my_o . \cosec^2 my_o \qquad 3.21$$

Rearranging equation 3.16

$$m^2 . \cot my_0 = g \qquad\qquad 3.22$$

which when substituting in equation 3.21 gives

$$\delta p = -4m^2 g\eta^2 \rho(a-\eta)\cosec^2 my_0 \qquad\qquad 3.23$$

Plotting in figure 3.1 the pressure defects appears negative, vanishing at the wave crest. The defect remains small over a long distance either side of the wave crest and vanishes at mean level. It peaks at $\eta = 2/3a$ having a value of $-(16/27)g \ m^2 a^3 \cosec^2 my_0$. This pressure distribution is distributed to be least effective and does not invalidate the theory of McCowan.
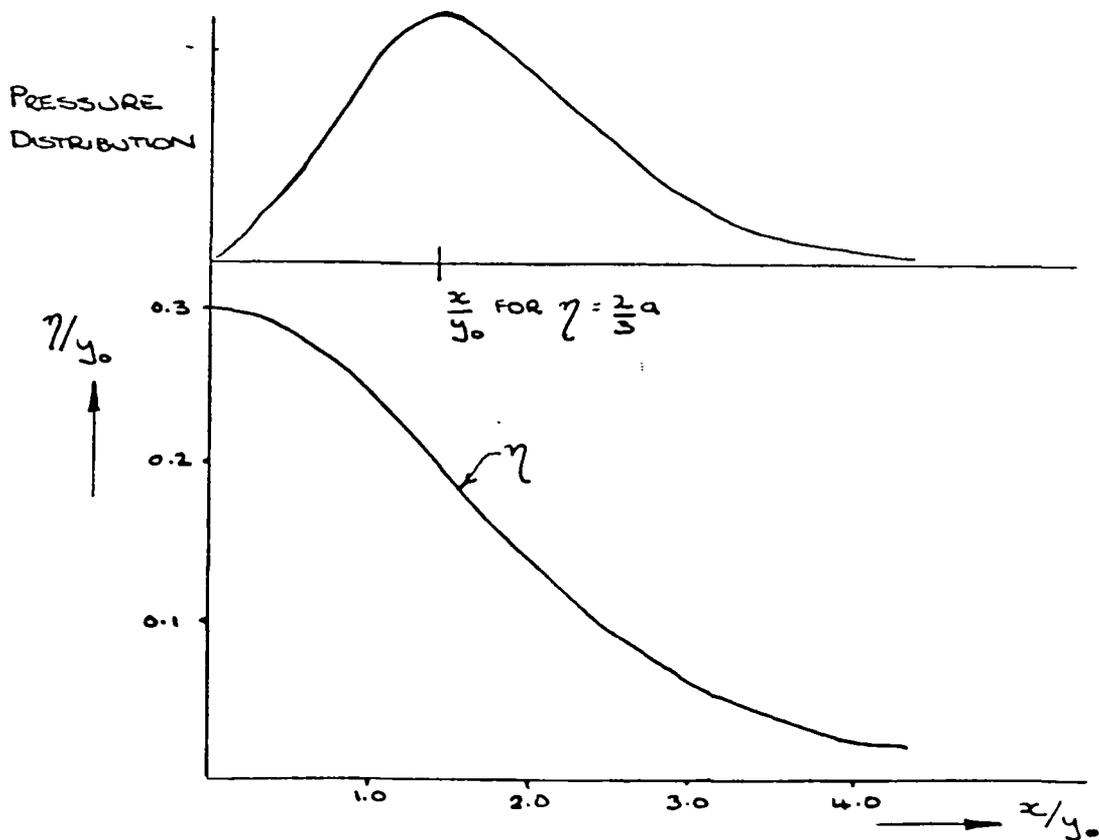
Figure 3.1 - Theoretical pressure distribution

(After McCowan)

Expanding the sine and cosine terms of equation 3.13 and neglecting terms of $m^2y_o^2$ it becomes after simplification

$$\eta = a.\text{sech}^2 \tfrac{1}{2}mx \qquad\qquad 3.24$$

my_o being a small quantity of the first order.

This result was first obtained by Boussinesq and later by Lord Rayleigh.

Using a similar technique with equation 3.18 and 3.19 gives to the first approximation

$$m = \sqrt{(3a/y_o)} \qquad\qquad 3.25$$

Using this in an expansion of equation 3.22 gives to the second approximation

$$c^2 = g(y_o + a) \qquad\qquad 3.26$$

which was obtained by Boussinesq and Rayleigh and originally deduced experimentally by Scott Russell.

Munk (1949) took the results of McCowan and using non-dimensional parameters it was shown that the horizontal and vertical particle velocities become

$$U = N(1 + \cos MZ \cosh MX)/(\cos MZ + \cosh MX)^2 \qquad\qquad 3.27$$

where the non-dimensional parameters M and N are functions of a/y_o. (figure 3.2) and are exactly defined by equations

$$a/y = (N/M)\tan\tfrac{1}{2}[M(1+a/y_o)]$$
      3.29

$$N = (2/3)\sin^2[M(1+2a/3y_o)]$$
      3.30

As the parameter cannot be determined explicitly a method of calculating a first approximation was required.
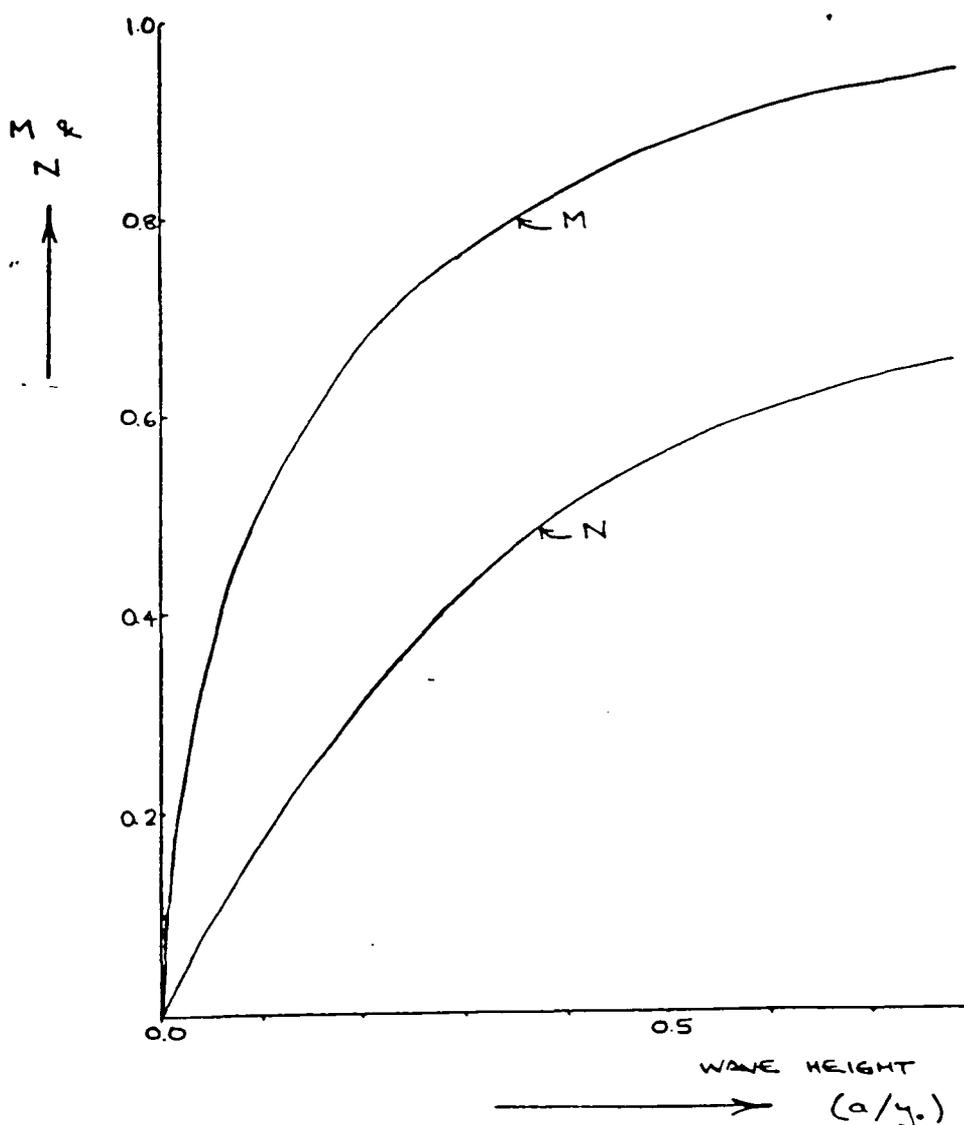
Figure 3.2 - Non-dimensional parameters

(After Munk)

Taking

$$M = (3a/y_o)$$ 3.31

precise values for M and N can be found using a
Newton-Raphson iteration process.

Differentiating equation 3.8

$$\delta u / \delta t = \frac{c^2 m^2 a \sinh mx [2 + \cos mz . \cosh mx - \cos^2 mz]}{(\cos mz + \cosh mx)}$$ 3.32

or after Munk

$$\delta u / \delta t = \frac{c^2 NM . \sinh MX [2 + \cos MY . \cosh MX - \cos^2 MY]}{y_o \ (\cos MY + \cosh MX)}$$ 3.33

with $X = x/y_o$ and $Y = z/y_o$, with m having the dimensions 1/L
and a the dimensions, L.

.

3.2.3 Analysis by Boussinesq (1871)

Boussinesq considered a rectangular horizontal channel of
uniform cross section and infinite length, containing fluid
perfectly at rest. With some external force acting for a short
time, the free surface of the fluid in the channel will deform.
With this force parallel to the direction of the channel and
constant throughout the whole depth of the liquid, the
deformed surface will move with a constant velocity
constituting a translation wave.

The resulting motion of the liquid under the deformed free
surface will be irrotational and possess a velocity potential
thus

$$u = -\delta \Phi / \delta x$$ 3.7

$$w = -\delta\Phi/\delta z \qquad\qquad 3.34$$

where Φ is a $f(x,z,t)$ and satisfy Laplace's equation 2.3. The pressure equation reduces to

$$p/\rho = \delta\Phi/\delta t - gz - \tfrac{1}{2}(u^2 + w^2) + F(t) \qquad\qquad 3.35$$

For a point at infinity on the free surface $F(t)$ can be evaluated, thus obtaining the dynamic surface condition

$$\delta\Phi/\delta t - g\eta - \tfrac{1}{2}(u^2 + w^2) = 0 \qquad\qquad 3.36$$

With a fluid particle of the free surface remaining on the free surface.

$$w = \delta y_o/\delta t + u\delta y_o/\delta x \qquad\qquad 3.37$$

the kinematic surface condition applies.

At the bottom surface of the channel the velocity component normal to the bottom vanishes (z=0)

$$\delta\Phi/\delta z = 0 \qquad\qquad 3.38$$

As this is the case the potential Φ may be assumed a power series expansion of the form

$$\Phi = \sum_{n=0}^{\infty} \Phi_n z^n \ , \Phi = 0$$

where $\Phi_h = f(x,t)$.

Substituting in Laplace's equation $\nabla^2\Phi = 0$ and equating coefficients of z^n to zero term by term, a convergent series is found

$$\Phi = \Phi_0 - z^2\frac{\delta^2\Phi_0}{2!\delta x^2} + z^3\frac{\delta^4\Phi_0}{4!\delta x^4} - z^5\frac{\delta^6\Phi}{6!\delta x^6} + \ldots\ldots \qquad 3.39$$

Differentiating with respect to z,

$$\delta\Phi/\delta z = -z\frac{\delta^2\Phi_0}{\delta x^2} + x^3\frac{\delta^4\Phi_0}{3!\delta x^4} - z^5\frac{\delta^6\Phi_0}{5!\delta x^6} + \ldots \qquad 3.40$$

Retaining the first two terms in Φ and $\delta\Phi/\delta z$

$$\Phi = \Phi_0 + \frac{y_0^2}{z}\frac{\delta^2\Phi_0}{\delta x^2} \qquad 3.41$$

$$\delta\Phi/\delta z = -(\eta + y_0)\frac{\delta^2\Phi_0}{\delta x^2} + \frac{y^3}{6}\frac{\delta^4\Phi_0}{\delta x^4}$$

Differentiating with respect to t and to the first approximation of $\delta\Phi_0/\delta x$.

$$g\eta - \frac{\delta\Phi}{\delta t} + \frac{g}{2}(\eta^2 + y_0^2\frac{\delta^2\eta}{\delta x^2}) = 0 \qquad 3.42$$

and $$\frac{\delta\eta}{\delta t} - y_0\frac{\delta^2\Phi}{\delta x^2} + \sqrt{gy_0}\frac{\delta}{\delta x}(\eta^2 - \frac{y_0^2}{6}\cdot\frac{\delta^2\eta}{\delta x^2}) = 0$$

Eliminating Φ_0

$$\delta^2\eta/\delta t^2 = gy_0\frac{\delta^2\eta}{\delta x^2} + gy_0\frac{\delta^2}{\delta x^2}(\frac{3\eta}{2y_0} + \frac{y_0^2}{3}\frac{\delta\eta}{\delta x}) \qquad 3.43$$

which is the fundamental wave equation to the second approximation in which the effects of the height and curvature of the wave profile are included.

This assumes the liquid in the channel is undisturbed at infinity and that the disturbance changes only slowly in a reference frame moving to the right with speed $\sqrt{gy_o}$.

Korteweg & deVries (1895) derives a more general equivalent which allows for any uniform translation of the reference frame and incorporates surface tension.

$$\delta\eta/\delta t = \frac{3}{2}\sqrt{(g/y_o)}\frac{\delta}{\delta x}((1/2)\eta^2 + (2/3)\alpha\eta + (1/3)\sigma\delta^2\eta/\delta x^2) \qquad 3.44$$

where $\alpha = (1/3)y_o^3 - Ty_o/g$; T= capillary tension at water

surface

In Boussinesq's equation for stationary waves $\delta\eta/\delta t$ must be zero, integrating twice gives

$$\eta = a.\text{sech}^2 x/y_o\sqrt{(3a/4y_o)} \qquad 3.45$$

and also

$$c^2 = gy_o(1+a/y_o) \qquad 3.46$$

3.3 Forces on small submerged bodies

To fully understand and appreciate the complexity of fluid loading in accelerated flows, it is necessary to consider the similarity with steady current forces which are better documented, though this does not imply that there is any greater understanding.

Both fluid velocity and acceleration cause forces on a submerged body. The velocity dependent force, the drag force, is exactly analogous to the drag force in steady currents and is taken to be proportional to the velocity squared.

The acceleration dependent force, the inertia force, is similar to the usual body "force=mass*acceleration" and is thus proportional to acceleration. It is perhaps easiest to use an analogy with buoyancy. The horizontal force due to the fluid acceleration may be considered a horizontal, continually varying, buoyancy. In ordinary buoyancy a pressure gradient exists on any body immersed in fluid. The pressure gradient is due to the increasing head of water with depth. It is this pressure gradient over the body which causes the buoyancy force on the body. In wave motion there is a similar pressure gradient, due to the acceleration of the fluid, and this causes a force on the body.

Morison et al. (1952) proposed that the force at any instant of time on a body could be considered to be the instantaneous summation of drag and inertia forces. This assumption was widely accepted as an over simplification. However the formula is adequate under certain conditions.

Considerable research has been performed which attempts to determine when the equation which usefully describes the

forcing accurately and try to determine suitable values of drag and inertia coefficients.

Morison's equation uses terms dependent upon velocities and accelerations. These may be determined from theories as if the body was absent. It must be assumed the body has negligible effect on the waves, otherwise velocities and accelerations calculated as if the body were absent would not be applicable. Consequently Morison's equation may be applied to cases where the body is small compared with the wavelength.

The choice of suitable coefficients is possibly the most complex problem in the use of Morison's equation. There is a proliferation of data on coefficients obtained from both laboratory studies and in the ocean. They show a very large scatter particularly in Cd.

Additional information may be gleaned on the values of the force coefficient by studying the accelerated flow beneath the solitary wave with a ratio of vertical to horizontal fluid velocity remaining small for all waves.

3.3.1 Drag Forces

The development of a wake behind the horizontal cylinder will lead to a drag force. For a cylinder in a steady flow this wake forms behind the cylinder on the side diametrically opposite the direction of the oncoming flow. An oscillatory flow is generally described as a rotation velocity vector moving clockwise about the centre of the body. The magnitude of the velocity vector under the wave being a maximum when the velocity is horizontal in the direction of wave propagation, and a minimum when the vector points vertically upwards or downwards.

As a result, one might expect the wake to rotate about the cylinder in phase with the velocity vector. For flows with v/u=1.0 (corresponding to deep water waves where the velocity vector is constant magnitude) the wake, once established, will rotate with a velocity vector, leading to a constant drag force on the cylinder.

For flows where the value of v/u is less than unity (corresponding to intermediate and shallow water waves) the magnitude of the velocity vector is continuously varying as it rotates. In this case the drag force will vary in phase with the velocity vector, the magnitude of the force being maximum at instants of maximum velocity and minimum when the velocity vector is vertically upwards or downwards. When v/u is zero the velocity vector no longer rotates but is always horizontal of continuously varying magnitude. If the drag force does act in phase with the velocity this would produce a stationary drag force vector also of varying magnitude.

Consequently it is possible for both in-line and lift forces to be generated by the motion of the fluid under a wave. This contrasts with previous studies where the velocity vector representing the fluid motion does not rotate in the plane of the cylinder. This is because the majority of investigations have been on vertical cylinders. For these, forces generated perpendicular to the axis of the cylinder are only likely to be produced by the action of asymmetric vortex growth or the influence of free vortices shed from the body in previous cycles, since inertia and drag forces will not have components which act in the lift force direction.

3.3.2 Inertia Force

The inertia force on a body is made up of two components

1) since the fluid in the wave is accelerating there must be a force field to cause the acceleration, the force being expressed in terms of the fluid mass. A body in the force field will experience a force which may itself be expressed in terms of the mass it displaces.

2) The fluid in the wave must move round the object, thus additional accelerations related to the curvature of the flow develop forces on the body.

The latter component of the force is determined by the form of the wake. Both components of the inertia are 1* Vu, thus the total force on the body in an ideal flow will be 2* Vu. Assuming the form taken by Morison, Cm=2, which should apply at very low flow velocities. As fluid velocities increase eddies form and subsequently separate from the cylinder. With this separation the flow no longer travels all the way to the rear of the cylinder and Cm will be reduced. With longer wakes more disturbance downstream causes Cm to increase. Therefore one would expect the minimum value of the inertia coefficient to occur when eddies are just shed from the cylinder.

3.3.3 Dimensional Analysis

In the first instance consider a time dependent fluid oscillation which may be described as

$$u = u_m f_1(t)$$

<div align="right">3.47</div>

$$v = v_m f_2(t)$$

where u and v are instantaneous components of horizontal and vertical fluid velocity; u_m and v_m are characteristic maximum velocity amplitude; f_1 and f_2 are functions of time indicating the temporal variation of velocity. The force per unit length on a cylinder immersed in such a flow may be expressed in general terms as :-

$$F/l = f_3(\rho, \mu, D, u_m, v_m, T, t) \qquad 3.48$$

where F is the instantaneous force on the cylinder of diameter D, length l, which is rigidly supported in fluid density ρ, viscosity μ and period of oscillation T. t represents the time measured within a particular oscillation.

For cylinders held rigidly beneath a free surface wave, the values u_m and v_m are dependent on the gross wave parameters, so that

$$u_m, v_m = f_4(g, T, H, h, z) \qquad 3.49$$

To obtain an expression for the force on a cylinder subject to a wave which is generated in a wave tank, and therefore

subjected to constraints due to the apparatus, substitute for u_m and v_m so that

$$F/l=f_5(\rho,\mu,D,u_m,v_m,du/dt,T,t,g,L,h,z_c) \qquad 3.50$$

where L is the wavelength.

Dimensional analysis relates the force coefficients, C_t to the variables

$$C_t=F/(\tfrac{1}{2}\rho u_m^2 Dl) \qquad 3.51$$

$$C_t =f_6(D(du/dt)/u_m^2,vt/D,\rho u_m D/\mu,t/T,z_c/y_o,$$
$$v_m/u_m,y_o/L,D/y_o,u_m^2/g(z_c-D/2))$$

$$3.52$$

This represents the full collection of dimensionless groups required to describe the forces on a cylinder subjected to a periodic motion generated by the passage of a progressive wave. These dimensionless groups may be reduced by those not necessary in the experiments described here.

As the solitary wave is translatory, the period T is infinite as is the wavelength. Consequently

$$t/T \to 0 \; ; \; h/L \to 0$$

Groups z/y_o and d/y_o indicate the clearance of the centre of the cylinder from the channel bed and the diameter of the cylinder compared to the water depth, respectively. Together they may be seen as characterising the clearance of the underside of the cylinder from the channel bed in terms of the cylinder diameter, more conveniently denoted e/D. This may be

disregarded when the cylinder is in the body of the fluid i.e. $e/D \geq 2$.

For horizontal cylinders beneath waves $u_m\sqrt{(z_c - D/2)g}$, a form of Froude number indicates the influence of the body on the wave. Results presented later show the cylinder has negligible effects on the wave profile; so

$$u_m\sqrt{(z_c - D/2)g} \rightarrow 0$$

Within the body of the fluid v_m is small compared to u_m, therefore v_m/u_m and may be considered as

$$v_m/u_m \rightarrow 0$$

For this investigation.

$$F/(\tfrac{1}{2}\rho u_m^2 Dl) = C_t \qquad\qquad 3.53$$

$$= f_6(u_m t/D, \rho u_m D/\mu, D(du/dt)/u_m^2)$$

The coefficient C_t can be considered a total coefficient embodying drag and inertia effects.

Alternatively it may be considered to represent a drag component only, by recombining variables it becomes

$$F/(\rho D^2 du/dt) = Cm \qquad\qquad 3.54$$

$$= f_7(u_m t/D, \rho u_m D/\mu, D(du/dt)/u_m^2)$$

- 86 -

Consequently the resistance coefficients are in general functions of a Reynolds number; an acceleration parameter $D.(du/dt)u_m^2$ often referred to as Iverson's number and a parameter ut/D.

In the case of an unsteady motion started from rest, the Re alone may be insufficient to describe the state of vortex development, at least during the first instants of motion. Enough motion must occur to supply the separated boundary layers, or vorticity sheets, which eventually form the vortices.

As an integral ut/D can be related to the distance of fluid moves past the object, s. As a wave passes over the cylinder, vortices will form and begin to grow as s/D increases, provided that the velocity is sufficiently large to permit separation. As s/D increases, the initial vortices will shed and be replaced with additional ones assuming that the rate of vortex formation is large enough for shedding to be necessary, indeed s/D may reach such a value that a fully developed Karmen trail is formed.

3.3.4 Stream Function Analysis

A stream function analysis may be used to calculate fluid velocities and accelerations. These can then be used in the calculation of forces on submerged cylinders.

Dean (1965) developed a direct numerical technique for the calculation of the free surface of a nonlinear gravity wave.

He identified the problem as one of determining an analytic function which represented water wave motion in a mathematical form of a boundary value problem. He proposed a nonlinear stream function expression implicitly defining it at the predicted water surface by setting $y = \eta$.

Using a numerical perturbation procedure the unknown parameters in the expression could be determined to provide a least squares best fit to a measured profile. Unless the boundary conditions at the free surface are exactly satisfied the representation would be inaccurate. Indeed any discrepancies would be magnified in the calculation of fluid velocities, accelerations and ultimately forces.

As is usual, Dean considered the motion irrotational and the fluid incompressible. The wave system was represented by either the stream function, ψ or velocity potential, Φ, each of which must satisfy Laplace's equation throughout the interior of the fluid.

Dean considered a stream function of the form:

$$(x,z)=(\tfrac{L}{T}-Uc)y+\sum_{n=4,6,8\ldots}^{N-1} \sinh(n-2)\tfrac{\pi}{L}(y_0+y).\qquad 3.55$$

$$[X(n)\cos(n-2)\tfrac{\pi}{L}x+X(n+1)\sin(n-2)\tfrac{\pi}{L}x]$$

giving a free surface of:

$$\eta = \frac{(x,\psi)}{[(L/T)-Uc]} - \frac{1}{[(L/T)-Uc]} .$$

$$\sum_{n=4,6,8\ldots}^{N-1} \sinh(n-2)\tfrac{\pi}{L}(y_0+\eta).[X(n)\cos(n-2)\tfrac{\pi}{L}x+$$

$$X(n+1)\sin(n-2)\tfrac{\pi}{L}x]\qquad\qquad 3.56$$

The parameters in the stream function expression are determined so as to provide a best fit to the measured profile.

Differentiation of the stream function gives the fluid velocities and accelerations beneath that wave. These may be used in Morison's equation to calculate forces as shown previously.

A total error is made up of two components, that due to the non uniformity of the Bernoulli constant and that which represents the error component due to deviations between the measured and calculated water profiles. A Lagrange multiplier provides the relative weight to the error components. An approximate initial solution is determined by minimizing the measured free surface by direct least squares.

Dean applied the numerical solution to nonlinear periodic waves. By definition a solitary wave is entirely above the mean water surface, having an infinite wavelength and period. An exact numerical solution using the stream function proposed by Dean which is inherently periodic would seem impossible.

However if the proper weights are associated to the kinematic and dynamic free surface boundary conditions a "best solution" may be proposed.

This "best solution", though providing minimum errors for the free surface boundary conditions, does not necessarily provide all the wave parameters of interest with acceptable accuracy. This was investigated whilst carrying out this research work.

It was found that Dean's Stream Function analysis was unable to accurately match the solitary wave profile. Increasing the weighting coefficient to diminish the error between the measured and predicted free surface profiles improved accuracy but failed to improve the accuracy of the predicted fluid velocity profile. Fluid velocities were compared to those measured using a Hot Film Anemometer.

It was concluded that Dean's Stream Function was not able to model the solitary wave to sufficient accuracy for use in this study. This was because it was inherently periodic and with a weighting which gave a "best" fit, was unable to give fluid velocities and accelerations to acceptable accuracy.

It was felt that if Dean's series was modified to include a 'tanh' term (which was successfully used in McCowan's theory) then it would be more accurate and possibly enable its use in the calculation of forces on submerged cylinders. This was beyond the scope of this thesis but is recommended for further investigation.

3.4 Summary

Chapters 6 and 7 will investigate the correlation of experimentally derived results using the parameters given here with a view to establishing dependencies between force coefficients and wave characteristics.

Measurements are verified against the following theories:

Fluid profile   against   **Boussinesq's theory**

$$\eta = a.\mathrm{sech}^2 x/y_o \sqrt{(3a/y_o)} \qquad\qquad 3.45$$

Wave attenuation   against   **Keulegan's theory**

$$(a_2/y_o)^{-\frac{1}{4}} - (a_1/y_o)^{-\frac{1}{4}} = 1/_{12}(1+2y_o/B)\sqrt{(\ /(g^{\frac{1}{2}}y_o^{\frac{3}{2}}))}x/y_o \qquad 7.1$$

Wave celerity   against   **Boussinesq's theory**

$$c^2 = gy_o(1+a/y_o) \qquad\qquad 3.46$$

Fluid velocities   against   **McCowan's theory (Munk)**

$$U = N(1+\cos MZ.\cosh MX)/(\cos MZ + \cosh MX)^2 \qquad 3.27$$

Forces   against   **Morison's equation**

$$F = \tfrac{1}{2}Cd\rho Du|u| + \tfrac{1}{4}Cm\rho\pi D^2\ddot{u} \qquad\qquad 5.1$$

The total force coefficient, C_t is defined as:

$$C_t = F/(\tfrac{1}{2}\rho u_m^2 Dl) \qquad\qquad 3.53$$

CHAPTER4   APPARATUS AND EXPERIMENTAL TECHNIQUE

4.1 Introduction

The experimental study is described in two main parts. The
first contains a description of the apparatus and experimental
techniques used to calibrate the Hot Film Anemometer immediately
prior to the passage of a solitary wave. The second describes
the apparatus and techniques used to investigate loads a solitary
wave imposed on circular cylinders, held rigid, horizontal and
perpendicular to the channel wall at three elevations below the
free surface.

4.2 Wave Measurement

4.2.1 The wave tank

Experiments were conducted in a glass sided wave flume sealed
at both ends to prevent the loss or ingress of water. The
channel was approximately 20 metres long, 300 mm wide with still
water depths varying between approximately 160 and 190 mm.
(Figure 4.1) The channel could be tilted but was used
horizontally in this series of experiments (+-0.003 degrees).

Solitary waves were generated by the manual translation of a
board, (figure 4.2) standing upright at the one end of the
channel. This was adapted from a method used successfully by
Daily and Stephen at M.I.T. in 1952.

The advantage of this method was that the motion was infinitely variable and required no control and feedback equipment.
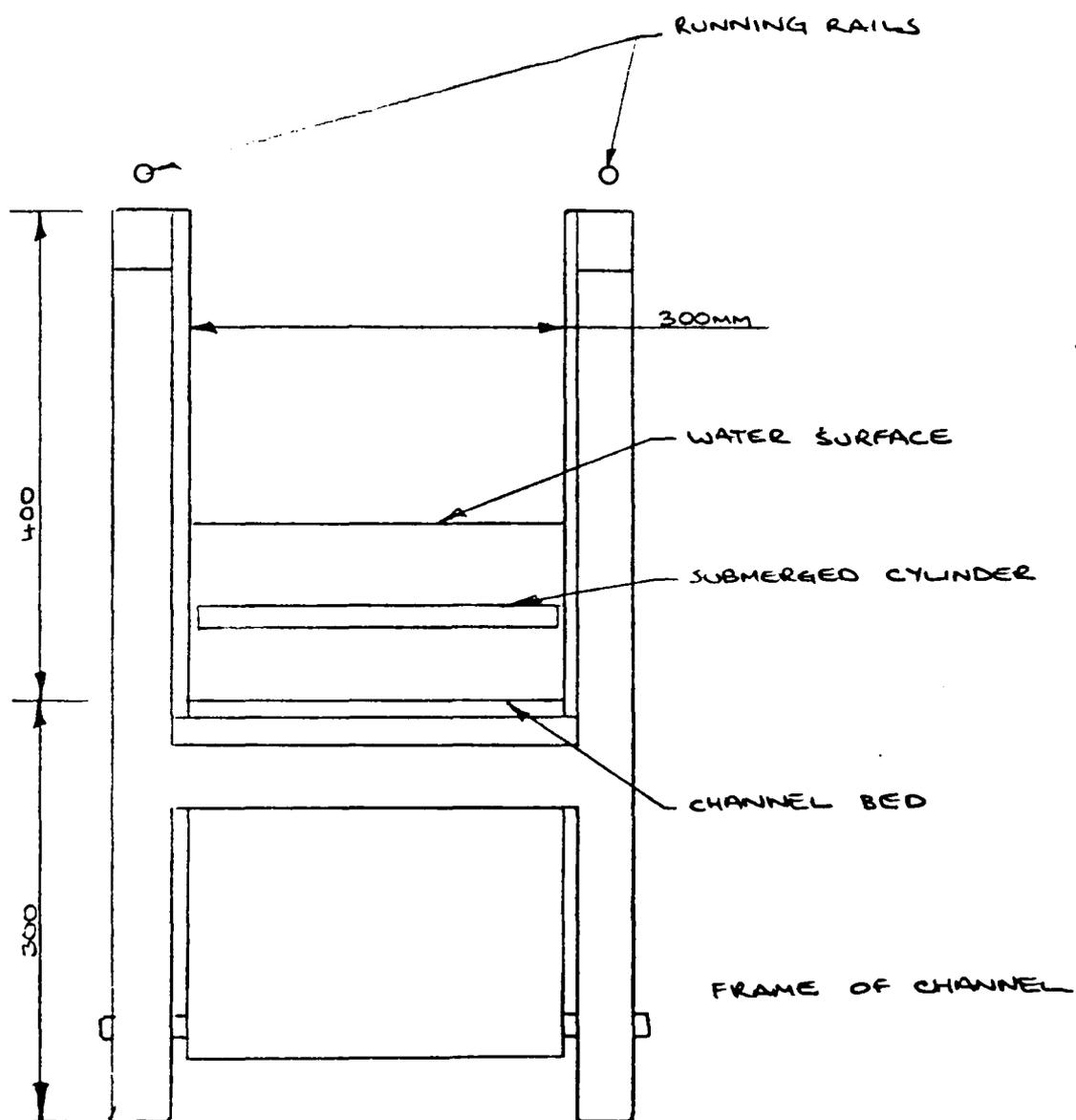
Figure 4.1 - Cross Section through channel
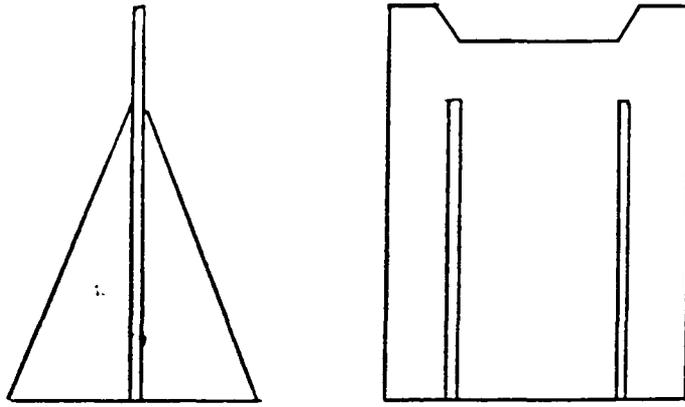
Figure 4.2 - The wave generator

No vibrations were transmitted through the channel walls to the semi-conductor strain gauges mounted on the submerged cylinder. The waves were unique and could not be repeated to an acceptable degree of accuracy. This was unimportant since all wave characteristics were measured accurately as the wave passed through the test section. Wave profiles show this to be an effective method of wave generation (Section 6.2.3).

Other methods have been used by experimenters with similar results (Daily and Stephen; Camfield and Street; Ippen and Kulin; Naheer; Skjelbreia and Raichlen; Longuet Higgins).

As the wave was translatory no reflections reached the test section during the passage of the wave. Though not strictly necessary, a beach was provided to speed the dissipation of energy in the transient disturbances. This reduced the time between tests before the water became still.

The beach was a metre long perspex sheet hinged at its top, extending from the channel bed to approximately 30mm above the undisturbed free surface.

As a wave ran up the beach the crest began to topple. The upper portion of the wave ran over the top of the beach converting its purely horizontal motion to a mixture of vertical and horizontal motion. A portion of the wave was reflected back along the channel.

Though crudely constructed, the beach quickly split the disturbance into numerous smaller ones, dissipating a large amount of energy in the process. The smaller disturbances readily dissipated with surface tension, bed and side friction effects, etc.

The choice of the position of the cylinder, about 8 metres from the wave generator, was made so that the wave attained its final form on reaching the test section. This was confirmed in preliminary experiments.

Most theoretical solutions for the behaviour of the solitary wave are based on the conditions of irrotational two dimensional motion of a liquid satisfying boundary conditions two of which are

1)   The wave form is permanent

2)   The motion vanishes at infinity in both directions.

Waves were generated close to the solitary form. After travelling between 5m - 6m, they ceased to deform perceptibly.

As the wave approaches its permanent form the deformation rate becomes very slow (Keulegan and Patterson, 1940) and may possibly oscillate about a permanent shape. Friction causes continual alterations even after the stable form has been attained. However, should the wave profile oscillate, frictional damping would ultimately eliminate these. Consequently, if the rate of loss of amplitude is near that expected from friction, the wave will probably have reached its final form.

4.2.2 Wave height and Profile measurement

Water surface elevation was measured using a purpose built amplifier based on a design from the Hydraulic Research Station, Wallingford.

The probes were twin parallel stainless steel conductor wires (1.5mm diameter) separated at their base (12.5 mm apart) by a thin perspex plate. (Figure 4.3)

The conductance, and hence immersion length, was measured by applying a potential difference between the wires and measuring the current which flowed. The current was proportional to the probe immersion so long as the water conductivity remained constant.

The probe responded to changes in conductivity. If the conductivity of the water changed, the probe calibration also changed. However as the wave probe calibration was "linear", adjusting the energising voltage to obtain the same reading for a given depth of immersion restored calibration.

Calibration was linear to the tolerances applied to this experimental programme. Changes in water conductivity were negligible, with no change in water level between experiments.

The polarisation capacitance at the wire/water surface meant that D.C. voltages and currents could not be used. Consequently, the probe was energised with high frequency alternating voltage.

The wave probe amplifier was extremely reliable, the signal not drifting with time and was easily calibrated over the range of wave heights used.
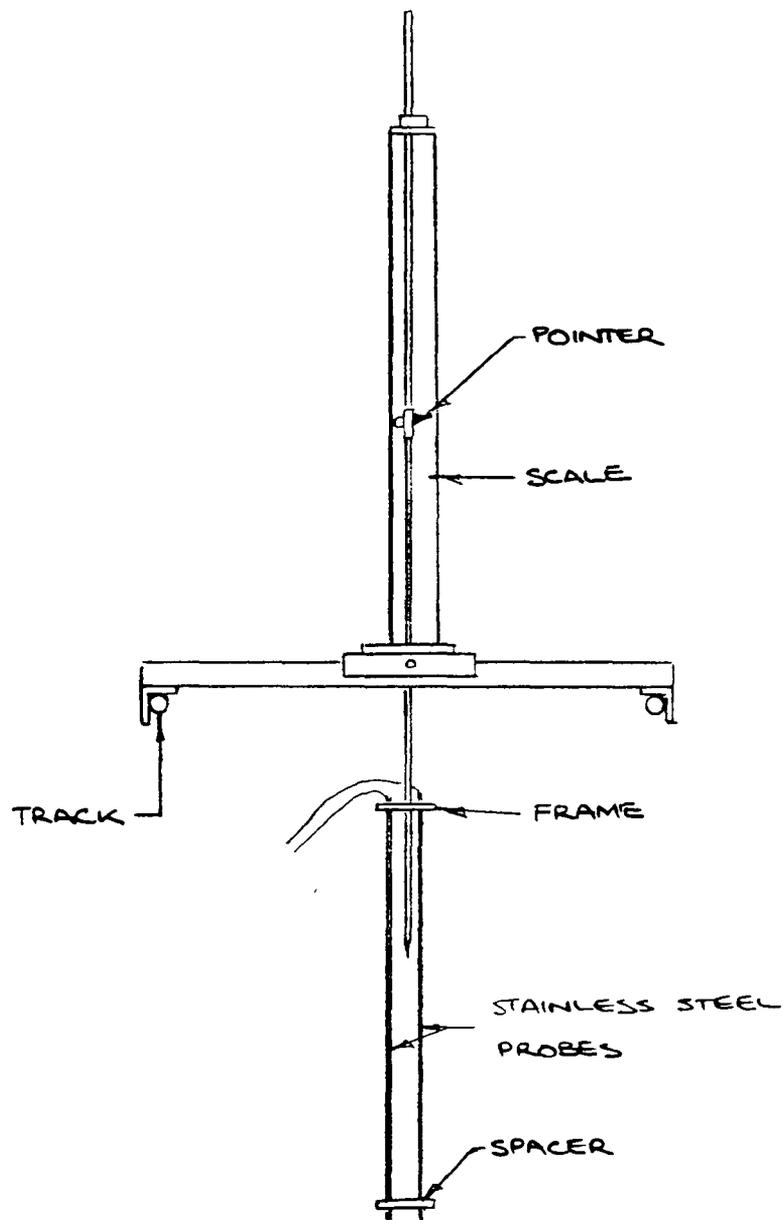
Figure 4.3 - The wave probe

4.2.3 Velocity Measurement

4.2.3.1 Introduction

The calibration of the Hot Film Anemometer (H.F.A) was difficult because of the velocities to be measured in a wave were small and of short duration. The practical problem of generating these velocities in a known and controlled way for the calibration were immense.

Frequently experimenters interpolate between easily determined points or extend a fitted curve from a calibration performed at higher velocities. Both methods are liable to error since the calibration is nonlinear, with maximum sensitivity at low velocities decreasing towards high velocities.

The situation is further complicated since the basic variable is mass flow. With constant density, velocity is measured.

H.F. Anemometry has been used to measure temperature, velocity, mass flow, thermal conductivity, pressure, basic heat transfer and mass fraction because of the many variables that can be sensed. Consequently care must be taken to isolate or control all variables not of interest. Temperature compensation is particularly important when measuring velocity or mass flow.

Consequently the system adopted to calibrate the H.F.A was continuous over the range of velocities to be measured and incorporated a number of checks on the basic calibration.

4.2.3.2. Hot Film Sensor and Anemometer Apparatus

Fluid velocities were measured using a TSI Hot Film Anemometer (1050) with conical Hot Film Sensor (1230W) (figure 4.4). This dual system anemometer incorporated two linearisers, correlators and signal conditioning units, though only the correlator and signal conditioning units were used. The linearisers used either a 4th. or 10th. order polynomial to match the sensor response curve. These were tedious to set up and were liable to error with drift of calibration, thus mathematical linearization using a modified King's Law was performed during analysis of the data.
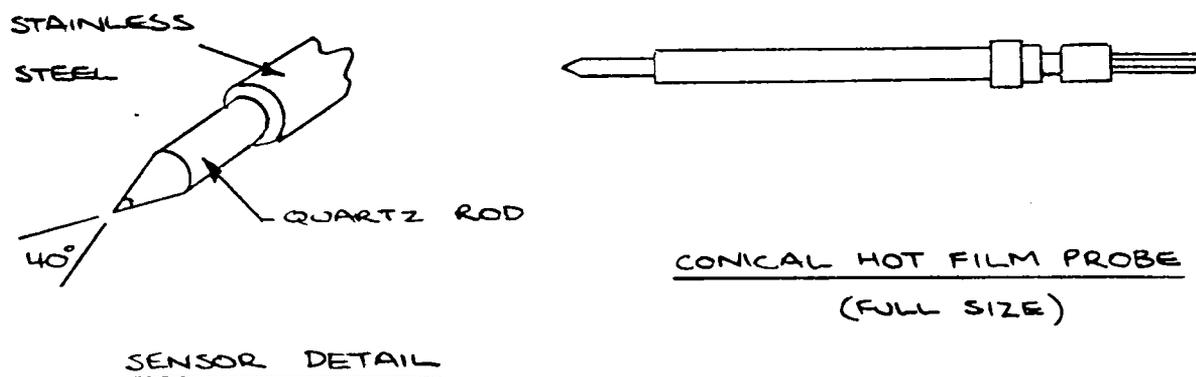
Figure 4.4 - Sensor detail

The Hot Film Sensor is a conducting film on a ceramic substrate, the one used in this series of experiments was of so called "ruggedised" design which reduces effects from water contaminates.

The sensor acted as a small resistance element which was heated and controlled at an elevated temperature. The amount of electrical energy dissipated in the sensor was a measure of the cooling effect of the fluid passing the heated sensor. The rate of cooling depended upon the mass flow and the temperature difference between the sensor and the fluid. The relationship between bridge voltage and mass flow or mass flux was

$$E^2 R / (R + R_3)^2 = A + B (\rho V_f)^{1/n} (t_s - t_e) \qquad 4.1$$

Set to "standby" there was no electrical feedback to the sensor and it was entirely safe to remove it from the water, though this was never done during a series of tests. With the Anemometer set to "Run" the feedback circuit was connected. If removed from the water the heat conduction from the sensor would increase. Consequently the feedback current would instantaneously increase in an attempt to maintain the sensor temperature. This would have burnt out the sensor within a matter of seconds.

With the anemometer turned to "Run" current flows through the Wheatstone bridge. The amplifier senses the out of balance and feeds back more or less current until the bridge comes back into balance. Thus the basic variable measured is the rate of heat transfer from the film to the fluid. As this is not the variable of interest, the bridge voltage versus the velocity of flow must be calibrated.

Assuming that over the period of the experiment the fluid and sensor operating temperatures are constant, equation 4.1 may be written thus

$$E^2 \propto A+B(v)^{1/n} \qquad\qquad 4.2$$

and called the modified King's Law.
Plotting E^2 versus $(v)^{1/n}$ with a suitable value for n gives a straight line.

The stability of this generalised King's Law for the conical sensor was expected since heat transfer from the film was controlled by the boundary layer. For the cone this depended on velocity in a simple manner. However for the modified King's Law to be used velocities must be high enough for forced convection to predominate.

Hot Film sensor orientation has been shown (Zakanycz, Wright and Elrod, 1974) to be important during calibration. Though, since the sensor was calibrated in-situ immediately prior to the passage of a wave, this was not a source of error.

A conical Hot Film sensor is recommended for use in water since it is less susceptible to fouling, is more durable and easier to clean than Hot Wire sensors. The Hot Film itself is platinum because of its oxidation resistance and long term stability.

The Hot Film sensor was mounted on a 90 degree angle section at the end of a 457mm probe support. Rubber rings at connection points prevented water from penetrating.

To prevent vibration of the support arm and sensor, a brass sleeve was fed round the support arm clear of the water surface. This increased rigidity, raising its natural frequency

above that expected from wave induced oscillations without disturbing fluid flow.

This was suspended beneath a trolley along with a wave probe to permit easy calibration (figure 4.5). The trolley was capable of being drawn along the channel with a motion that was recorded by a tachogenerator and potentiometer.
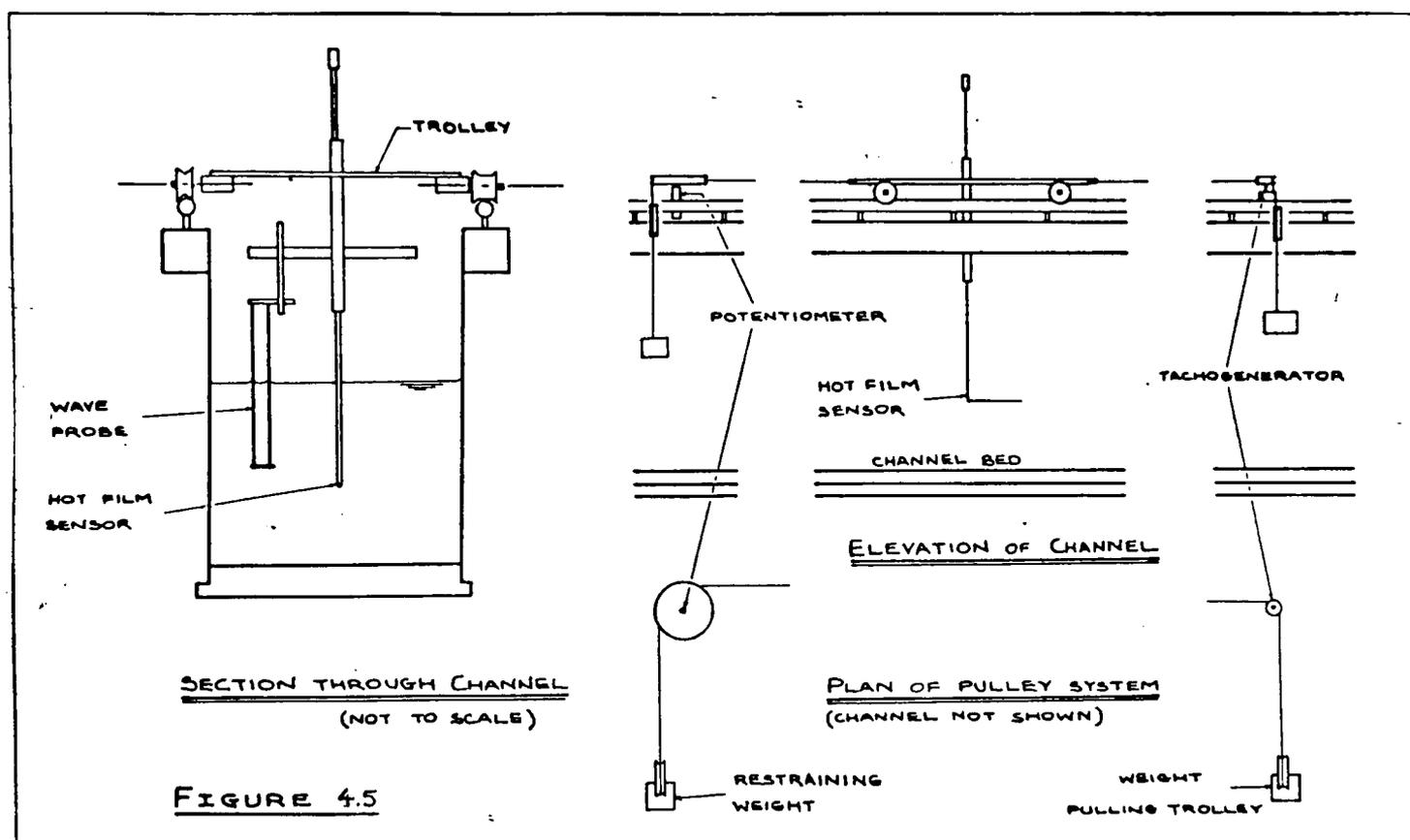
Figure 4.5 - H.F.A, trolley and channel

4.3 Force Measurement

4.3.1. Test cylinder design

Four circular cylinders of external diameters 47.5, 33.5, 27 and 13mm were used in this experimental programme.

The smallest cylinder was a hollow copper pipe. The remainder were hollow UPVC pipes with wall thicknesses varying from 2mm to 5mm for the largest cylinder. A 10mm square section brass bar was prepared, 300mm long to fit inside the UPVC pipes. End caps were turned to fit each cylinder. The three largest end caps were cut so that the 10mm bar fitted into the end caps protruding 1mm beyond one end. The other end of the bar was screw threaded internally to take a brass bolt that fixed the cylinder to the channel wall. (Figure 4.6)

Kyoto semi-conductor strain gauges were selected for their high gauge factors and mounted just inside the end cap on each of the four faces of the brass bar. The two sets of orthogonally mounted strain gauges allowed simultaneous lift and in-line forces to be measured.

Preliminary tests had developed techniques for waterproofing the gauges without damaging them or affecting their performance. Waterproofing was only necessary on the smallest of the four cylinders since the strain gauges had to be mounted externally in this case.

Preliminary tests also demonstrated that drift often associated with this type of strain gauge was minimal after they had been energised for 3 - 4 hours. (figure 4.7) The strain gauge bridge was re-balanced before testing commenced.
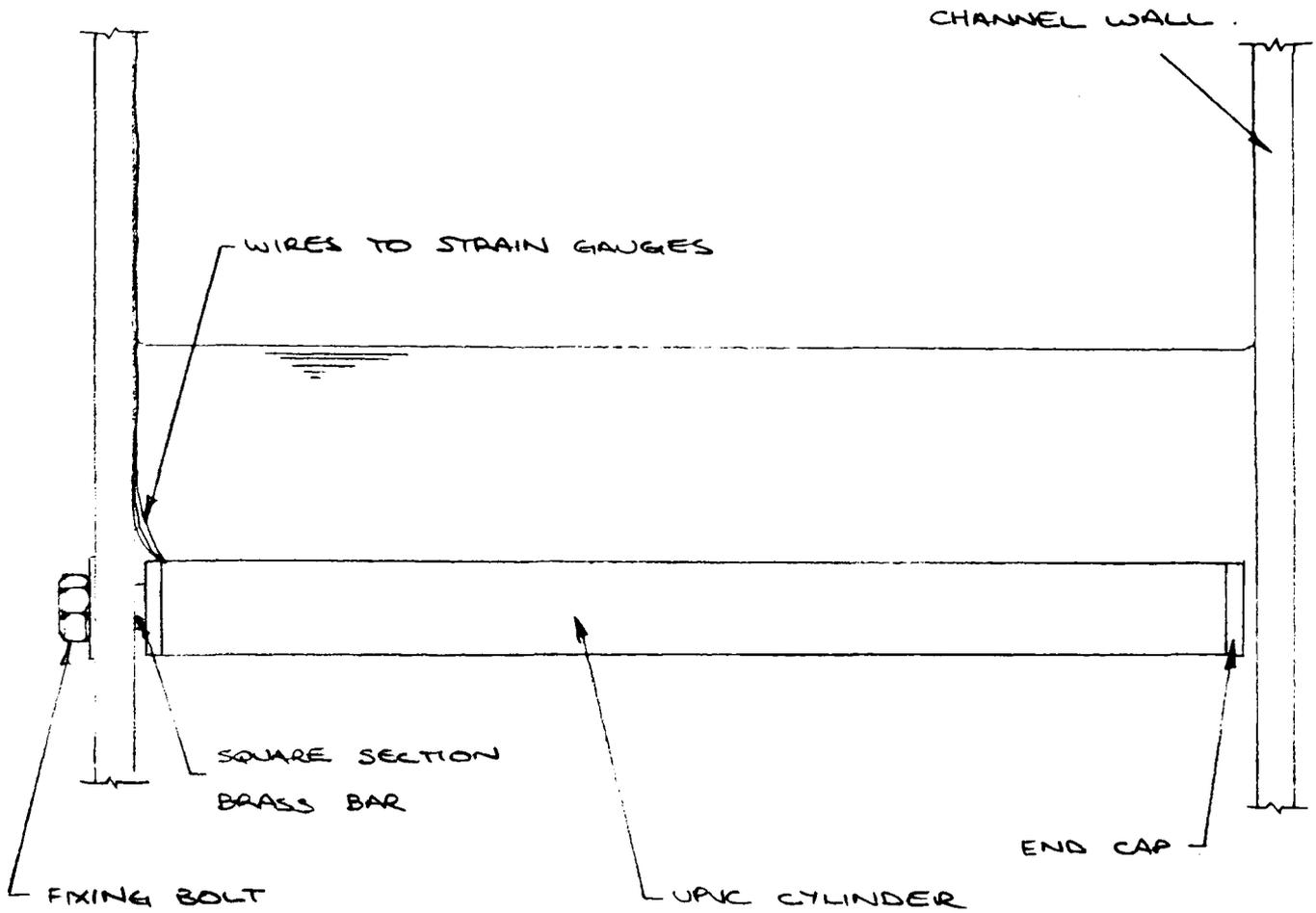
Figure 4.6 – Test cylinder details

Scanned Strain Gauge Output
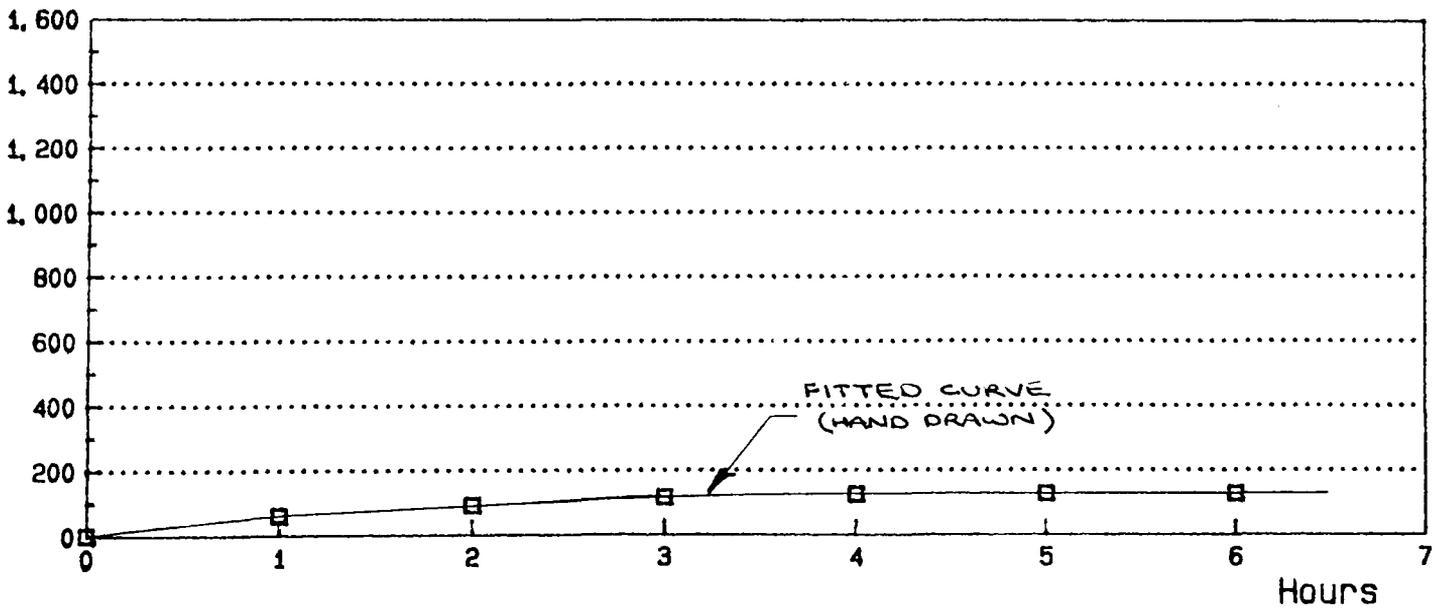
Figure 4.7 – Drift in strain gauge output

The strain gauges were mounted on a brass bar fixed inside the cylinder. After completing tests on one cylinder the bar was then mounted inside another cylinder of different diameter and the tests repeated. This gave greater scope for investigating cylinder diameter, roughness and shape at low cost. The number of cylinder diameters tested was limited by theoretical and practical considerations.

The high sensitivity strain gauges allowed a rigid cylinder (i.e. large section brass bar) to be used, maintaining a high natural frequency, far beyond the wave frequency. As it was rigidly fixed as postulated in theory, there was no modification of the flow field through cylinder movement.

The force balance was designed to measure both horizontal and vertical forces. In preliminary experiments only the horizontal force on the cylinder was measured (figure 4.8). A similar vertical cantilever support apparatus was considered for this series of experiments using the twisting and bending of a bar to give horizontal and vertical loads. The combined response of these two types of bending would give a non-linear response to applied loads. The advantage of this type of cantilever would have been that any movement of the cylinder would have been nearly uniform along its length, except where the support of either end of the cylinder was different.

Different support conditions would give a differential movement as is the case with the horizontal cantilever. Despite the difficulty in interpreting the results, manufacture would have required a consistency of material and construction that could not be guaranteed. Thus it was decided to use a horizontal cantilever design that was capable of measuring forces in two orthogonal directions with minimum movement under applied loads.
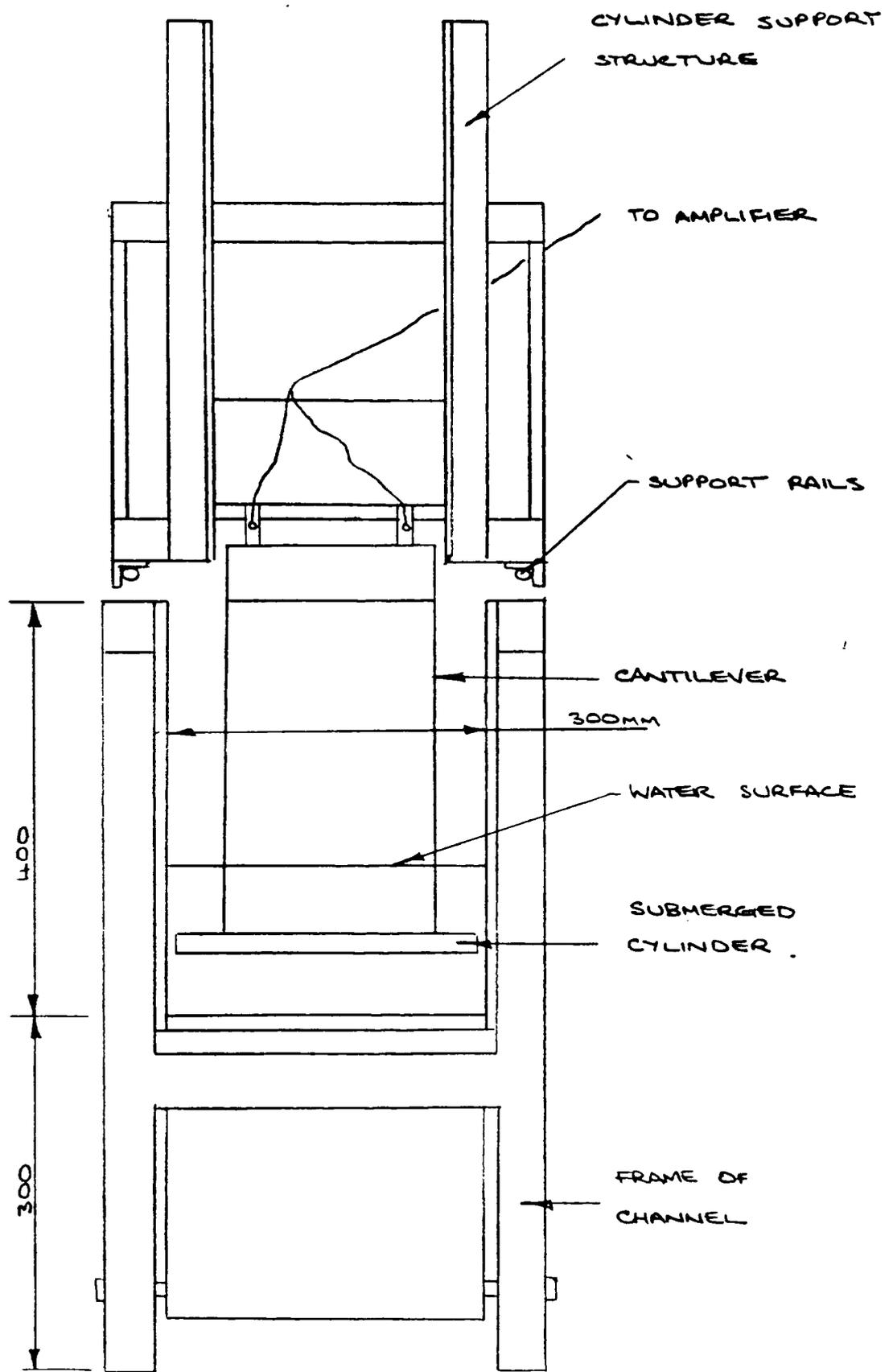
Figure 4.8 - Preliminary test equipment

Labels in figure:
- CYLINDER SUPPORT STRUCTURE
- TO AMPLIFIER
- SUPPORT RAILS
- CANTILEVER
- 300mm
- WATER SURFACE
- SUBMERGED CYLINDER
- FRAME OF CHANNEL
- 400
- 300

4.3.2 Force Transducers

Strain gauges were mounted as shown in figure 4.9 at the root of each bar.

Each pair of strain gauges formed two arms of a Wheatstone Bridge. At the beginning of a series of tests the cylinder was rotated about its long axis in the channel until one set of gauges was in such a position as to monitor the bending stresses at the cylinder root produced by lift forces and the other set those due to in-line forces. As a preliminary test, loads were applied through a pulley system to the cylinder in the horizontal direction. (figure 4.10) This tested whether horizontal loads gave any response in the lift force transducer and was repeated for loads applied in the vertical direction. In both cases "crosstalk" was small though noticeable. During calibration the "crosstalk" was recorded and accounted for in the analysis of the force traces.

The strain gauge system was sensitive to moment rather than force.

In this study it was assumed that the load distribution along the length of the cylinder was uniform and that it may be resolved to equal point loads acting at the end of the cylinder.

Sarpkaya (1976) makes a similar assumption though using a cylinder supported at both ends rather than the cantilever used here. Sarpkaya's measurements of moment at either support produced identical traces which showed that this assumption is not unreasonable. Movement of the tip of the cantilever would invalidate this assumption.

KYOTO SEMI-CONDUCTOR STRAIN GAUGES

TO AMPLIFIER

SCREW THREADED FOR FIXING BOLT

BRASS BAR.
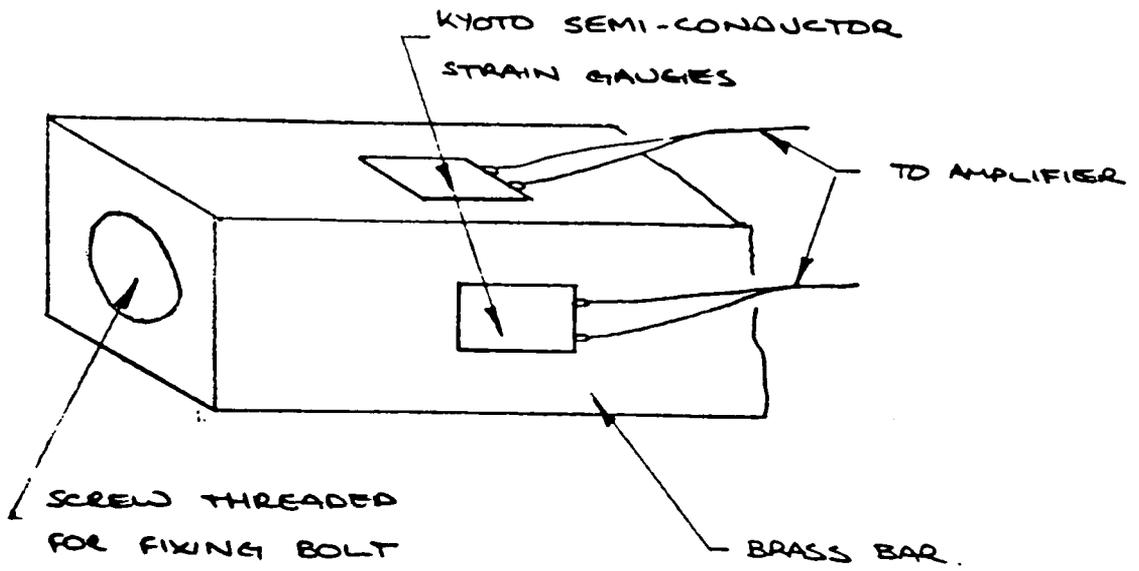
Figure 4.9 - Strain gauge detail

WATER SURFACE

FRAME OF CHANNEL

PULLEY (SUPPORTS NOT SHOWN).

WEIGHTS

WIRE CABLE

SUBMERGED CYLINDER
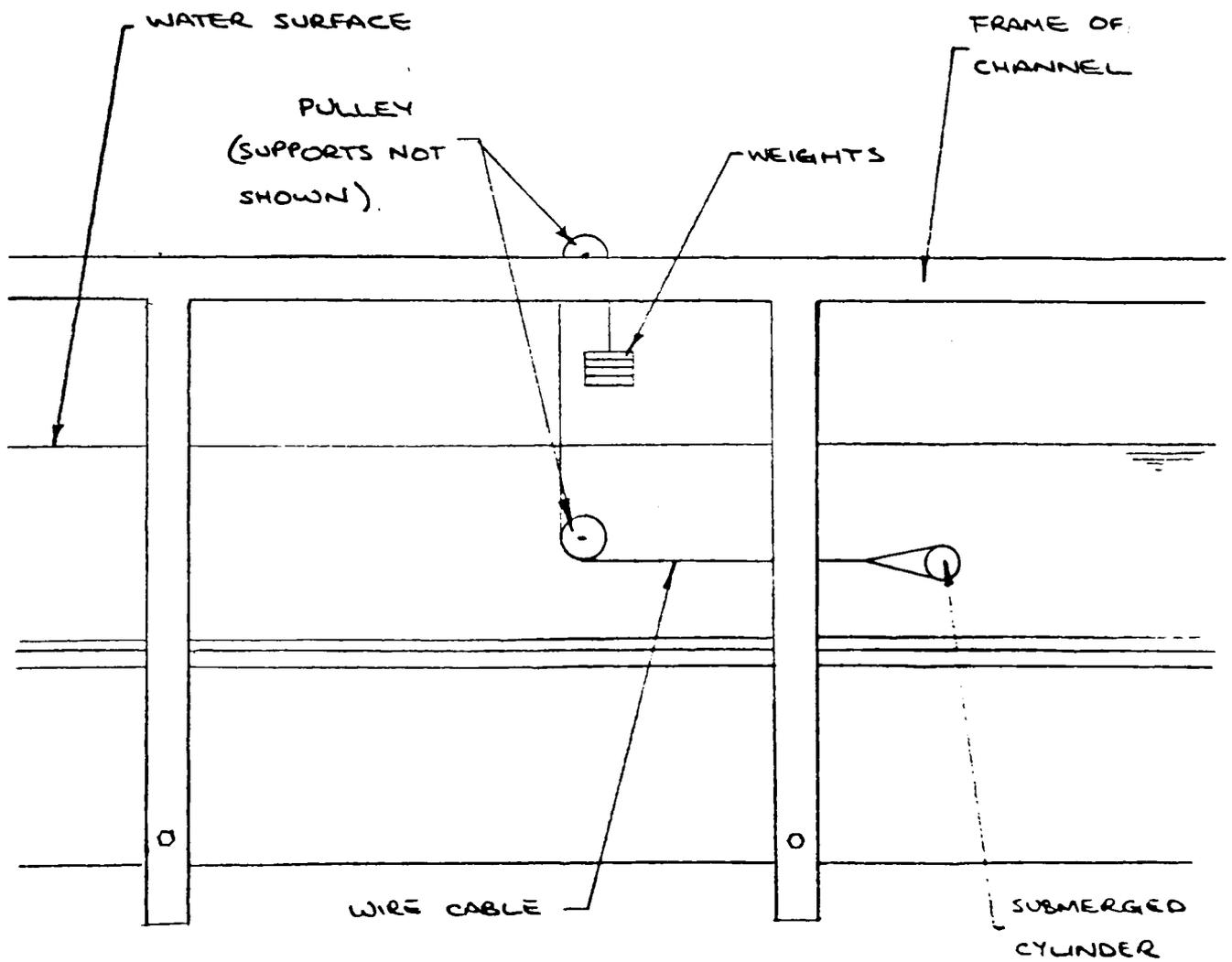
Figure 4.10 - Cylinder calibration

The direct measurement of force would require two extra sets of semi conductor strain gauges some distance from the original set, measuring moment at a second position. Subtraction of the two gauge signals would lead to a reduced signal possibly requiring smaller sections of brass bar. This would bring the natural frequency unacceptably close to the wave frequency. It would give no more information regarding the non uniformity of the force distribution than would the measurement of moment.

Monitoring a combination of force and moment would give an estimate of the point of action of the resultant. Indeed this may vary between tests and furnish no relevant information regarding the mechanics of the wave induced loading.

For these reasons the moment sensitive system was used. Any three dimensionality in loading would then give a transducer output proportional to the average force which was used throughout.

4.4 Instrumentation

The out of balance signal from the force transducers was monitored and amplified by two of a six channel bridge conditioning unit (SE995). These had carrier frequencies of 3kHz and a bridge voltage of 5 volts. Both channels had phase and frequency locked oscillators to prevent beating.

Recording of the transducer signals was on a Racal dual standard 14 channel frequency modulating tape recorder. Tape speeds from 15/16 ins/sec (2.38 cm/sec) to 60 ins/sec (152.4 cm/sec) were available and a voice track permitted verbal comments, notes etc., to be recorded. An attenuator on each of the channels allowed variation of the strength of the input signal, so that best use could be made of the signal to noise ratio of the tape recorder.

During testing the transducer signals were inspected for quality and strength using a Telequipment D1011 dual channel cathode ray oscilloscope.

4.5 Calibration Procedures

4.5.1 Calibration of Force Transducers

Calibration of the force transducers was carried out 4 - 5 hours after the bridge was first energised. The calibration was performed in-situ to remove any end effects the fixing may have had on the response. To calibrate in the horizontal direction forces were applied to the centre of the span of the cylinder through a pulley system. (figure 4.10) With the pulley at over 1 metre from the test cylinder the error in the direction of application of the force was kept within 0.1%.

A similar pulley system was used to calibrate the force transducers in the vertical direction. At the lowest cylinder position the force transducers could be calibrated in the vertical upward direction only because of the proximity of the channel bed. This was satisfactory since the response of the force transducers to applied loads was linear. (figure 4.11)) Signals from the strain gauge amplifier were amplified and filtered to remove high frequency noise (>1kHz). This filtering did not introduce a perceptible phase shift or drift and was ignored.

Whilst calibrating in the horizontal direction, signals from both sets (horizontal and vertical) of force transducers were monitored with the tape recorder set to a suitable sensitivity. The cylinder was loaded in the horizontal direction then the vertical direction. In both cases the loads were applied in small increments to cover the range of forces expected on the cylinder. The range was determined by several preliminary tests with waves of near maximum amplitude.
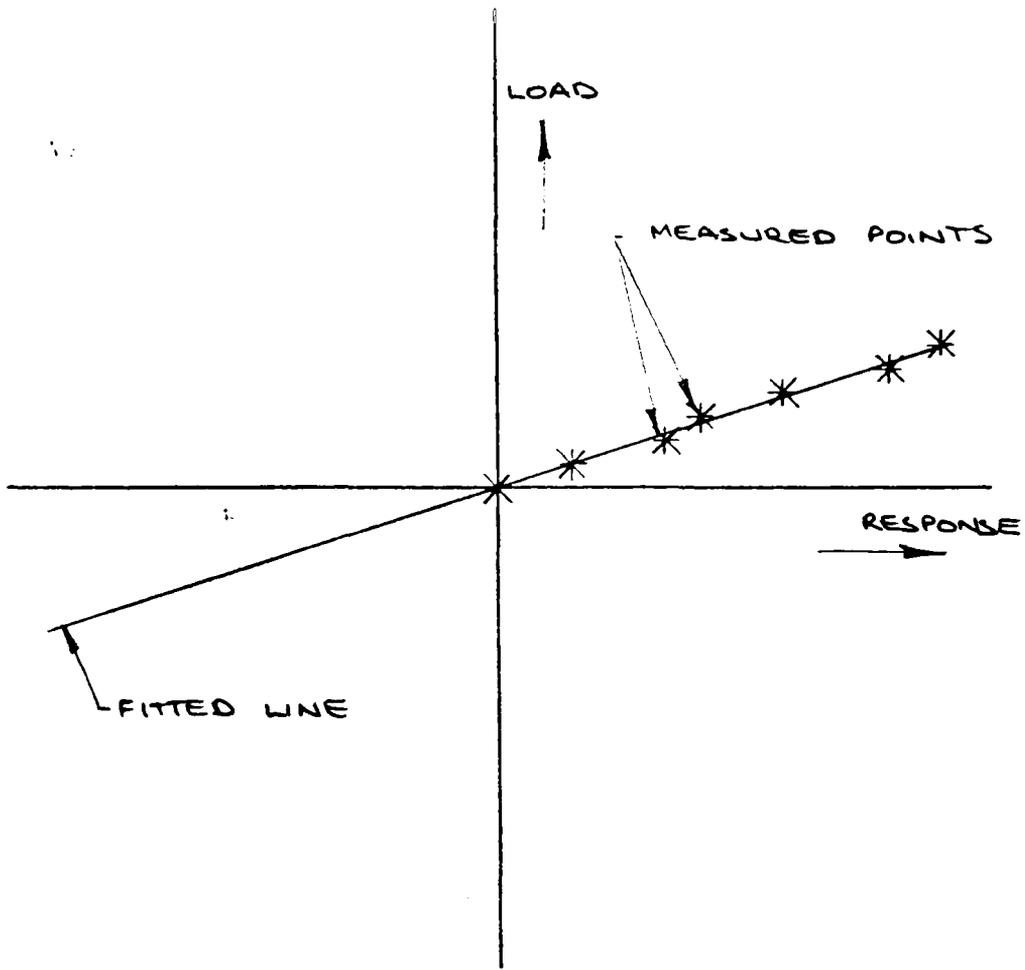
D=27mm; Ht. of cylinder=36mm
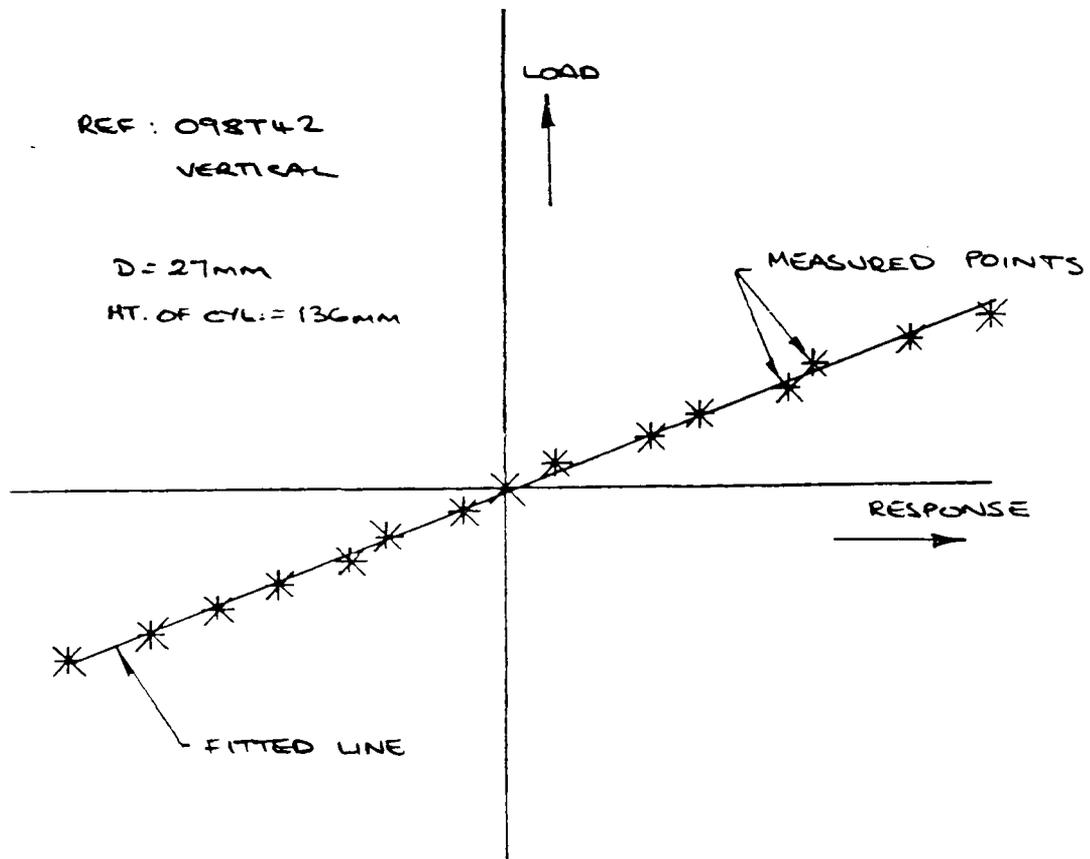
D=27mm; Ht. of cylinder=136mm

Figure 4.11 - Force Transducer calibration graphs

4.5.2 Calibration of Hot Film Anemometer

The position of the trolley was given by a ten turn linear potentiometer mounted in the line of the trolley's motion over the centre of the channel (figure 4.12)

The potentiometer linearly divided a voltage according to position. Calibration was performed by identifying one trolley position along the channel with a pointer fixed to the trolley. For this static but known position and voltage was recorded. The trolley was then moved to another extreme position and the new lower voltage recorded. Thus the change in voltage per unit distance was determined (figure 4.13). Also during this calibration it was possible to set the sensitivity range on the tape recorder.

The tachogenerator was calibrated using a strobescope and lathe. Whilst monitoring the output voltage from the generator the angular speed of the lathe was set using a strobescope. The calibration gave a linear relationship between angular speed and generation voltage (figure 4.14).

The voltage was related to the response of the tape recorder by applying a known and near maximum generated voltage (typically 1.5 volts) to the tape recorder.

Using a pulley wheel of known diameter the angular velocity of the pulley was converted to a linear speed of the trolley. Thus the trolley speed at an instant of time could be determined by monitoring the voltage output from the tachogenerator.

As the trolley moved along the channel it closed two micro switches approximately 1 metre apart. A "flip-flop" circuit
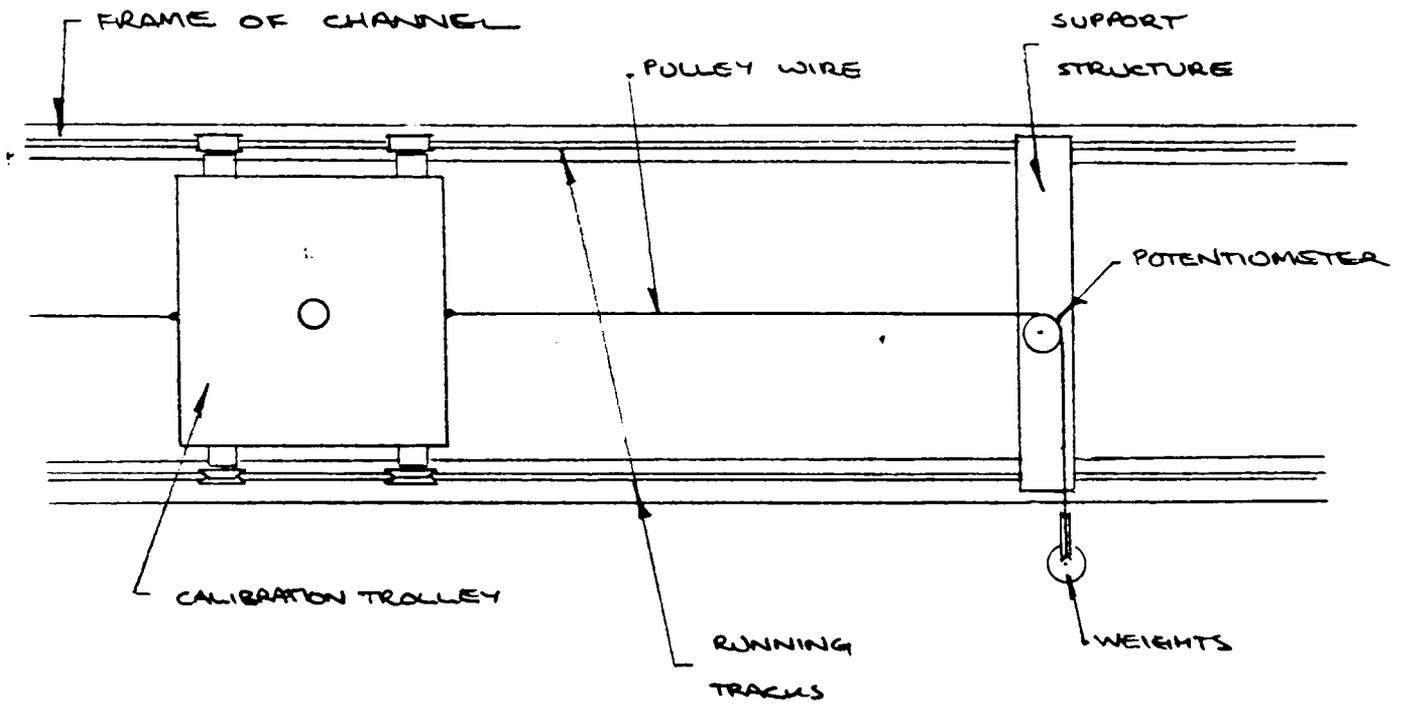
Figure 4.12 – Plan of channel

(showing potentiometer)
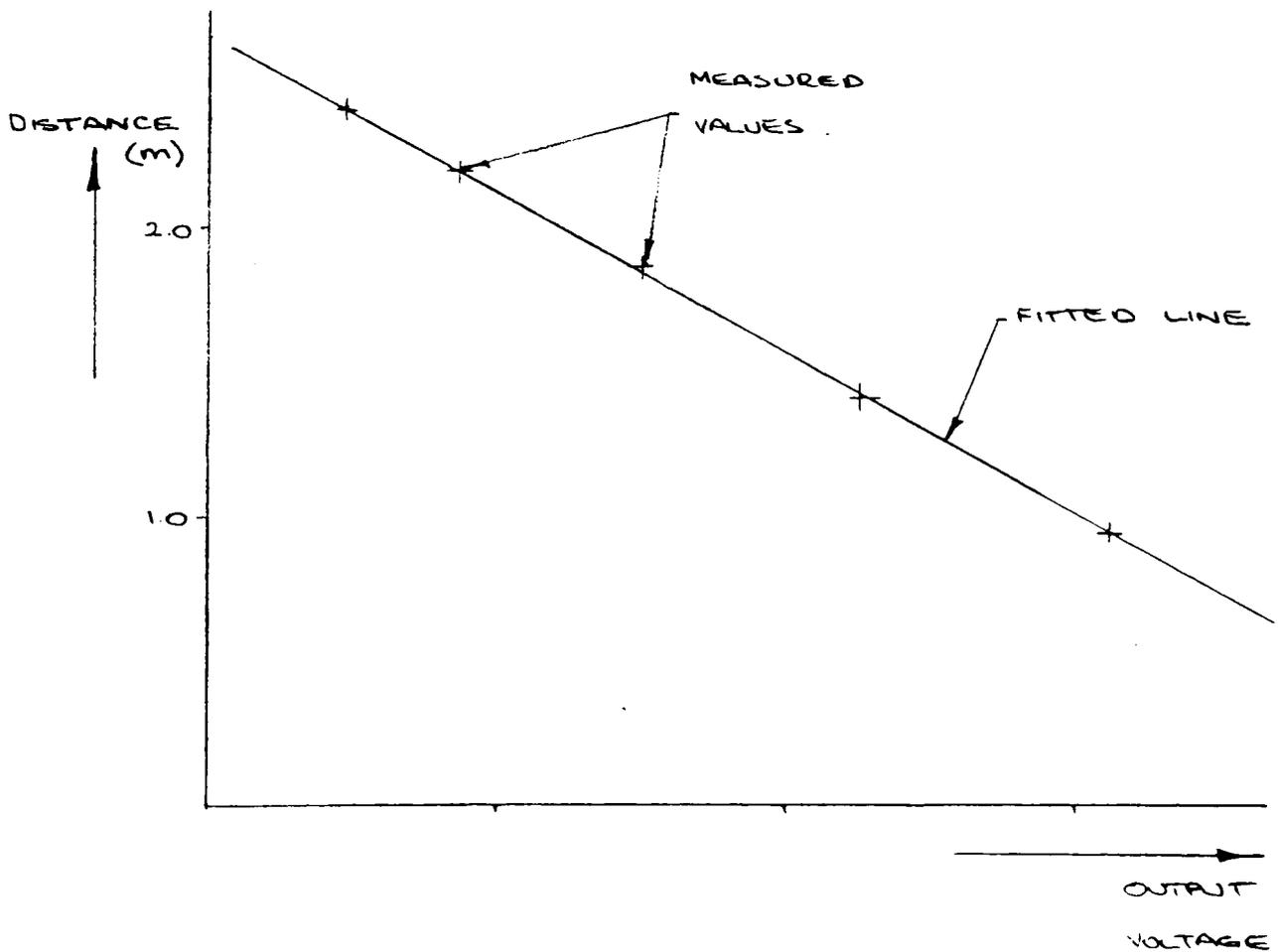
Figure 4.13 – Calibration graph of potentiometer
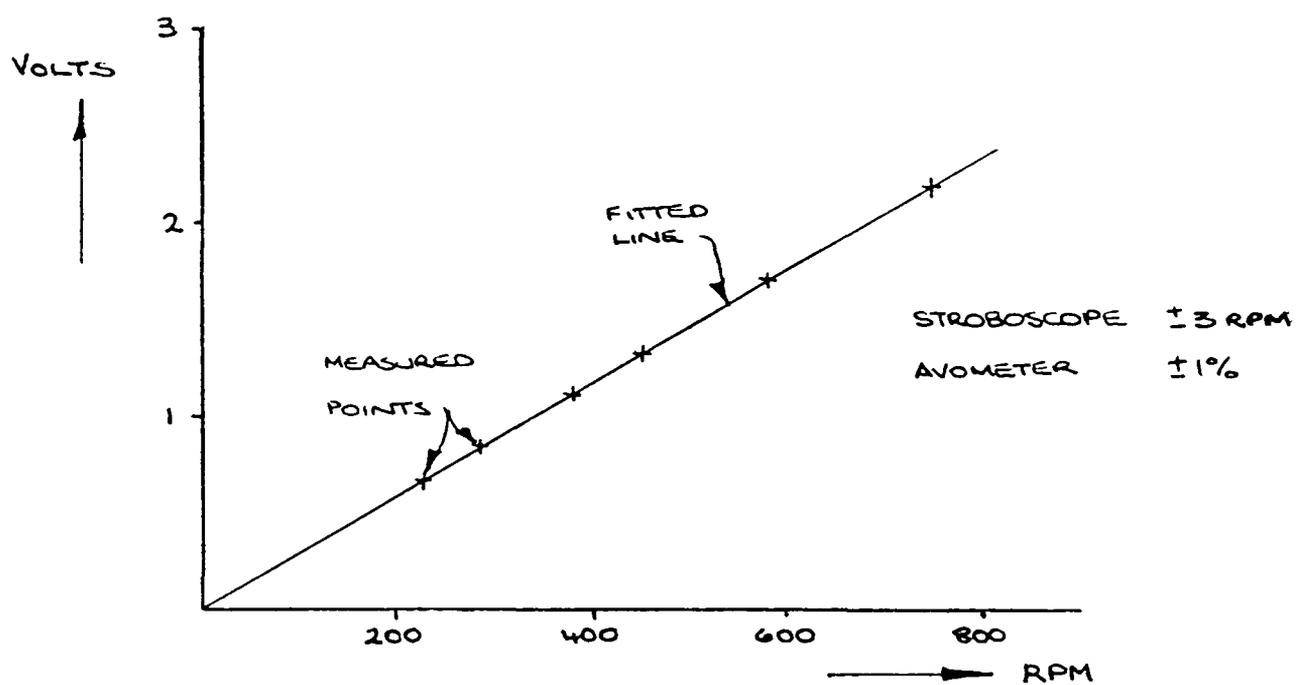
Figure 4.14 - Calibration of tachogenerator

applied 5 volts D.C to the tape recorder when one switch had been pressed. Thus it was possible to establish the positions of the micro switches in both the tacho-generator and potentiometer output records to within 0.01 sec. by monitoring the output from the "flip-flop" circuit. Having measured the distance between the switches this could be compared with that from the potentiometer and tacho-generator output.

The "flip-flop" circuit also activated a timer as the first switch was passed and stopped as the second switch was passed. This gave the time to travel between the micro switches and hence the trolleys average speed. This was compared with the time and average velocity computed from the tacho-generator output.

The wire was prevented from slipping over the pulley wheel by winding the wire several times around it.

Thin copper wire was chosen to pull the trolley since it was strong, would not stretch significantly without breaking and quite flexible without being "springy". This last point was important since the trolley had to be accelerated smoothly to maintain forced convection from the sensor during calibration. Also by accelerating the probe smoothly from rest more closely represented the fluid motion as the wave passed.

Linearity of response of the potentiometer was established by moving the trolley to known positions along the channel and recording the D.C voltage output of a divided stable potential. As the trolley moved it turned the potentiometer, dividing the applied potential according to position. (figure 4.13)

The trolley itself had a rectangular perspex base (335*380mm) 5mm thick, with a brass axle mounting at each corner. The wheels were perspex machined so that two, on one side of the base were "V" grooved, the others having a central flat. This was done to prevent irregularities in the line of the track causing vertical movements of the trolley. The axle was screwed securely into a brass sleeve. Contact between these surfaces was minimised by machining the axle to be marginally larger diameter mid way between the wheel edges. The brass sleeve inside the wheel was made in two halves, so that when fixed together they formed a 'U' shaped channel. The points of the contact act as knife edges thereby minimising friction and play.

Hooks were positioned at the front and rear of the trolley so that towing and restraining cables could be securely fixed. The Hot Film sensor was mounted centrally through the base of the trolley. It's height in the water was fixed with a locking bolt held in a sleeve around the probe extension piece.
A capacitance wave probe was mounted adjacent to the Hot Film sensor (figure 4.15) so that the wave profile could be measured as it passed.

A lateral extension arm was fixed to the trolley base so that cables from the Hot Film sensor and the wave probe would clear the wave channel support columns, and not be fouled as the trolley moved along the channel.

It was possible to move the trolley forward approximately 1.5 metres under the action of a falling weight. The pulley system included both pulling and restraining weights. (figure 4.16) This enabled close control of the motion of the trolley though sensibly different each time the trolley made a calibration run. Throughout, the philosophy was maintained that a predetermined motion was unimportant though the accurate determination of the motion was essential.

4.5.3 Calibration of wave probes

Three wave probes were used to measure water surface elevation. Two were some distance either side of the cylinder, the other immediately in front of the cylinder adjacent to the Hot Film sensor. (figure 4.16)

Each wave probe was calibrated statically immediately prior to a day's tests. This was performed by moving the probes up and down in steps of 10mm either side of the amplifier balanced position.

The wave probes were dynamically calibrated over a range of frequencies. This was to determine the relation between wave frequency, phase shift and amplitude reduction.
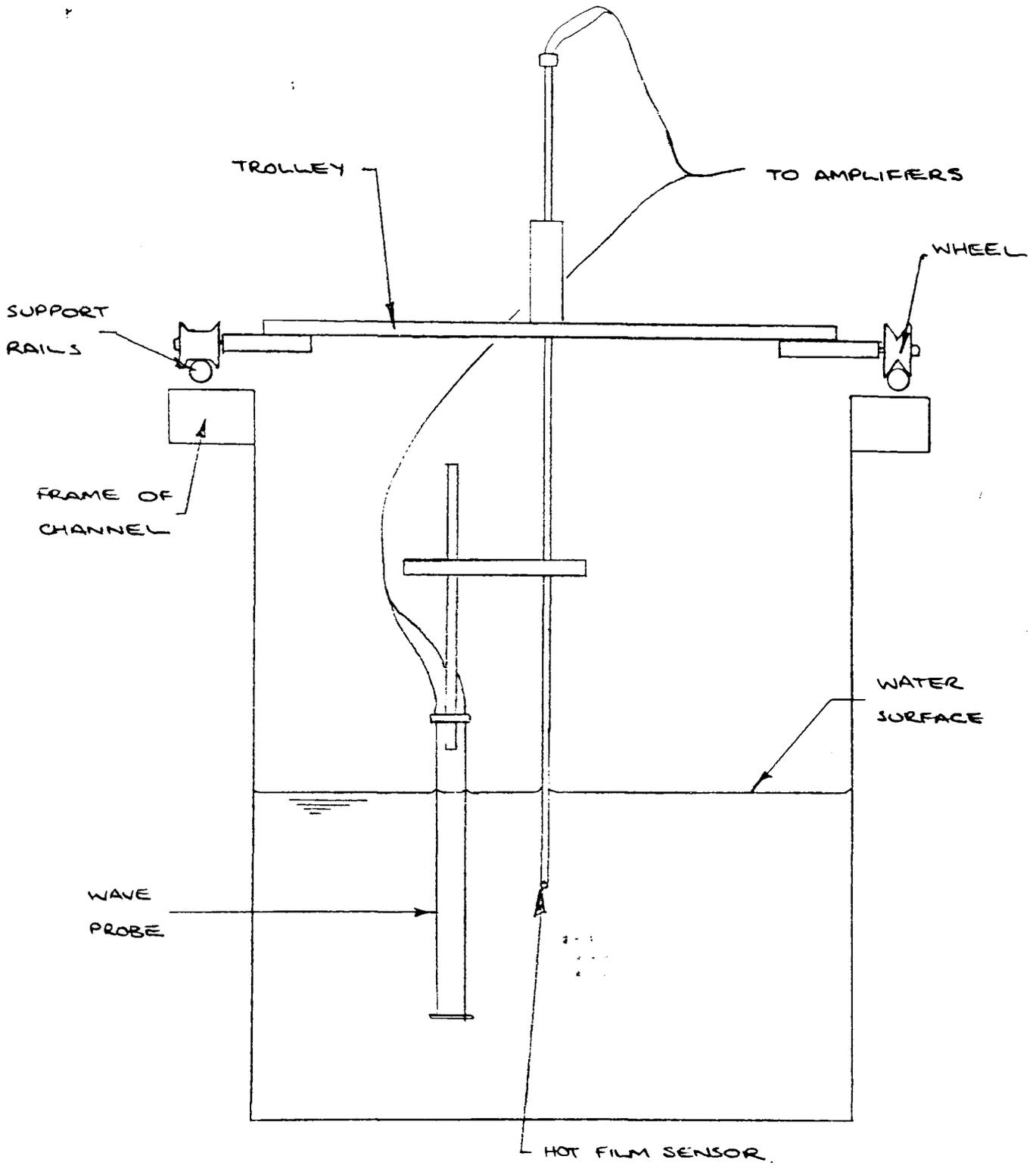
Figure 4.15 - Wave probe, HF Sensor, trolley and channel section
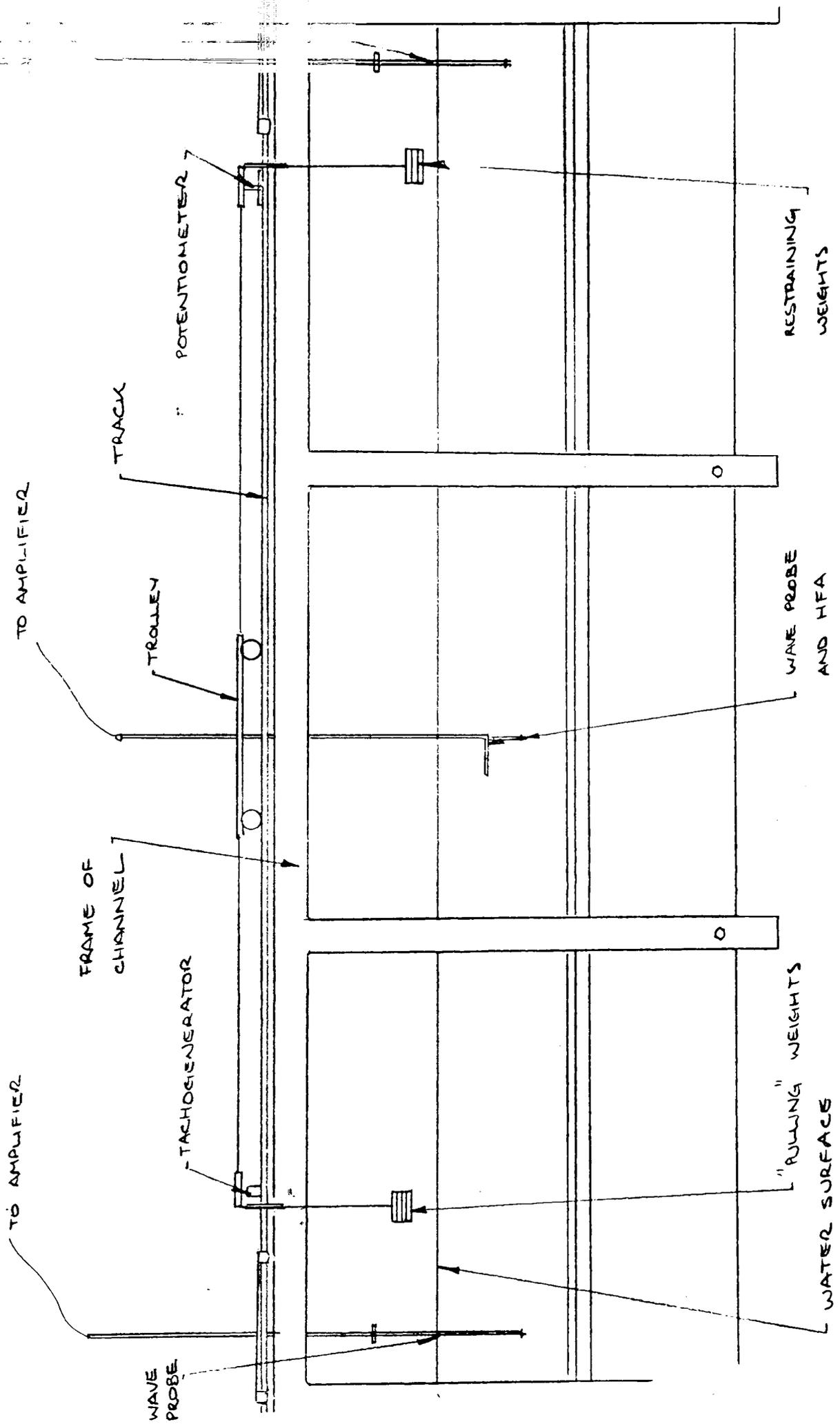
Figure 4.16 – Elevation of channel showing pulley system, trolley, wave probes and H.F. Sensor

Fixing the wave probe to a hydraulic ram and moving it sinusoidally enabled phase lag to be determined. The feedback for the ram was compared with the wave probe amplifier output for frequencies up to 1Hz. The phase shift was measured at 0.04 sec. with negligible amplitude reduction. Clearly the phase shift was significant (0.04 sec. is equivalent to typically 0.056 metres wave movement) and was corrected before comparison with other transducer signals. No frequency dependent phase lag or amplitude reduction was found with any other piece of instrumentation.

4.6 Test Procedure

At the beginning of a day's testing, the wave channel was levelled and the sliding gate at the generator end of the channel was sealed whilst dry. The beach was lowered into the channel which was then filled with filtered water from a main storage tank. This was done slowly so as not to increase the dissolved air content of the water which may affect the stability of the HFA calibration.

The cylinder was lowered into position and secured with a brass fixing bolt to the channel wall. A rubber collar and washers (figure 4.6) were fitted around the bolt to stop water leaking through the fixing hole.

The cylinder was rotated to orientate the strain gauges so that one pair measured horizontal, and the other pair measured vertical forces. By loading the cylinder in the horizontal direction whilst monitoring the signal from the strain gauges orientated to measure the vertical forces, the "crosstalk" was minimised.

The channel bed was levelled by measuring the water depth at either end of the channel and altering the bed slope so that the water depth was constant along the channel.

The trolley was mounted on runners along the edge of the channel. (figure 4.15)

The "flip-flop" circuit and timer were checked.

The Hot Film Anemometer and Sensor were adjusted for maximum frequency response as detailed in TSI literature. As this was an entirely standard procedure it will not be reproduced here.

When not in use the Anemometer was switched to 'standby' and was only switched to 'Run' immediately prior to measurements being taken.

The position of the trolley was recorded prior to the Hot Film sensor calibration run. The temperature of the water was taken, along with the time. The Anemometer was switched to 'Run' and the voltage output from the potentiomenter was checked to be within the sensitivity range set on the tape recorder. The output voltage from the HFA was checked for stability and zero offset. The time was reset at zero and the 'flip-flop' circuit was set so that no voltage was applied to the tape recorder. The tape speed and sensitivity settings on the 9 channels were checked. The tape was started.

After two or three seconds the trolley was released from its position by releasing a falling weight. This was sufficient to overcome friction in the pulley/trolley system. The weight, now falling freely pulled the trolley, whilst the towing wire turned the tacho-generator and potentiometer. As the trolley moved along the channel it activated the micro switches, starting then stopping the timer.

The trolley motion ceased once the falling weight touched the ground, the restraining weight acting as a brake. The system was arranged so that the 'pulling' weight only hit the ground after the trolley had passed the last microswitch. The impact of the weight on the floor was cushioned by a thick foam pad which prevented vibrations being transmitted through the wave channels support structure to the force transducers.

After all motion had ceased the tape recorder was stopped. The trolley's final position was recorded along with the time taken to travel between micro switches. The HFA was then switched to 'standby'.

So that velocities in the wave could be recorded as if the cylinder was absent the trolley was moved and fixed between the cylinder and the wave generator. This position was measured and recorded.

The Anemometer was again switched to 'Run' and the tape recorder started. A solitary wave was generated at the far end of the wave channel, propagating along its length. The recording was stopped once the disturbance reached the far end of the channel.

Fifteen minutes was allowed for the water to return to rest, during which time the trolley was moved back to its pre-calibration position. The instruments and signals were checked in preparation for the next calibration run.

4.7 Summary

A simple but innovative design of apparatus and experimental techniques have been described. These give calibration and results of high accuracy and consistency. In chapters 6 and 7 these results and their inter-relationships will be used to gain a better understanding of the generation of forces.

CHAPTER 5   ANALYSIS OF RESULTS

5.1 Introduction

This thesis gives results of high accuracy and consistency.
This was achieved by logging, scanning and analysing data
using a series of computer programmes enabling huge quantities
of data to be systematically processed, quickly and easily.

The first section outlines the hardware used to analyse the data
together with a programme used to transfer data from one
computer to another.   The process is summarised in figure 5.1

5.1.1 Data Logging and Scanning

Output signals from the measuring equipment used in this
experimental program were stored on magnetic tape.   These were
scanned and logged using an Intercole Systems Ltd Compulog
four PDP11-23.   The high speed scanning system, designed and
manufactured by Intercole, provided 13 software selectable
speeds of scanning from 1 Hz to 25 kHz.   A scanning frequency
of 3.3kHz was used throughout the series of experiments.   Eight
switch selectable scales (20mV to 5V full scale deflection) for
input voltage were available.   A scale compatible with the 2 volts
peak - peak output from the tape recorder was selected.
Storage of data was on double density floppy discs (512kBytes)
and two 5Mbyte cartridge discs.

Transducer signals were monitored at a scan speed of 25k
channels per sec. with a real time delay of 0.015 secs.
Scanning speed was determined primarily by the conversion time
of the analogue to digital converter, which in this case is $12\mu s$.
Combined with the data acquisition time of effectively $15\mu s$, gave
a maximum scan speed of 25kHz.

```
┌─────────────────┐          ┌─────────────────┐
│ Set up exp.     │◄─────────│ Calibrate       │
│ Apparatus       │          │ Tachogenerator  │
└─────────────────┘          └─────────────────┘
         │
         ▼
┌─────────────────────────┐
│ Calibrate               │
│   Wave probes, Cylinder │
│   Potentiometer,        │
│   Micro switches.       │
└─────────────────────────┘
         │
         ▼
┌─────────────────────────┐
│ Set ranges              │      - Racal tape recorder
│   Take init. readings   │
└─────────────────────────┘
         │
         ▼
┌─────────────────┐
│ Take pre-HFA    │◄──────────────────────┐
│ calib. readings │                       │
└─────────────────┘                       │
         │                                │
         ▼                                │
┌─────────────────┐                       │
│ Calibrate HFA   │                       │
└─────────────────┘                       │
         │                                │
         ▼                                │
┌─────────────────┐                       │
│ Take post HFA   │                       │
│ calib. readings │                       │
└─────────────────┘                       │
         │                                │
         ▼                                │
┌─────────────────┐                       │
│ Record wave     │                       │
└─────────────────┘                       │
         │                                │
         ▼                                │
       ╱   ╲           Yes        ┌───────────────┐
      ╱ Any ╲────────────────────►│ Reset         │
      ╲more? ╱                    │ Equipment     │
       ╲   ╱                      └───────────────┘
         │
         │ No
         ▼
┌─────────────────┐
│ Scan tape       │          - PDP11-23
│ Recordings      │
└─────────────────┘
         │
         │ Data Transfer
         ▼
┌─────────────────┐
│ Data processing │          - Honeywell 66
│ and Output      │
└─────────────────┘
```

**Figure 5.1 - Flow chart showing the procedure used
to analyse results.**

Interleaved scanning allowed effective scanning speed of up to 50kHz by scanning channels in parallel though this facility was not used in this series of experiments.

Data generated by the scanning was logged on the dual cartridge disc storage system. Programmes used for the data logging and scanning were based on Intercole library routines.

5.1.2 Data transfer

Data was scanned and logged using the dedicated mini computer described earlier. Though this had excellent programming facilities it had limited memory, hardware and software facilities. To allow comprehensive large scale data processing, printing and plotting of results a mainframe computer was used. Data from the mini computer was transferred to the mainframe computer using software on the mini computer to emulate an ordinary mainframe terminal. This involved programming the required response to prompts from the mainframe. Thus data collected on the mini computer from laboratory experiments was transferred for analysis to a main frame computer.

5.2 Introduction

Having established an efficient method of scanning and handling the data, programmes were developed on the Honeywell mainframe computer to determine calibration constants in a systematic and consistent way. This eliminated inconsistencies introduced in the processing of data by hand.

5.2.1 Calibration of force transducers

The calibration of the force transducers is outlined as a flow chart in figure 5.2

Basic data collected in the laboratory for the calibration of the force strain gauges, included weights applied during calibration, lever arm length together with the primary transducer output along with the corresponding transducer "crosstalk".

Several scans were made for each applied load during calibration. An average value for each load was computed and ·taken as the response of the force transducer to that applied loan.

As the cylinder was loaded in both horizontal directions (left and right) a calibration was obtained for both "positive" and "negative" responses of the transducer. Since the response in the vertical direction was monitored whilst loading in the horizontal direction, calibration could be repeated for the "crosstalk".

Loads applied during calibration in the vertical direction were analysed in the same way, including the "crosstalk" in the horizontal direction due to a vertically applied load.

```
                    ┌──────────────────────┐
                    │   Install  cylinder  │
                    └──────────┬───────────┘
                               │
                               ▼
                    ┌──────────────────────┐
                    │   Fix  cylinder      │
                    │   orientation        │
                    └──────────┬───────────┘
                               │
                               ▼
                    ┌──────────────────────┐        ┌──────────────┐
                    │   Load  in  horiz.   │◄───────│   Rotate     │
                    │   direction          │        │   cylinder   │
                    │   and  monitor.      │        └──────┬───────┘
                    └──────────┬───────────┘               ▲
                               │                           │
                               ▼                           │
                          ╱─────────╲                      │
                        ╱  "Crosstalk" ╲      No           │
                       ╱   minimised?    ╲────────────────┘
                        ╲               ╱
                          ╲─────────╱
                               │
                               │ Yes
                               │
                               ▼
                    ┌──────────────────────┐
                    │   Load  in  horiz.   │
                    │   direction  and     │
                    │   record.            │
                    └──────────┬───────────┘
                               │
                               ▼
                    ┌──────────────────────┐
                    │   Load  in  vert.    │
                    │   direction  and     │
                    │   record.            │
                    └──────────┬───────────┘
                               │
                               ▼
                    ┌──────────────────────┐
                    │   Linear  regression │
                    │   of  results.       │
                    └──────────┬───────────┘
                               │
                               ▼
                    ┌──────────────────────┐
                    │   Derive  calib.     │
                    │   formula.           │
                    └──────────────────────┘
```
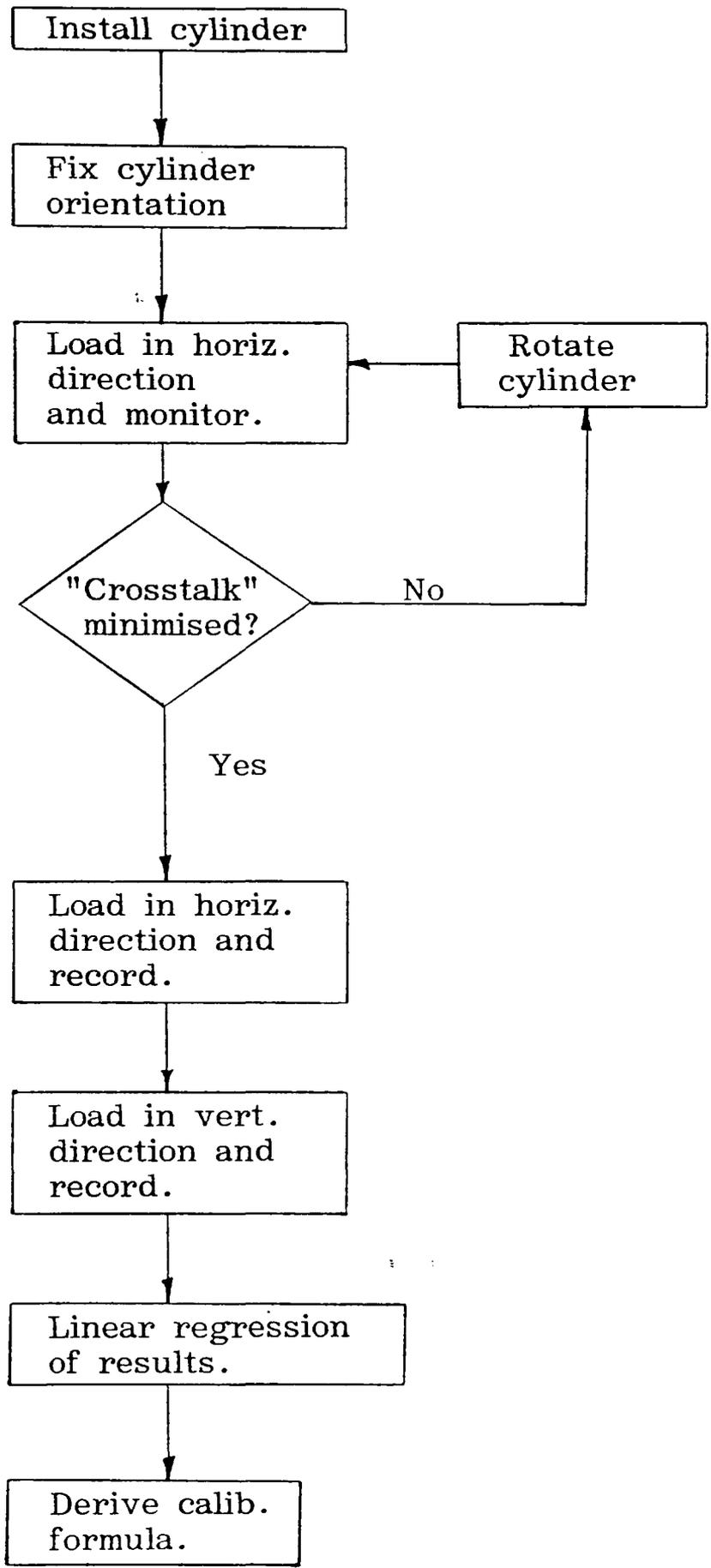
Figure 5.2 - Flow chart showing the procedure used
to calibrate force transducers

The data was transferred to the mainframe computer and a routine used to perform a linear regressions of the four sets of data, giving gradients and intercepts of the fitted lines. The date and fitted lines were plotted using the GINO-F series of graphic subroutines. (figure 6.62 a,b)

The regressed lines were subsequently used to obtain the forces on the cylinder in the horizontal and vertical directions. Corrections were made to remove any 'crosstalk' from these so that a direct comparison could be made with results from Morison's equation.

5.2.2 Calibration of the Hot Film Anemometer

The calibration of the Hot Film Anemometer is summarised in figure 5.3.

The first step in calibrating the Hot Film Anemometer was to relate tacho-generator output to an applied voltage.

The numerical value corresponding to zero applied voltage was computed by averaging the scanner response over a number of scans, typically 20 covering a 30 sec. interval. This was repeated for an accurately determined calibration voltage (typically 1.5 volts).

From this the computer had numeric values corresponding to zero and some other known applied voltage. The computer calculated the changes in scanner output corresponding to a change of applied voltage of 1 volt.

With a linear relation between applied voltage and scanner output (figure 5.4), any scanner output could immediately be converted to an applied voltage. Thus the magnitude of a voltage generated by the tacho-generator could be found. With the relation between generated voltage with angular velocity

```
┌─────────────────┐
│ Reset timer.    │
│ Record postion  │
│ of trolley.     │
└────────┬────────┘
         │
         ▼
┌─────────────────┐
│ Switch on       │
│ tape and HFA    │
└────────┬────────┘
         │
         ▼
┌─────────────────┐
│ Release trolley │
└────────┬────────┘
         │
         ▼
┌─────────────────┐
│ Stop trolley &  │
│ fix in position │
└────────┬────────┘
         │
         ▼
┌─────────────────┐
│ Stop tape.      │
│ Switch off HFA  │
└────────┬────────┘
         │
         ▼
┌─────────────────┐
│ Record: Timer   │
│ reading and final│
│ trolley position.│
└────────┬────────┘
         │
         ▼
┌─────────────────┐
│ Prepare for wave.│
└─────────────────┘
```
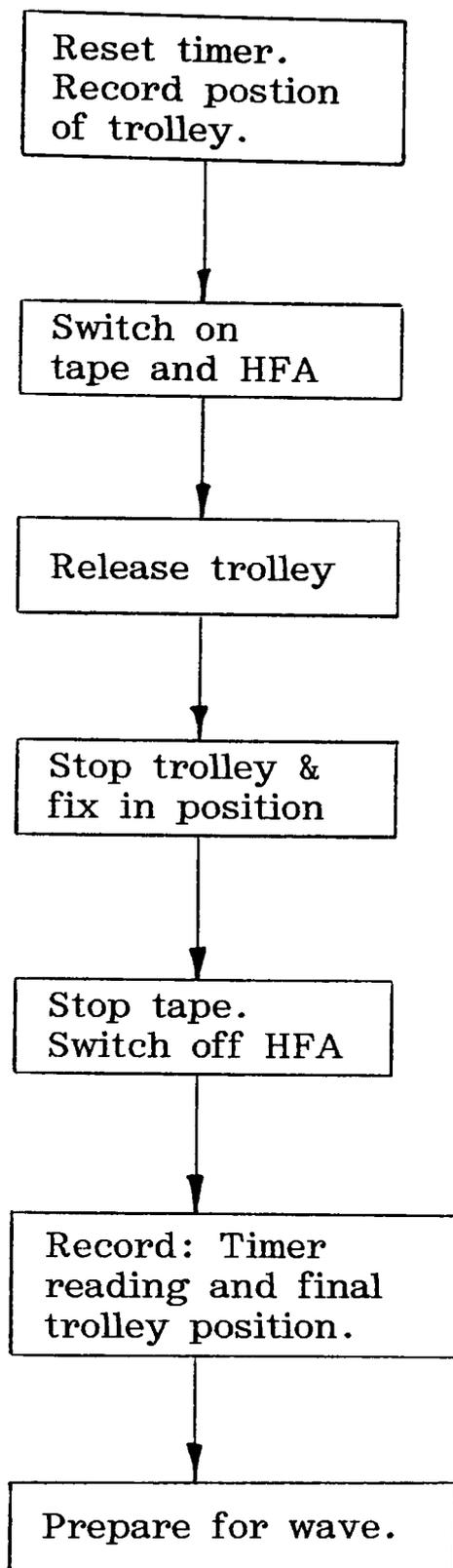
**Figure 5.3 - Flow chart showing the procedure used
to calibrate Hot Film Anenometer.**

Scanner Output
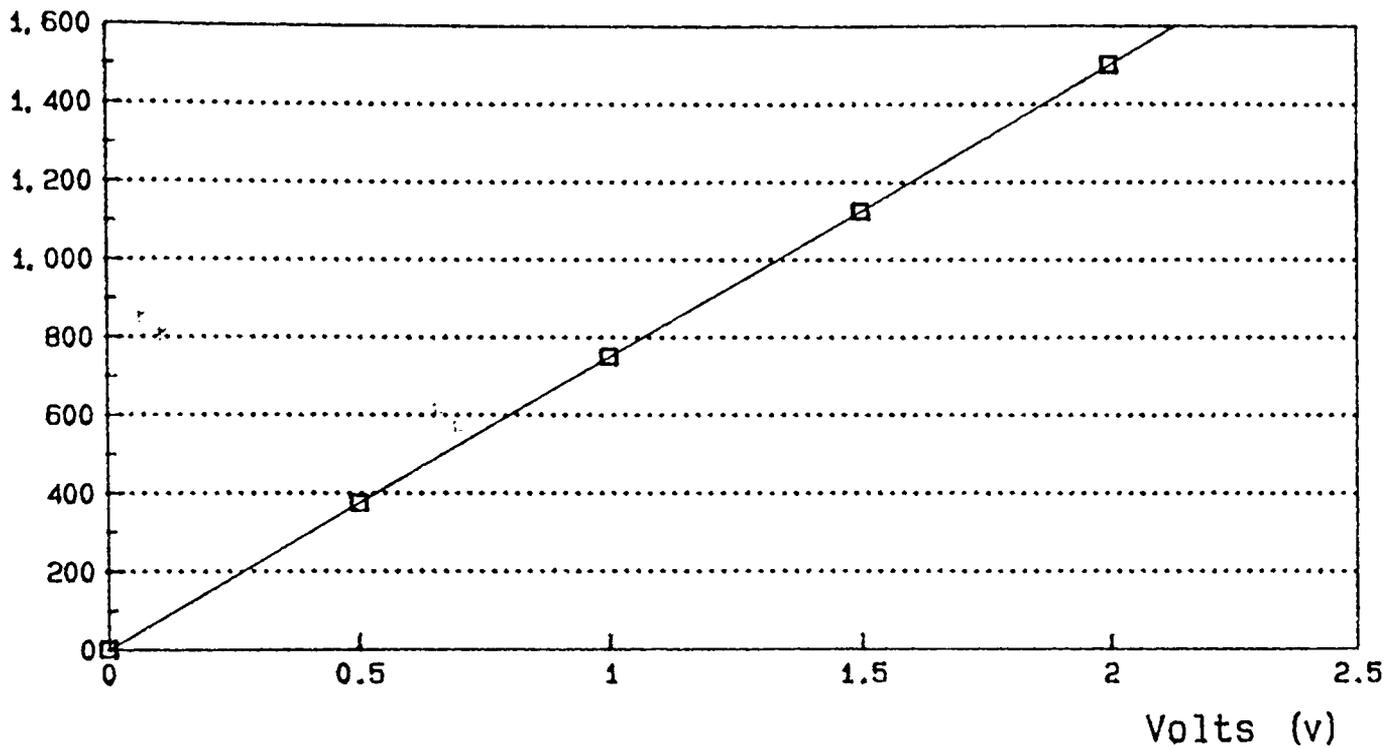
Figure 5.4 - Graph of scanner output versus applied voltage.

(figure 5.5) the speed of the trolley was found from the tacho-generator output.

The potentiometer was calibrated by scanning the output voltage for two measured positions of the trolley along the channel. As before an average value of scanner output was calculated for each position. The relation between trolley position and output voltage was linear, as was the relation between applied voltage and scanner output. Thus changes of scanner output could be directly related to the distance moved by the trolley.

To calibrate the Hot Film Anemometer, the trolley supporting the sensor was allowed to move freely along the channel. The transducers used to measure the position and speed of the trolley were scanned as the trolley moved along the channel. The tacho-generator output gave the linear velocity of the trolley, and was used to calibrate the Hot Film Anemometer.

Using the tacho-generator enabled continuous calibration of the Hot Film Anemometer and was clearly an improvement over previous techniques which calibrate the Hot Film sensor only at discrete velocities. To obtain calibration curve in this situation intermediate values had to be interpolated from measured values. Large errors are readily introduced using this technique since errors of adjacent measured points manifest themselves in the interpolated values.

Integration of the velocity data using Simpson's rule gave the distance travelled from rest. This was compared directly with the potentiometer output and converted to distance moved.

The Hot Film Anemometer calibration data was fitted with a high order polynomial using a library routine. The order of the polynomial was determined by minimising deviation from the fitted curve.
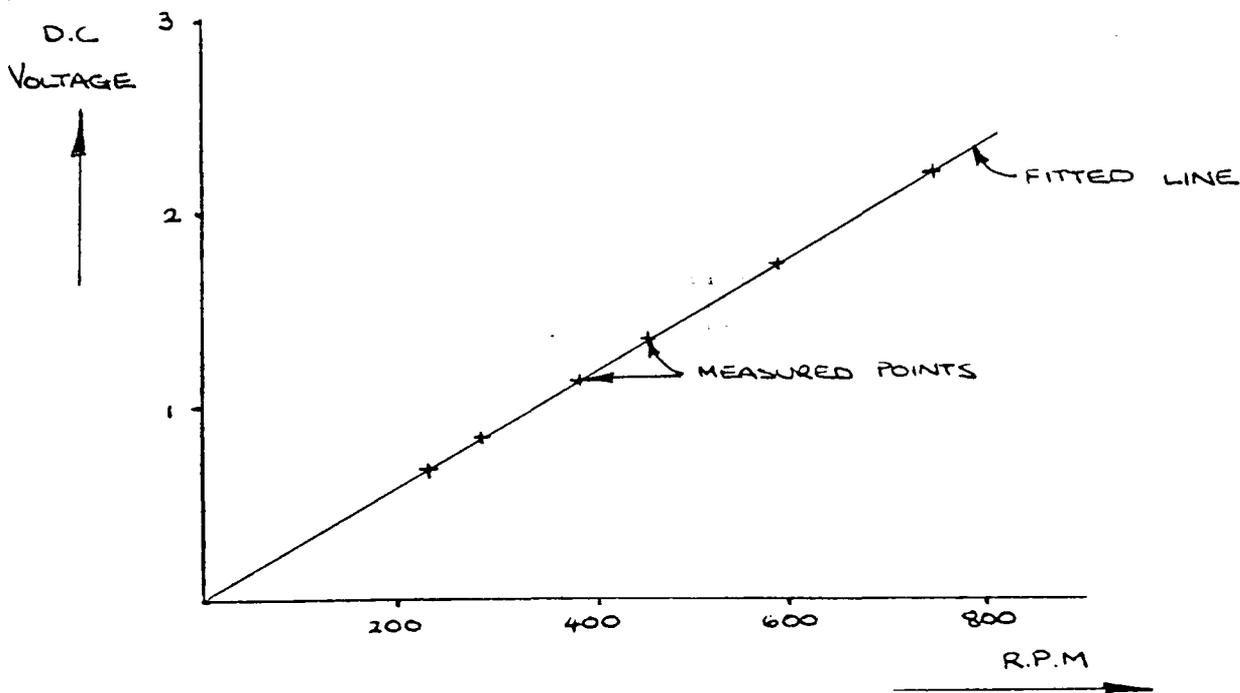

Figure 5.5 - Calibration graph of the tachogenerator

The Hot Film Anemometer data was linearised using a linear regression to fit a modified King's Law expression, maximising the regression coefficient for best fit. The intercept and gradient of the fitted line was calculated.

The linearised expression was used to reduce the Hot Film Anemometer output to velocities as the wave passed.

5.2.3 Calibration of Wave probes

Figure 5.6 summarises the process used to adjust and calibrate the wave probes.

The wave probes were scanned continuously during calibration. Plateaus were found in the data to correspond to the centimetre lifts and falls of the wave probe. The numbers in these plateaus were averaged. A polynomial, usually of the fifth order was then fitted to those averaged values. The order of the polynomial was chosen by the computer to give "best fit" of the curve to the data. This process was repeated for each wave probe to obtain calibration curves necessary. (figure 6.1.6)

The polynomial was used to determine the surface elevation of the water as the wave passed.

```
                    ┌─────────────────┐
                    │ Install         │
                    │ Wave probes (WP)│
                    │ in channel      │
                    └────────┬────────┘
                             │
┌─────────────┐    ┌─────────▼───────┐    ┌─────────────┐
│ Adjust      │───▶│ Balance WP      │◀───│ Adjust WP   │
│ sensitivity │    │ amplifier       │    │ height      │
└─────────────┘    └─────────┬───────┘    └─────────────┘
      ▲                      │                    ▲
      │            ┌─────────▼───────┐  Out of     │
      └────────────│ Pass test       │──range──────┘
                   │ wave            │
   incorrect       └─────────┬───────┘
   sensitivity               │
                             │         ┌─────────────────┐
                             │◀────────│ Record ht. of   │
                             │         │ WP and output   │
                   ┌─────────▼───────┐ └────────▲────────┘
                   │ WP calib. to    │ No  ┌────┴────────┐
                   │ max. wave ht?   │────▶│ Lower WP    │
                   └─────────┬───────┘     └─────────────┘
                             │
                            Yes
                             │         ┌─────────────────┐
                             │◀────────│ Record ht. of   │
                             │         │ WP and output   │
                   ┌─────────▼───────┐ └────────▲────────┘
                   │ WP calib. to    │ No  ┌────┴────────┐
                   │ min. wave ht?   │────▶│ Raise WP    │
                   └─────────┬───────┘     └─────────────┘
                             │
                            Yes
                             │         ┌─────────────────┐
                             │◀────────│ Record ht. of   │
                             │         │ WP and output   │
                   ┌─────────▼───────┐ └────────▲────────┘
                   │ Balanced WP     │ No  ┌────┴────────┐
                   │ amplifier?      │────▶│ Lower WP    │
                   └─────────┬───────┘     └─────────────┘
                             │
                            Yes
                             │
                   ┌─────────▼───────┐
                   │ Calibration     │
                   │ complete.       │
                   └─────────────────┘
```
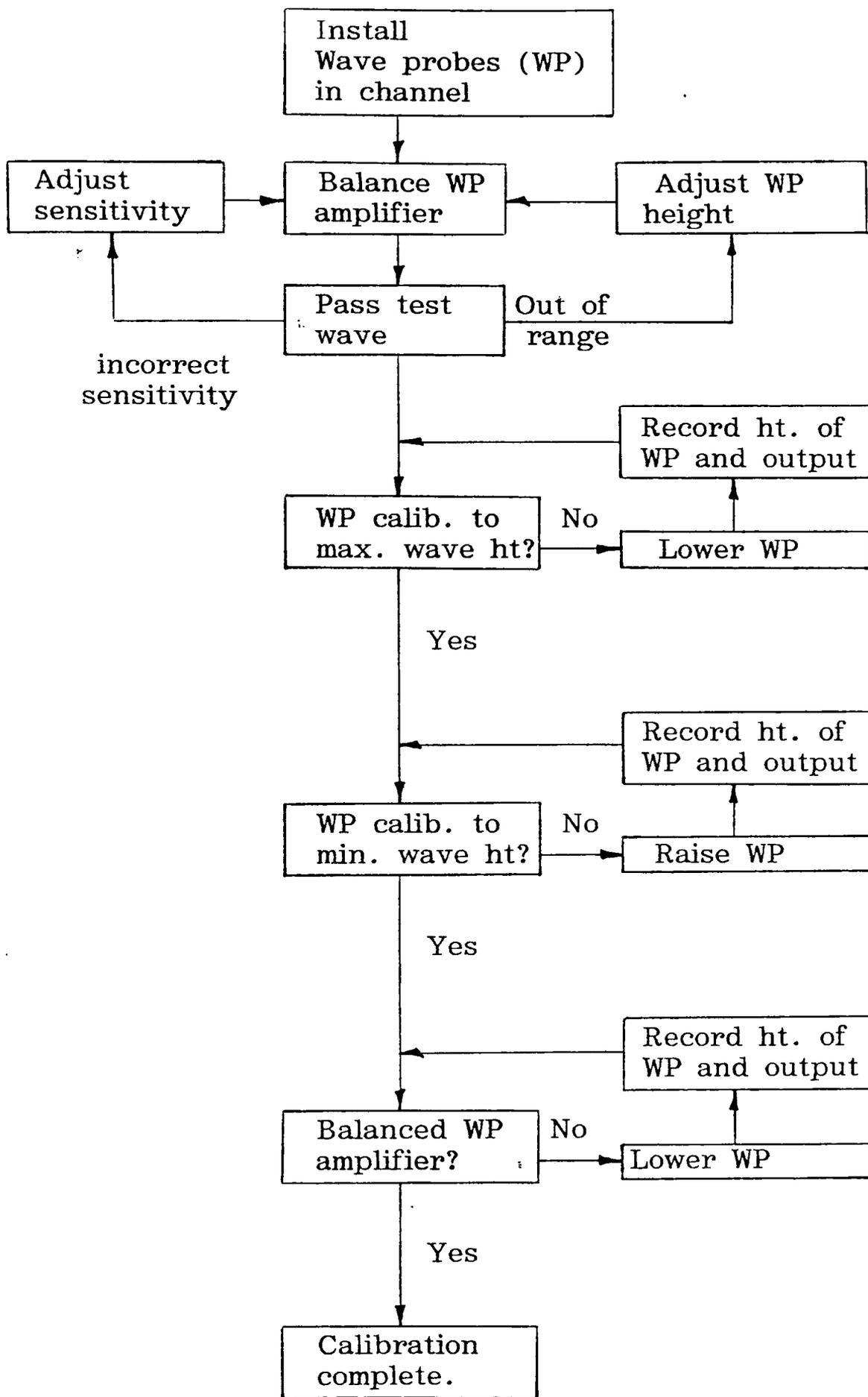
Figure 5.6 – Flow chart showing the procedure used
to calibrate the wave probes.

5.3 Manipulation of wave force, fluid velocity and wave profile data

As the transducers were located at several positions along the channel (i.e. the wave probes and Hot Film sensor were some distance from the cylinder) and because of phase shifts introduced by the amplifiers used, it was necessary to shift the data records of the transducers to an orientation as if the transducers were coincident. Left uncorrected this would obscure some of the history and cumulative effects in the wave data records. The corrections were small, consequently it could be assumed that the wave characteristics were constant over the test section.

The Hot Film sensor and the strain gauges on the cylinder had imperceptible phase shifts, their response being practically instantaneous. The data records were only corrected for position along the channel.

The wave probe output records had to be corrected for both position and phase shift, the latter being sensibly constant over the range of frequencies encountered here. (figure 6.4)

Corrections were made by calculating the required shift in time to each transducer output, according to its distance from the submerged cylinder and the wave celerity. Allowing for any phase shift introduced in amplifying and filtering the transducer signal it was found that peak fluid velocity occurred at wave peak as expected.

5.4 Introduction

Having performed all necessary calibration manipulations and corrections to the data, the wave parameters and characteristics of interest were computed and presented. A flow chart relating the physical movement of data to the logical view is included in figure 5.7.

5.4.1 Overview of test procedure and data analysis

The tests were carried out in four parts

1 - Calibration and set up of fixed transducers, called 'C' data.
(e.g. wave probes, cylinder, potentiometer, etc.)

2 - Calibration of HFA immediately prior to wave generation, called 'R' data.

3 - Measurement of wave characteristics, called 'W' data.

4 - Analysis and presentation of results.

5.4.2 Calculation of Wave amplitude

For each set of wave profile data a polynomial was fitted through the twenty one points symmetrical about the apparent wave profile peak.

Logical view   **Physical view**

Transducer
Calibration   'C' DATA

                    Calib. for
                    Tachogenerator
                    Potentiometer
                    Microswitches

                                     Calib. for
                                     Cylinder
HFA   Waveprobes
Calibration   'R' DATA

Wave
Generation   HFA Calib.   'W' DATA
                (linear &
                nonlinear)

Anymore?
                                     Wave profile
         Yes   Fluid vel. data
                                     Force measurements

No

Analysis &   Basic Analysis Programs
Presentation

                  Wave profile   Celerity
Wave amp.   Vel. profile   Amplitude
y_o Vert.& Horiz.Force   Attenuation

Wave attn. (Keulegan)
Wave profile (Bousq.)   Further analysis and
Celerity (Boussinesq)   comparison with theory
Fluid vel. (McCowan)

                Morison's coeff.   Keul.& Carp.nos.
                Reynold's nos.   Wave characteristics
                Wave profile   Fluid vel. profile
                Force profiles

Figure 5.7 - Flowchart showing procedure for
             calculating wave parameters and
             characteristics.

The highest numerical value was not necessarily the wave amplitude. Noise and other irregular signals frequently gave a local high in the data output, sensibly higher than the average value of the signal at that instant.

By fitting a polynomial through the apparent wave peak the actual wave amplitude and the time of the peak was found. This was repeated for the other two sets of wave probe data generated during the passage of the wave.

5.4.3 Calculation of celerity

The celerity calculated and used in subsequent analysis was the average of wave speeds calculated for the passage of the wave between two sets of wave probes. Wave profile data from three wave probes together with the corresponding calibrations were used in the calculations.

Using the distances in metres between the wave probes, wave speeds were calculated between the first and second wave probe. Also between the second and third wave probes. The two values were then averaged to give the wave celerity used in subsequent calculations.

The wave amplitudes recorded at each wave probe were used in Boussinesq's equation to calculate a theoretical wave speed.

5.4.4 Presentation of wave characteristics

Since the computer programme determined wave celerity using the wave profile measured at three locations, it was extended to plot the three wave profiles in the same spatial relation as the positions of the wave probes in the channel. The measured profile was plotted along with that calculated using the theory of McCowan for a wave with the same amplitude. This graphical output (with wave amplitudes) show how the wave changes shape with distance from the point of generation. (figure 6.6 to 6.17)

The nonlinear and linearised Hot Film Anemometer calibration data with the fitted curves were plotted (figure 6.21) as was the measured wave profile and that according to Boussinesq.

5.4.5 Computation of Cd and Cm

Force coefficients were calculated in three different ways;

1. Cd at zero acceleration; Cm at peak acceleration

2. using a least squares analysis (LSA) to fit Morison's equation to measured forces

3. by solving Morison's equation across the wave crest

Discussing each in turn, firstly calculating Cd and Cm at zero and peak acceleration respectively

Morison's equation is given as;

$$F = \tfrac{1}{2}Cd\rho Du|u| + \tfrac{1}{4}Cm\rho\pi D^2\dot{u} \qquad 5.1$$

$$F = A_m\dot{u}Cm + B_mu^2Cd \qquad 5.2$$

where the constants, A_m & B_m, are related to physical quantities.

At zero acceleration (peak velocity) Morison's equation reduces to

$$F = B_mu^2Cd \qquad 5.3$$

With the computer, Cd was calculated for each wave using velocities measured with the Hot Film Anemometer. The calibration curve determined immediately prior to generating the wave was used.

Assuming Cd constant through the wave, Cm may be calculated at any other position. Peak acceleration was chosen since it may be assumed that inertia effects are maximum giving higher accuracy for the value of Cm calculated.

To calculate the acceleration, the computer fits a high degree polynomial to fluid velocities measured with the Hot Film Anemometer. The polynomial is used to smooth the velocity history and is of no physical significance. It was then differentiated twice and used to compute the time of maximum acceleration. Hence the fluid velocity and acceleration was calculated.

Cm was found by substituting in Morison's equation the measured force and the value of Cd at zero acceleration.

Using these values of Cd and Cm, horizontal forces were calculated for the entire wave using Morison's equation and compared with those measured. At zero and peak acceleration measured and calculated forces coincide because Cd and Cm were calculated at these points.

Forces are plotted non dimensionally using $F/(\frac{1}{4}aD^2g\rho)$ in an attempt to reduce dependance on the size of the cylinder.

The second method for calculating Cd and Cm is outlined in appendix A.

The analysis involves the theory of "least squares" analysis of the measured horizontal force. The square matrix is determined by summing products of fluid velocity and acceleration for each point in the wave included in the analysis. This was inverted using the Gauss-Jordan method as a standard routine for inversion. A value for Cd and Cm was found as a product of the sum of forces multiplied by the inverted matrix. These were valid for the entire wave.

As before the values of Cd and Cm were substituted back into Morison's equation to calculate forces which were non dimensionalised and plotted with those measured.

The last method of calculating Cd and Cm was by solving Morison's equation simultaneously across the wave crest. This was in the belief that though Cd and Cm may change as the wave moves past the cylinder their value being immediately a product of the fluid velocities.

If it were possible to generate a wave of perfect solitary form, fluid velocities and accelerations would be equal in magnitude across the wave crest, though the accelerations would be of opposite sign. This was not the case with the waves generated in the laboratory since they often exhibited a degree of asymmetry. Consequently fluid velocities and the computed accelerations were used here.

Values for Cd and Cm were computed using measured fluid velocities, derived accelerations and measured horizontal forces. (Appendix B)

This gave a series of values for Cd and Cm through the wave that matched values of measured and calculated forces. Consequently, there was little to be gained by plotting these.

Since the values of Cd and Cm are assumed to be a direct result of the fluid velocities, Cd and Cm were plotted against Reynolds and Keulegan and Carpenter numbers which themselves change as the wave passes. Both are non-dimensional and therefore can be plotted directly.

5.4.6 Ratio of Drag/ Inertia, F_d/F_i

The total horizontal force on a cylinder as given by Morison's equation 5.1, separates into drag and inertia forces, F_d and F_i respectively. The ratio F_d/F_i gives an indication as to the level of confidence that may be given to the drag and inertia coefficients calculated for a particular solitary wave.

From 5.1

$$F_d = \tfrac{1}{2} Cd \rho Du|u| \qquad\qquad 5.4$$

$$F_i = \tfrac{1}{4} Cm \rho \pi D^2 \dot{u} \qquad\qquad 5.5$$

Substituting $u=Uc$, $Z=z/y_o$ and $X=x/y_o$, with U given by equation 3.27, equation 5.4 becomes:

$$F_d = \tfrac{1}{2} Cd \, \rho Dc^2 N^2 \frac{(1+\cos Mz/y_o \cdot \cosh Mx/y_o)^2}{(\cos Mz/y_o + \cosh Mx/y_o)} \qquad 5.6$$

F_d reaches a maximum at wave crest (x=0) where equation 5.6 reduces to:

$$F_d = \tfrac{1}{2} Cd \rho Dc^2 N^2 / (1+\cos Mz/y_o)^2 \qquad 5.7$$

To calculate the maximum value for F_i, the position x, at which $\delta u/\delta t$ is a maximum can be found from equation 3.33. Determining these using an analytical approach is complicated, therefore a numerical analysis has been used which gives:

$$\delta u/\delta t = c^2 NM/5y_o \qquad\qquad 5.8$$

which agree to within 10% of experimental results.

Consequently equation 5.5 reaches:

$$F_i = \tfrac{1}{4} Cm \rho \pi D^2 c^2 NM / 5 y_o \qquad 5.9$$

at maximum. Consequently using equation 5.7 and 5.9

$$F_d / F_i = 10 y_o CdN / Cm \pi DM (1 + \cos Mz / y_o)^2 \qquad 5.10$$

Taking $1/\pi (1 + \cos Mz / y_o)^2$ approximating to $1/10$, consequently:

$$F_d / F_i \approx N/M \cdot y_o / D \cdot Cd / Cm \qquad 5.11$$

For oscillatory waves a definition of Nkc is

$$Nkc = \pi H / D \qquad 5.12$$

$$\text{or} \qquad Nkc = F_d / F_i \cdot Cm / Cd \cdot \pi^2 \qquad 5.13$$

Substituting for F_d / F_i as given in 5.11, 5.13 becomes

$$Nkc = N/M \cdot y_o / D \qquad 5.14$$

Consequently this parameter is the equivalent Keulegan Carpenter number for the solitary wave case. Applying the range of sensitivity used for oscillatory waves

$$Nkc < 5 \qquad F_d / F_i < 10\% \qquad \text{inertia regime}$$

$$Nkc > 25 \qquad F_d / F_i > 90\% \qquad \text{drag regime}$$

the confidence level in values of Cd and Cm with Nkc can be determined.

In oscillatory fluid motion, the Keulegan-Carpenter number is usually taken as the amplitude of fluid motion relative to the cylinder size. This is expressed as $u_m T/D$, where u_m and T are the velocity amplitude and period of flow respectively.

For a solitary wave, T is infinite but may be approximated as λ/c giving

$$Nkc = u_m \lambda /c.D \qquad 5.15$$

From experiments performed here, Nkc as defined in 5.15 can be found by multiplying the values presented in this thesis by approximately "3".

5.5 Summary

A method of

- scanning
- logging
- manipulating
- analysing

and presenting

results are given here. The use of a structured systematic approach has ensured the consistency and quality of results. Through the analysis of large quantities of detailed wave and force data, results can be presented (chapter 6) which are comprehensive and accurate. The procedures detailed here enable a clear and confident discussion in chapter 7.

CHAPTER 6   EXPERIMENTAL RESULTS

6.1 Introduction

The first chapters of this thesis give an introduction to the investigation undertaken here, with a description and classification of the waves and wave loadings expected. Consideration of the nature of these waves and imposed forces led to the development of techniques capable of collecting and reducing data to a useful form. The following chapters present and discuss the data gathered in the course of the experiments.

This chapter contains the experimental results gathered on horizontal cylinders under solitary waves aligned parallel to the wave crests. The cylinder varied both in diameter and in position above the channel bed.

6.2 The Waves

6.2.1 Introduction

The data gathered on the solitary wave mostly relate to its shape and how this changed relative to Boussinesq's theory with height and position along the channel.

A full description is given of the changes observed in the wave shape as it progressed along the channel. Descriptions of the wave are presented in the following amplitude bands.

$$a/y_o \leq 0.20$$
$$0.20 < a/y_o \leq 0.25$$
$$0.25 < a/y_o \leq 0.30$$

$$0.30 < a/y_o \leq 0.35$$
$$0.35 < a/y_o \leq 0.40$$
$$0.40 < a/y_o \leq 0.45$$
$$0.45 < a/y_o \leq 0.50$$
$$0.50 < a/y_o$$

Wave attenuation data is presented as wave heights at wave probes and as gradients between adjacent wave amplitude measurements. Wave celerity calculated between adjacent wave probes is presented, as are the average values used in subsequent calculations.

The waves generated past cylinders of four different diameters gave Reynolds and Keulegan & Carpenter in the range:-

$$2,800 \leq Re \leq 26,000$$
$$1.0 \leq Nkc \leq 10.0$$

6.2.2 Wave Probe Calibrations

Figures 6.1 and 6.2 show typical wave probe calibration graphs. The graphs show measured elevations of the water surface plotted with the corresponding digitised response of the wave probe amplifier. Measured points at centimetre raising/lowering of the water surface were fitted with a fifth order polynomial. The response was linear within experimental tolerances of $+-0.5$mm (or approximately $+-0.003$ in a/y_o) for a calibrated range of -50mm to +100mm water elevation.
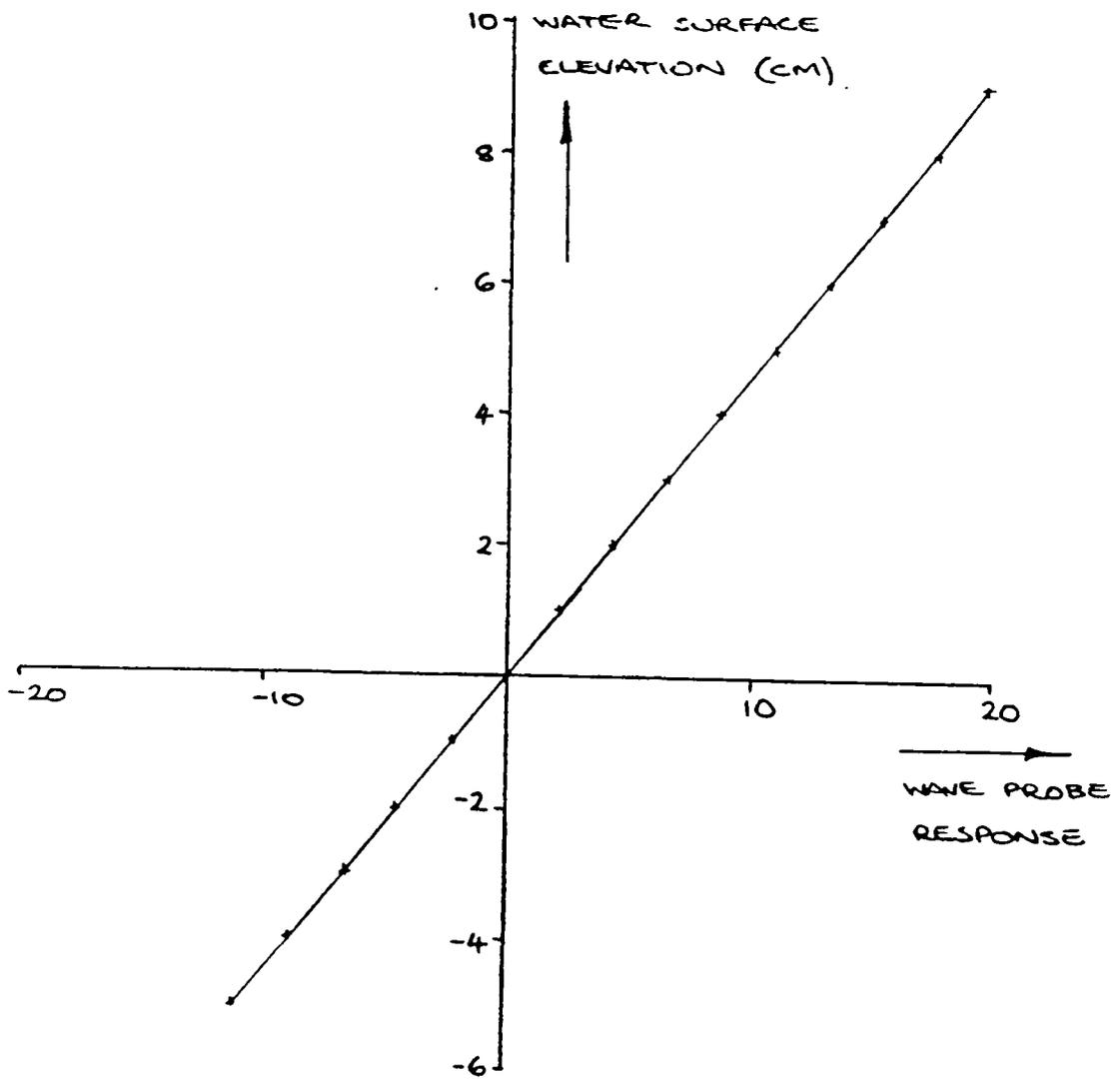
Figure 6.1 - Wave probe calibration graph
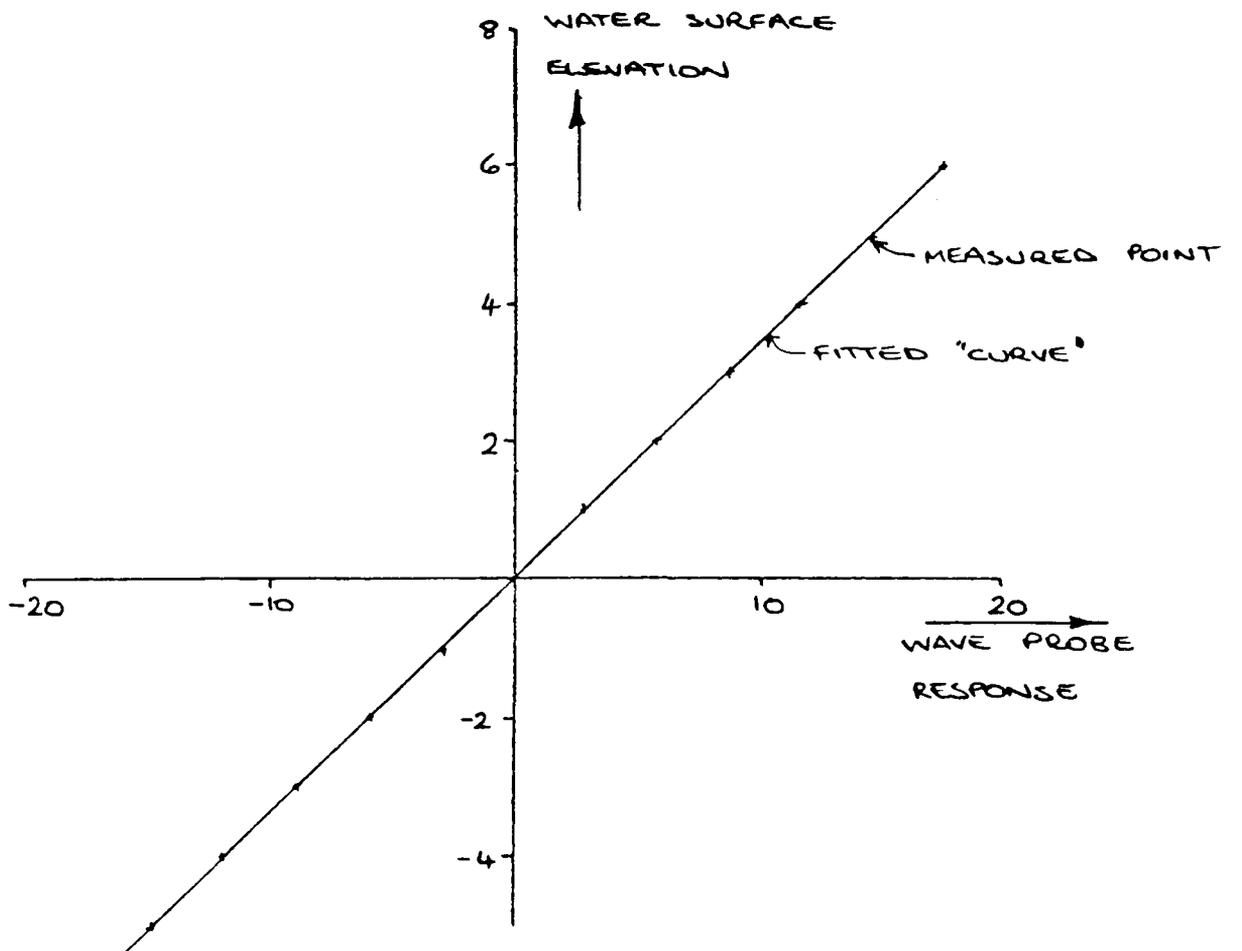
Figure 6.2 - Wave probe calibration graph

A dynamic calibration of wave probe response up to 1Hz showed a 3% under estimate of the wave amplitude from the scanned output. (figure 6.3) This is equivalent to approximately 2mm for a wave of 70mm amplitude (a/y_0 approximately 0.5).

The dynamic calibration also showed a phase shift was introduced by the wave probe amplifier of approximately 0.038 secs. for the frequencies up to 1Hz. (figure 6.4) This phase shift was corrected in the presentation of wave profile data.
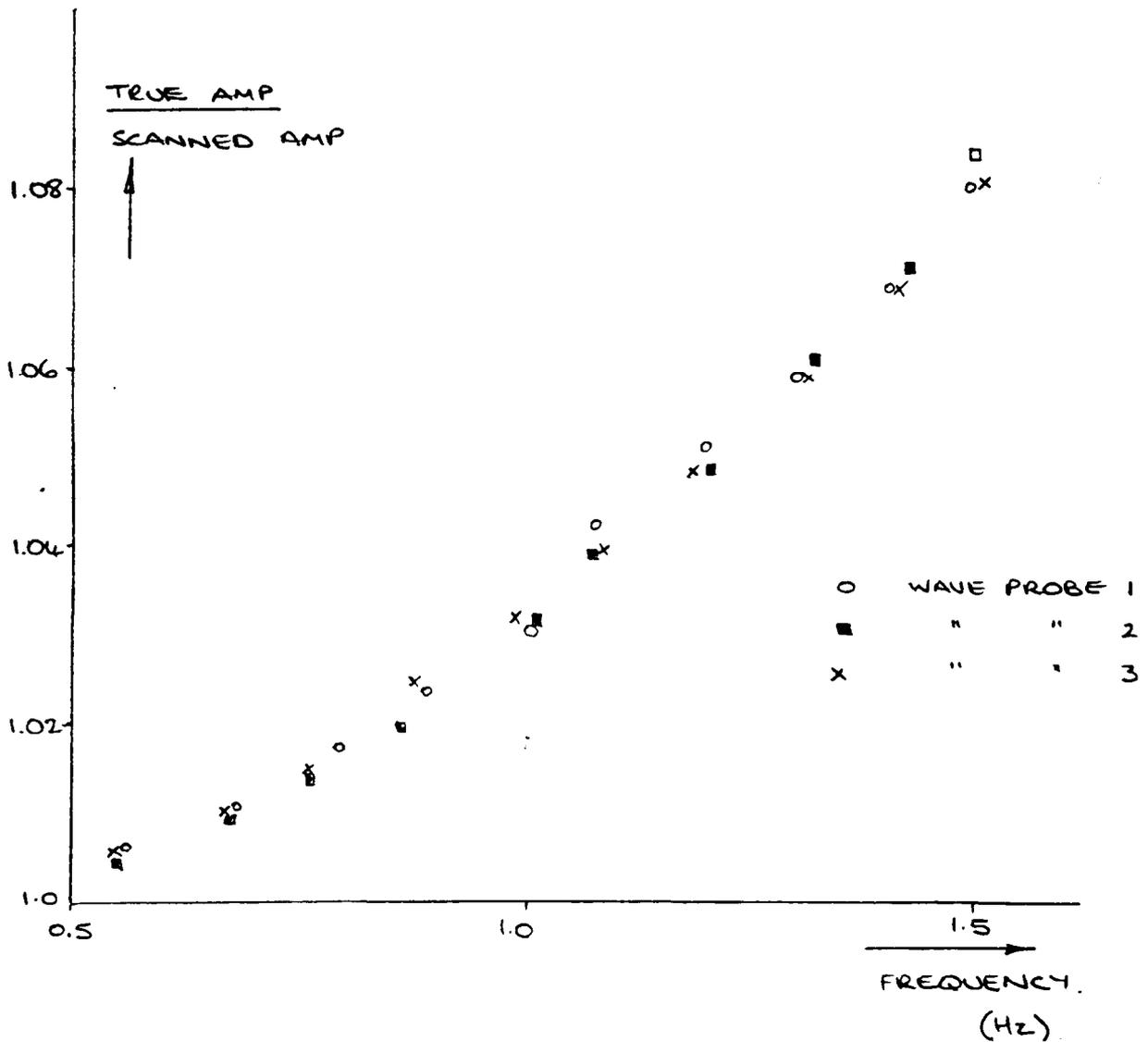
Figure 6.3 - Amplitude reduction with wave frequency.
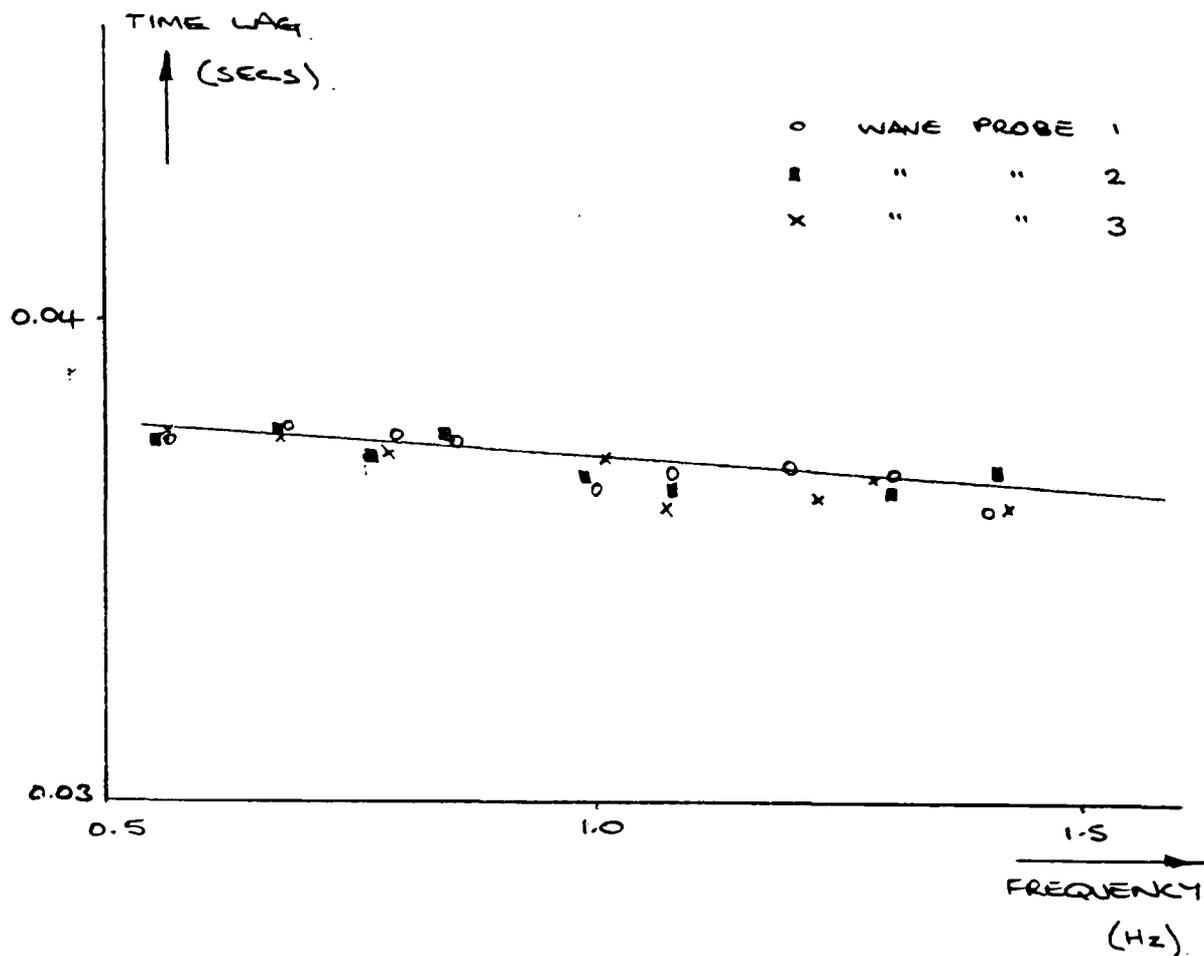
Figure 6.4 - Phase shift with wave frequency.

6.2.3 Wave Profile

The wave profile was determined at three positions along the channel. Results are presented as the time variation of surface elevation at these positions within the water. For simplicity these positions are numbered 1, 2 and 3, position No.1 being closest to the wave generator.

Wave generator at chainage (approx.)	19.4m
Wave probe No.1 at chainage (approx.)	6.4m
Wave probe No.2 at chainage (approx.)	5.7m
Cylinder at chainage (approx.)	5.5m
Wave probe No.3 at chainage (approx.)	3.3m

These chainages are 'approximate' and are only intended to act as a guide. The accurate position of a wave probe and generator changed between successive tests. The accurate positions were determined at the time of testing and vary by

- 152 -

only small amounts from those given above relative to the length of the wave.

Figure 6.5 labels the information presented for each set of results. The measured values are shown by an asterix (*) and are compared with the wave profile calculated using Boussinesq's theory, shown as a solid line.

The measured values are the time variation of water surface elevation as the wave moves down the channel, wave probe no.1 being closest to the wave generator. In essence the graph shows a 5sec. time slice of the life of the wave as recorded at three positions along the channel. It is not a true pictorial representation of the wave at a moment in time, though it can be considered a close approximation.

The calculation of wave amplitudes is covered in section 5.4.2, their manipulation is covered in section 5.3.

Results for waves with $a/y_o <= 0.2$ (figure 6.6) showed good agreement with the theory of Boussinesq over the main part of the wave (i.e. between points of surface profile inflection). The surface profile at the rear of the wave in all three positions showed trailing depressions. The effect of these depressions of the main portion of the wave diminished as it moved down the channel but never ceased (figure 6.6). This was most noticeable for the very low waves $a/y_o < 0.15$.

The correlation between the measured wave profile and that calculated over the length of the wave was good. Generally, agreement improved as the wave moved along the channel. The effect of trailing disturbances was greater as the wave amplitude decreased.
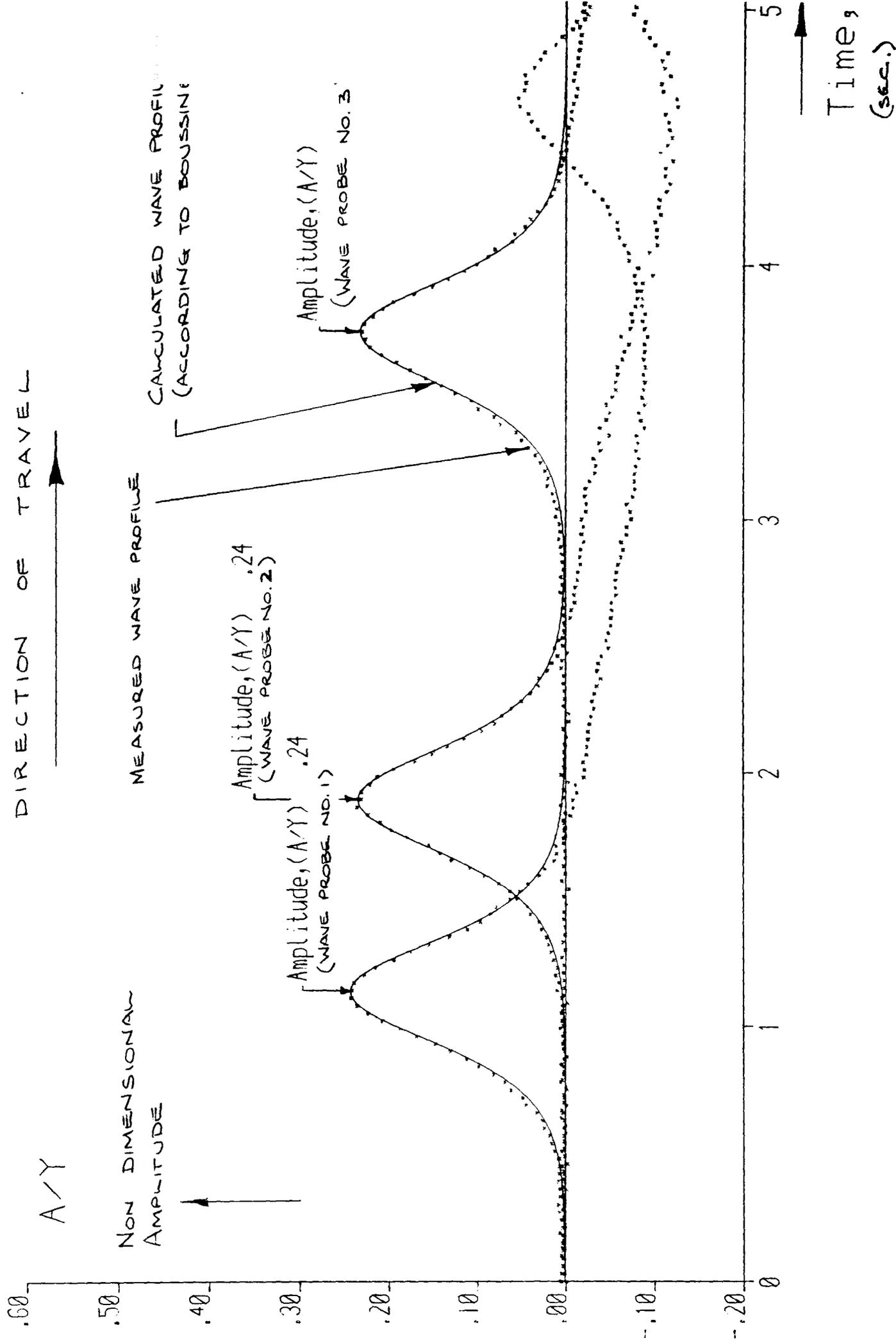
Figure 6.5 - Measured and Boussinesq wave profiles
Cyl. dia., $D/y_o = 0.20$; $z_c/y_o = 0.22$

- 154 -
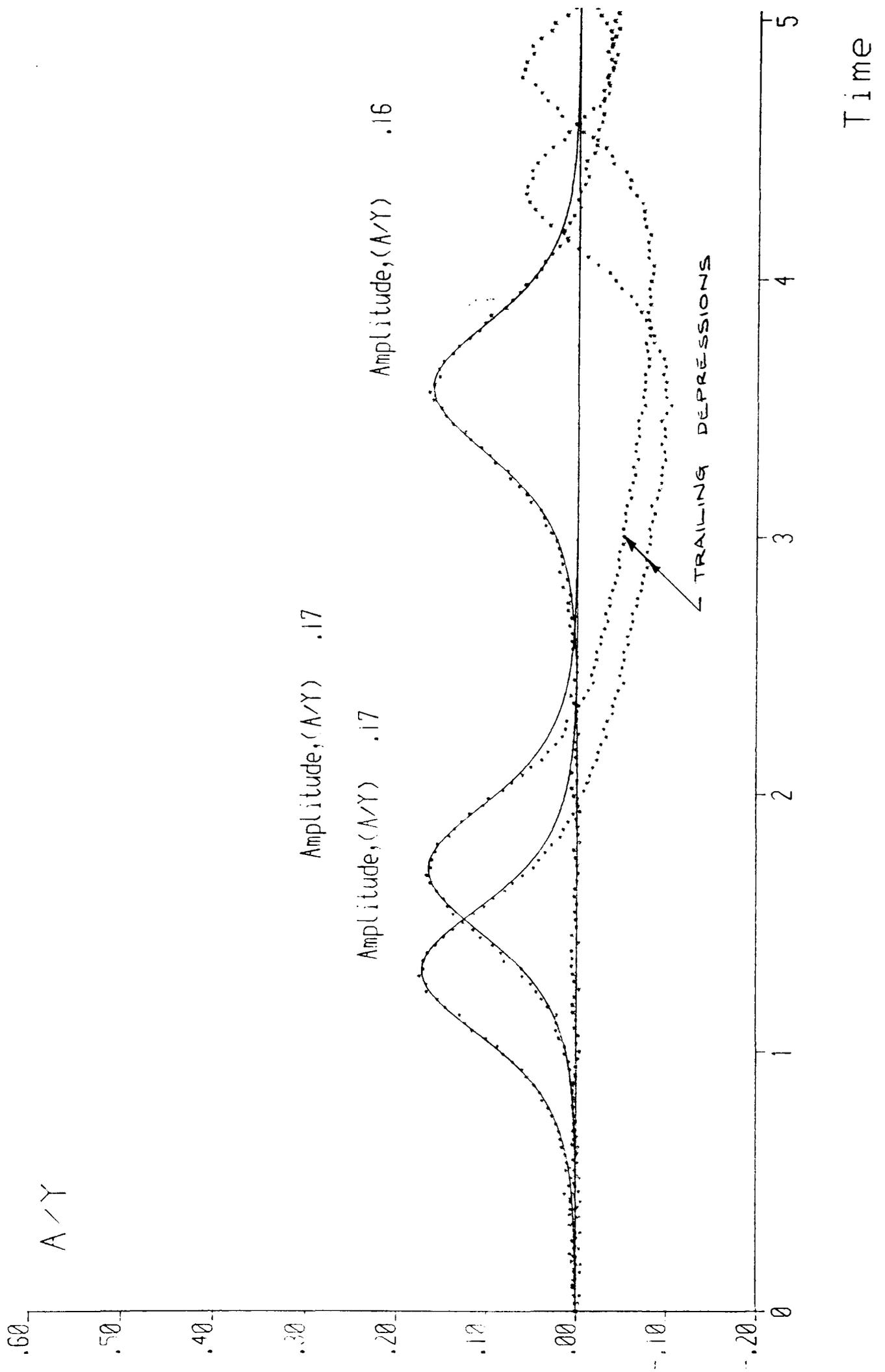
Figure 6.6 - Measured and Boussinesq wave profiles
Cyl. dia., $D/y_o=0.07$; $z_c/y_o=0.78$

- 155 -

For waves with $0.2 < a/y_o \leq 0.25$ (figure 6.7/ 6.8) agreement was good over the central portion of the wave as previously. The measured surface profile shows a small elevation at the front of the wave and depression at the rear, for position No.1 (figure 6.7). As the wave moved along the channel their was no significant improvement in agreement at the front or rear of the wave.

With $0.25 < a/y_o \leq 0.3$ (figure 6.9/ 6.10) measured wave profiles were generally higher than theory over the front part of the wave (figure 6.9). This is a significant change over figure 6.8 with only a 13mm increase in amplitude. As before, agreement with theory was best over the central portion of the wave.

At the rear of the wave trailing depressions lowered the measured profile below the theoretical profile.

For waves with $0.3 < a/y_o \leq 0.35$ (figure 6.11/ 6.12) agreement with theory at the front of the wave was poor. The measured surface profile was higher than theory the difference reducing to the wave crest (figure 6.11). At the rear of the wave the measured profile was initially higher than theory, but as before the trailing disturbances took the measured surface below that predicted by theory (figure 6.11). As the effect of these disturbances diminished a small 'lump' appeared at the rear of the wave where surface curvature was greatest (figure 6.11). Waves with $0.35 < a/y_o \leq 0.4$ (figure 6.13) showed little effect from trailing disturbances for each position along the channel.

The wave profile measured at position No.1 was essentially the same as measured at position No.2 both being higher than theory predicted. At position No.3 the wave appeared to have a flatter crest than at positions 1 and 2.
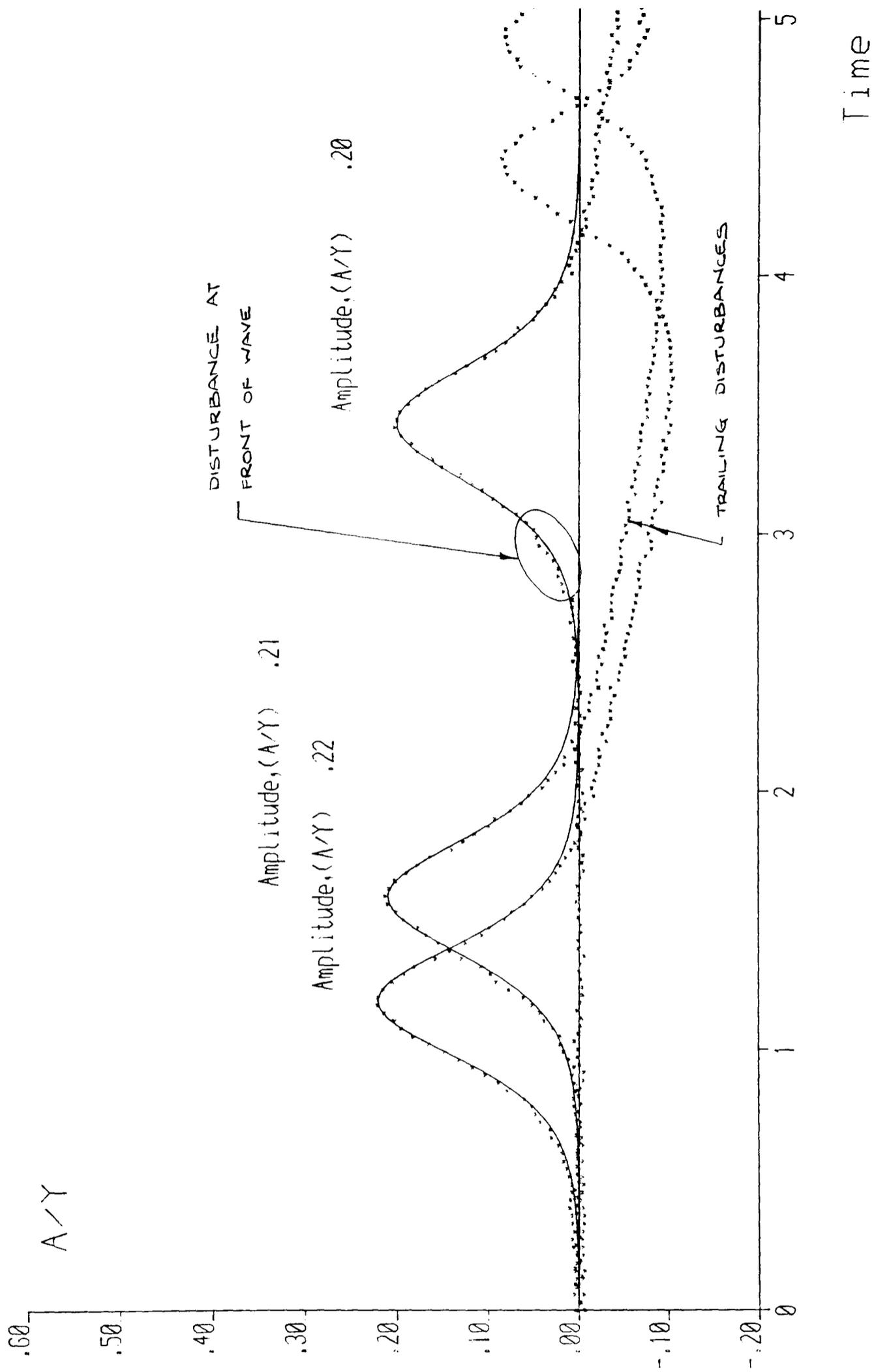
Figure 6.7 - Measured and Boussinesq wave profiles

Cyl. dia., $D/y_o = 0.15$; $z_e/y_o = 0.78$

- 157 -
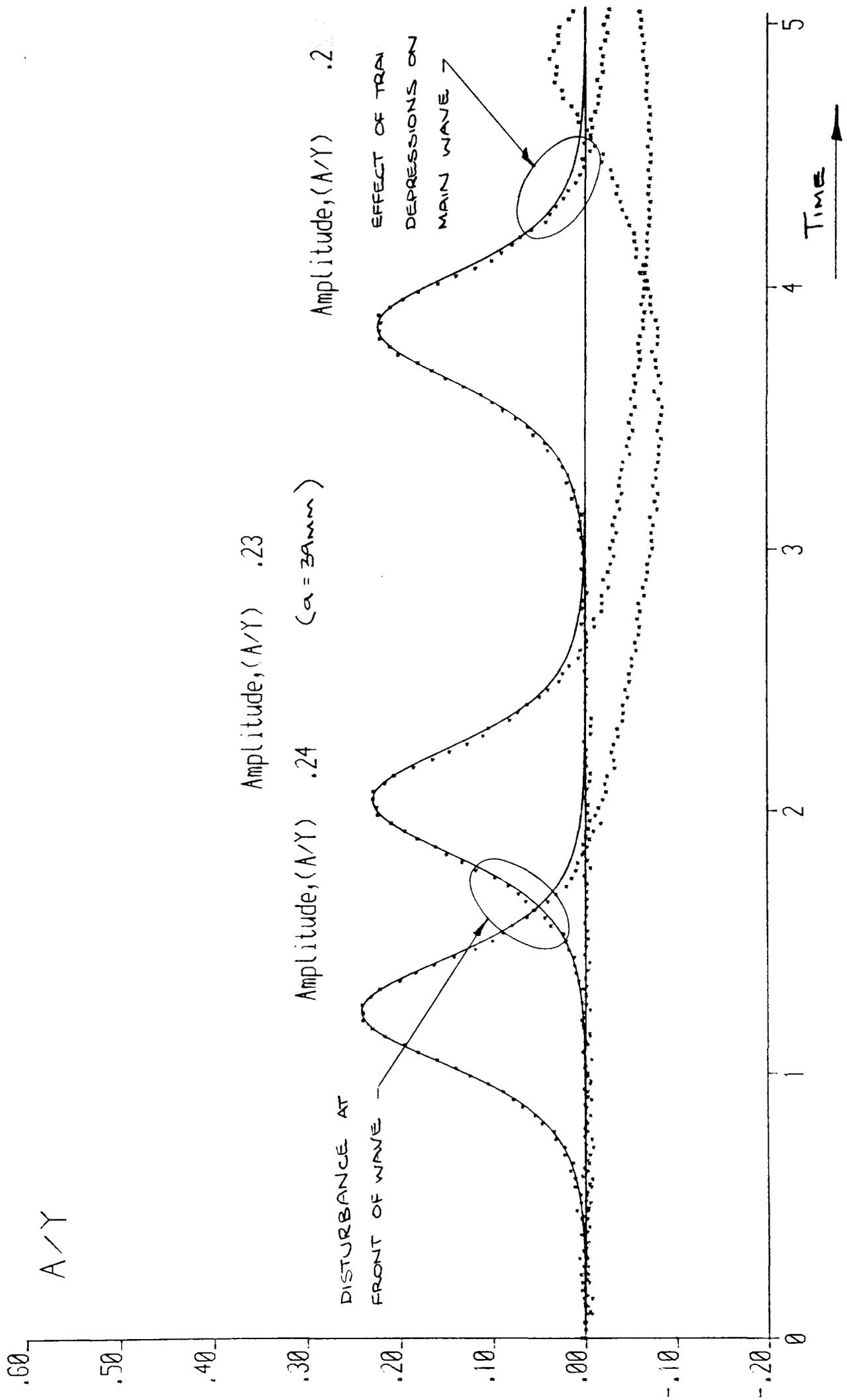
Figure 6.8 - Measured and Boussinesq wave profiles
Cyl. dia., $D/y_o=0.20$; $z_e/y_o=0.52$

- 158 -
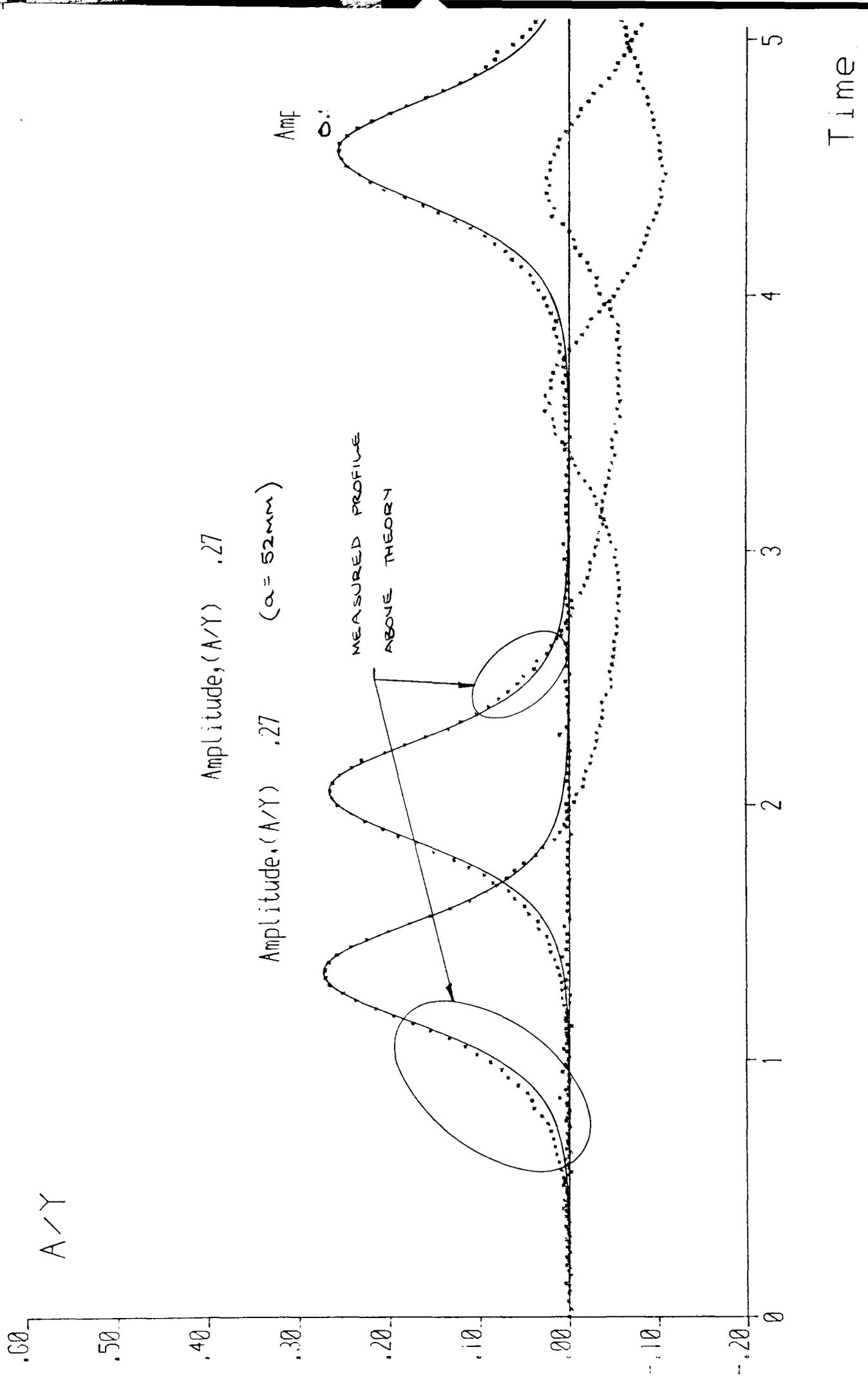
Figure 6.9 - Measured and Boussinesq wave profiles
Cyl. dia.,D/y_o=0.25; z_c/y_o=0.71

- 159 -
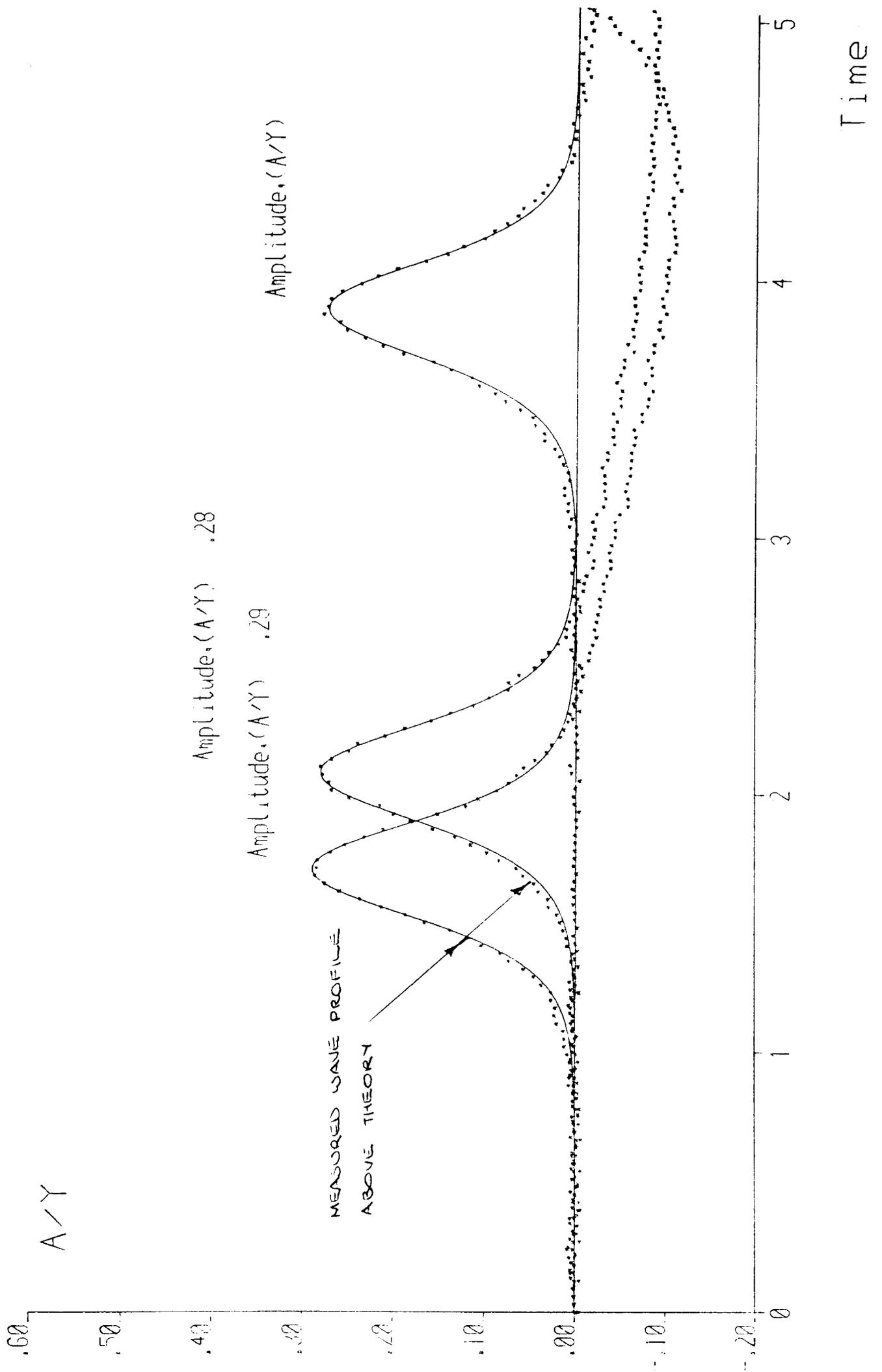
Figure 6.10 - Measured and Boussinesq Wave profiles

Cyl.dia., $D/y_o=0.07$; $z_c/y_o=0.78$
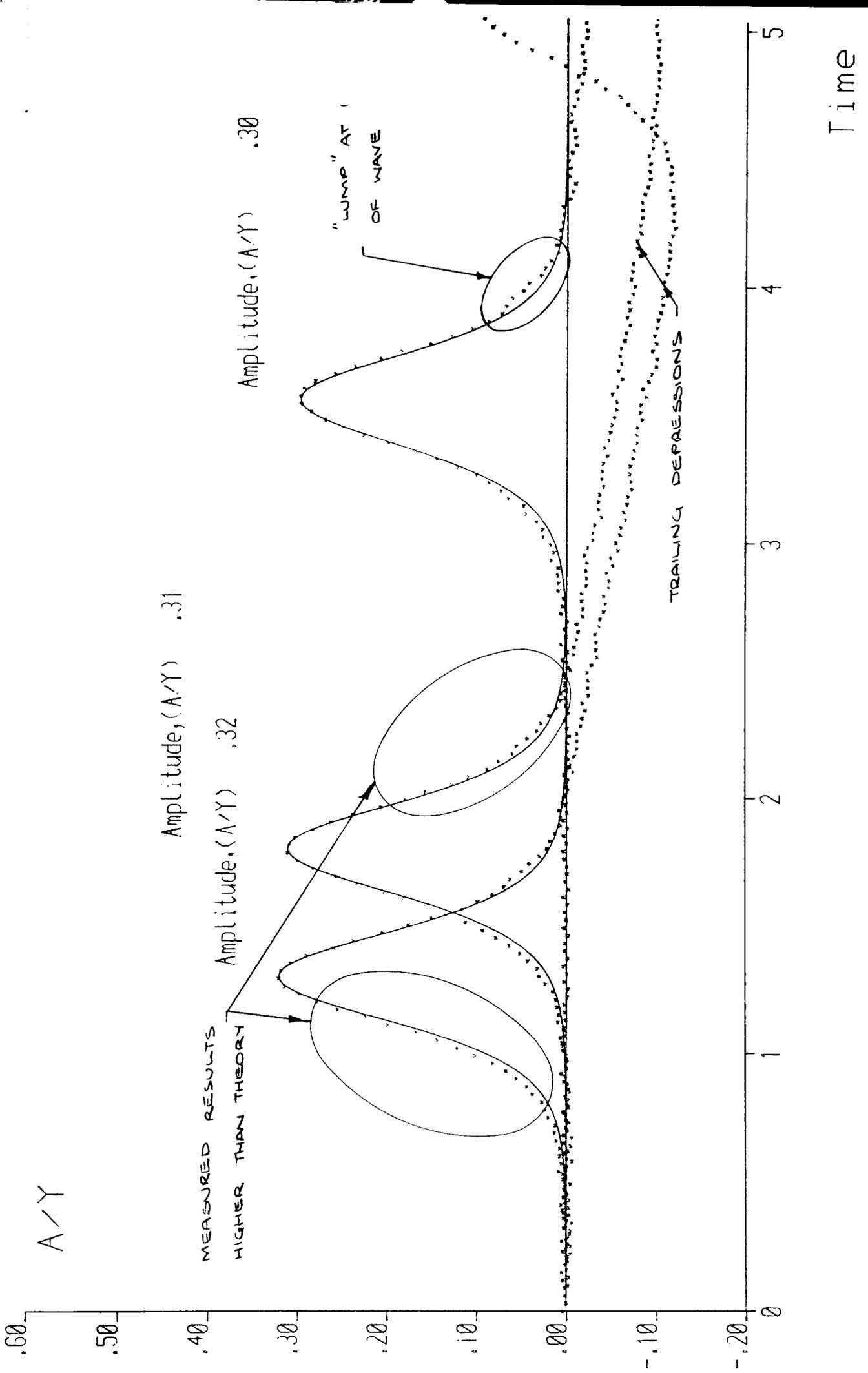
Figure 6.11 - Measured and Boussinesq Wave profiles

Cyl.dia., $D/y_o = 0.15$ $z_c/y_o = 0.78$

- 161 -
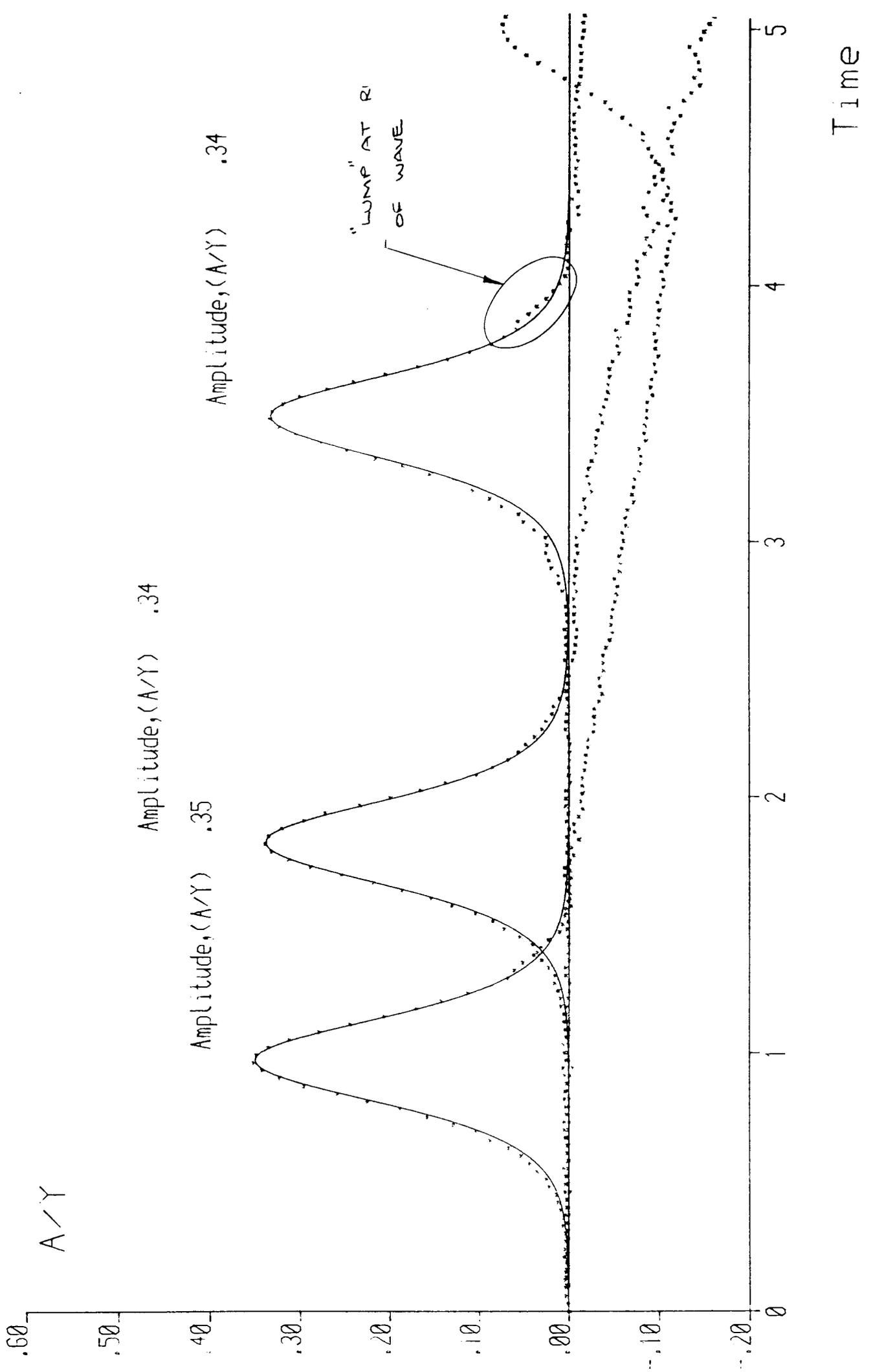
Figure 6.12 - Measured and Boussinesq Wave profiles

Cyl.dia., $D/y_o=0.20$ $z_c/y_o=0.22$

- 162 -
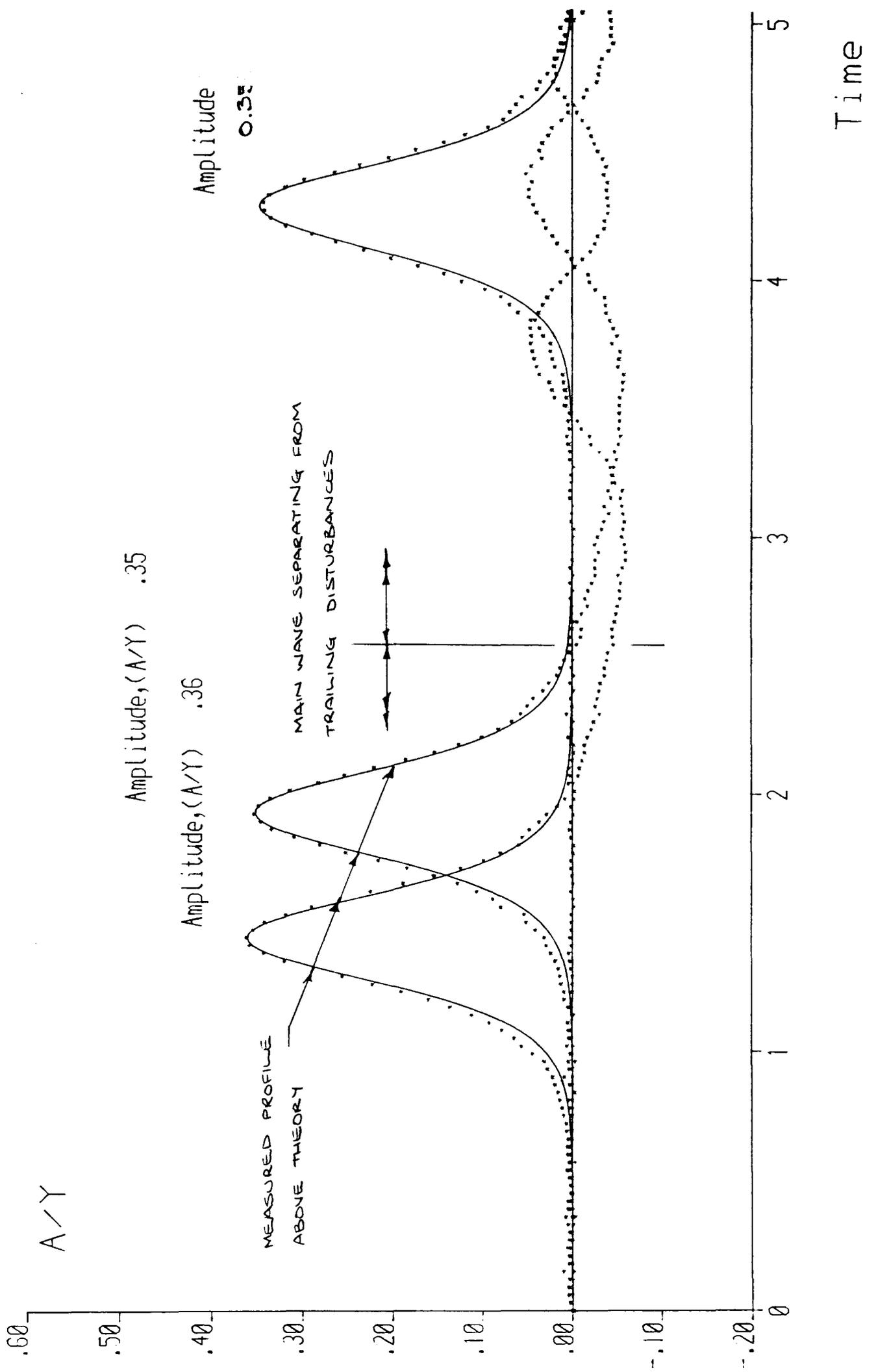
Figure 6.13 - Measured and Boussinesq Wave profiles
Cyl.dia., $D/y_o=0.07$ $z_c/y_o=0.19$

For waves $0.4 < a/y_o \leq 0.45$ (figure 6.14/ 6.15) and $0.45 < a/y_o < 0.5$ (figure 6.16) the measured profiles were consistently higher than theory with small disturbances immediately in front and behind the wave. There was little change in profile as the wave progressed along the channel.

The measured surface profile for waves with $a/y_o > 0.5$ (figure 6.17) was always above that given by theory though by no greater amount than for waves of lower amplitude. Symmetry improved with increasing a/y_o though waves above $a/y_o = 0.55$ were difficult to generate.

Summary

To summarise, low amplitude waves generally showed good agreement with theory of Boussinesq. Disturbances lowered the rear of the generated waves below theory.

As the wave amplitude increased, a disturbance at the front of the wave had an increasing effect generally raising the profile above the theoretical profile up to the wave crest. Above $a/y_o \approx 0.35$ the disturbances at the rear of the wave became separated from the main wave. For higher waves the measured profile was always above theory with a 'lump' in the profile at both the front and rear of the wave. At the rear of the wave trailing disturbances, which were normally below the general shape of the wave, disturbed the wave profile. Their effect diminished with increasing wave amplitude and distance from the wave generator.

High amplitude waves showed evidence of being unstable and were difficult to generate, though their shape was more symmetrical than waves with low amplitude.
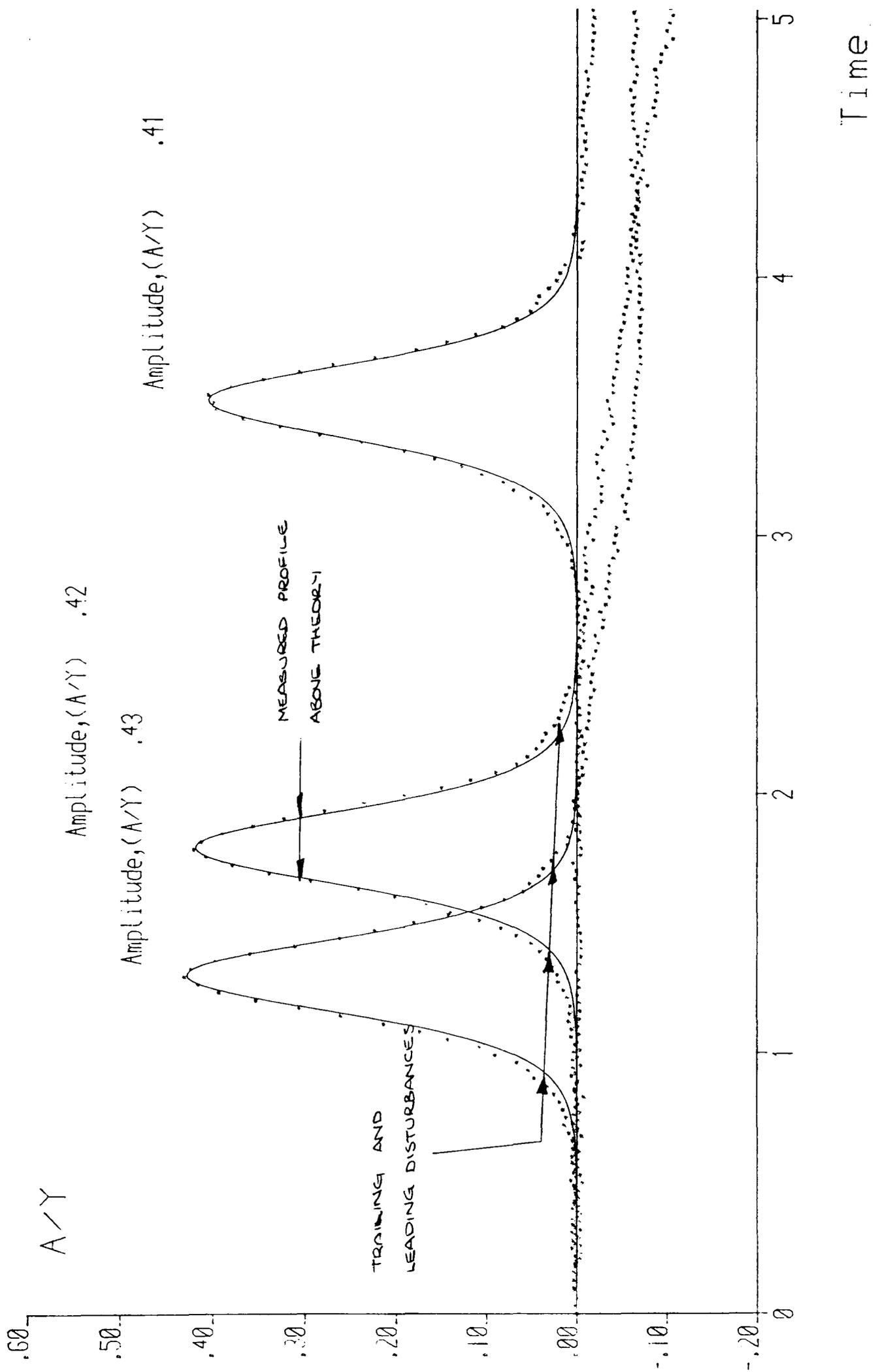
Figure 6.14 - Measured and Boussinesq Wave profiles
Cyl.dia., $D/y_o = 0.16$ $z_c/y_o = 0.51$
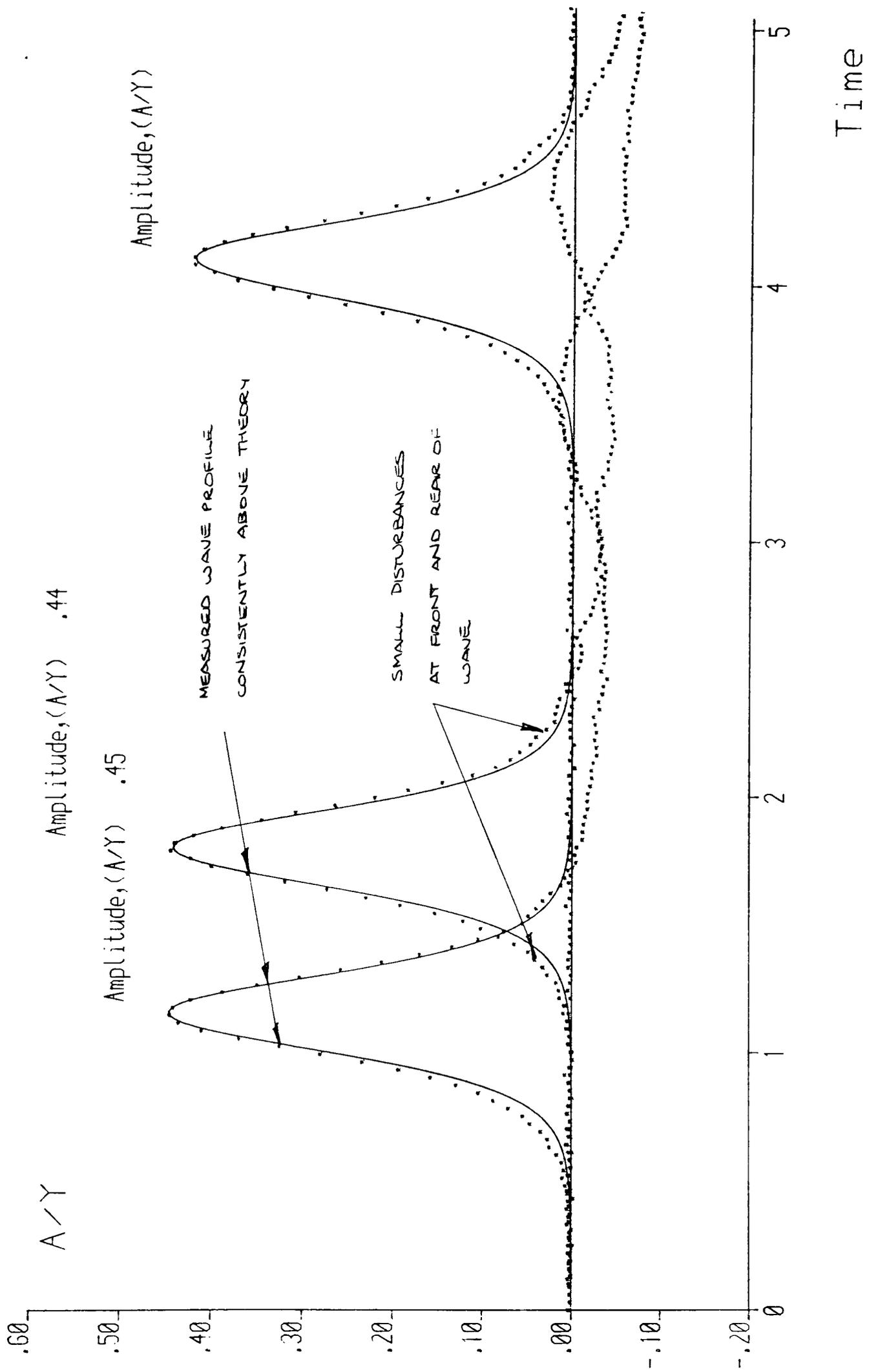
Figure 6.15 - Measured and Boussinesq Wave profiles
Cyl.dia., $D/y_o=0.25$ $z_c/y_o=0.71$
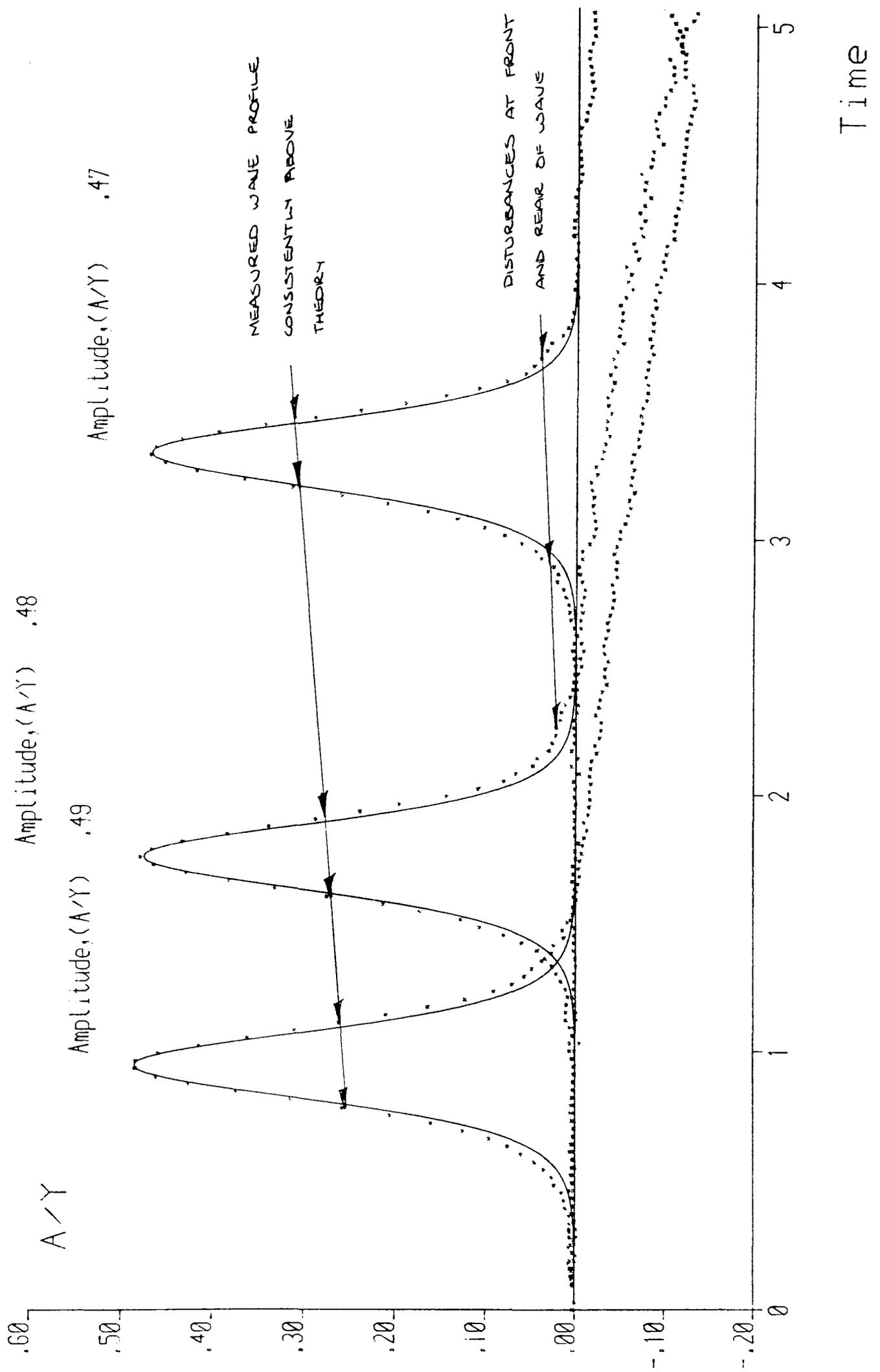
Figure 6.16 - Measured and Boussinesq Wave profiles
Cyl.dia., $D/y_o=0.20$ $z_c/y_o=0.22$
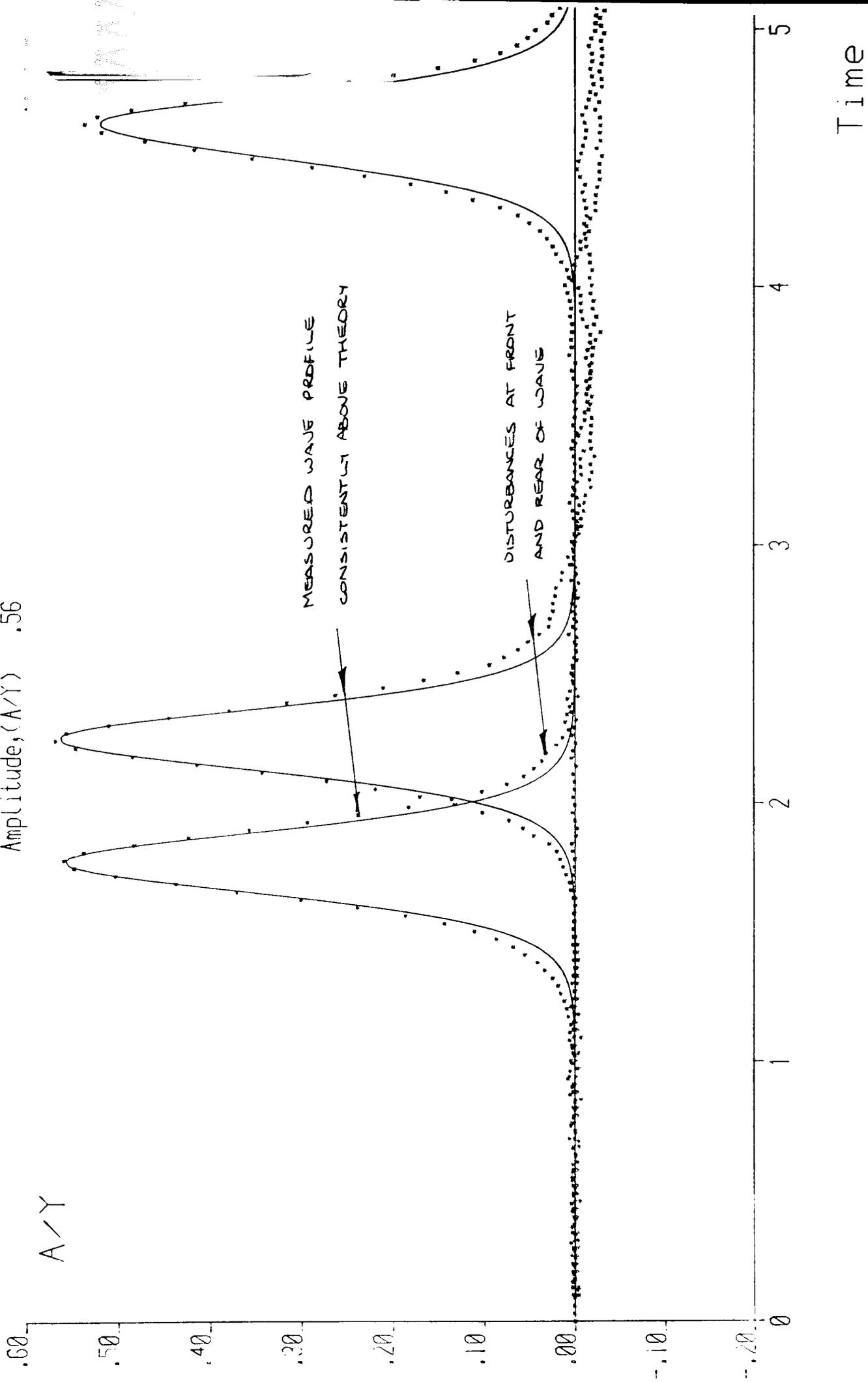
Figure 6.17 - Measured and Boussinesq Wave profiles
Cyl.dia., D/y_o=0.29 z_c/y_o=0.21

- 168 -

6.2.4 Wave Amplitude and Time of Peak

Wave amplitude and the position of the wave crest was determined by fitting a polynomial to the top twenty one points (approximately 200mm either side of the apparent wave crest) symmetric about the maximum measured profile value. Differentiating the polynomial gave the magnitude and position of the 'true' wave crest. This reduced the error in the position of the wave crest to below 0.6 secs (approximately 84mm) and in amplitude below $a/y_o = 0.01$ (approximately 1.5mm).

The actual error in results could not be determined explicitly since it depended upon the accuracy with which the polynomial fit the results and also the degree to which the results were influenced by noise in the signal. Reducing the error in determining the wave amplitude was important since it also reduced the errors in derived quantities (i.e. wave celerity, fluid particle velocity, etc.)

6.2.5 Wave Attenuation

Close inspection of results shows that the wave attenuation was greater between positions 1 and 2, both before the cylinder, than between positions 2 and 3 (after the cylinder - figure 6.5). Typically, the initial wave attenuation gave a gradient between positions 1 and 2 of the order of 0.0015 to 0.0025. No apparent simple correlation between wave amplitude and initial gradient was found. Equally there was no correlation of the gradient between positions 1 and 2 and that between positions 2 and 3. A small number of waves increased in height as they moved down the channel between positions 2 and 3, though no parameters that would predict this effect could be identified, in this study.

As would be expected with a reduction in wave amplitude there was a corresponding reduction in wave celerity. Neither the

reduction in wave amplitude or celerity correlate to Nkc, Re or wave loading.

However there was clear evidence that the wave attenuation may be determined using the theory of Keulegan (1948). For several generated waves Keulegan's equation was used to calculate the amplitude at the adjacent wave probe. Plotting the measured amplitude at wp2 against that predicted (figure 6.18a) shows close agreement between the two values, generally less than 2% error. This agreement was irrespective of initial wave height.

For the 34 and 48mm dia. cylinders close to the free surface, the error increased to between 5% and 10% in wave amplitude at wp3 (after the cylinder). In both cases the generated waves were higher than predicted, demonstrating the effect of the submerged cylinder. It also justified the removal of these test results from this analysis.

To gain such good agreement it was necessary to change the constant of proportionality in Keulegan's equation (equation 7.1) from $1/_{12}$ to unity. This had the effect of increasing the attenuation predicted by theory. This was contrary to other experimental reports which indicate theory over predicts the wave attenuation.

With the constant of proportionality equalling 1/12, the error increases to between 2-5% with the calculated attenuation being less than measured. (figure 6.18a).

Varying the constant of proportionality affects the predicted wave amplitude as shown in figure 6.18b. This demonstrates that above unity the predicted wave amplitude is only slightly changed. Consequently in the absence of any other information it appears satisfactory to assume the sufficiency of unity.

This also highlights that there is little significance in the difference in wave attenuation predicted by Daily and Stephan
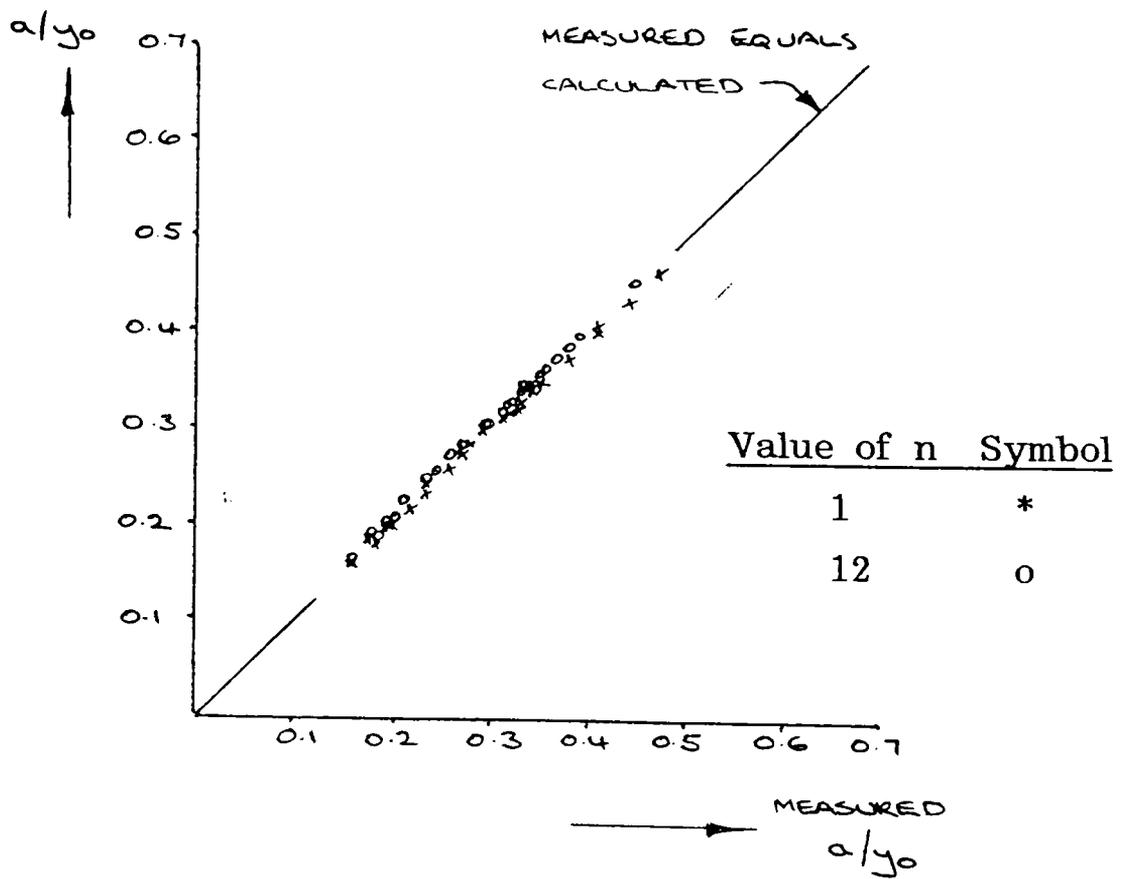
Figure 6.18a - Comparison of measured wave height to that calculated by G.H.Keulegan after attenuation.
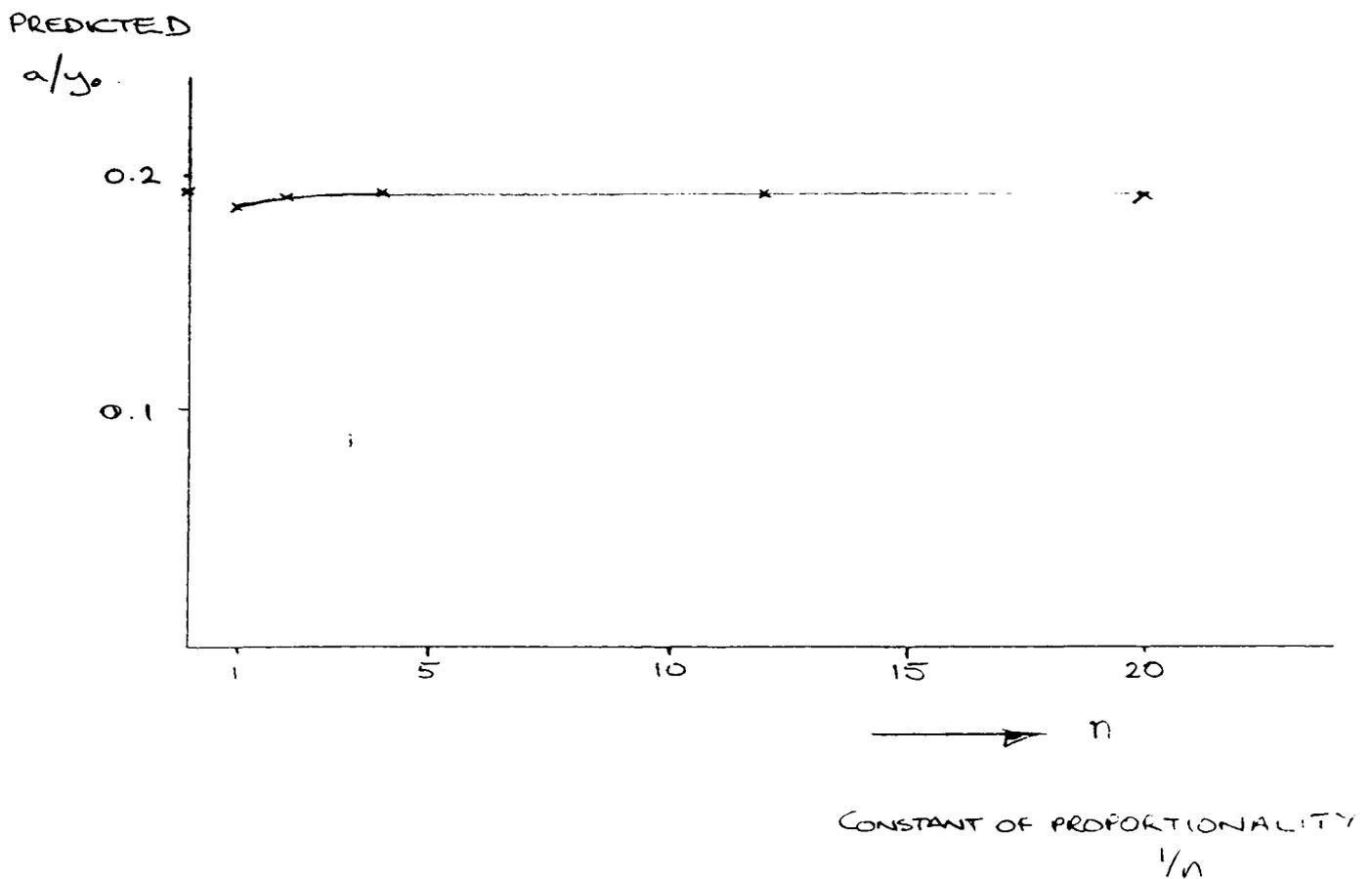

Figure 6.18b - Variation of amplitude with 1/n

and the theory of Keulegan, which was of the order of 0.1%. This can be equally applied to the results obtained here which are of the order of 3% different to those given by Keulegan's theory.

6.2.6 Wave Celerity

Wave celerity was calculated between adjacent wave probes (i.e. between wp's no.1/2 and 2/3) in the wave channel. The error between the two calculated wave speeds was generally 1% but peaked at 2.5%.

The measured celerity reduced as the wave progressed along the channel. This was approximately in line with reduced wave amplitude. The scatter of results and the small values being measured prevented the accurate correlation of results.

The average of the two measured values varied from that calculated using the theory of Rayleigh/Boussinesq by approximately 1% (figure 6.19).

C (measured)
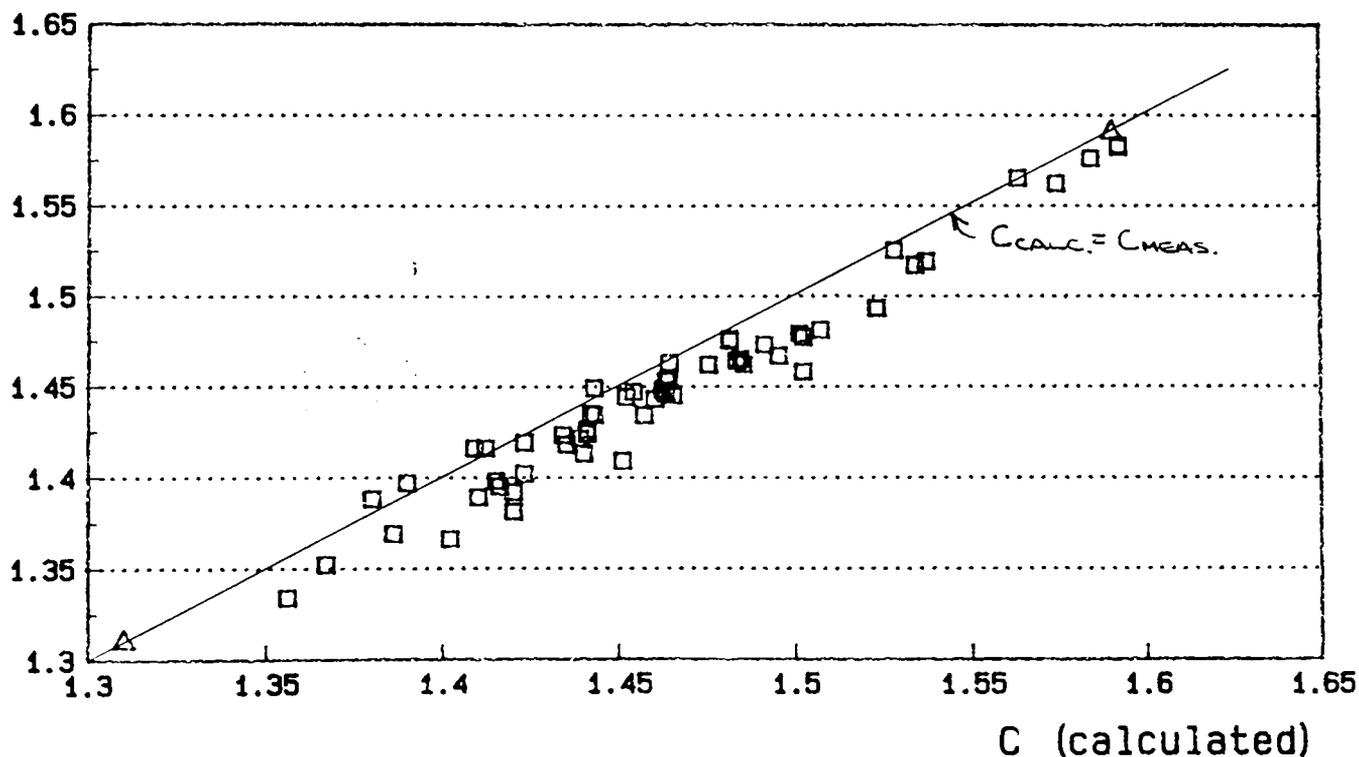
Figure 6.19 - Graph showing agreement between
measured and calculated celerity

The graph of non dimensional amplitude versus celerity clearly shows the simple relation between them (figure 6.20).
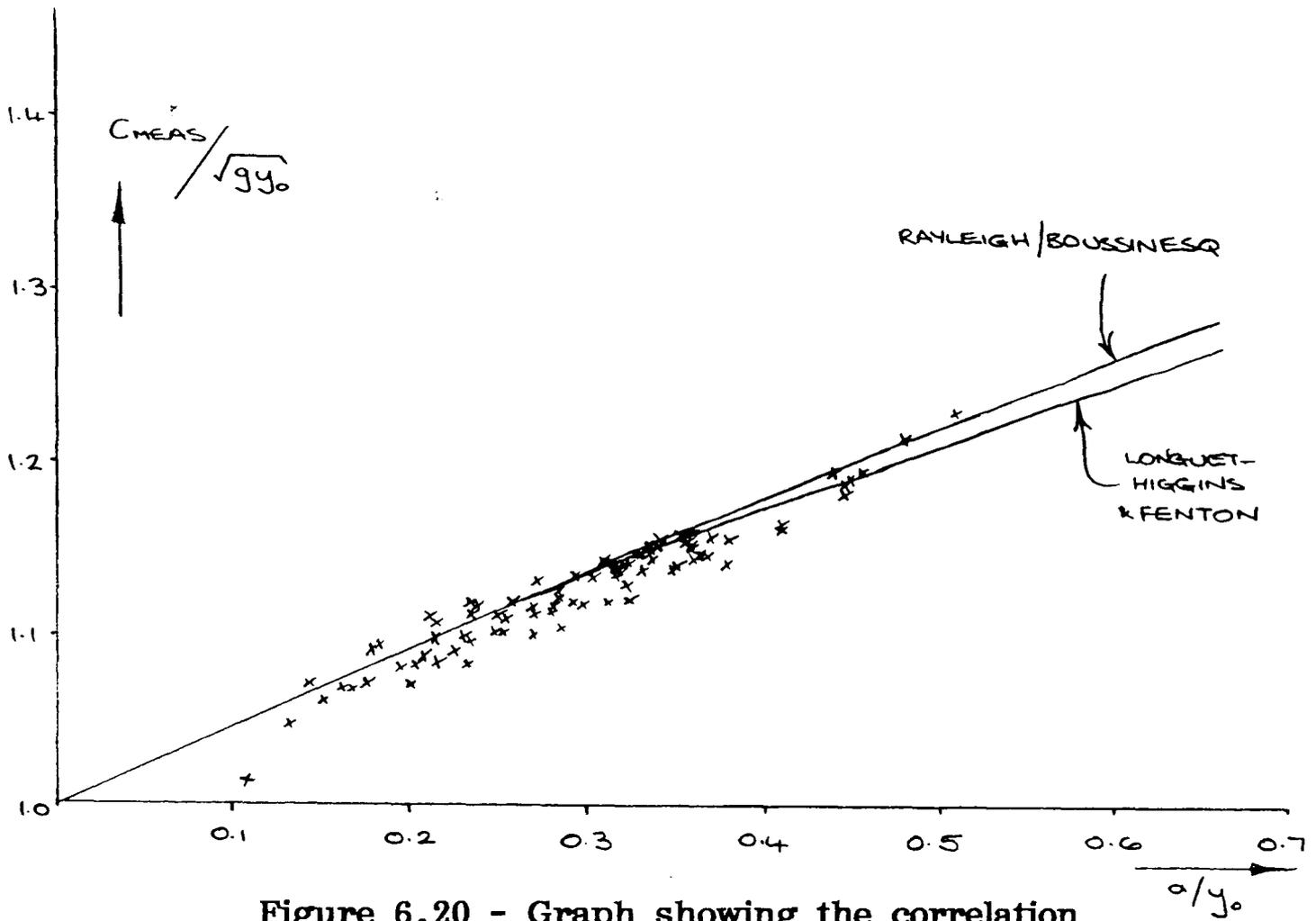
Figure 6.20 - Graph showing the correlation between a/y₀ and celerity

6.3 The Fluid Velocities

6.3.1 Introduction

A very important part of this research was the accurate measurement of fluid velocities beneath the generated waves, since these will subsequently be used to calculate the predicted force on the cylinder. These are then correlated with the measured forces. It is this correlation that will prove, or otherwise, the use of Morison's equation. Consequently considerable effort went into obtaining these velocities, which were small and of short duration, with maximum accuracy.

Results already presented show the deficiencies in the method of generation of a solitary wave. Consequently it was most important to accurately record the wave parameters of interest so that the effect of these on the calculation of forces may be assessed. An important factor in the measurement of velocity using the Hot Film Anemometer was its calibration and the application of the calibration to the measurements of velocities under the wave. Both are discussed in full.

6.3.2 Hot Film Anemometer Calibration

The Hot Film Anemometer was calibrated by allowing the sensor, whilst attached to a rail mounted trolley, to move along the channel under the action of a falling weight (4.3.1). As the trolley moved along the rails it activated micro switches at known positions along the channel. The measured distance between the micro switches was compared with that calculated by integration of the line regressed to the Hot Film Anemometer calibration graph. The differences between the two varied between zero and 60mm, a maximum error of 6%. Calibrations with a high regression coefficient (i.e. best fit) generally covered a much smaller range than this with a maximum error of 4%.

Figure 6.21 shows typical nonlinear and linearised calibration graphs for the Hot Film Anemometer and demonstrate the accuracy of the fitted curves for the chosen value of N.

Noise on the anemometer output gave the x axis intercept. This was not a response by the anemometer to fluid velocities and was removed for clarity. Because of the magnitude of this noise, very low velocities could not be measured. When raised to the power, N the graph became offset from zero.

Velocities above the 'noise threshold', but below approximately 0.03m/s lie in a region where free convection predominates. This region is not well represented by a simplified King's Law. Above approximately 0.03m/s King's Law applied and good agreement was achieved between measured values and the fitted curve.,

Points in the free convection region were included in the regression analysis because it was unclear at the time of analysis what the lower velocity limit was for each wave. However, the calibration graph does show the limit of the application of King's Law, and the number of points in the region was small compared to the total number of scans in the regression analysis. They had little effect on the choice of N and consequently the fitted line.

Any scatter from the fitted curve was primarily due to sensor deterioration, dirt particles and air in the water all of which affected the conduction of heat from the sensor.

A large percentage (75%) of all test results had a linear regression coefficient better than 0.9975 (1.0 perfect) with 90% better than 0.9960 (figure 6.22). The regression coefficient not only reflected the accuracy of the fit of the line to the measured data but also the scatter of the results. The line may have been in good agreement with the data but with a large scatter in the data the regression coefficient would be poor.

The values for the power to which the velocities were raised to maximise the regression coefficient are plotted as a histogram in figure 6.23. The most common value was N=0.5 with 42% lying between $0.45 \leq N \leq 0.55$. The wide spread of results was due to
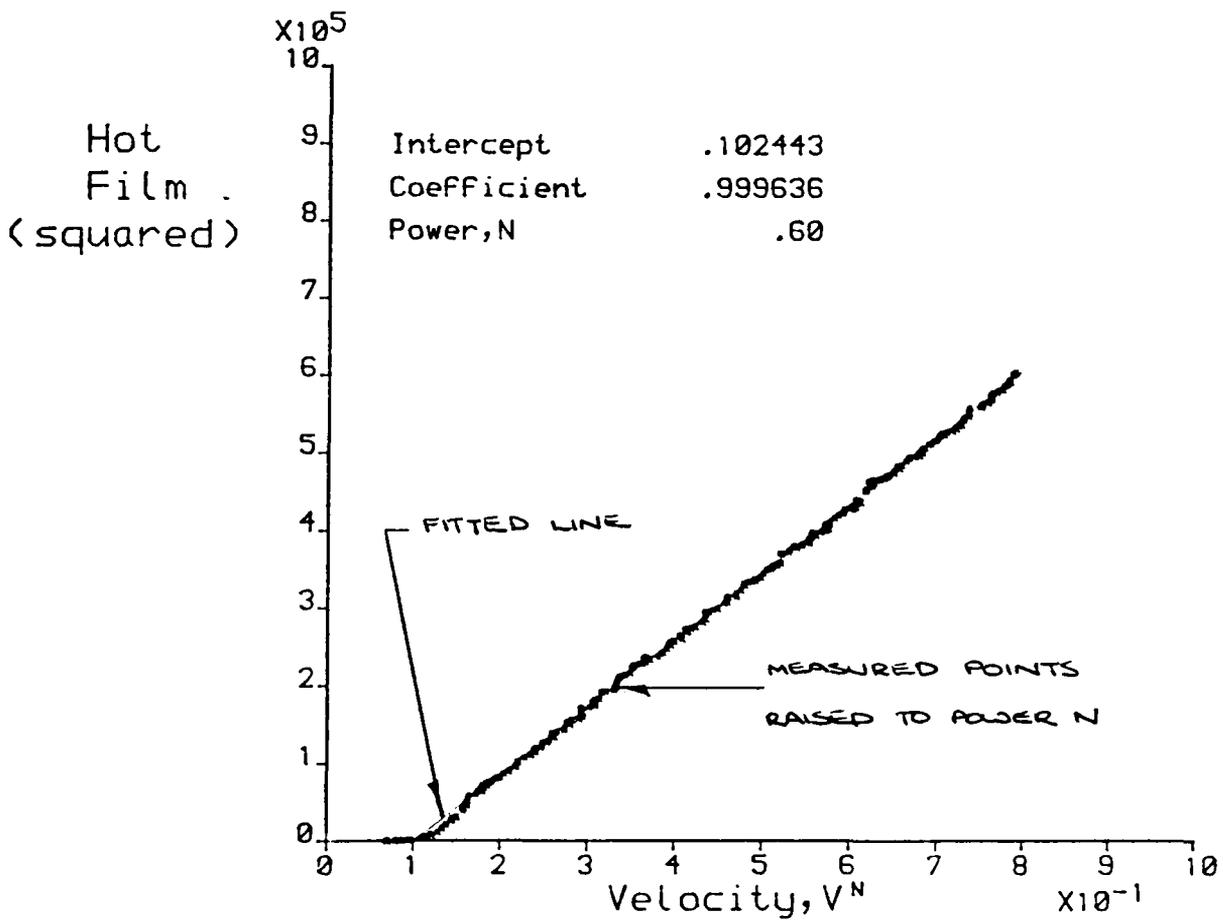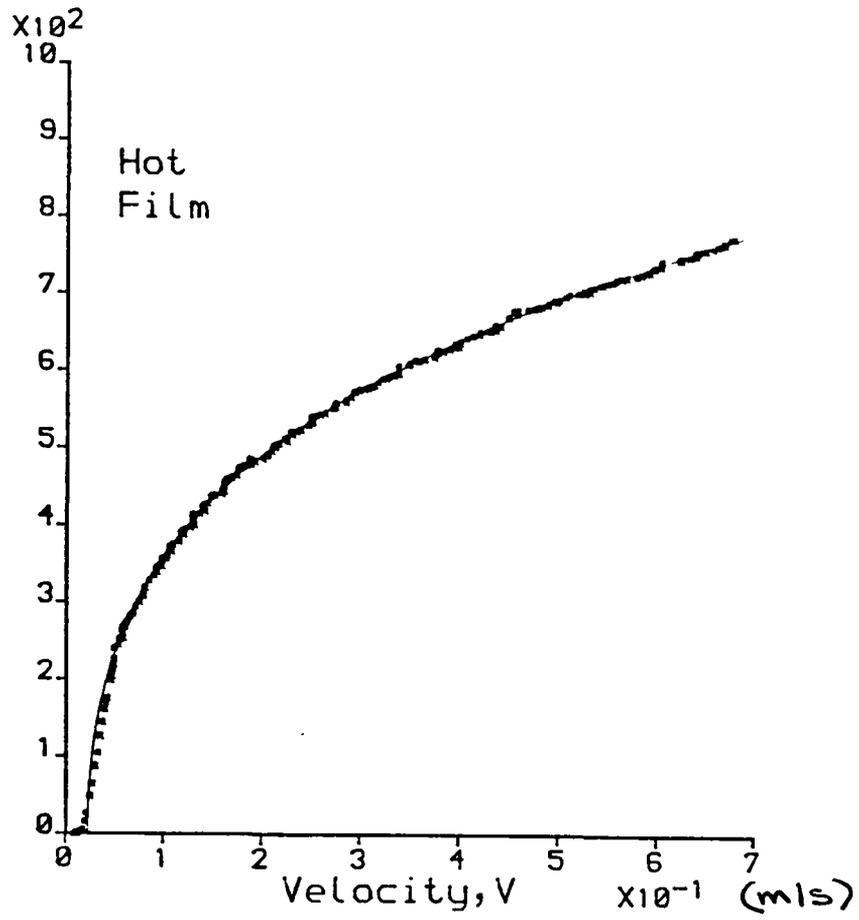
Figure 6.21 - Typical HFA calibration
graphs (linear and nonlinear)

each particular days tests of the Hot Film Anemometer being unique. This was of no consequence to this research so long as the calibration remained valid for the corresponding test.

Within a days tests the value for N varied within a range of +-0.05, each days tests being centred on a different mean value of N. Within this range approximately 60% of results fall within 0.05 of each other.

The drift in sensor calibration shown by the changes in N were probably due to changes in temperature and air content of the water.

Summary

Through the procedures and controls adopted in the calibration of the HFA, fluid velocities were measured and presented with a high degree of confidence and an error which appears to be better than 6%.
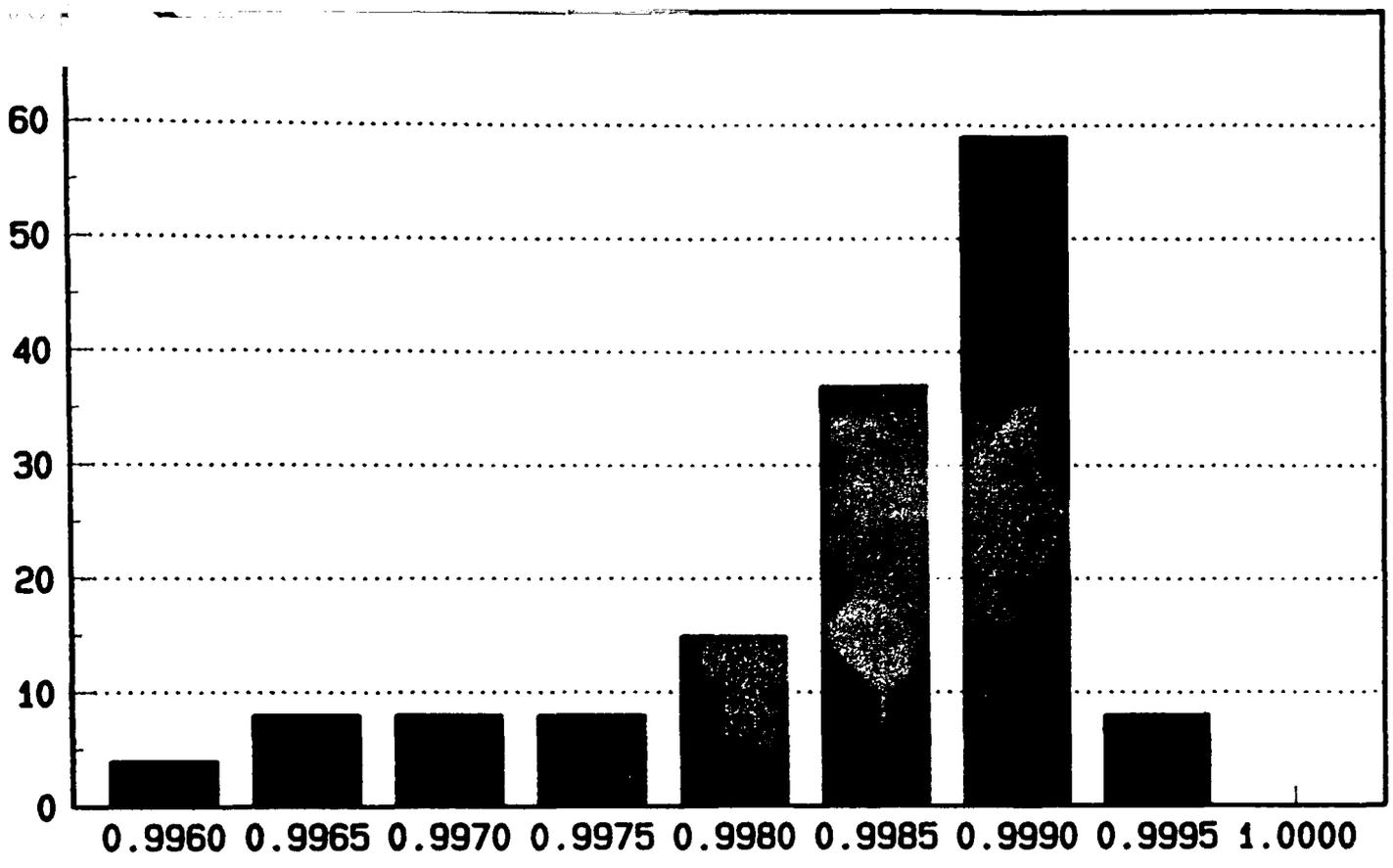
Figure 6.22 - Histogram showing accuracy of results

Frequency
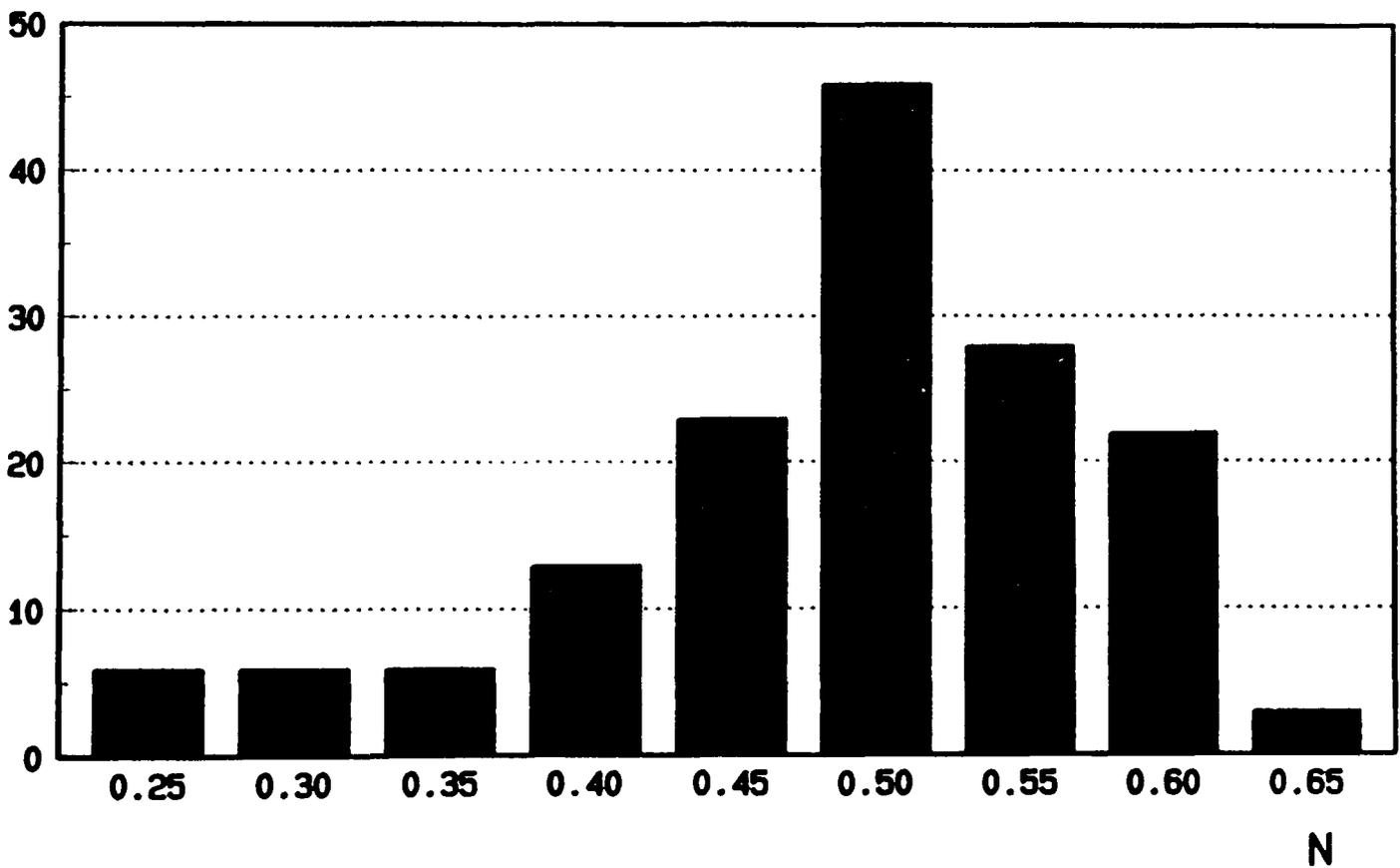
Figure 6.23 - Histogram showing values for N

6.3.3 Fluid Velocity measurements

Results are presented as the time variation of velocity at one point within the water. Measured velocities are presented with velocities calculated using McCowan's theory and a polynomial fitted to the measured velocities.(Figure 6.24). As the accurate determination of fluid velocities is so crucial to the validity of the thesis, it was the comparison with theory that was used as the acceptance criteria for the test results.

Accuracy of fit of polynomial to measured values

Generally the polynomial well represented the measured fluid velocity data, smoothing minor irregularities near peak velocity. (Figure 6.25) Their was good agreement between the polynomial and measured values over the central section of the wave, covering the main disturbance. However the polynomial failed to give consistently good results at the very front and rear of the wave. (Figure 6.26)

Very low fluid velocities (<0.01 m/s) were not measured because the calibration was not valid in this region (see 6.3.2) due to the predominance of free convection effects not modelled by King's Law. (Figure 6.27)

High fluid accelerations were not well represented by the smoothing polynomial. These were rare and were generally the result of signal noise.

Disturbances produced during the generation of the wave (discussed fully in section 7.1.6) and subsequently as it travelled along the channel (bed and free surface effects) may also have affected the measured values. However this seems unlikely since only minor irregularities are seen on the trace of measured velocities.
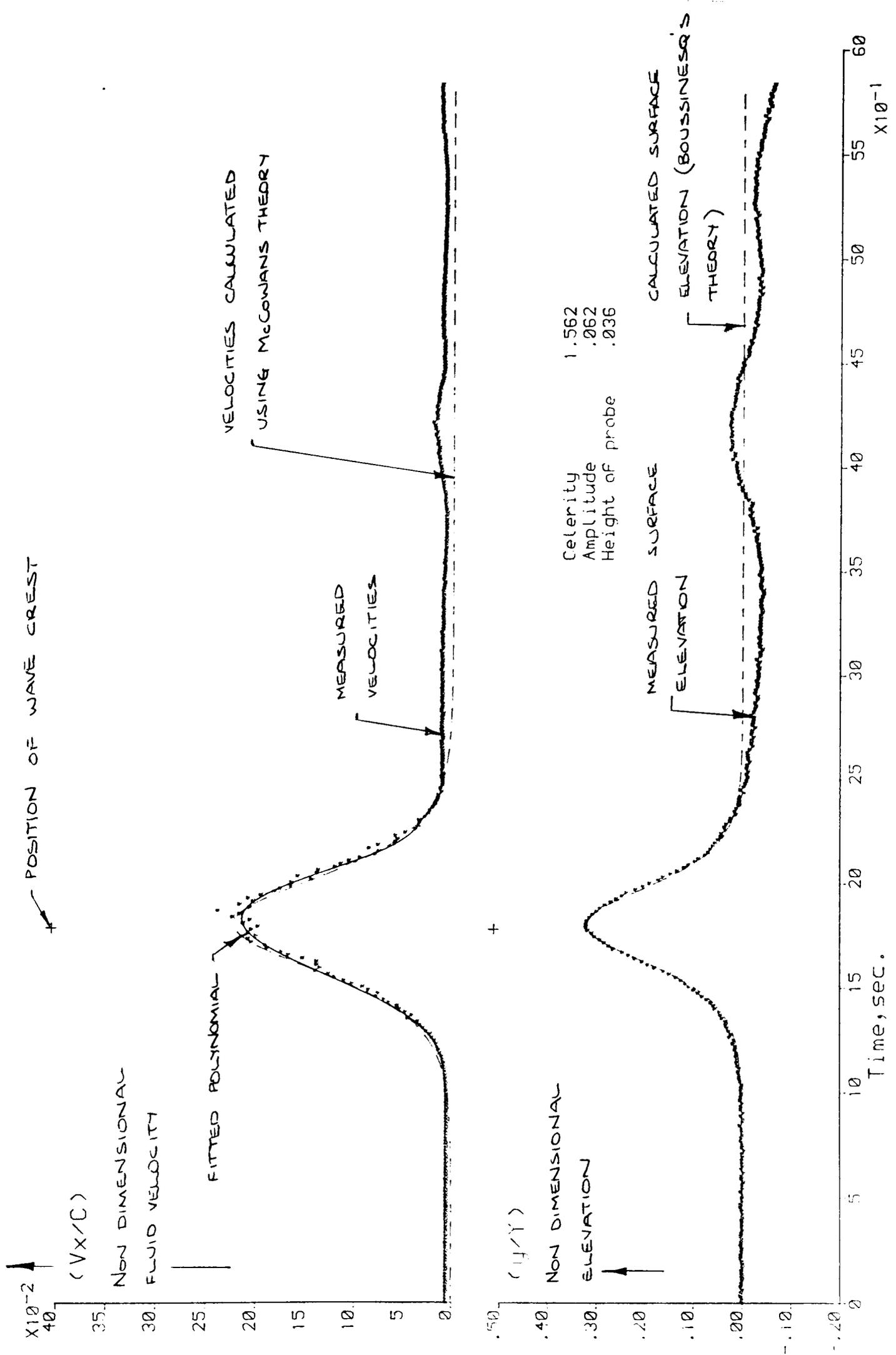
Figure 6.24 - Measured, Fitted (——) and McCowan's (---) fluid vels. Cyl.dia.D/y_o=0.07; Cyl.pos.,z_c/y_o=0.19

- 180 -
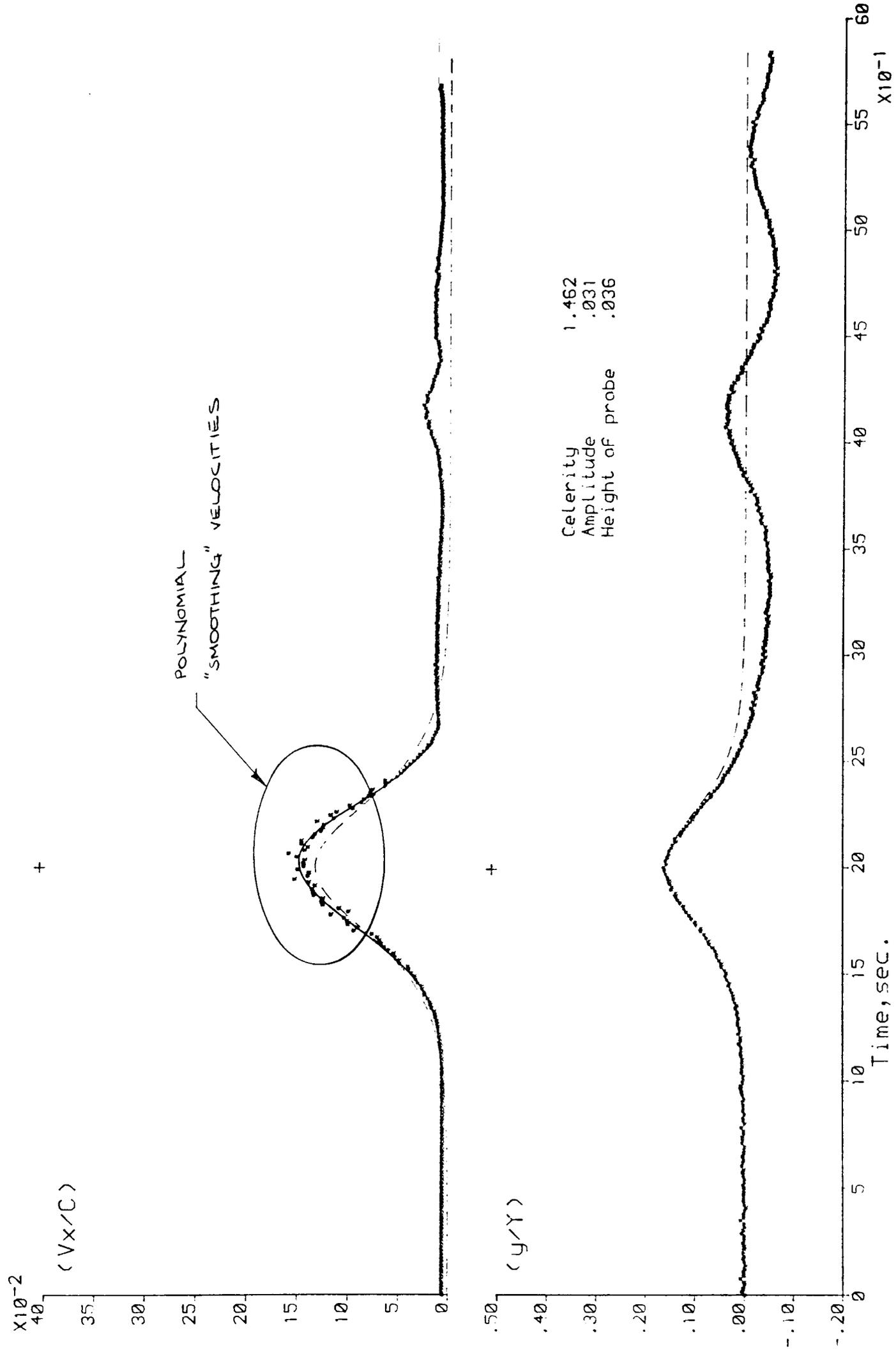
Figure 6.25 - Measured, Fitted (——) and McCowan's (---)
fluid vels. Cyl.dia.D/y_o=0.07; Cyl.pos.,z_c/y_o=0.19
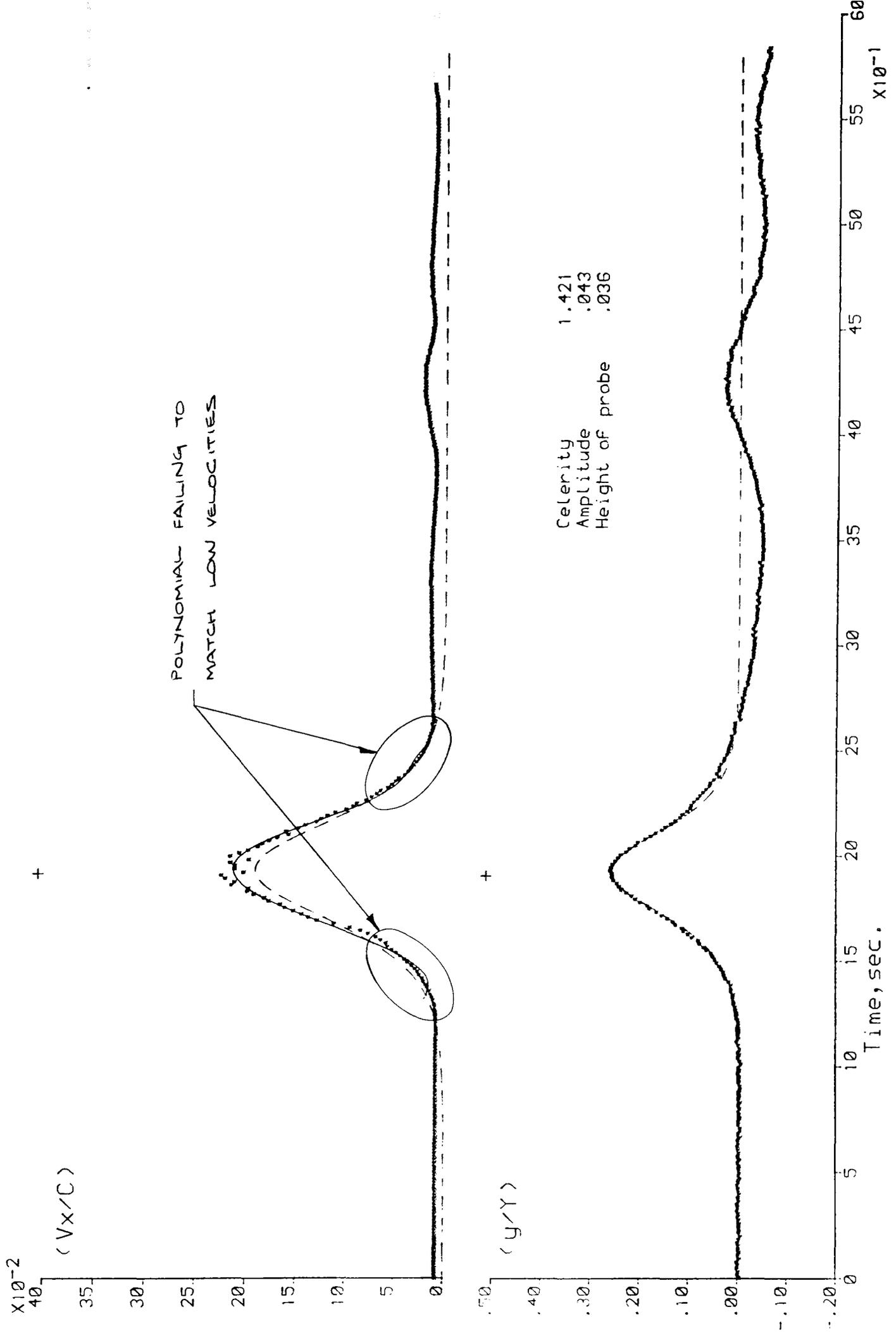
Figure 6.26 - Measured, Fitted (——) and McCowan's (---) fluid vels. Cyl.dia.D/y_o=0.29; Cyl.pos.,z_c/y_o=0.21

- 182 -
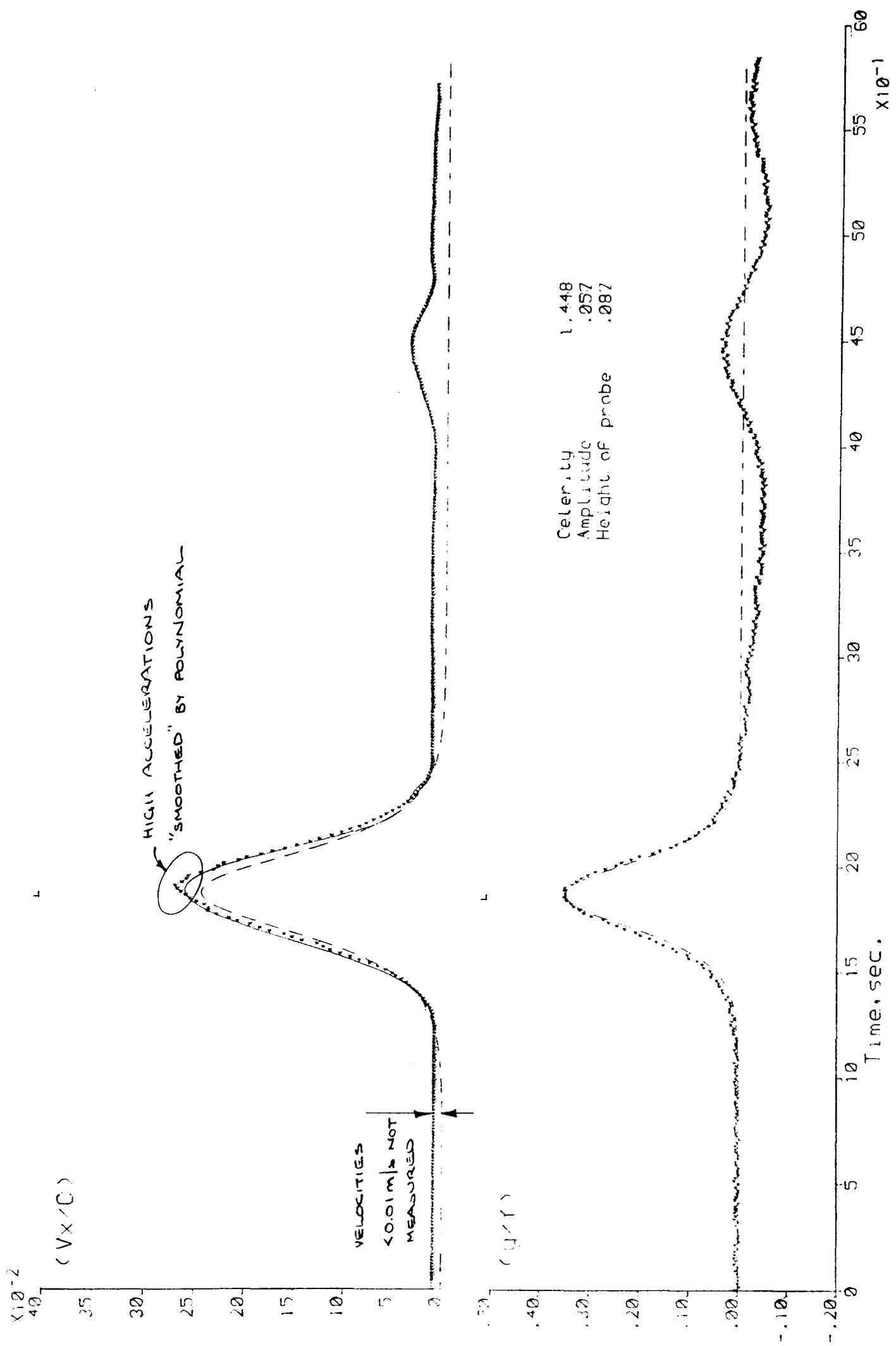
Figure 6.27 - Measured, Fitted (——) and McCowan's (---)
fluid vels. Cyl.dia.D/y_o=0.08; Cyl.pos.,z_c/y_o=0.54

- 183 -

Fluid velocity data was not affected by the size of the cylinder since measurements were made just before the wave reached the cylinder, and could be considered to be those as if the cylinder were absent.

The percentage error between measured peak fluid velocities and those determined from a fitted polynomial are presented as histogram in figure 6.28.

The average difference between the fitted polynomial and measured peak fluid velocities was 4% and was considered acceptable in view of the scatter in the measured values.

Frequency
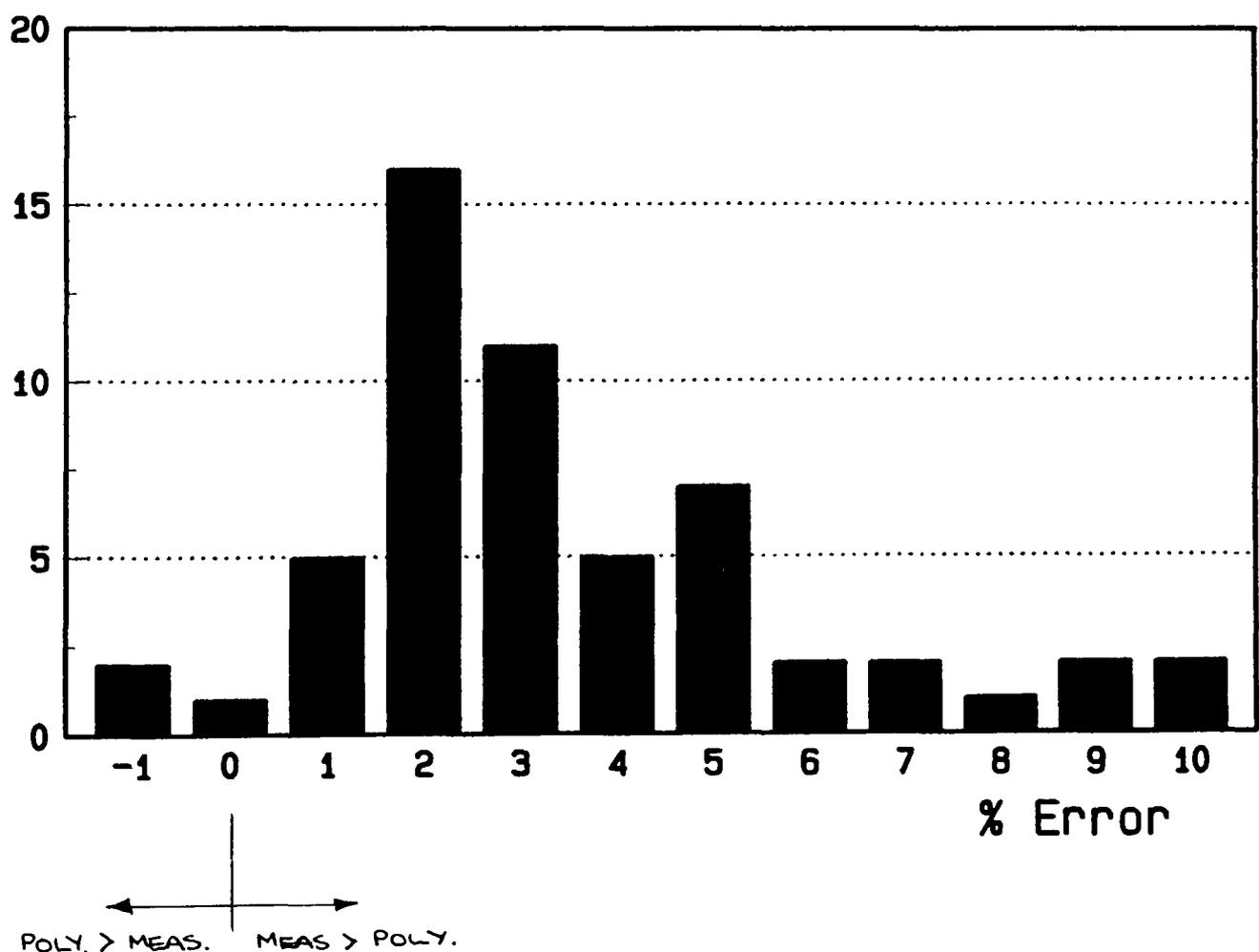
Figure 6.28 - Error between measured and smoothed peak velocities.

Smoothed fluid velocities compared with theory

Measured peak fluid velocities and those determined using the polynomial were compared with theory. At 0.036m above the channel bed the difference with theory was small, with the polynomial overestimating by on average, 1%. At 0.087m above the channel bed the situation was similar with zero average error. At 0.136m above the channel bed the error range was larger, with the polynomial over estimating by on average 5%.

A scatter of results was in some ways inevitable because of differences in accuracy with which the polynomial represented the measured values. Indeed at 0.136m above the channel bed the errors in the fluid velocities determined using the polynomial were greater than that between the measured values and those calculated.

The results may have been affected by the changes in the calibration of the anemometer. Though these effects were minimised by calibrating immediately prior to generating a wave.

Because the response of the HFA to changes in fluid velocity is nonlinear, the differences between the smoothed and theoretical fluid velocities would be greatest at the peak of the wave, as observed here. Even though this may account for some of the differences, it should not prevent the identification of any trends because the calibration of the HFA did not drift significantly between adjacent test. (Figure 6.29)
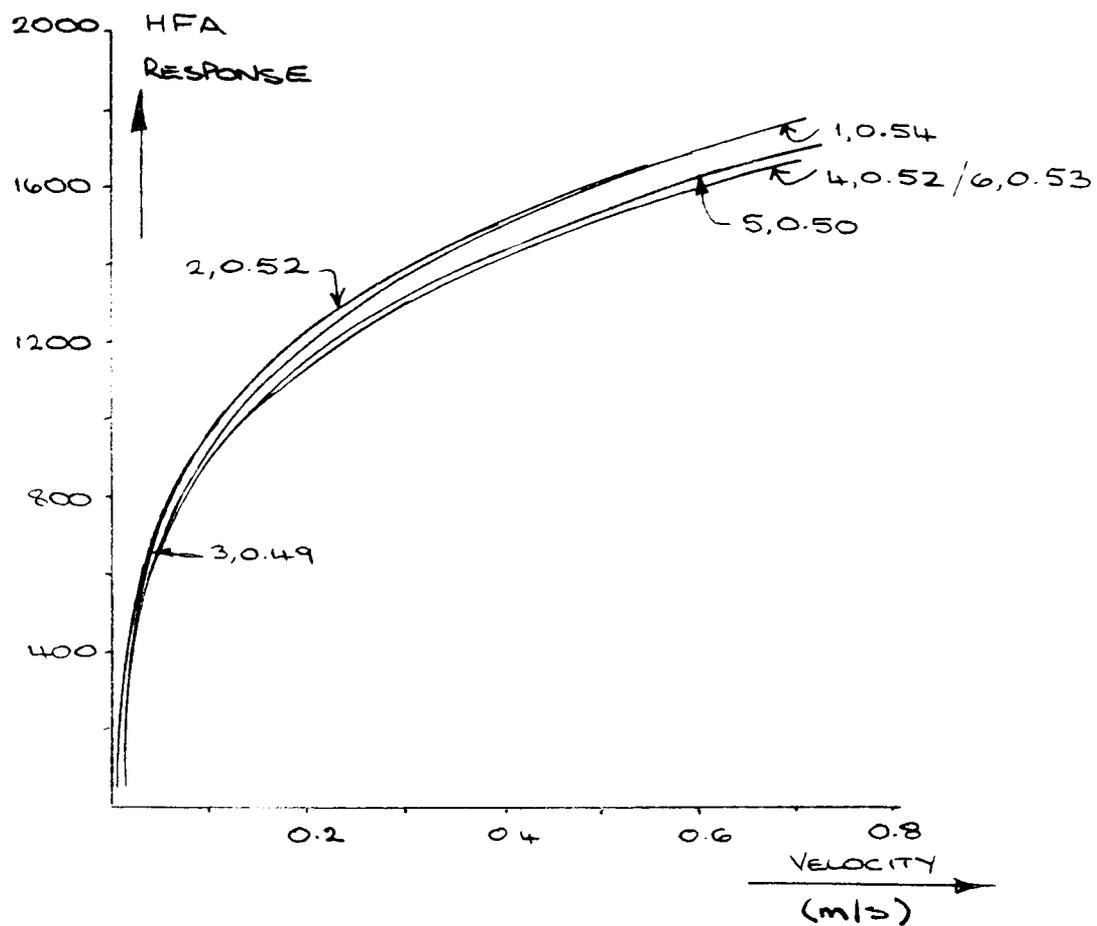
Figure 6.29 - Nonlinear calibration of HFA for sequential tests

As wave height increased the validity of McCowan's theory is thought to change. Consequently this would affect the correlation with measured results.

It is also reasonable to suggest that the validity of McCowan's theory would also vary with depth of immersion. This may well explain some of the scatter seen in the results presented here.

Essentially the comparison with theory is only of passing interest, since the measured values were used in the calculation of forces. Consequently the accuracy is of paramount importance and that has been shown previously.

Time of Peak

The fluid velocities calculated using the theory of McCowan were centred on the wave profile peak calculated from the polynomial fitted to the wave crest. Having corrected for electrical phase shifts, the measured peak velocity had an insignificant offset from the wave profile crest and could consequently be considered coincident as expected.

The time of peak velocity determined from the smoothing polynomial gave results of similar accuracy.

Errors in the measured data were sometimes significant because of 'noise' on the output from the Hot Film Anemometer giving a 'false' peak. This 'noise' had no effect on the results using a polynomial since the fitted curve smoothed the high frequency part of the signal. Consequently any high frequency turbulence was also lost. Though undesirable because turbulence would affect the formation, growth and separation of eddies causing the forces on the cylinder, this was clearly a limitation of using a HFA for measuring fluid velocities.

6.4. Forces on Cylinders

6.4.1 Introduction

One aim of this study was to generate a known velocity field of a simple type and avoid the complexities of history effects on the fluid motion. Having determined the velocity field, forces on the cylinders in the vertical and horizontal directions were measured using a force balance of semi conductor strain gauges. Results are presented here that are used to calculate the drag and inertia coefficients in Morison's equation.

The results are considered in two sections,
1) measurements made on cylinders away from the channel bed

and

2) measurements on cylinders close to the channel bed.

In both cases trends have been identified with respect to Reynolds number and Keulegan and Carpenter numbers. The interrelation between vertical and horizontal forces have been highlighted for each height above the channel bed.

The results for both drag and inertia coefficients are considered.

Forces on the cylinders in this investigation are primarily a result of the velocity/acceleration environment the cylinder was subjected to. Fluid velocities were represented by Reynolds number. The time available for the velocity effects to force the cylinder was represented by the Keulegan and Carpenter number giving the total time to form the eddies as a proportion of the total time of the disturbance.

In an attempt to non dimensionalise the forces with the diameter of the cylinder, $F/(\frac{1}{4}aD^2\rho g)$ was used when results were plotted. Figure 6.30 identifies the traces included in the results.

6.4.2 Natural Frequency of Cylinders

Table 6.1 gives the natural frequency of vibration both in air and water for the cylinders used in the study. As the same force balance system was used for the 27, 34 and 48mm diameter cylinders the measured natural frequencies in air are all very similar.

6.4.3 Force Balance Calibration

Figures 6.31a and b show typical calibrations of the force balance system to applied loads in either the horizontal or vertical directions (as marked). The graphs show output from each strain gauge pair.

With a load applied in the horizontal direction ideally the force should be registered by only one pair of strain gauges. Because of misalignment of the force balance system and material properties giving a Poisson effect, a load applied in the horizontal direction also gives a response in the strain gauges measuring forces in the vertical direction. This may be thought of as a secondary response since the primary response is given by the strain gauges measuring forces in the line of the applied load. The secondary response was never large and was calibrated along with the primary response. Its effect on the magnitude of the primary response was removed during the analysis of the force traces.
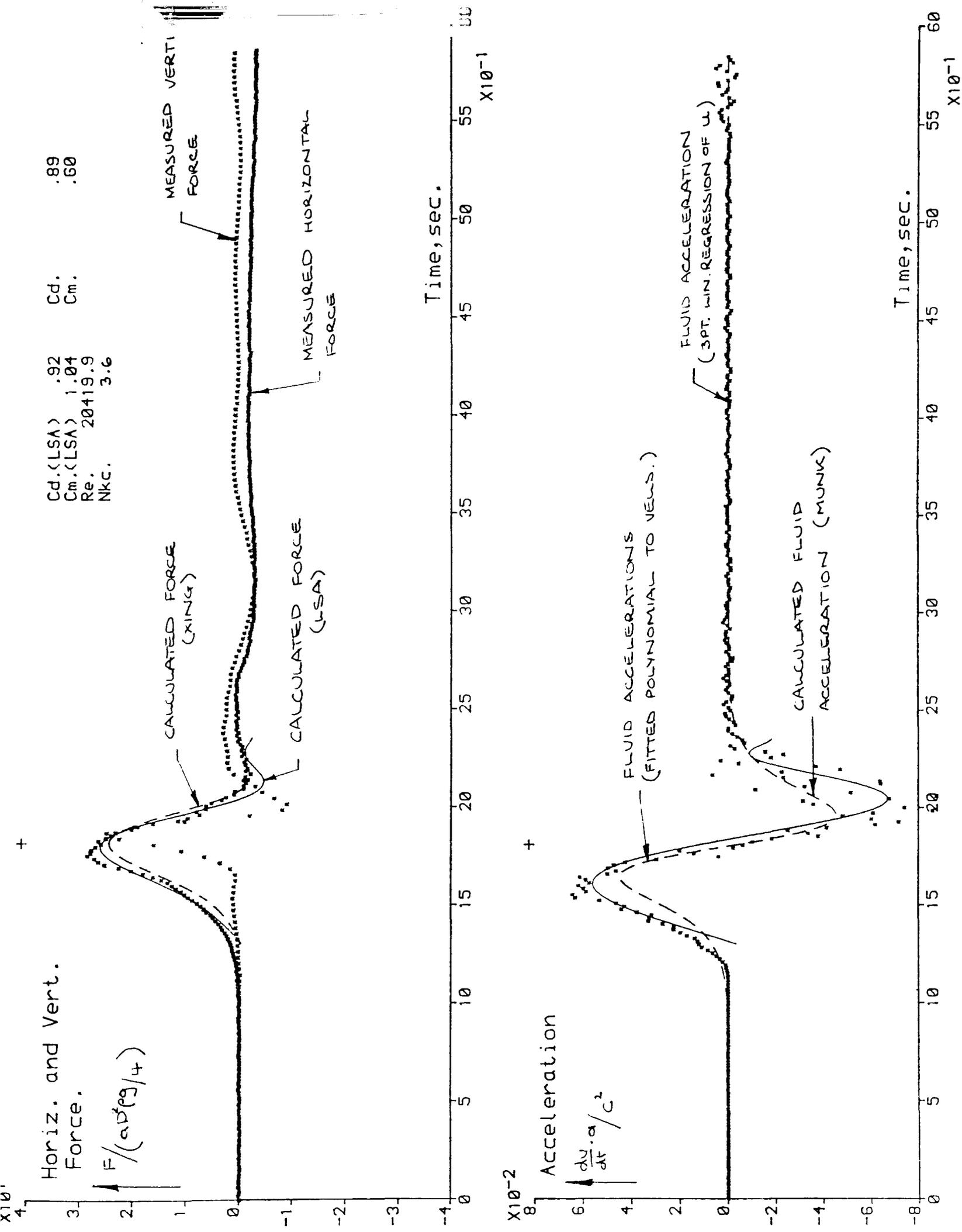
Figure 6.30 - Measured and Calculated forces.
(Morison: LSA [———]; XING [---])
Cyl.Dia.D/y_o=0.20; Cyl.pos.z_c/y_o=0.22
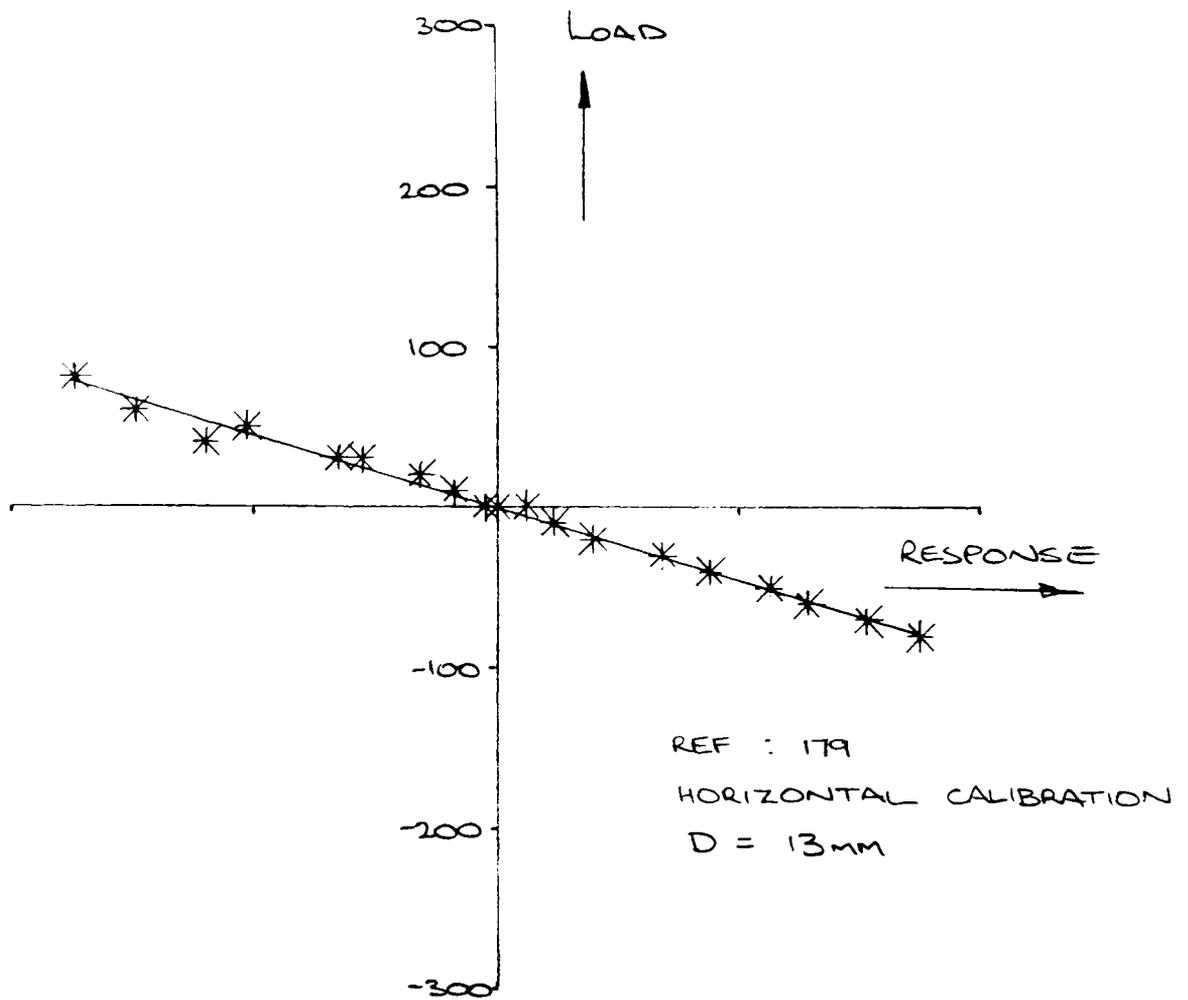
**Figure 6.31a – Typical force balance calibration (in horizontal direction)**
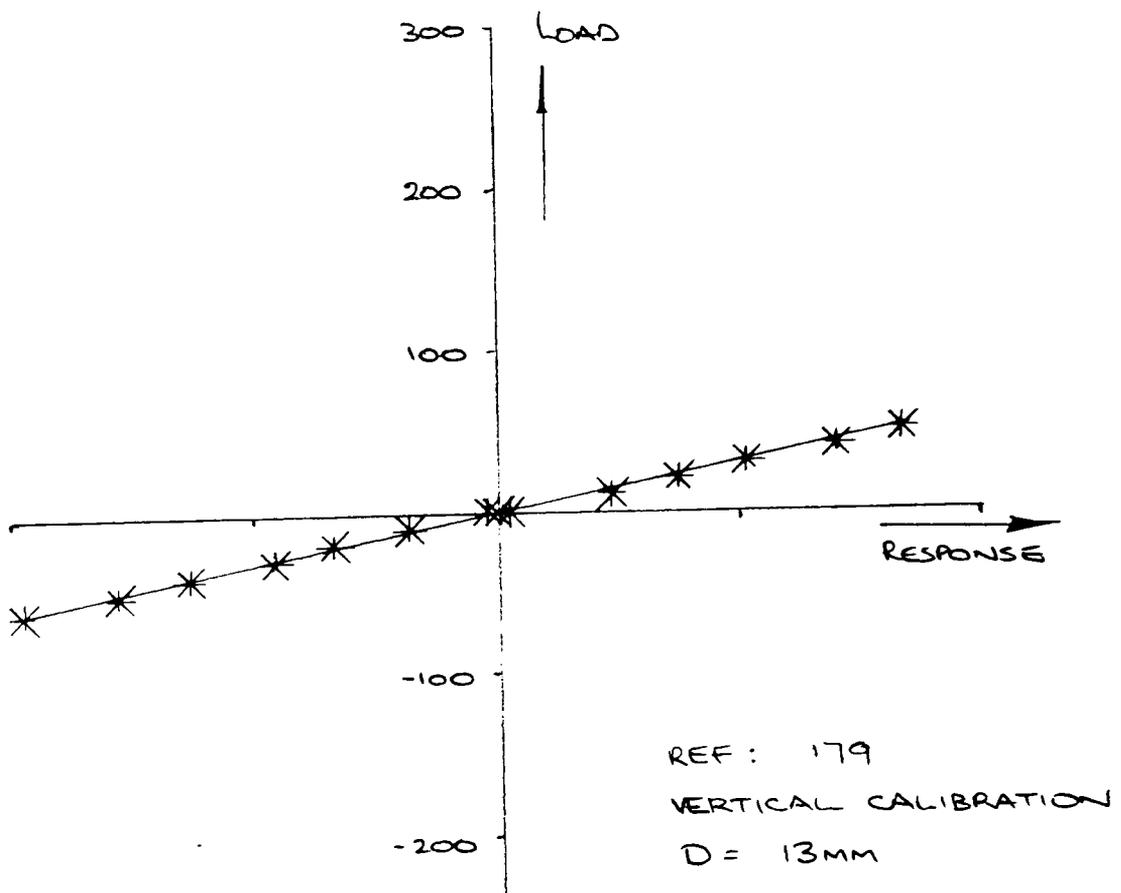
Figure 6.31b – Typical force balance calibration (in vertical direction)

Cylinder diameter (mm)	fn in air (Hz)	fn in water (Hz)
13	60.0	54.5
27	31.6	25.8
34	30.9	24.5
48	30.0	22.0

Table 6.1 - Frequencies of vibration

The results show that both the primary and secondary response are directly proportional to the loads in both the vertical and horizontal directions.

Typically the primary response graph had an offset from zero of less than 1% of the maximum applied load. This output from the strain gauges for zero applied load in the primary direction was also corrected during analysis of results.

The scatter of results from the regressed line was small considering the small loads applied during calibration. (figures 6.31a & 6.31b)

6.4.4 Forces on cylinders away from the channel bed

6.4.4.1 Measured Forces

13mm Diameter cylinder

Results for the smallest cylinder are characterised by the effects of low Reynolds number with high Keulegan and Carpenter number (i.e. relatively low velocities with time available for the formation and separation of eddies from the cylinder).

At low Re (<4000) the vertical force trace oscillated at approximately 2Hz with a peak occurring at approximately 0.15 secs. after the wave crest had passed (figure 6.32). This may be compared with the 0.04 secs. (approx.) for a disturbance to travel the diameter of the cylinder at near peak fluid velocity.

The highest vertical force was recorded between the wave crest and peak negative acceleration (figure 6.32). Its position relative to the wave crest remained constant for all Re at both heights above the channel bed though its magnitude decreased with increasing Re. The maximum vertical force was always towards the channel bed for this cylinder (figure 6.33). The maximum vertical force exceeded the maximum horizontal force by up to 100% at low Re (Nkc approx. 7.0).

With Re<4000 the horizontal force separated into two distinct peaks either side of the wave crest (figure 6.34). The central trough in the horizontal force trace generally coincided with the wave crest. The peak horizontal force occurred after the wave had passed and coincided with the maximum downward force.
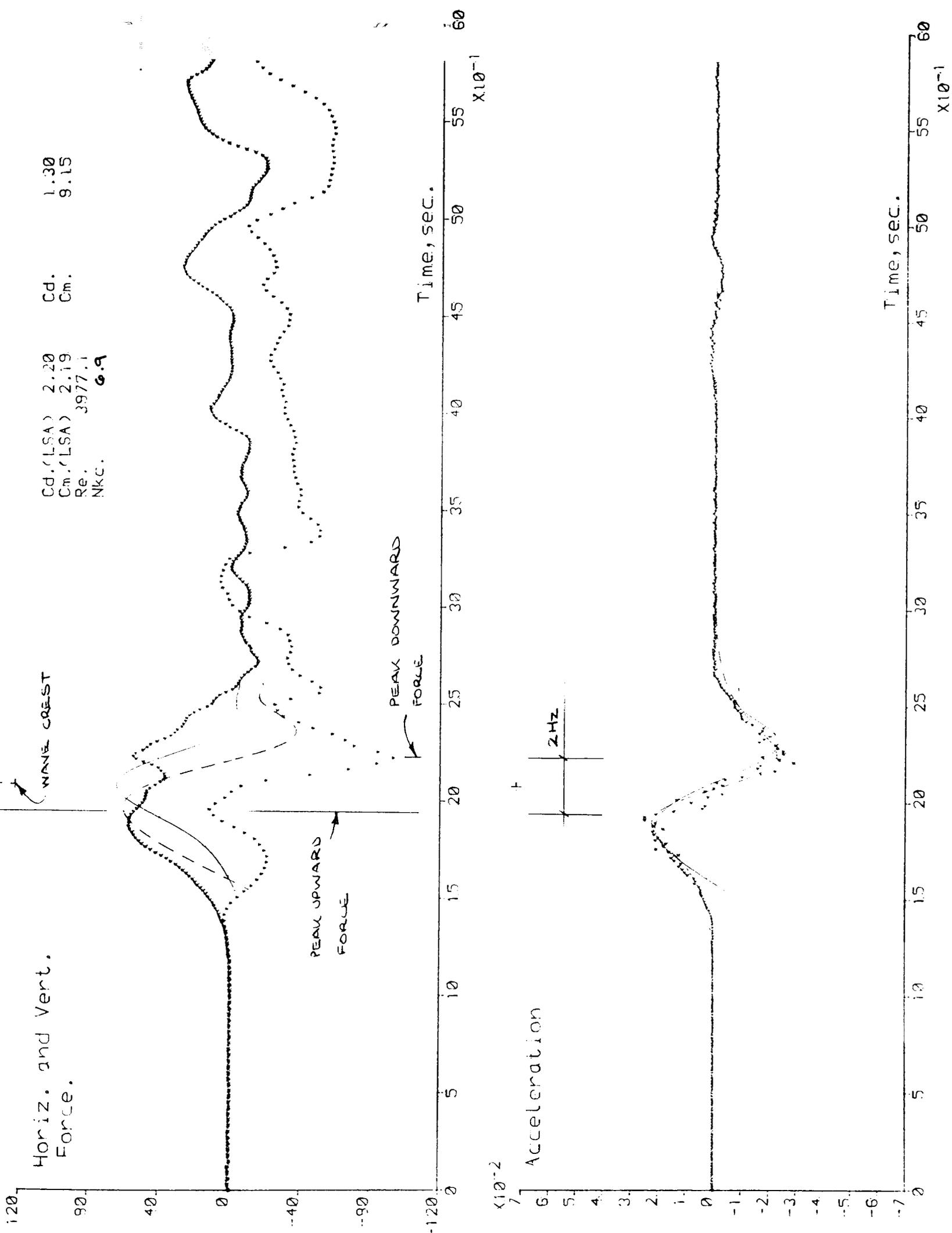
Figure 6.32 - Measured and Calculated forces.
(Morison: LSA [——]; XING [---])
Cyl.Dia.D/y_o=0.08; Cyl.pos.z_c/y_o=0.54

- 194 -
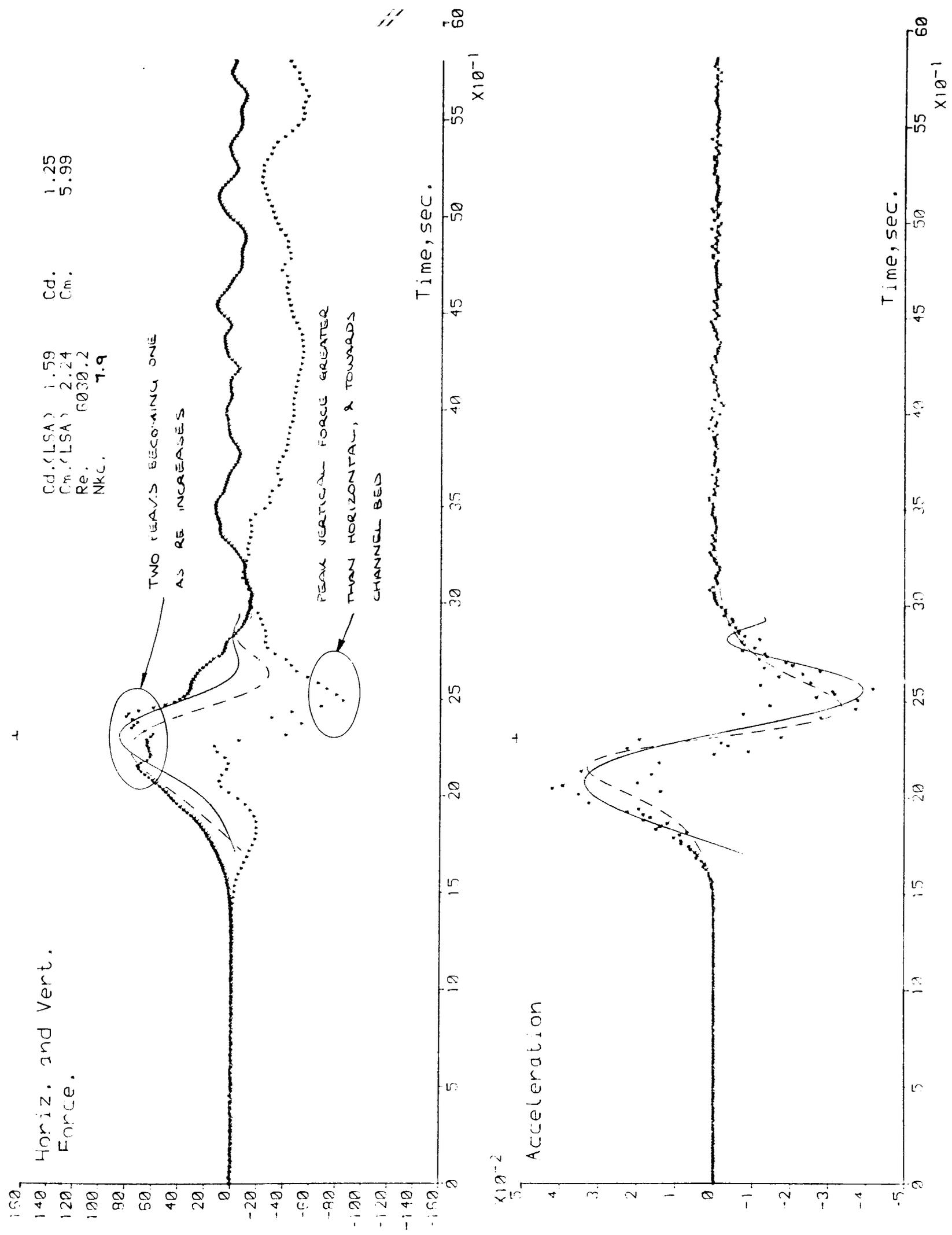
Figure 6.33 - Measured and Calculated forces.
(Morison: LSA [——]; XING [---])
$Cyl.Dia.D/y_o=0.07; \quad Cyl.pos.z_e/y_o=0.78$

- 195 -
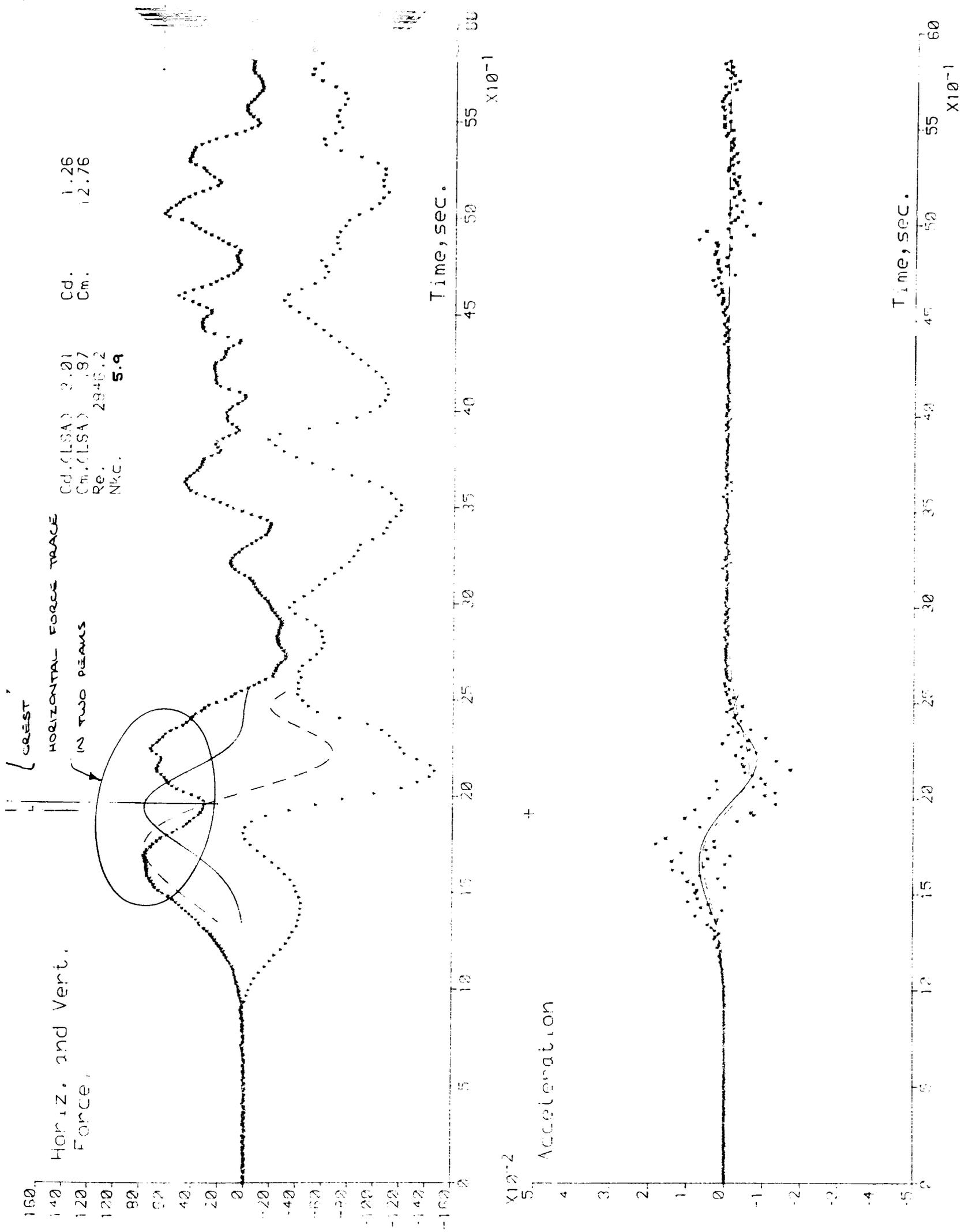
Figure 6.34 - Measured and Calculated forces.
(Morison: LSA [——]; XING [---])
Cyl.Dia.D/y_o=0.07; Cyl.pos.z_e/y_o=0.78

With Re approximately 6000, the trough in the horizontal force trace disappeared leaving a very broad and flat topped response (figures 6.33).

With Re increasing from 6000 the width of the horizontal force trace reduced forming a single peak by Re approximately 7000 ($Nkc=8.5$). The vertical force trace became less well defined with increased scatter particularly at the rear of the wave.

Changes between the dual crested horizontal force trace and the single peak when $Re>=7000$ were gradual and possibly indicate a "transition zone" of sorts.

Introduction : Large Cylinders

Results for the larger cylinders show a much simpler response for both horizontal and vertical forces.

27mm Diameter cylinder

At low Re (approx. 5500) the horizontal force trace for the 27mm diameter cylinder had two peaks, the second peak being only about 30% of the first. The main peak was much closer to the wave crest than the second (figures 6.35). As Re increased ($9500<=Re=10500$) the second peak reduced further and was effectively zero by $Re=10500$ ($Nkc=3.6$). This corresponded to a narrowing of the horizontal force trace and the main peak moving closer to the wave crest (figure 6.36).
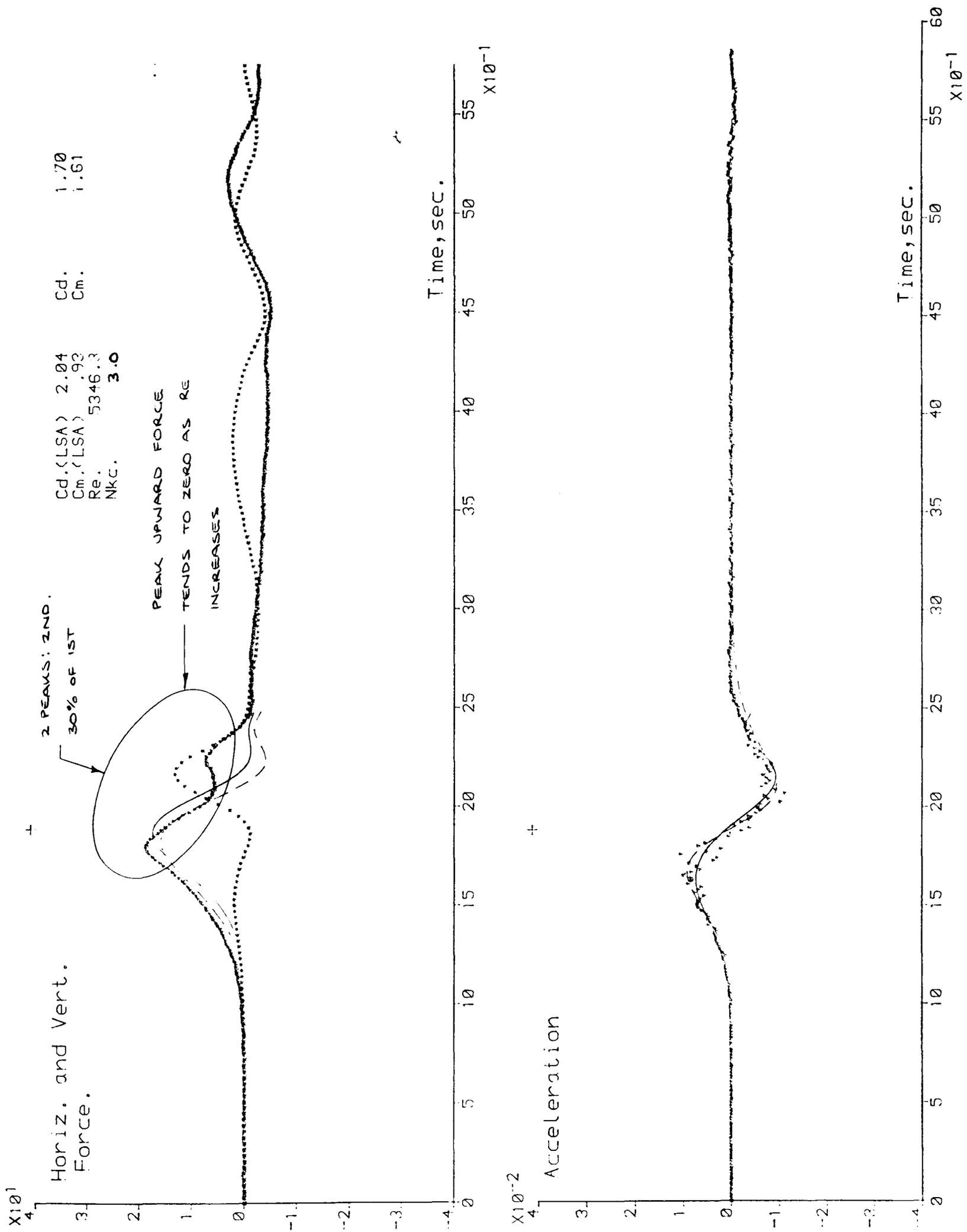
Figure 6.35 - Measured and Calculated forces.
(Morison: LSA [——]; XING [---])
Cyl.Dia.D/y_o=0.16; Cyl.pos.z_c/y_o=0.51

- 198 -
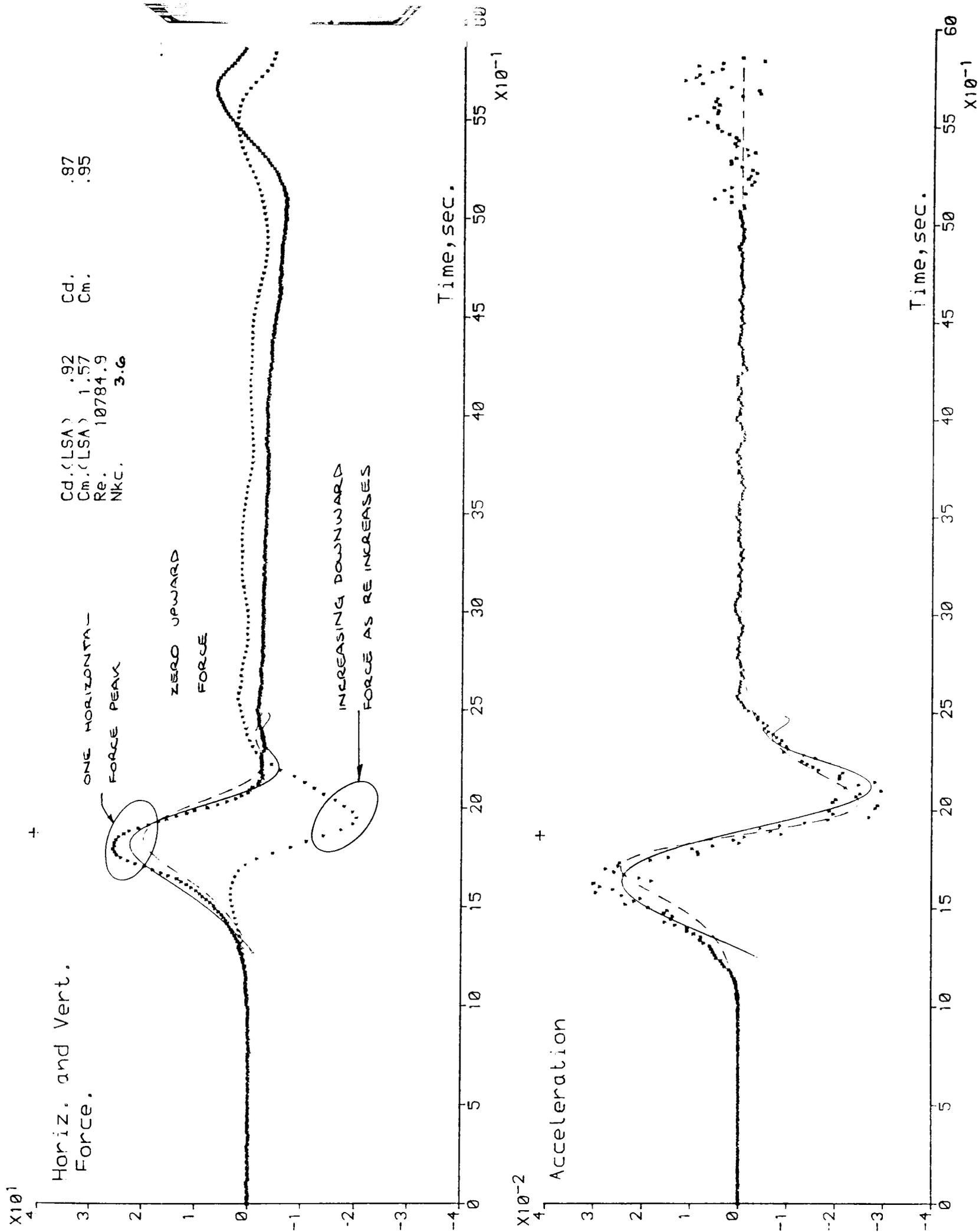
Figure 6.36 - Measured and Calculated forces.
(Morison: LSA [——]; XING [---])
Cyl.Dia.D/y_o=0.15; Cyl.pos.z_c/y_o=0.78

Close inspection of results for the 27mm diameter cylinder shows that as the second peak in the horizontal force trace reduced to zero, the main vertically upward force also reduced to zero. This was combined with a considerable increase in the downward force in the cylinder (figure 6.35/ 6.36). Clearly the fluid mechanics involved in this change are critical and are systematic of a reduction in Nkc from about 3.0 to about 3.7, with an increase in Re from about 9500 to about 11000.

With Re increasing from 10500, the downward force on the cylinder increased, the horizontal force trace becoming single asymmetric elevation with the trace rising more slowly to the peak than it falls (figure 6.37).

With Re<9500 the vertical force oscillated at approximately 1.75Hz, slightly higher than for the smallest cylinder (figure 6.38). The peaks and troughs of the vertical force trace generally occurred at the same time relative to the wave crest for waves in the range 5300≤Re≤17000 for the 27mm and 34mm diameter cylinders, though the vertical force trace of the largest cylinder (48mm diameter) oscillated at a slightly lower frequency (1.5Hz). Because of the different frequency, the peaks and troughs in the vertical force trace for the largest cylinder lag, by an ever increasing amount, the corresponding peaks/troughs of the smaller cylinders for the same Re.

For the 27,34 and 48mm diameter cylinders the vertical force never exceeded the peak horizontal force though at low Re (approx. 5500) the second peak of the vertical force trace became approximately 80% of the horizontal force. For the 34mm diameter cylinder the second peak of the vertical force trace never exceeded 70% of the peak horizontal and only 40% for the 48mm diameter cylinder
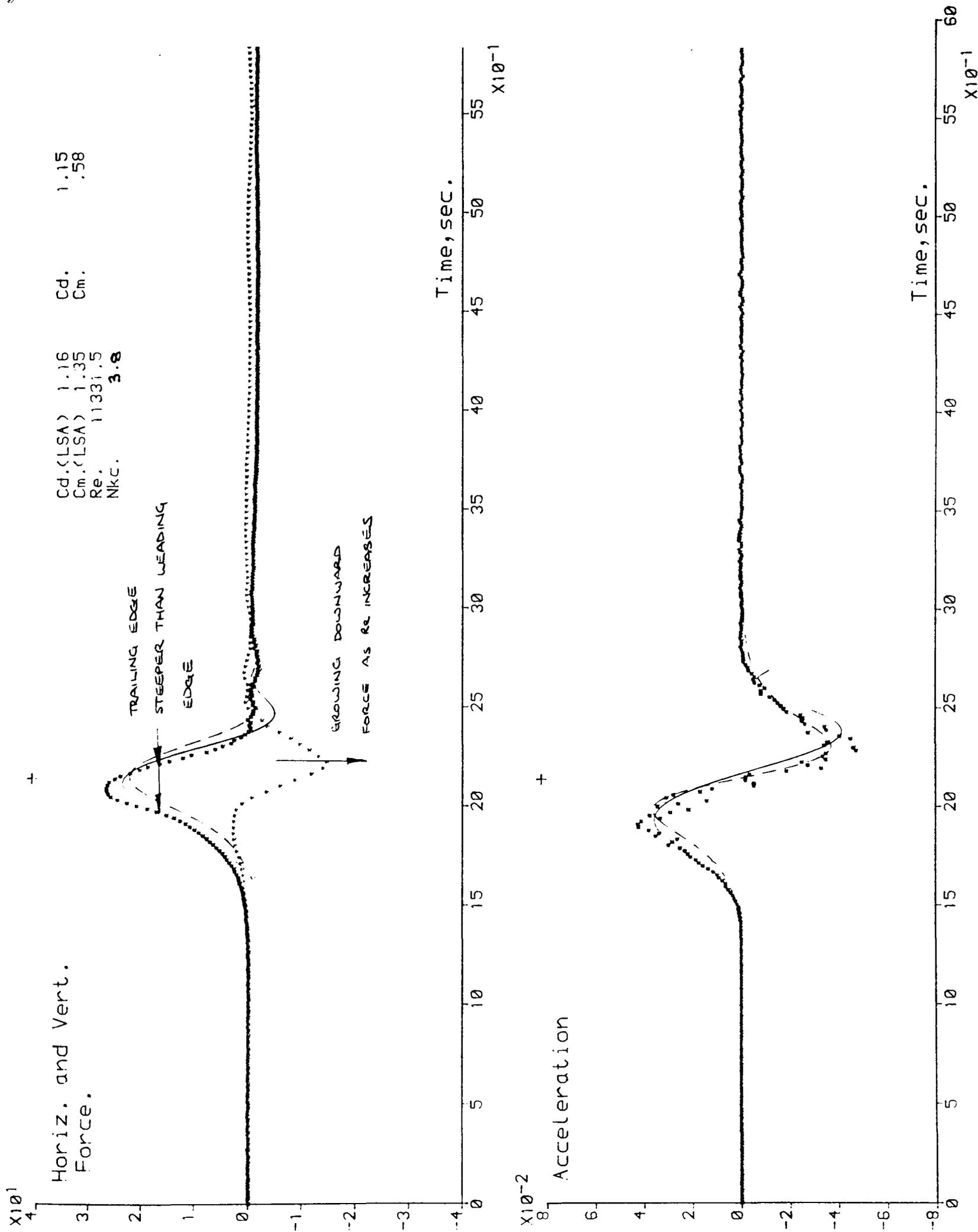
Figure 6.37 - Measured and Calculated forces.
(Morison: LSA [——]; XING [---])
Cyl.Dia.D/y_o=0.16; Cyl.pos.z_e/y_o=0.51

Horiz. and Vert. Force.

Cd.(LSA) 1.36   Cd. 1.19
Cm.(LSA) .61   Cm. .93
Re. 6932.5
Nkc. 3.1

WAVE CREST
PEAK UPWARD FORCE
1.75 Hz
PEAK DOWNWARD FORCE

Time, sec.

Acceleration

Time, sec.
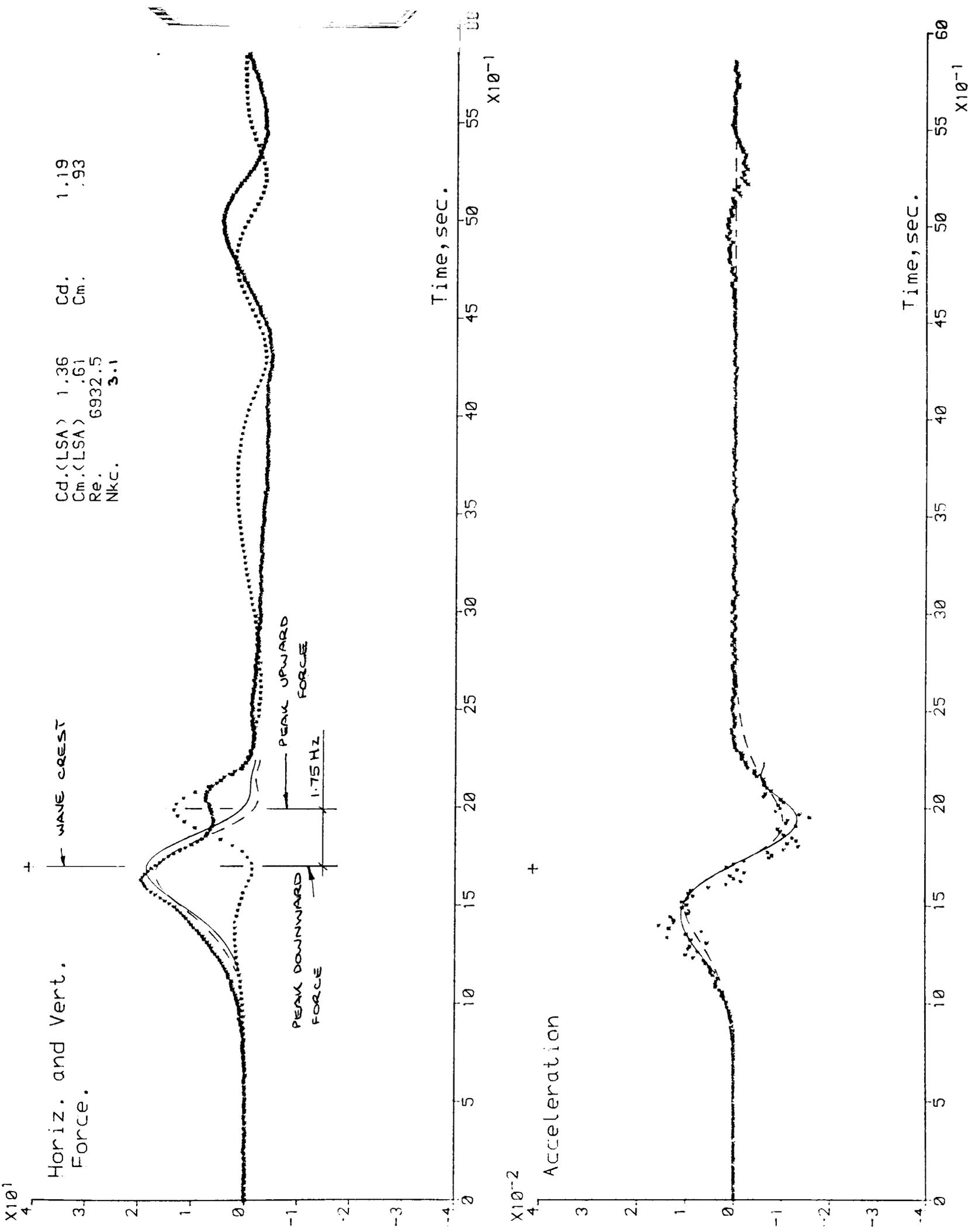
Figure 6.38 - Measured and Calculated forces.
(Morison: LSA [——]; XING [---])
Cyl.Dia.D/y_0=0.16; Cyl.pos.z_c/y_0=0.51

34mm Diameter cylinder

Results for this cylinder showed similar vertical force traces with increasing Re. (figures 6.39/ 6.40) This was because Nkc remained sufficiently small for the force from the second eddy to remain unaltered by the force from the generation and separation of the first eddy (i.e. there was sufficient time for both eddies to create opposing forces on the cylinder).

48mm Diameter cylinder

The results for the 48mm diameter cylinder were similar to those for the 34mm diameter cylinder with little change in the vertical force trace for a similar change in Re. Though as Re reached higher values the vertical downward force grew to a larger value than for the 27mm diameter cylinder. (figures 6.41/ 6.42/ 6.43)

The horizontal force trace increased in width with cylinder diameter with a slight negative force developing after the wave crest with increasing Re.For this cylinder it becomes more peaked with only a small reduction in peak width with Re>=10000.

The peak horizontal force led the wave crest by approximately 0.03 secs. for the largest cylinder, approximately 0.06 secs. for the 34mm diameter cylinder and approximately 0.09 secs. for the 27mm diameter cylinder. This remained near constant for all Re.

It is noted that the proximity of the water surface affected the generation of the vertical forces for the largest cylinder. Figure 6.44 shows how the direction of the vertical forces were reversed for the highest position in the channel.

A summary and detailed interpretation of results is given in chapter 7.
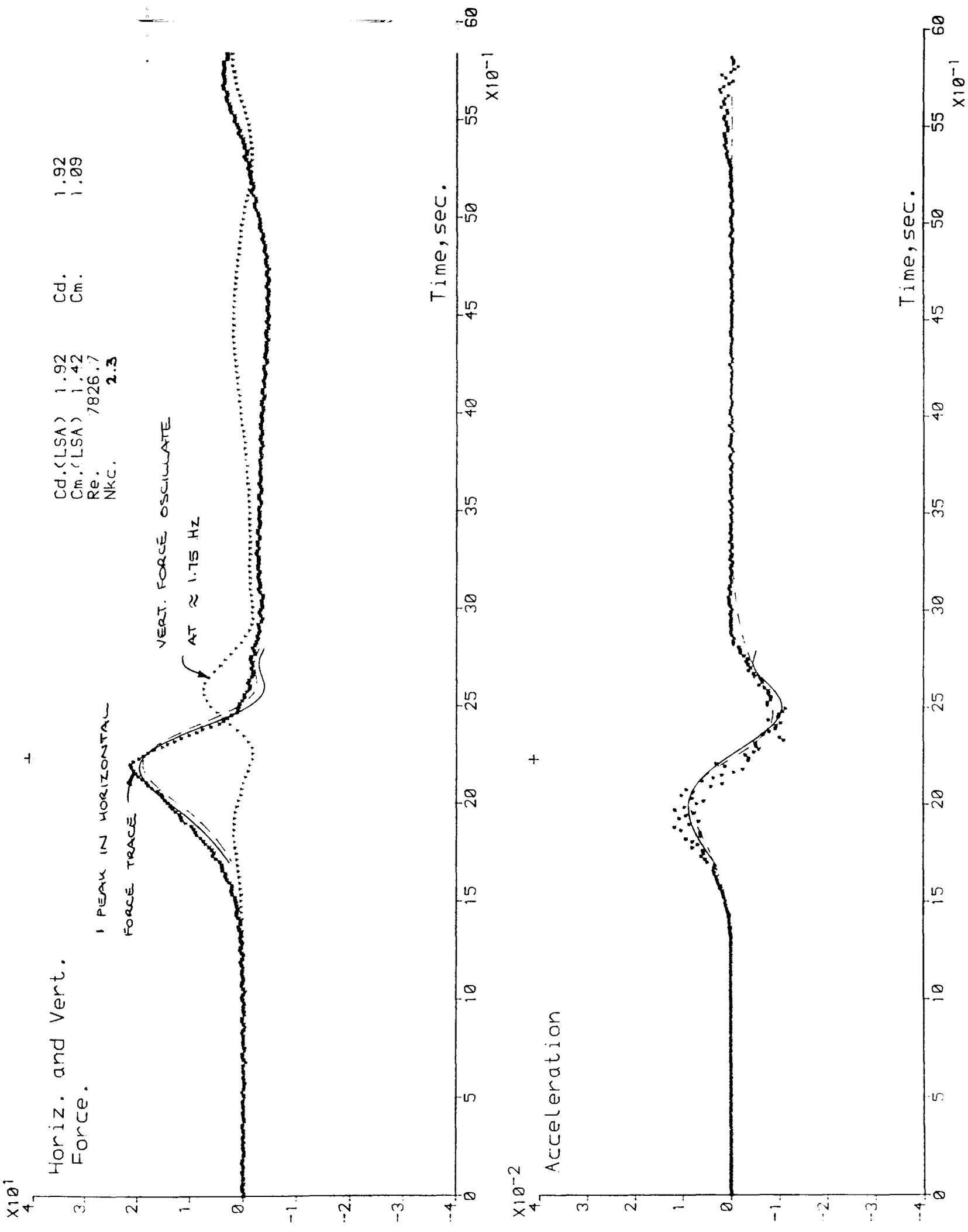
Figure 6.39 - Measured and Calculated forces.
(Morison: LSA [——]; XING [---])
Cyl.Dia.D/y_o=0.20; Cyl.pos.z_c/y_o=0.52
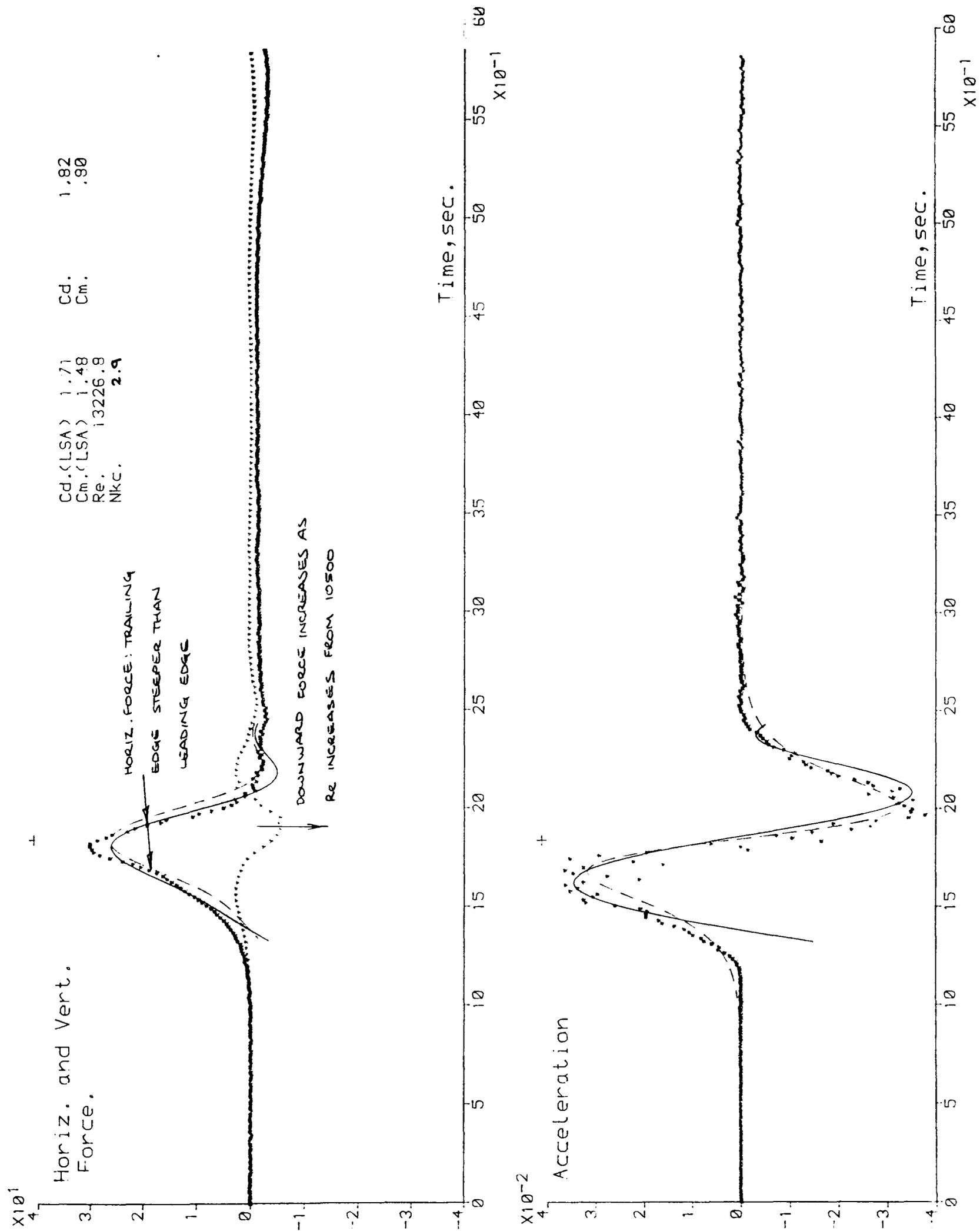
Figure 6.40 - Measured and Calculated forces.
(Morison: LSA [——]; XING [---])
Cyl.Dia.D/y_o=0.20; Cyl.pos.z_c/y_o=0.52
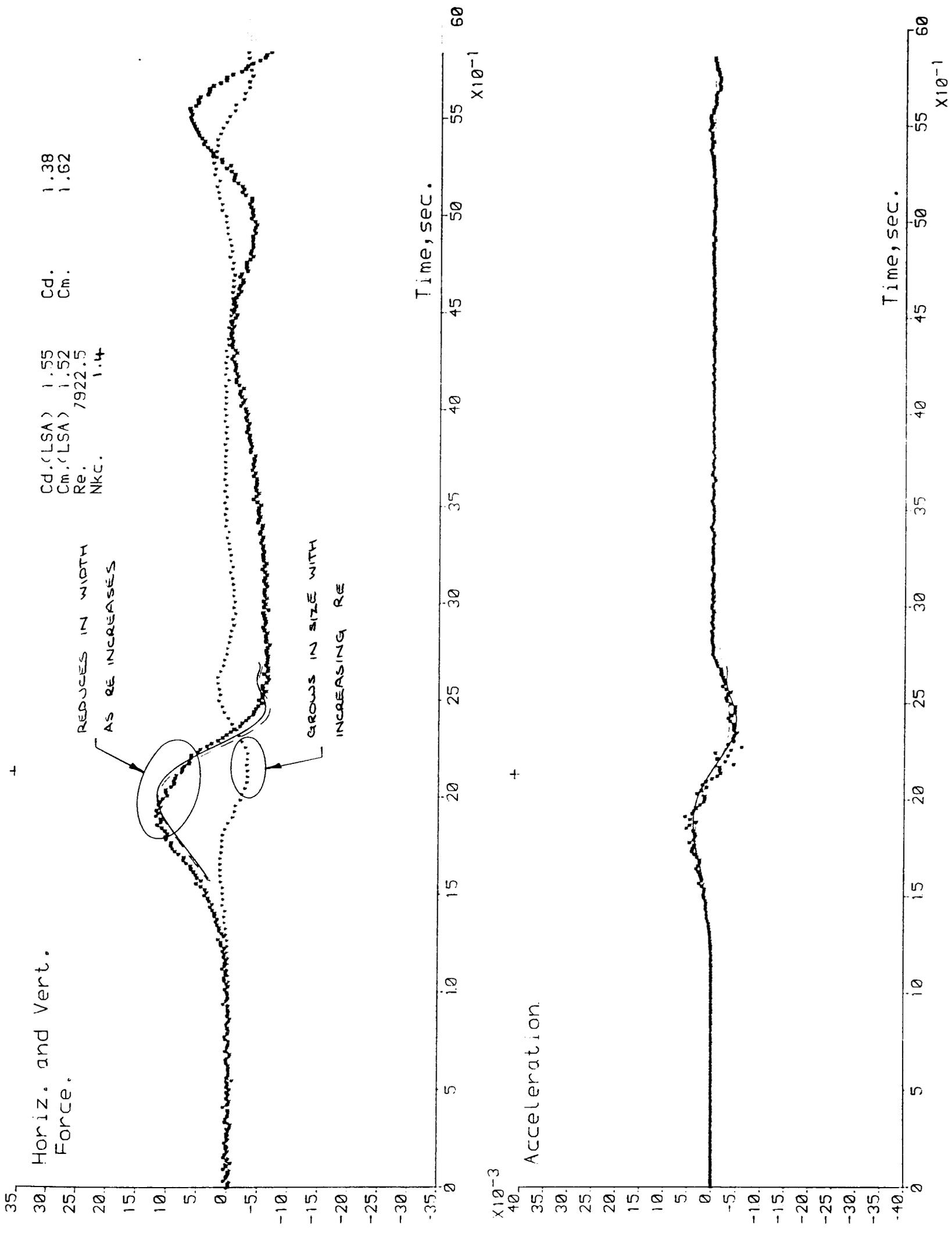
Figure 6.41 - Measured and Calculated forces.
(Morison: LSA [——]; XING [---])
Cyl.Dia.D/y_o=0.29; Cyl.pos.z_c/y_o=0.53
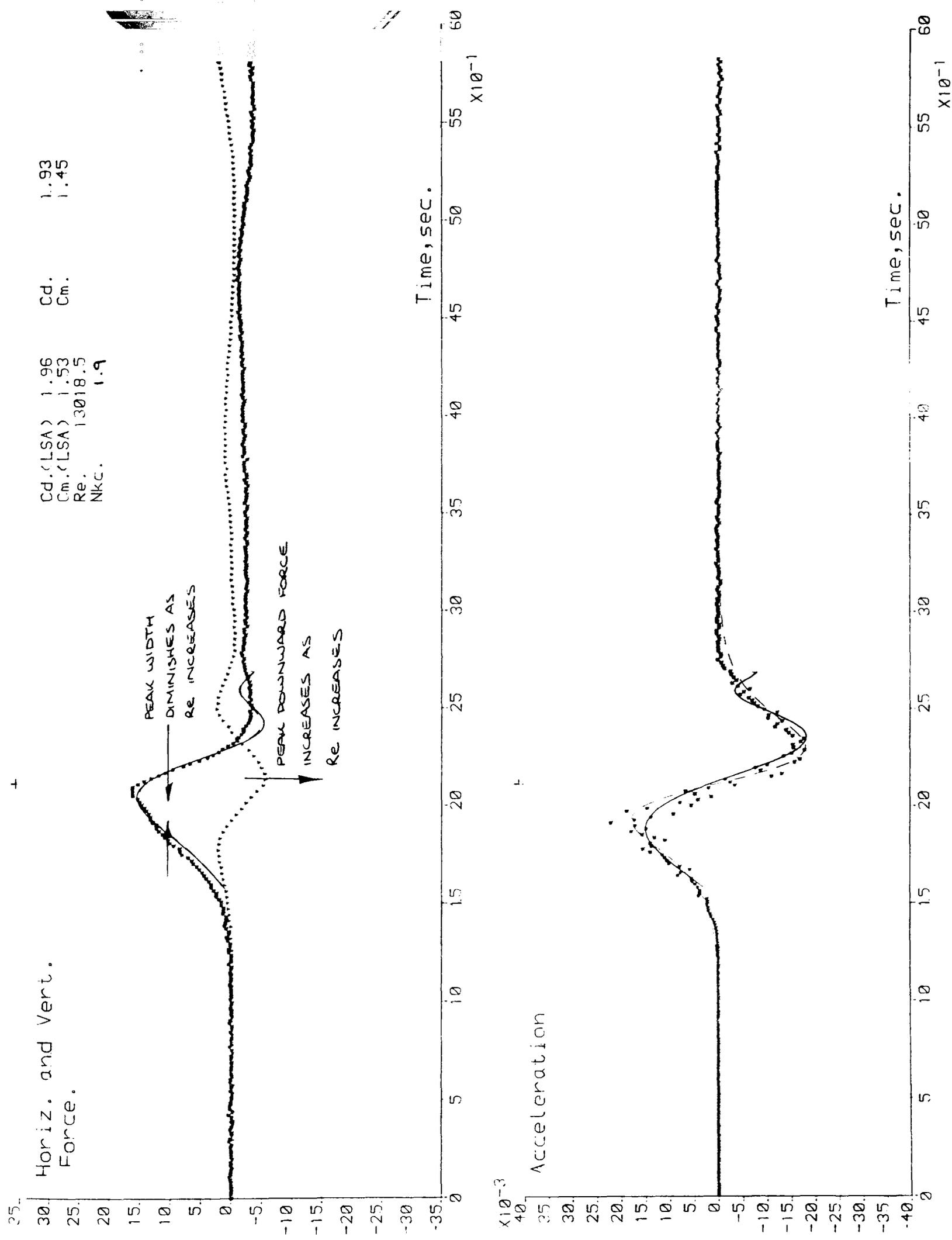
Figure 6.42 - Measured and Calculated forces.
(Morison: LSA [——]; XING [---])
Cyl. Dia. $D/y_o = 0.29$; Cyl. pos. $z_c/y_o = 0.53$
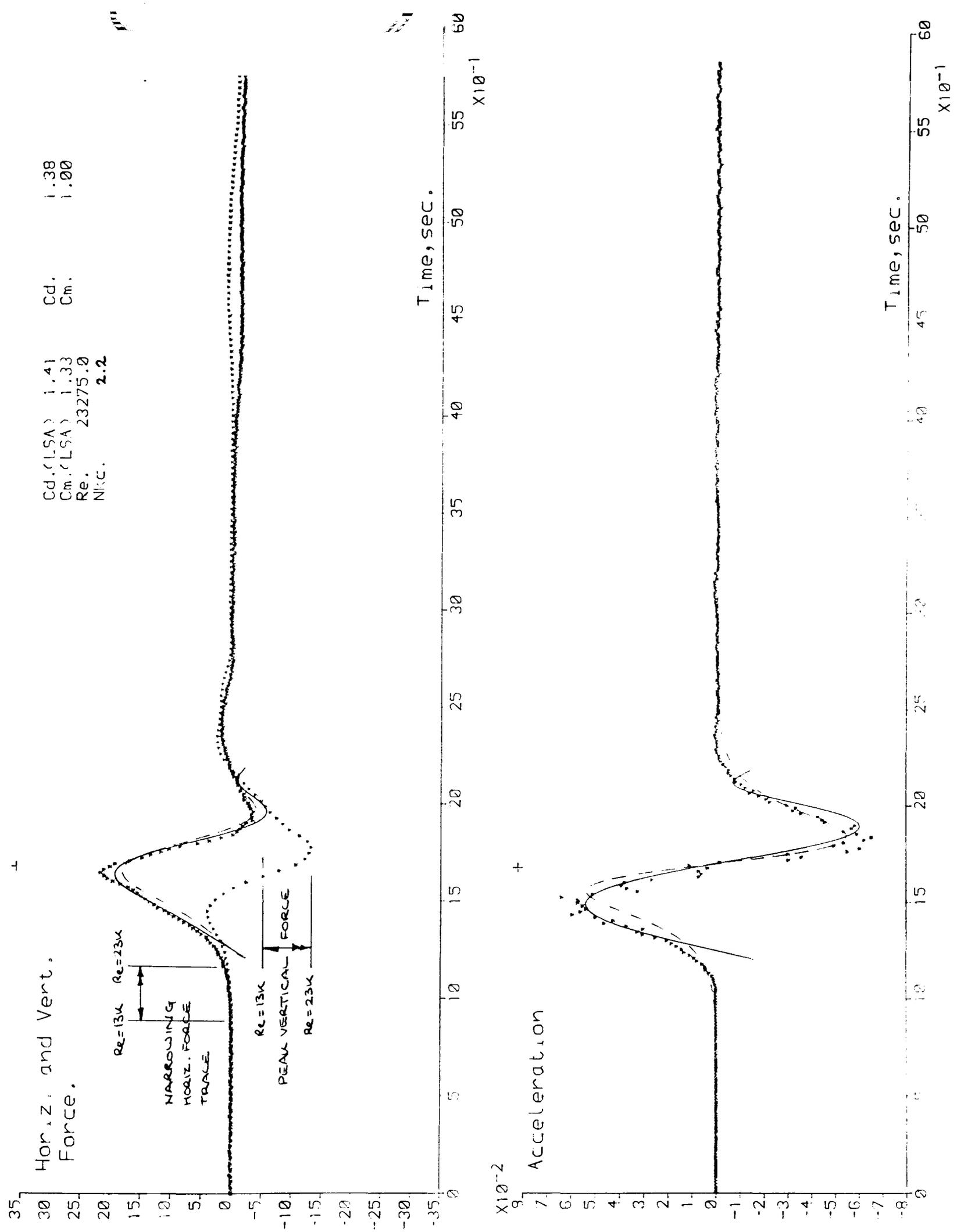
Figure 6.43 - Measured and Calculated forces.
(Morison: LSA [——]; XING [---])
Cyl.Dia.D/y_o=0.29; Cyl.pos.z_c/y_o=0.53
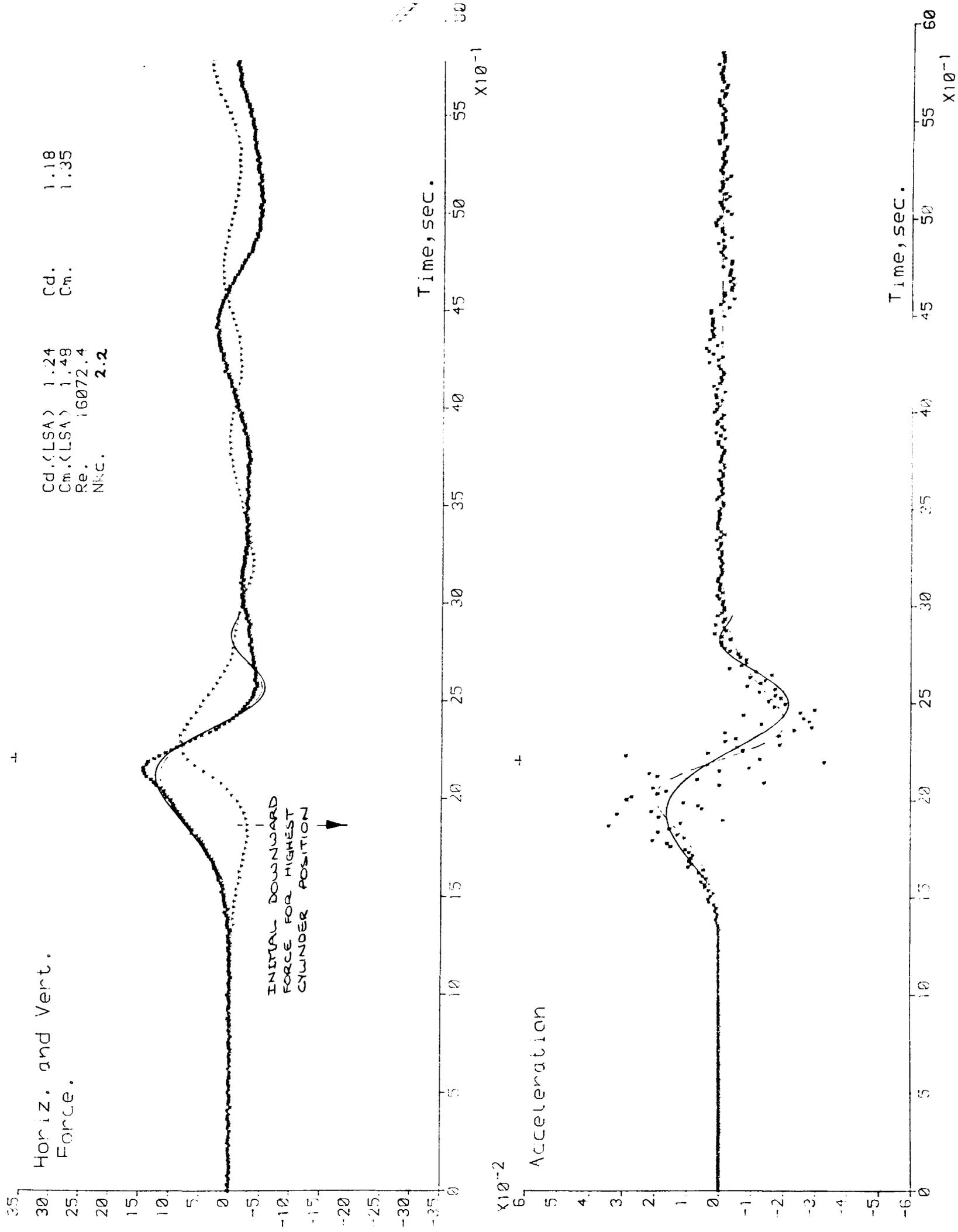
Figure 6.44 - Measured and Calculated forces.
(Morison: LSA [——]; XING [---])
Cyl.Dia.D/y_o=0.25; Cyl.pos.z_c/y_o=0.71

6.4.4.2 Calculated Forces

13mm Diameter cylinder

For the smallest cylinder neither analysis accurately matched the abrupt changes in the measured horizontal forces, though the LSA consistently gave better results with Re>6000, particularly for time of peak.

For Re<6000 the measured horizontal forces had two clear peaks with a central trough which was generally below the wave crest. This trough coincided with the peak force predicted by Morison's equation using the LSA (figure 6.45).

The crossing point method more correctly identified the first peak in the measured horizontal force trace but gave a trough under the second peak (figure 6.45).

As Re approached 7500 both analyses accurately represented the time and magnitude of peak force at the wave crest

27mm Diameter cylinder

Results for the 27mm diameter cylinder showed that at low Re (<7000) both analyses gave results for horizontal force at the front of the wave less than the measured, with the LSA giving marginally better results (figure 6.46). Whereas the crossing point method more closely predicted the time of peak force at low Re (<7000), the situation reversed at high Re (>8000) (figure 6.47).
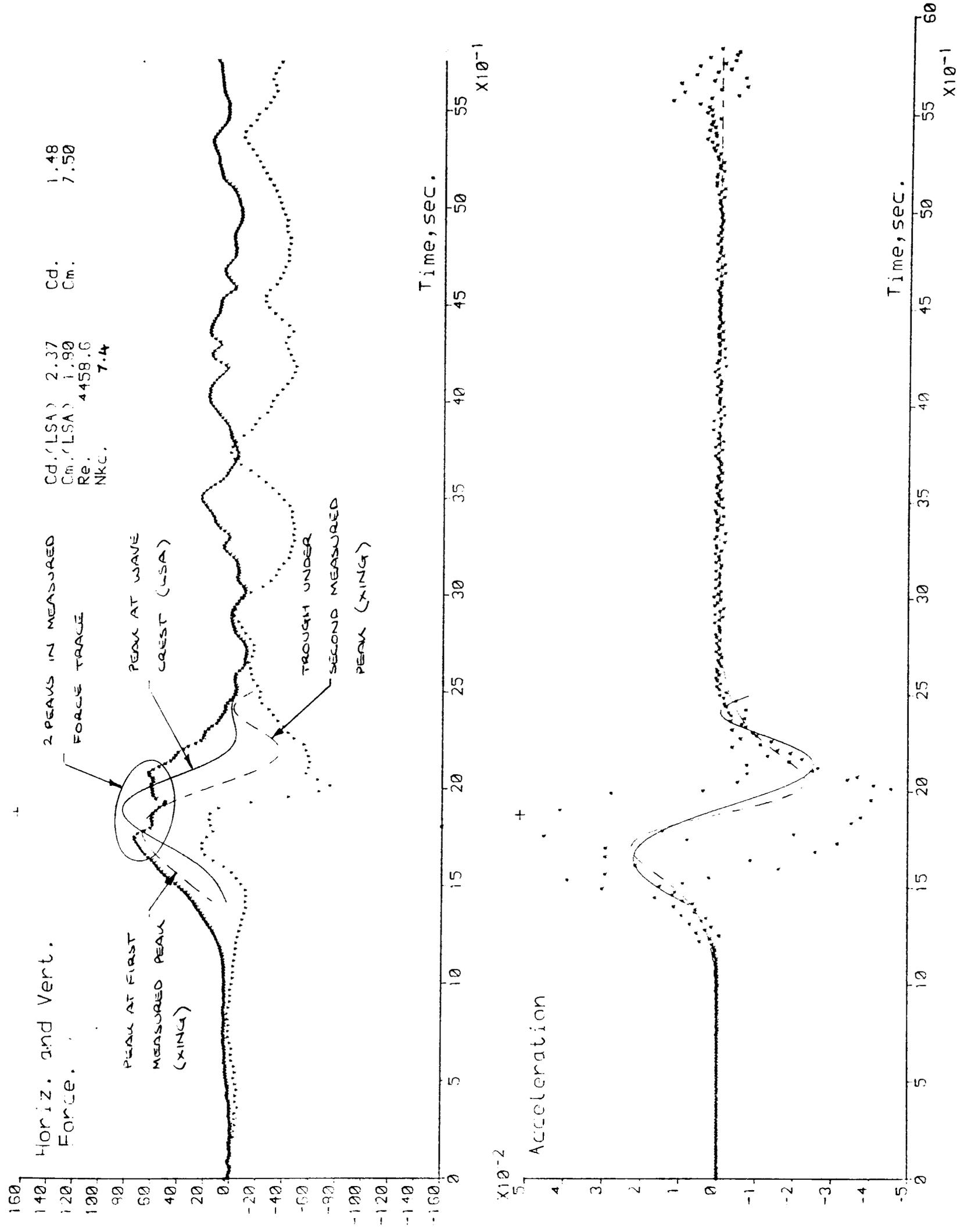
Figure 6.45 - Measured and Calculated forces.
(Morison: LSA [——]; XING [---])
Cyl.Dia.D/y_o=0.07; Cyl.pos.z_c/y_o=0.78
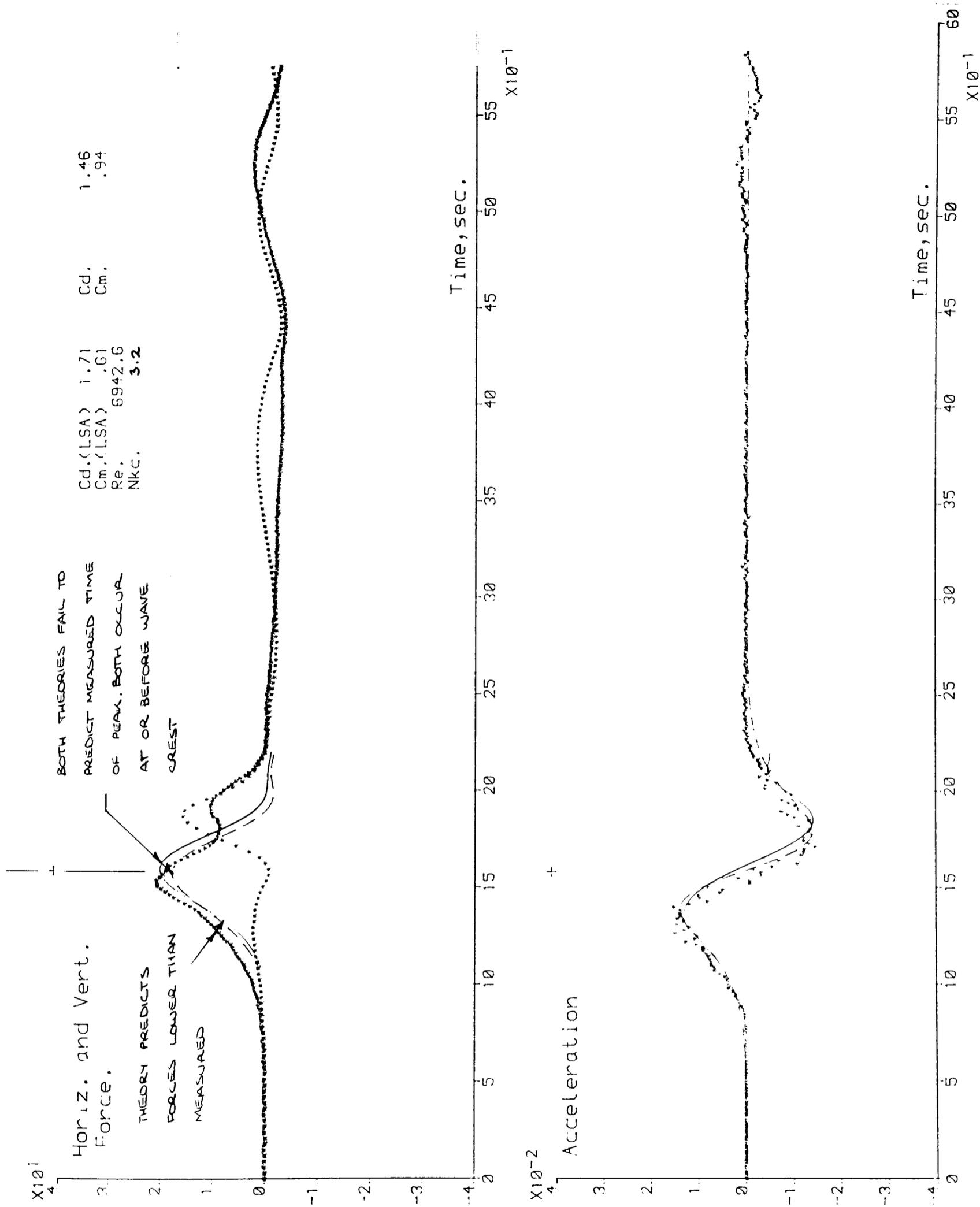
Figure 6.46 - Measured and Calculated forces.
(Morison: LSA [——]; XING [---])
Cyl.Dia.D/y_o=0.16; Cyl.pos.z_c/y_o=0.51

- 212 -
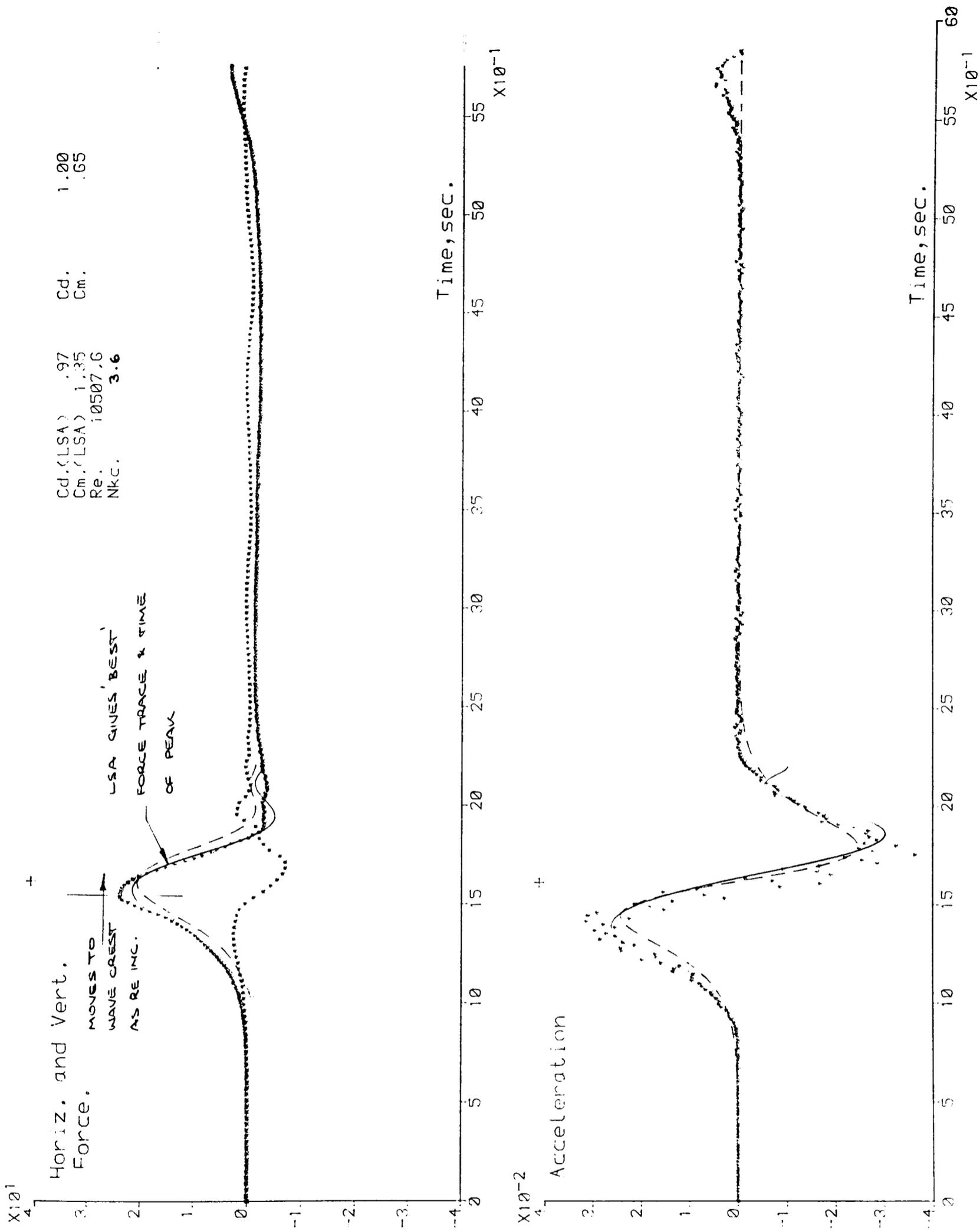
Figure 6.47 - **Measured and Calculated forces.**
(Morison: LSA [——]; XING [---])
Cyl.Dia.D/y_o=0.16; Cyl.pos.z_c/y_o=0.51

Morison's equation using coefficients calculated using the LSA predicted a peak force at or a little before the wave crest (figure 6.46). As Re increased the position of the highest measured force peak moved closer to the wave crest though never reached it by Re=17000 (figure 6.47).

For low Re<9500 the horizontal force trace had a secondary peak at the very rear of the wave, though this was never matched by the theory of Morison.

34mm Diameter cylinder

Results for the 34mm diameter cylinder showed that below Re=6000 both analyses gave excellent results, closely predicting the magnitude, time and shape of the horizontal force trace within the wave length (figure 6.48). The peak horizontal force was measured before the wave crest, with the force trace going negative at the rear of the wave to approximately 60% of the maximum positive value.

Between Re=6000 and Re=7000 the measured peak horizontal force increased markedly (figure 6.49). The LSA gave the best results over nearly all the wave however at peak horizontal force neither analysis matched the measured values for shape nor magnitude but came close by Re=8000.
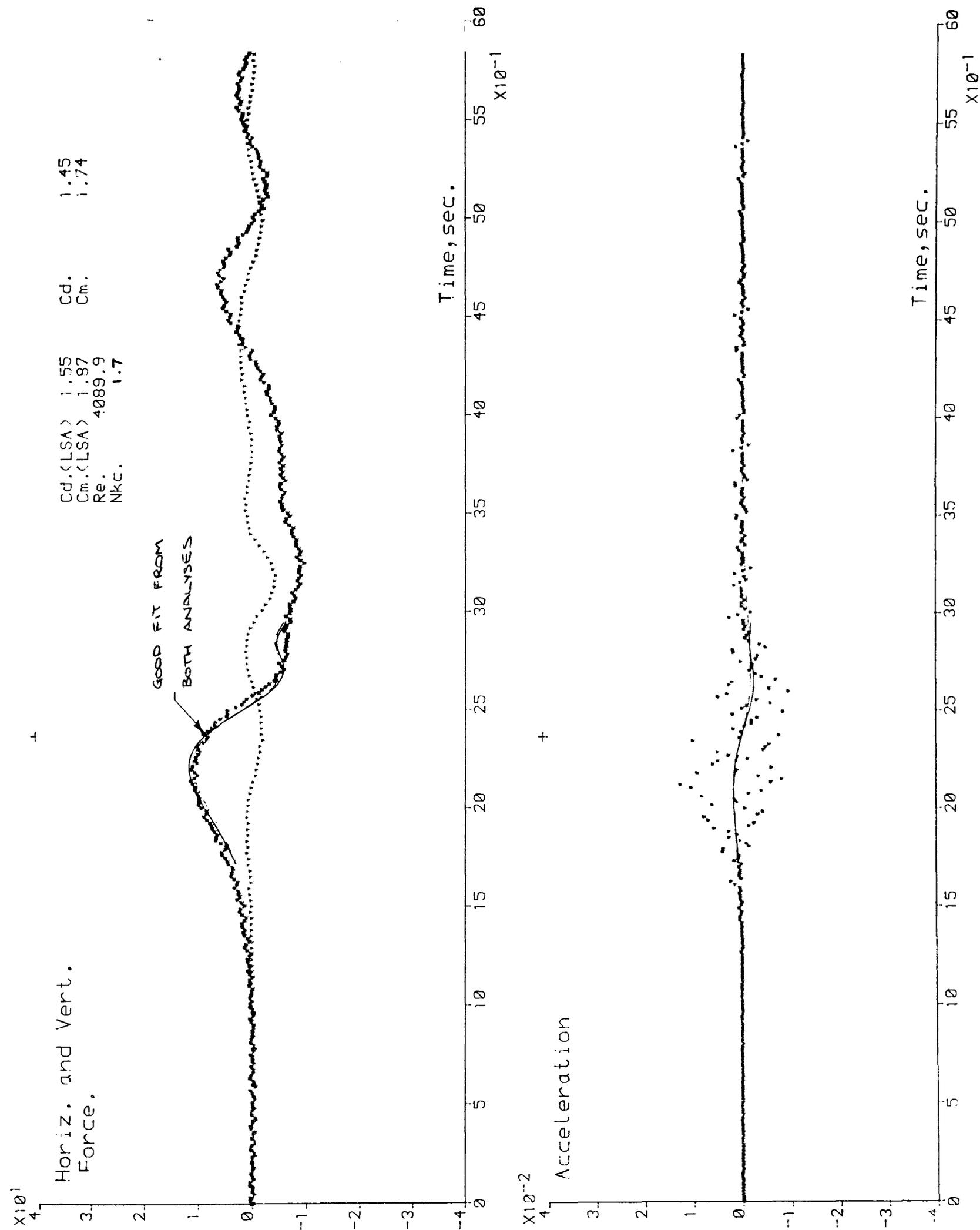
Figure 6.48 - Measured and Calculated forces.
(Morison: LSA [——]; XING [---])
Cyl.Dia.D/y_o=0.20; Cyl.pos.z_c/y_o=0.52
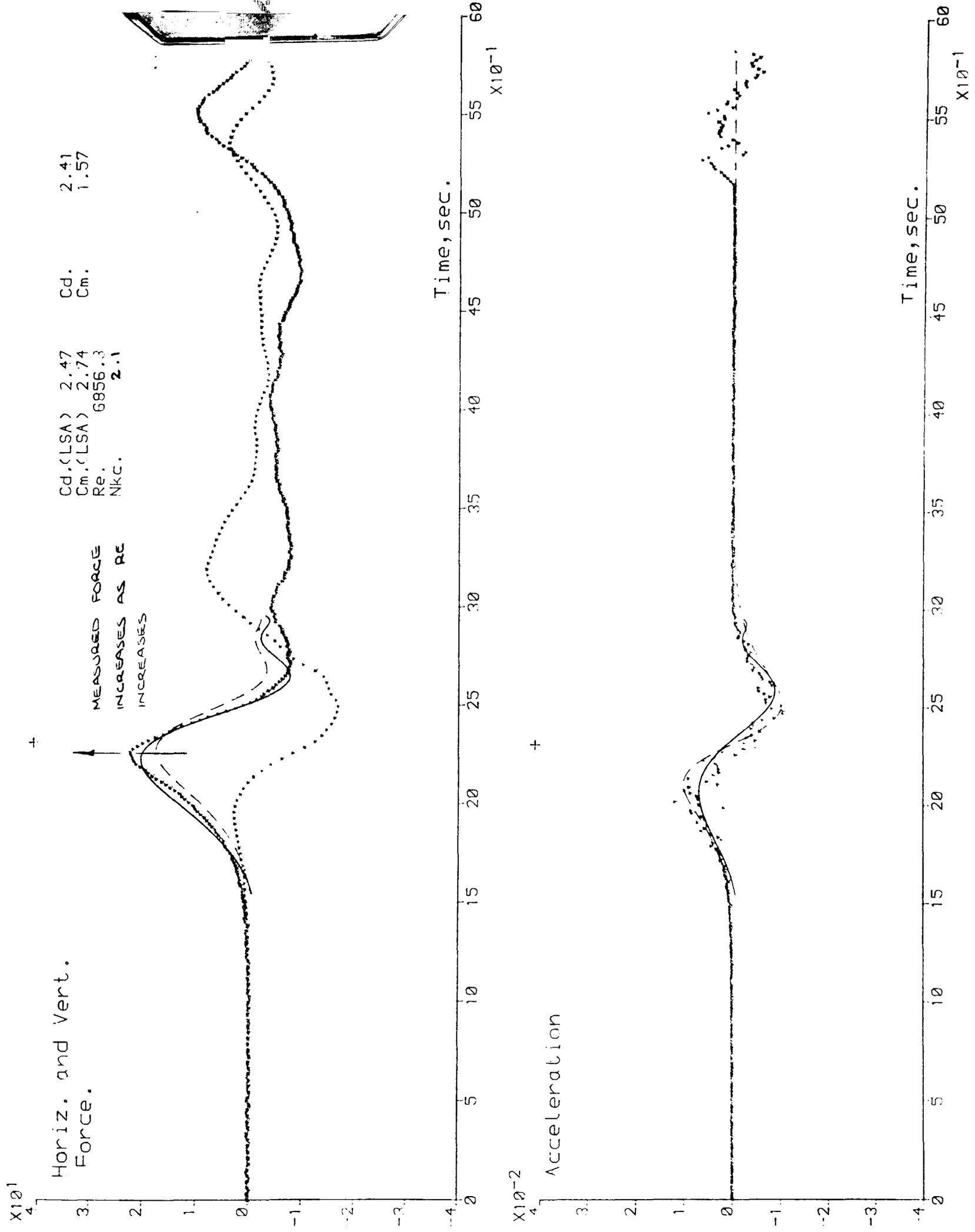
Figure 6.49 - Measured and Calculated forces.
(Morison: LSA [——]; XING [---])
Cyl.Dia.D/y_o=0.20; Cyl.pos.z_c/y_o=0.79

- 216 -

48mm Diameter cylinder

With Re<12000 both the LSA and crossing point method gave force traces which closely matched those measured for the largest cylinder (figure 6.50). They slightly under estimated the force at the front of the wave but matched the negative horizontal force at the rear of the wave. Results show only a slight discrepancy in matching the time and magnitude of the measured horizontal force peak for both analyses.

The agreement between the analyses and the measured forces deteriorate at the rear and peak of the wave for Re=16000 with the measured peak becoming sharper and the trough shallower (figure 6.51).
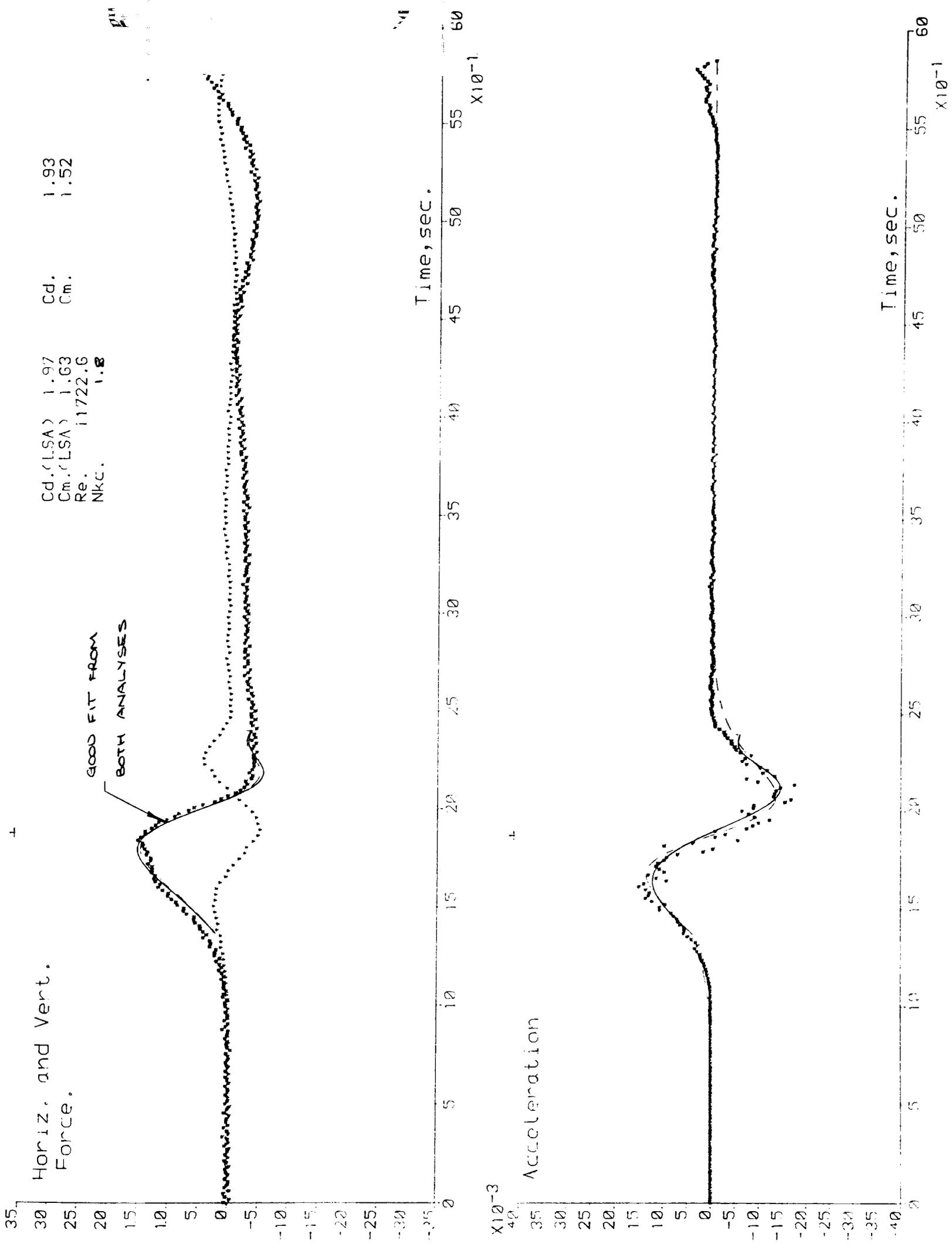
Figure 6.50 - Measured and Calculated forces.
(Morison: LSA [——]; XING [---])
Cyl.Dia.D/y_o=0.29; Cyl.pos.z_c/y_o=0.53

Cd.(LSA) 2.02   Cd.   1.97
Cm.(LSA) 1.90   Cm.   1.60
Re.   17955.2
NKC.   2.2

Horiz. and Vert.
Force.

AGREEMENT DETERIORATES
AS RE INCREASES

Time, sec.
X10⁻¹

Acceleration
X10⁻²

Time, sec.
X10⁻¹
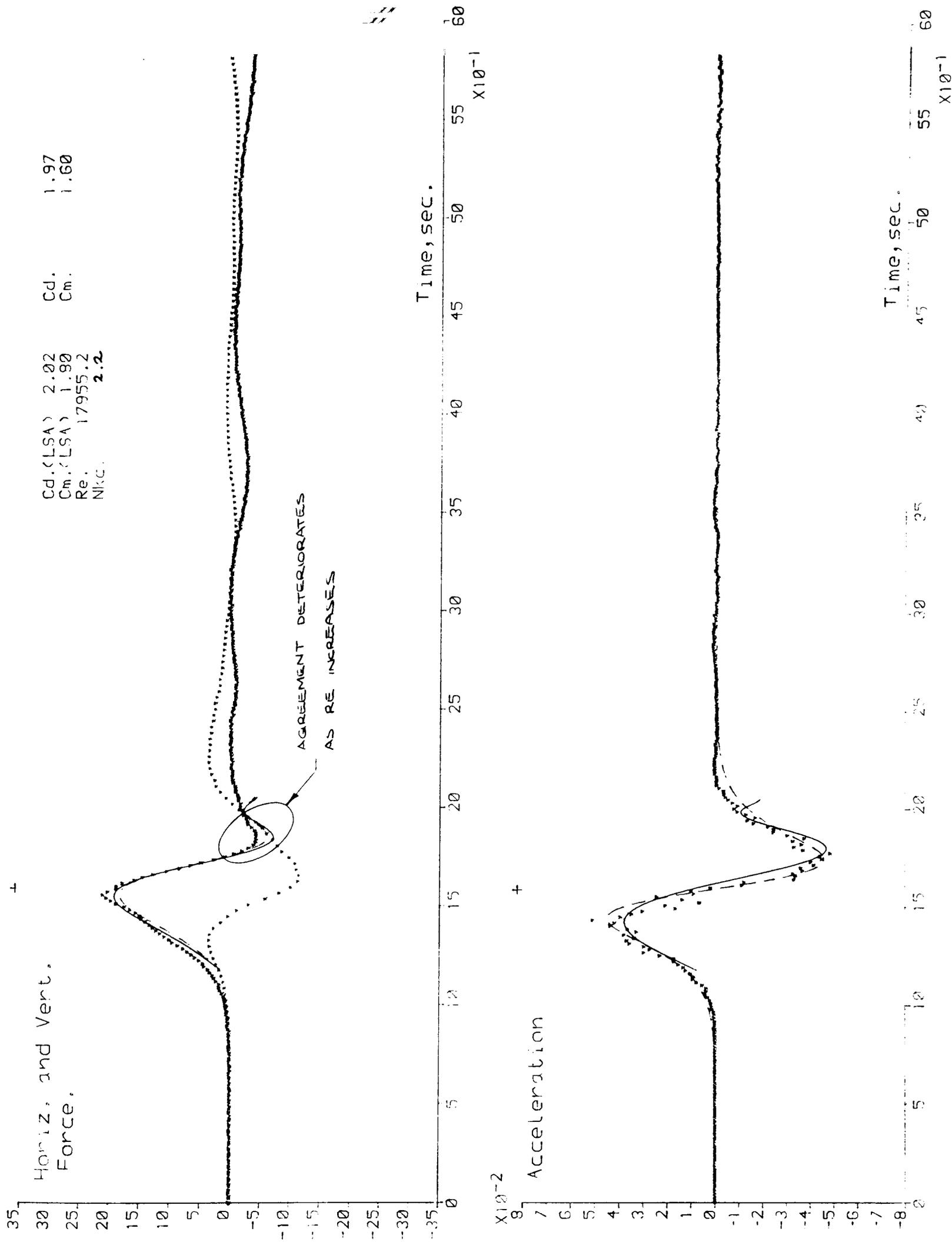
Figure 6.51 - Measured and Calculated forces.
(Morison: LSA [——]; XING [---])
Cyl. Dia. D/y_o=0.29; Cyl. pos. z_c/y_o=0.53

6.4.5 Forces on cylinders near the channel bed

6.4.5.1 Measured Forces

13mm Diameter cylinder
_____

As found previously, results for the smallest cylinder were characterised by the effect of a low Reynolds number with a high Keulegan and Carpenter number thus showing considerable oscillation in both the horizontal and vertical force traces.

Vertical and horizontal forces were recorded immediately fluid motion commenced, the vertical force initially being towards the channel bed. It acted for much longer than the initial horizontal force, which tended to be short and highly peaked (figure 6.52). Frequently the horizontal force dropped to zero at the wave crest.

The general shape of both the horizontal and vertical force trace remained the same for all Re.

$$2800 \leq Re \leq 26000$$
$$\& \ 1.0 \leq Nkc \leq 10.0$$

For this cylinder

$$e/D = 2.25$$

$$z_c/y_o = 0.81$$

$$D/y_o = 0.07$$
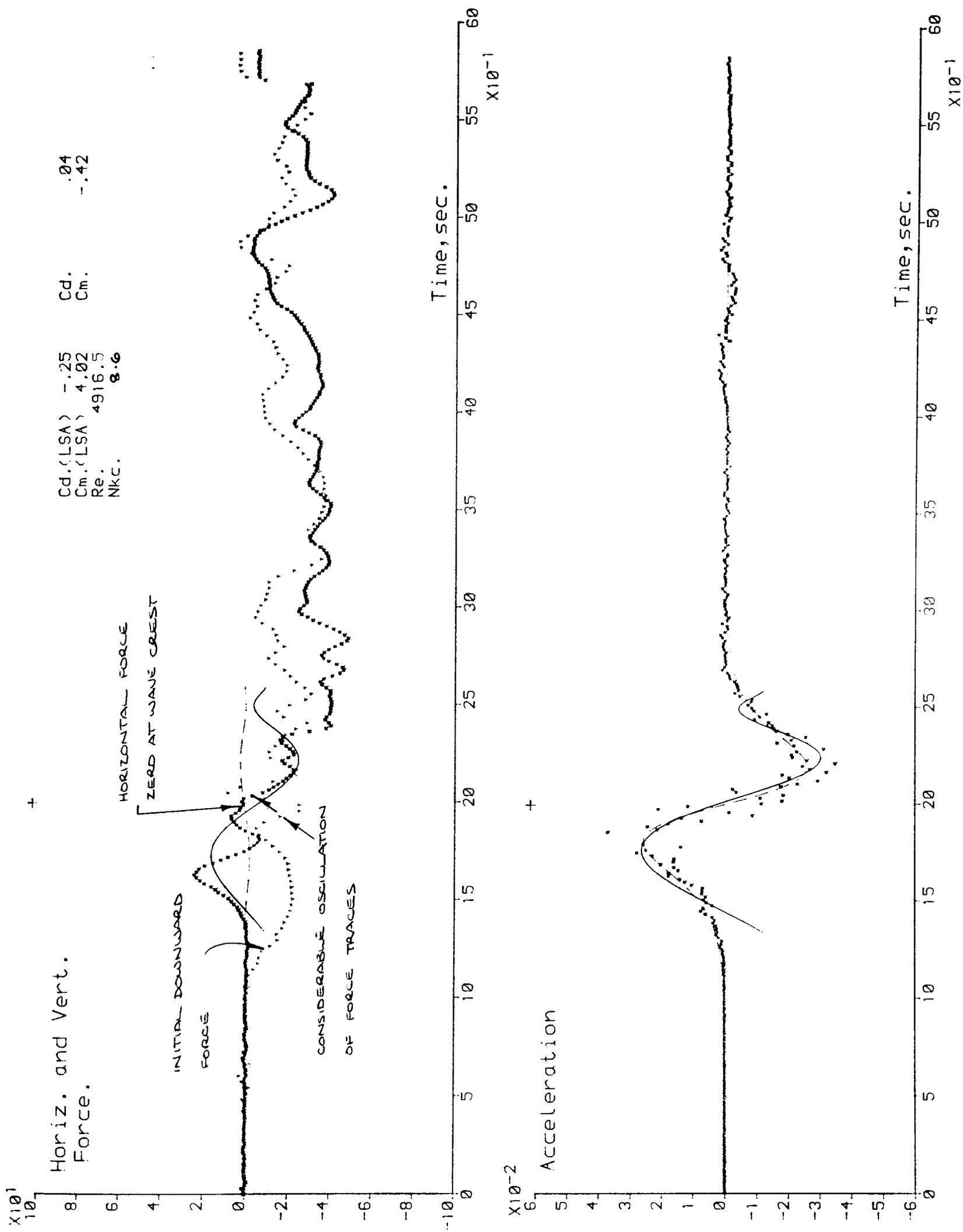
Figure 6.52 - Measured and Calculated forces.
(Morison: LSA [——]; XING [---])
Cyl.Dia.D/y_o=0.07; Cyl.pos.z_c/y_o=0.19

- 221 -

27mm Diameter cylinder

Results for the 27mm diameter cylinder had a different "characteristic" shape than those of the smallest cylinder.

The horizontal force trace reached a peak just prior to the wave crest, the front slope being greater than that at the rear. Close inspection showed irregular 'lumps' on the trailing edge of the force trace which diminished in amplitude with increasing Re (figures 6.53).

The vertical force trace remained essentially zero to just before the wave crest, going positive to approx. 80% of the maximum horizontal force. The vertical forces remained positive over the majority of the wave only becoming slightly negative at the very rear of the wave.

34mm Diameter cylinder

Results for the 34mm diameter cylinder showed that the maximum vertical force almost equalled the maximum horizontal force (figure 6.54).

Both vertical and horizontal force traces showed slight undulations after the wave had passed in contrast to the highly disturbed trace of the smallest cylinder.
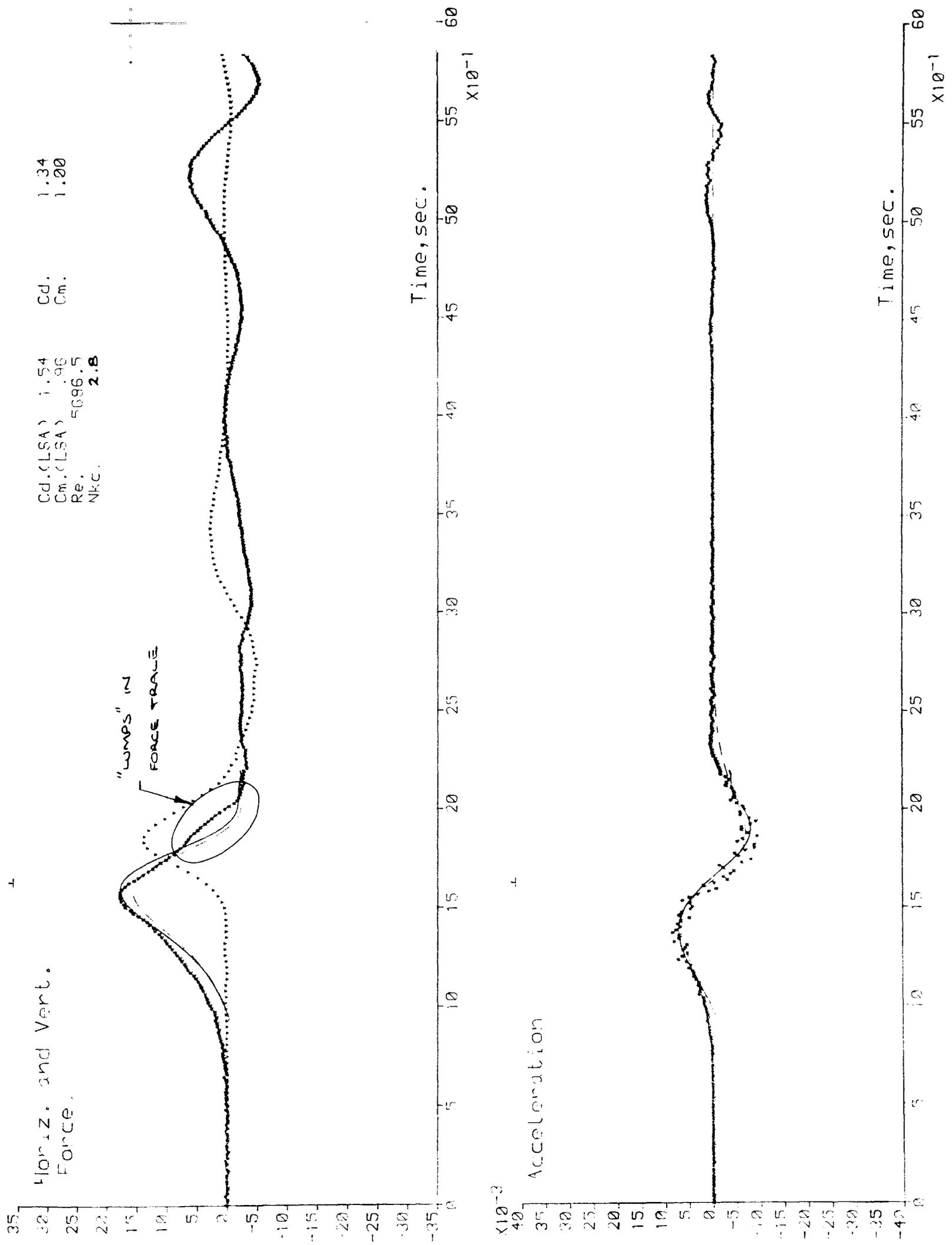
Figure 6.53 – Measured and Calculated forces.
(Morison: LSA [——]; XING [---])
Cyl.Dia.D/y_o=0.16; Cyl.pos.z_c/y_o=0.22

- 223 -
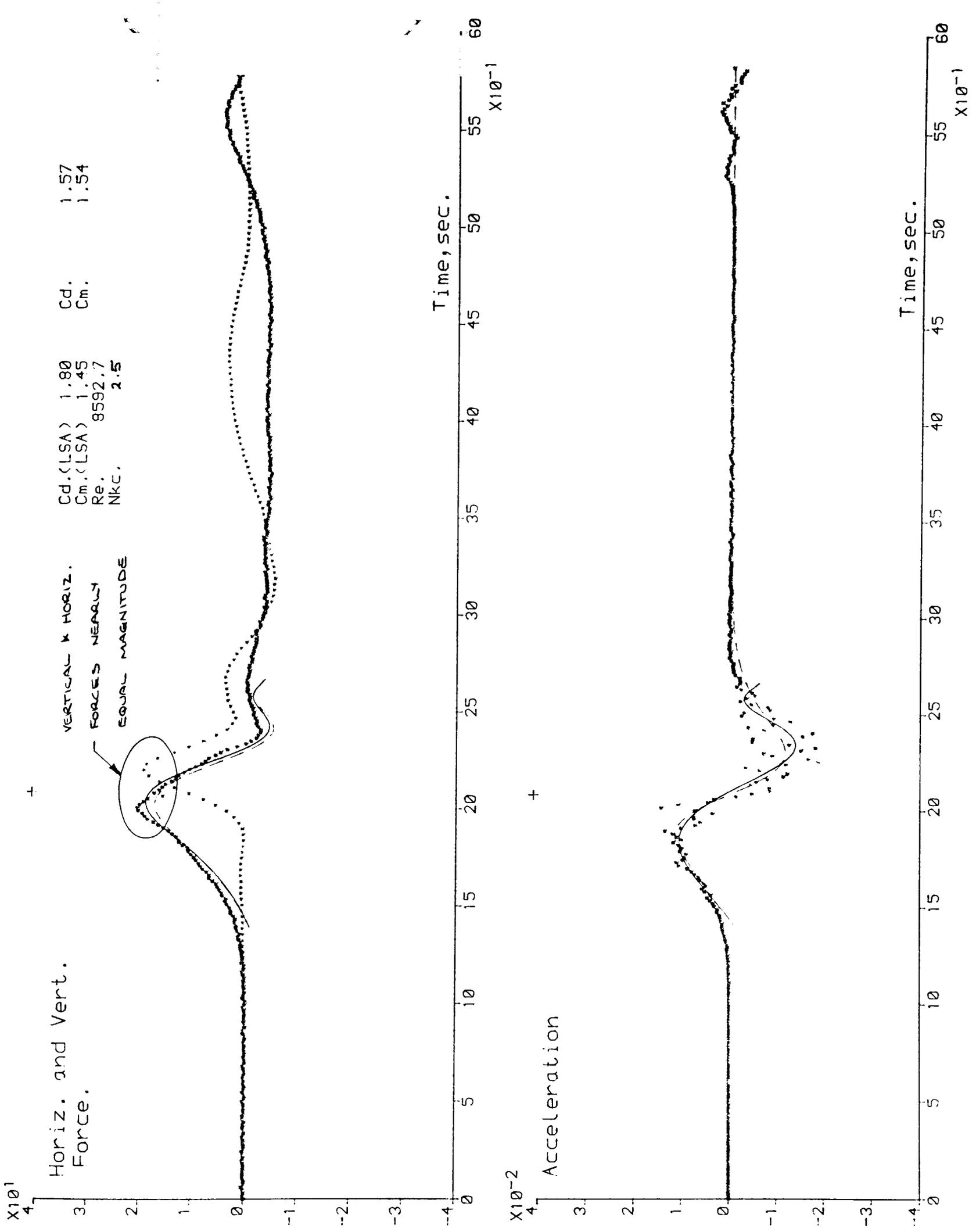
Figure 6.54 - Measured and Calculated forces.
(Morison: LSA [——]; XING [---])
Cyl.Dia.D/y_o=0.20; Cyl.pos.z_c/y_o=0.22

As Re increased beyond 9000 the vertical force trace developed a small trough at the rear of the main elevation. This was not consistent for all results (figure 6.55).

48mm Diameter cylinder

Close inspection of the figure 6.56 show that for the largest cylinder a small trough in the vertical force trace appeared immediately prior to the main peak, which remained constant size in the range $12000 \leq Re \leq 26000$ ($1.0 \leq Nkc \leq 2.0$).

It became noticeable that as the cylinder diameter increased the horizontal force trace became broader at its base with increasingly large negative force after the wave had passed. With Re approximately 13000 the horizontal force trace showed a broad trough which narrowed as Re increased further.

A summary and detailed interpretation of results is given in chapter 7.
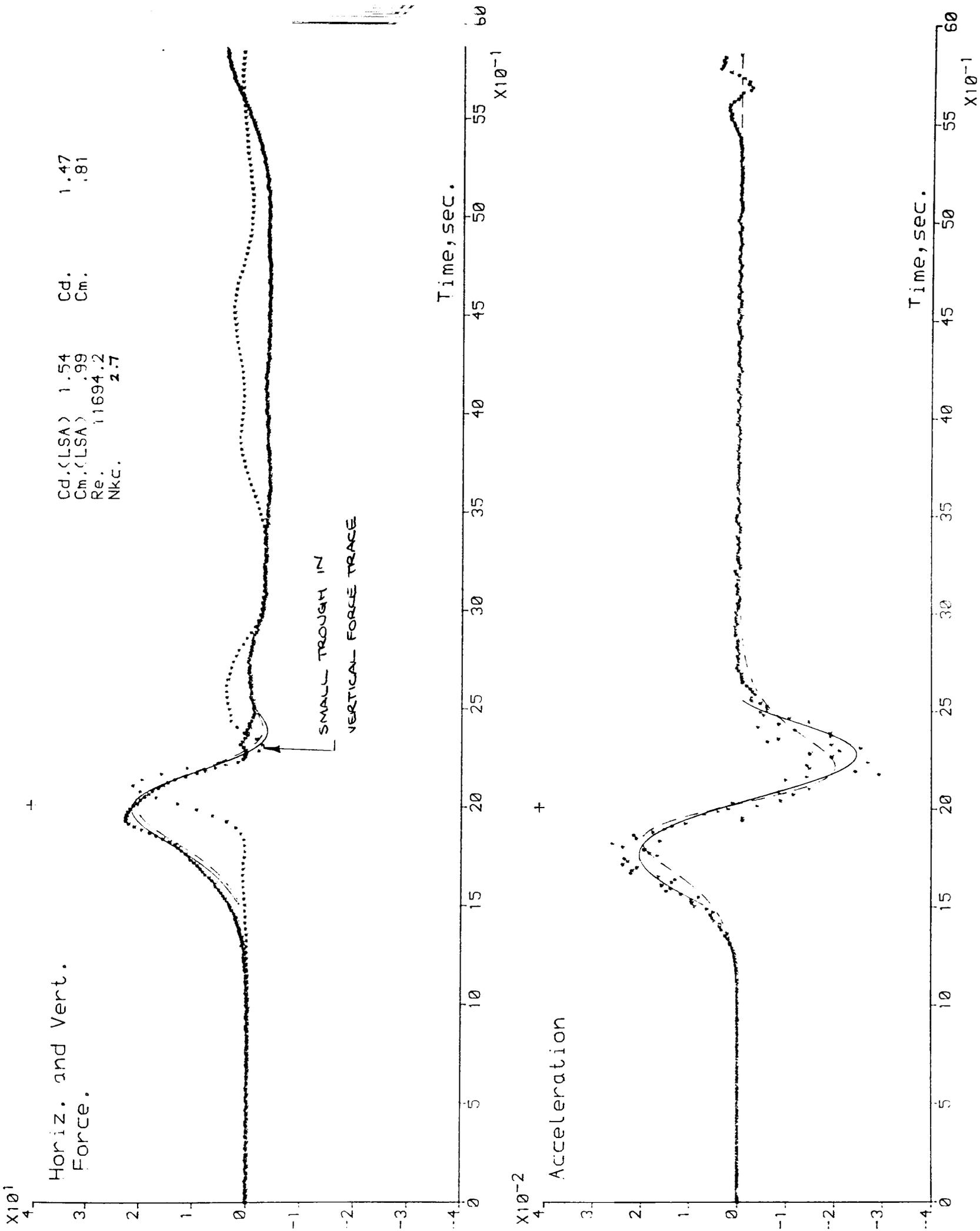
Figure 6.55 - Measured and Calculated forces.
(Morison: LSA [——]; XING [---])
Cyl.Dia.D/y_o=0.20; Cyl.pos.z_c/y_o=0.22
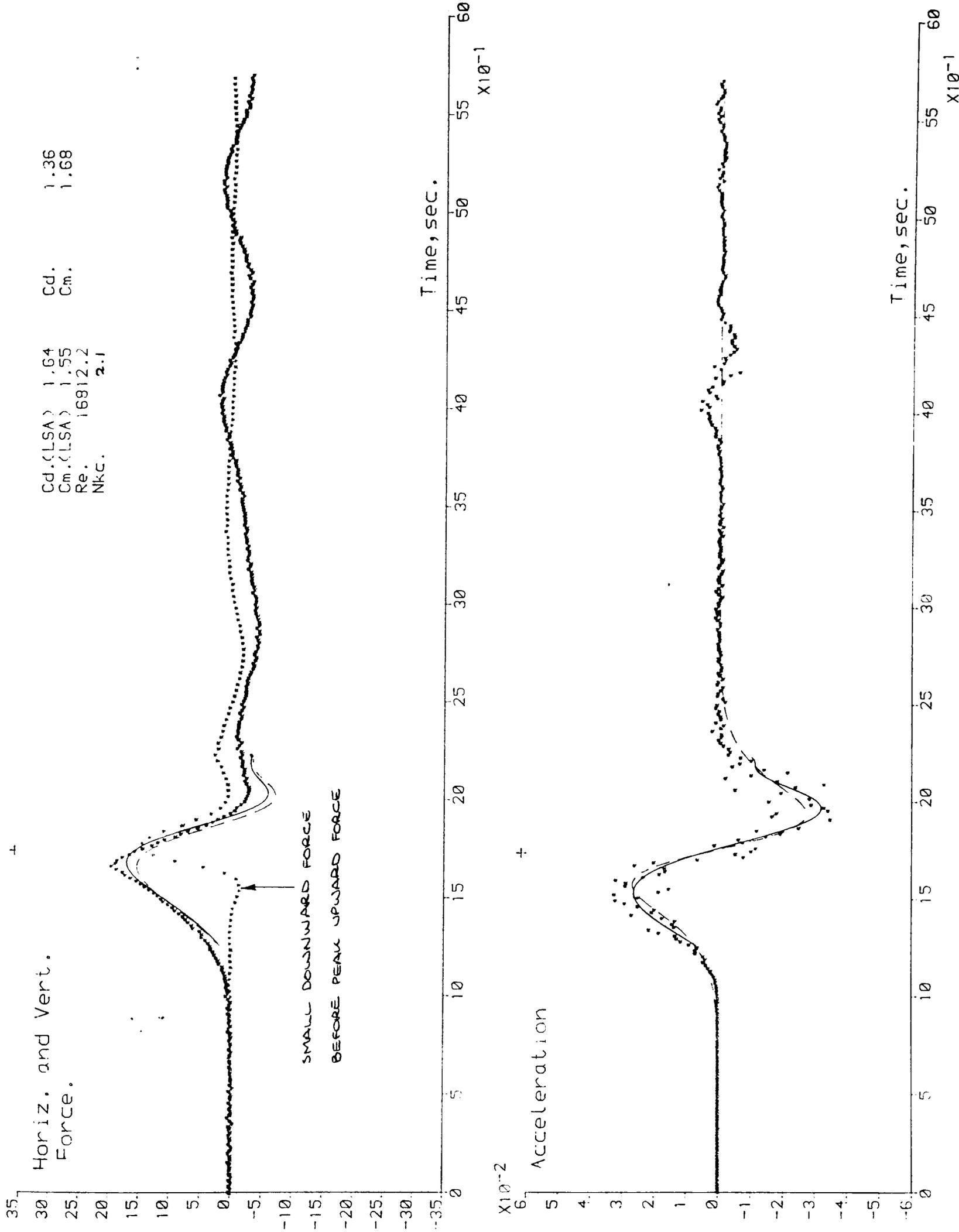
Figure 6.56 – Measured and Calculated forces.
(Morison: LSA [——]; XING [---])
Cyl.Dia.D/y_o=0.29; Cyl.pos.z_c/y_o=0.21

6.4.5.2 Calculated Forces

13mm Diameter cylinder

Results for the smallest cylinder showed that neither analysis accurately represented the measured values. However Morison's equation using coefficients calculated with the LSA gave consistently better results than with coefficients calculated using the crossing point method. Results using the LSA did not accurately match the abrupt changes in the horizontal force nor did it match the peak value or indeed the time over which it was applied. Frequently the crossing point method predicted zero horizontal force as the wave passed because the measured horizontal force was zero at both points where the Morison coefficients were calculated. The crossing point method proved unreliable and inconsistent here.

Morison's equation with coefficients calculated using the LSA gave peak values between 60% - 80% of those measured. The LSA predicted peak values closer to the wave crest than observed. Agreement between forces calculated using LSA and measured results was poorest at the very rear of the wave for all Re (2500 - 9900).

27mm Diameter cylinder

Results for the 27mm diameter cylinder (figure 6.57) show that at low Re Morison's equation using the LSA marginally under estimated forces at the front of the wave. It also gave forces which reached a peak of similar magnitude though closer the wave crest than measured. The measured force reached its

Horiz. and Vert.
Force.

Cd.(LSA)   2.31   Cd.   2.00
Cm.(LSA)   1.04   Cm.   .95
Re.   5848.2
Nkc.   6.6

"LSA" CLOSELY PREDICTS
MAGNITUDE & TIME OF PEAK
FORCE

UNDERESTIMATES
FORCE AT WAVE
FRONT

Time, sec.
X10⁻¹

Acceleration

Time, sec.
X10⁻¹
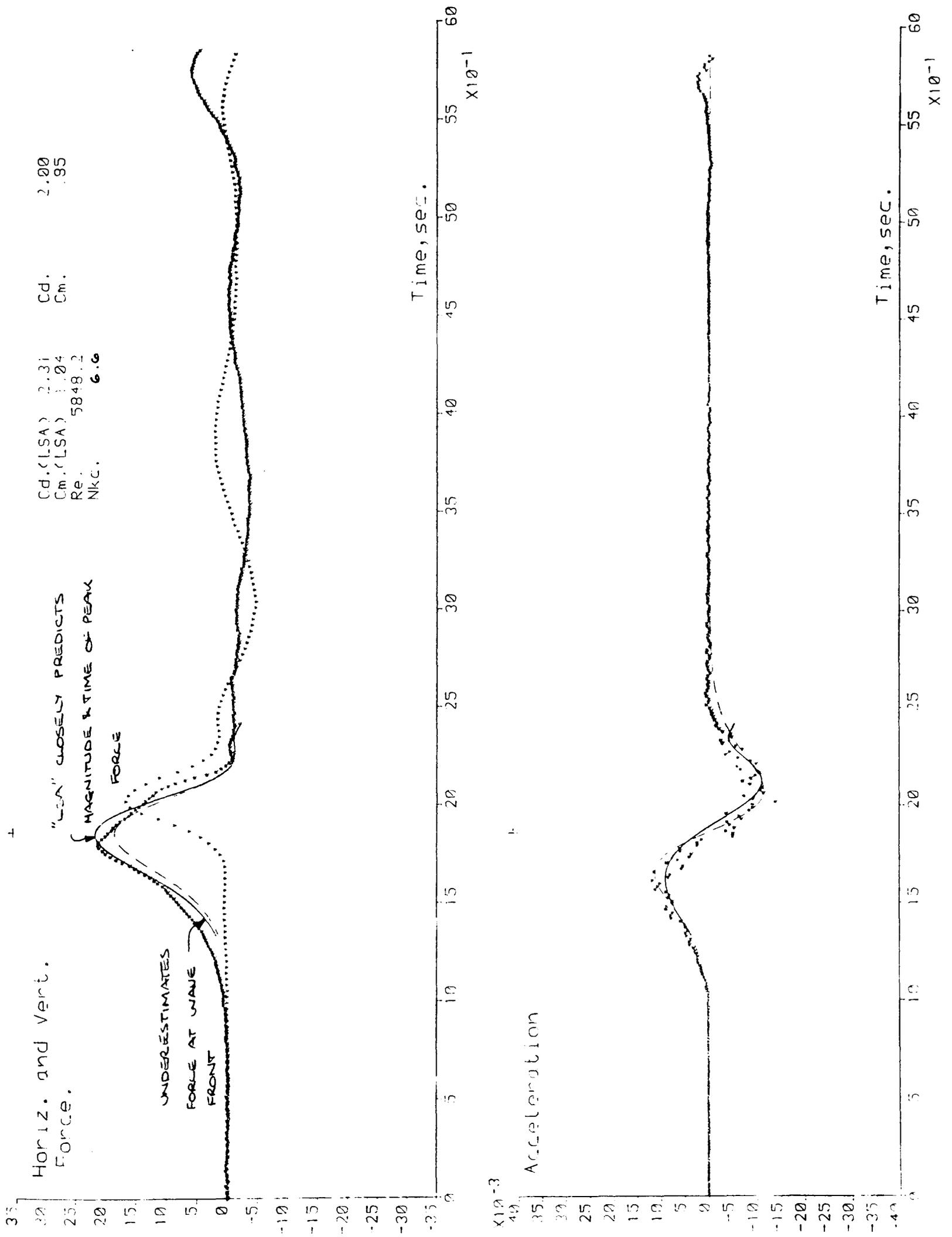
Figure 6.57 – Measured and Calculated forces.
(Morison: LSA [——]; XING [---])
Cyl.Dia.D/y_o=0.16; Cyl.pos.z_c/y_o=0.22

- 229 -

peak value before the wave crest. Using the crossing point method Morison's equation under estimated the horizontal force for all Re.

34mm Diameter cylinder

Over the entire range of results for the 34mm diameter cylinder (figure 6.58) (12000<=Re<=26000) Morison's equation using coefficients calculated using a LSA gave better results than with the crossing point method. In both cases Morison's equation marginally under estimated the horizontal forces before the wave crest though at the rear of the wave the LSA gave good agreement.

Both analyses showed consistently better agreement with measured forces at the rear of the wave, than for the smaller cylinders.

48mm Diameter cylinder

As with the 34mm diameter cylinder, Morison's equation using coefficients calculated using a LSA gave better results than with the crossing point method (figure 6.59). Neither method of calculating coefficients was able to match the sharp peak in the horizontal force trace, and over estimated the trough in the force trace following the wave crest.

As a whole, good agreement was achieved between Morison's theory and measured results.
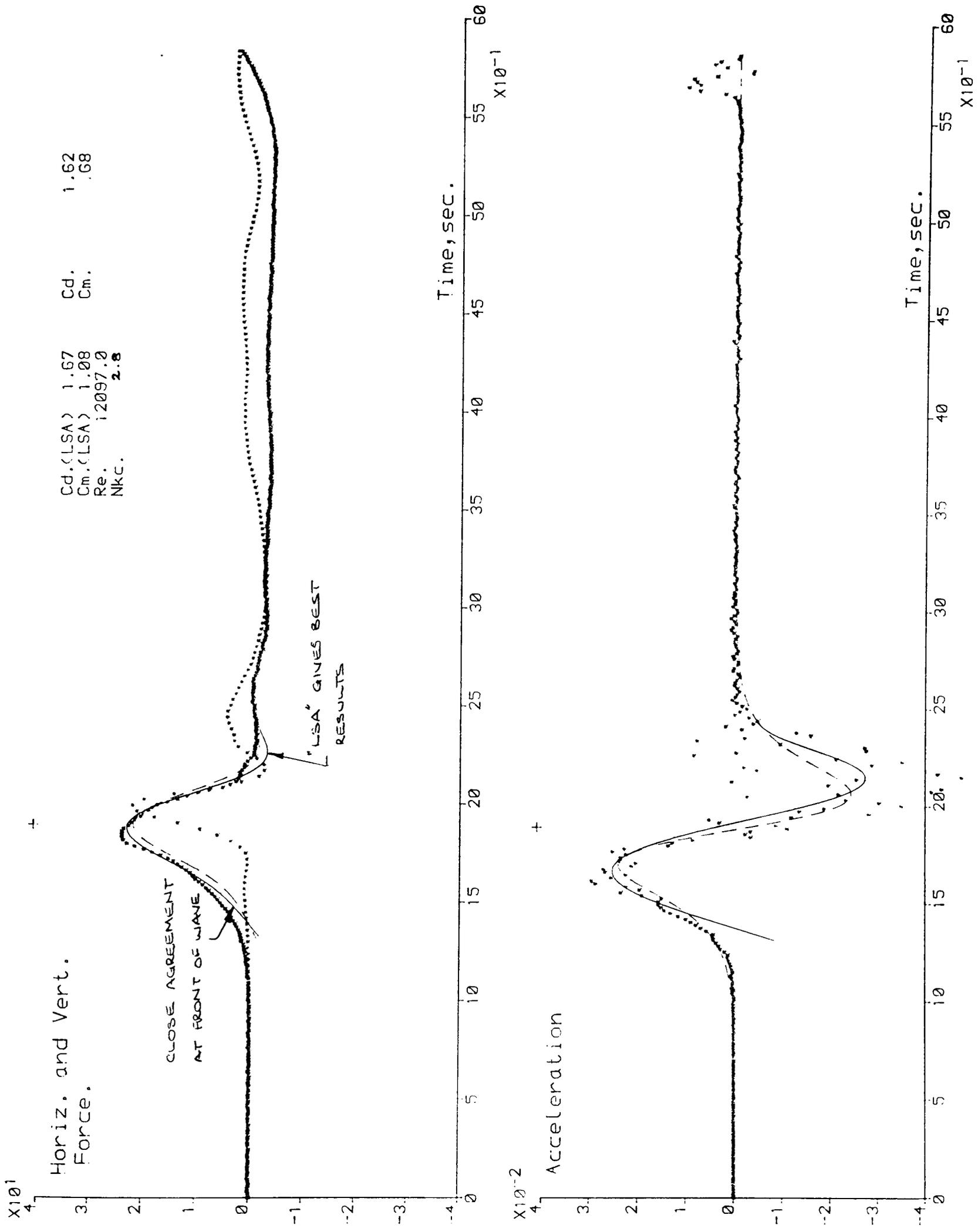
Figure 6.58 - Measured and Calculated forces.
(Morison: LSA [——]; XING [---])
Cyl.Dia.D/y_o=0.20; Cyl.pos.z_c/y_o=0.22
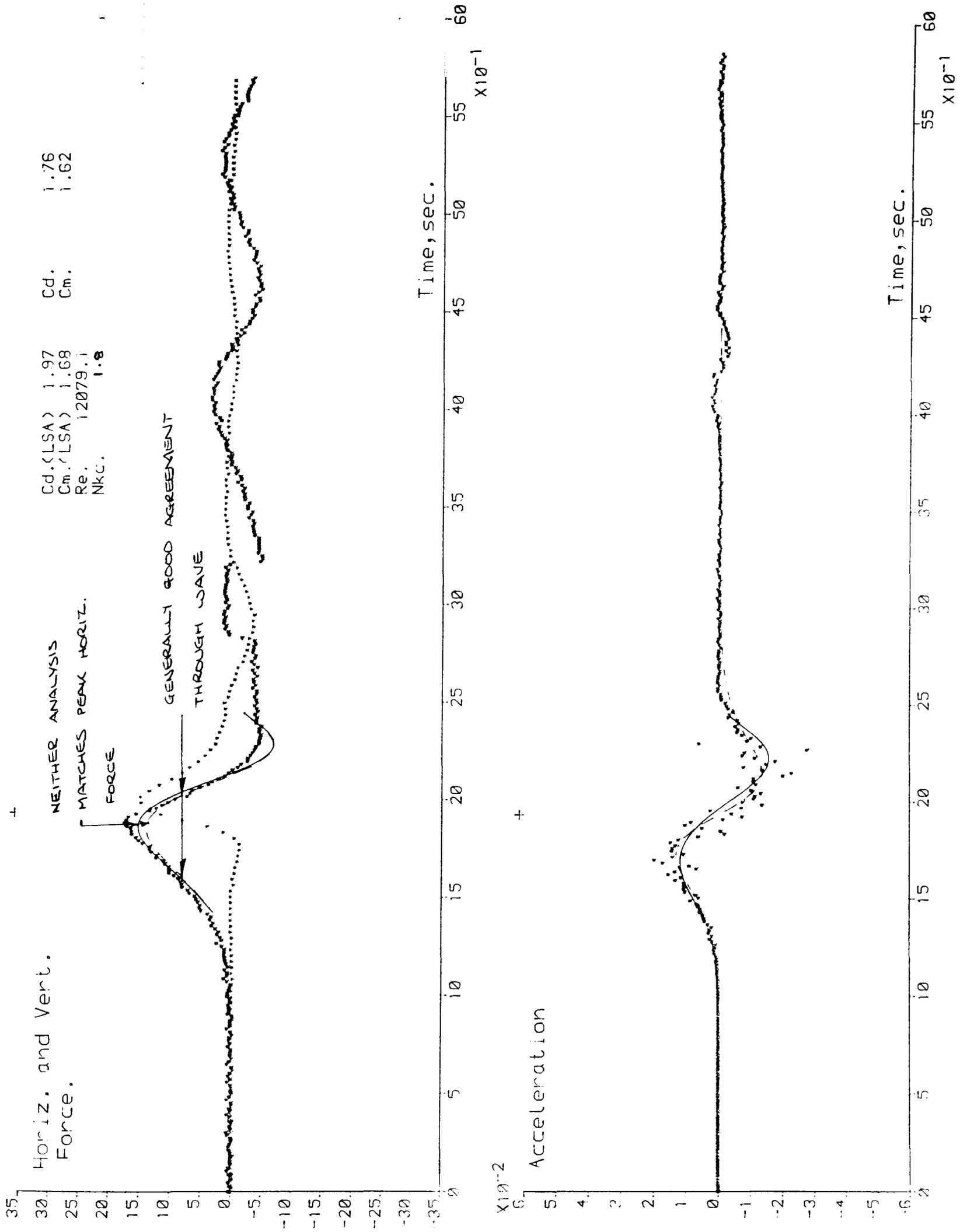
Figure 6.59 - Measured and Calculated forces.
(Morison: LSA [——]; XING [---])
Cyl.Dia.D/y_o=0.29; Cyl.pos.z_e/y_o=0.21

6.5. Force Coefficients

6.5.1 Introduction

Coefficients, Cd & Cm, used by Morison's equation to calculated forces on submerged cylinders are calculated in three ways:-

1)   With a least squares analysis (LSA) of the measured forces.

2)   Solution of simultaneous equations for given positions along the wave, where the velocity environments is known, usually peak velocity and acceleration (crossing point method), and

3)   the solution of simultaneous equations symmetrical either side of the wave crest where the velocity environment may be assumed to be identical. This gives an "instantaneous" coefficient for cylinder drag and inertia forces.

Method 3 makes the calculated and measured horizontal force traces equal at all points along the wave by choosing coefficients to suit.

Methods 1 and 2 calculate a value for each coefficient for each wave, this suggests Cd and Cm are sensibly constant and are reliant upon the "global" wave characteristics. However method 3 considers Cd and Cm as products of the particulate fluid characteristics and consequently change during the passage of the wave. Therefore the trend for Cd and Cm are considered for several waves.

Results show that the coefficients determined in each of the above ways are different for each particular wave considered. The problem remained that a parameter must be found that may be related in some predetermined way to one of the coefficients.

This was so that for a wave, of "known" characteristics, the values of Cd & Cm may be predicted.

Commonly Reynolds or Keulegan and Carpenter numbers are the "known" characteristics of a particular wave, so results are presented to show how the calculated coefficients relate to these.

Following the results of the dimensional analysis given in Chapter 3, the coefficients calculated by method 3, shall be related to ut/D which was seen to relate to the distance fluid travels past the object as the wave passes.

6.5.2 Drag Coefficient with Reynolds No.

"Least Squares Analysis" (LSA)

Results for Cd plotted with Re are given in figure 6.60.

The effects of the proximity of the channel bed is clearly demonstrated in results for the smaller cylinder where a different flow regime for some tests is evident.

The range of Re for each cylinder is small, though it overlaps for cylinders of different diameters. Consequently a trend of decreasing Cd, from Cd=1.8 to 1.5, with increasing Re can be seen when the results are considered together, despite some scatter.

The scatter is probably partially due to:-

- experimental inaccuracies which are amplified through the analysis

- to the inability of Morison's equation to completely model the forces.

Kulin's results for a 50mm diameter cylinder, lie within results presented here. Though the scatter in the results prevent a meaningful comparison being made, (figure 6.61) the trends are similar.

Results for the 48mm diameter cylinder are consistently above those calculated by Kulin for a 64mm diameter cylinder using as would be expected. They also lie above those calculated for steady flow.

Crossing Point Method (XING)

As with the LSA, results for Cd calculated using XING plotted against Re (figure 6.62) show some scatter. The trends are as with the LSA, with Cd averaging at 1.5 for all Re. At low Re the affects of the proximity of the channel bed are evident with Cd becoming negative.

Reynold's Number versus Cd (LSA)

Figure 6.60

- 235 -
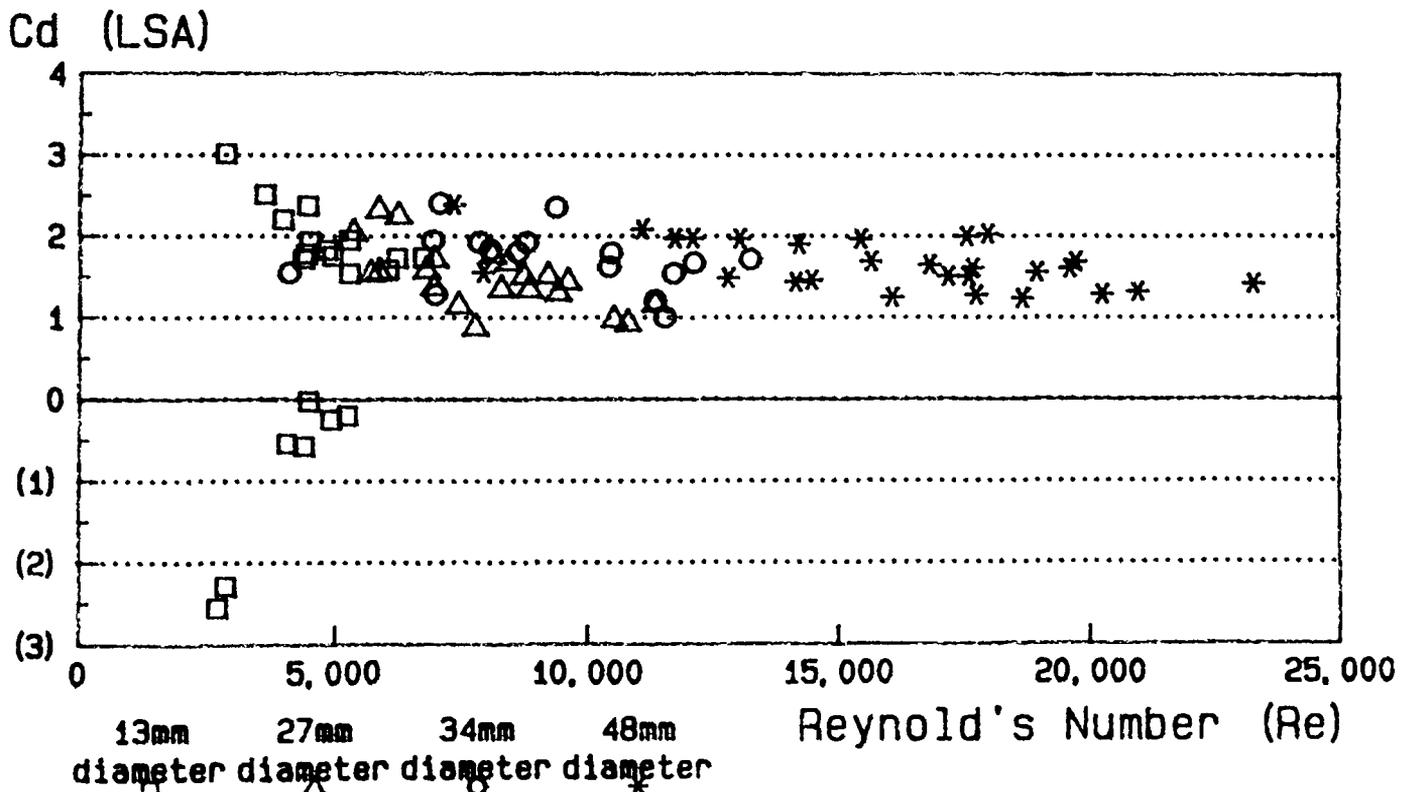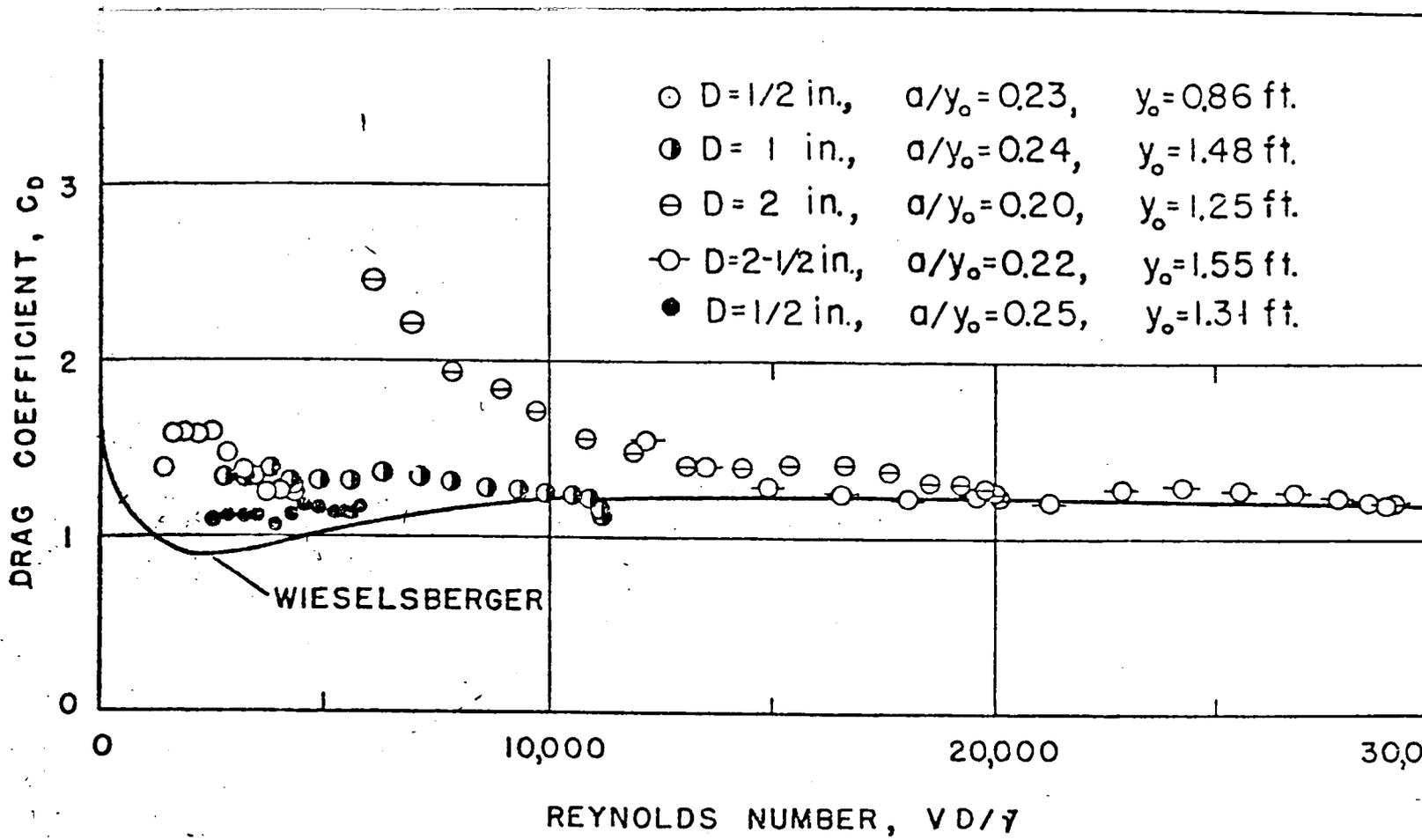
Figure 6.61 – Drag Coefficients based on
$$\underline{C_d(x) = C_d(-x) \text{ (after Kulin)}}$$

Reynold's Number versus Cd (XING)
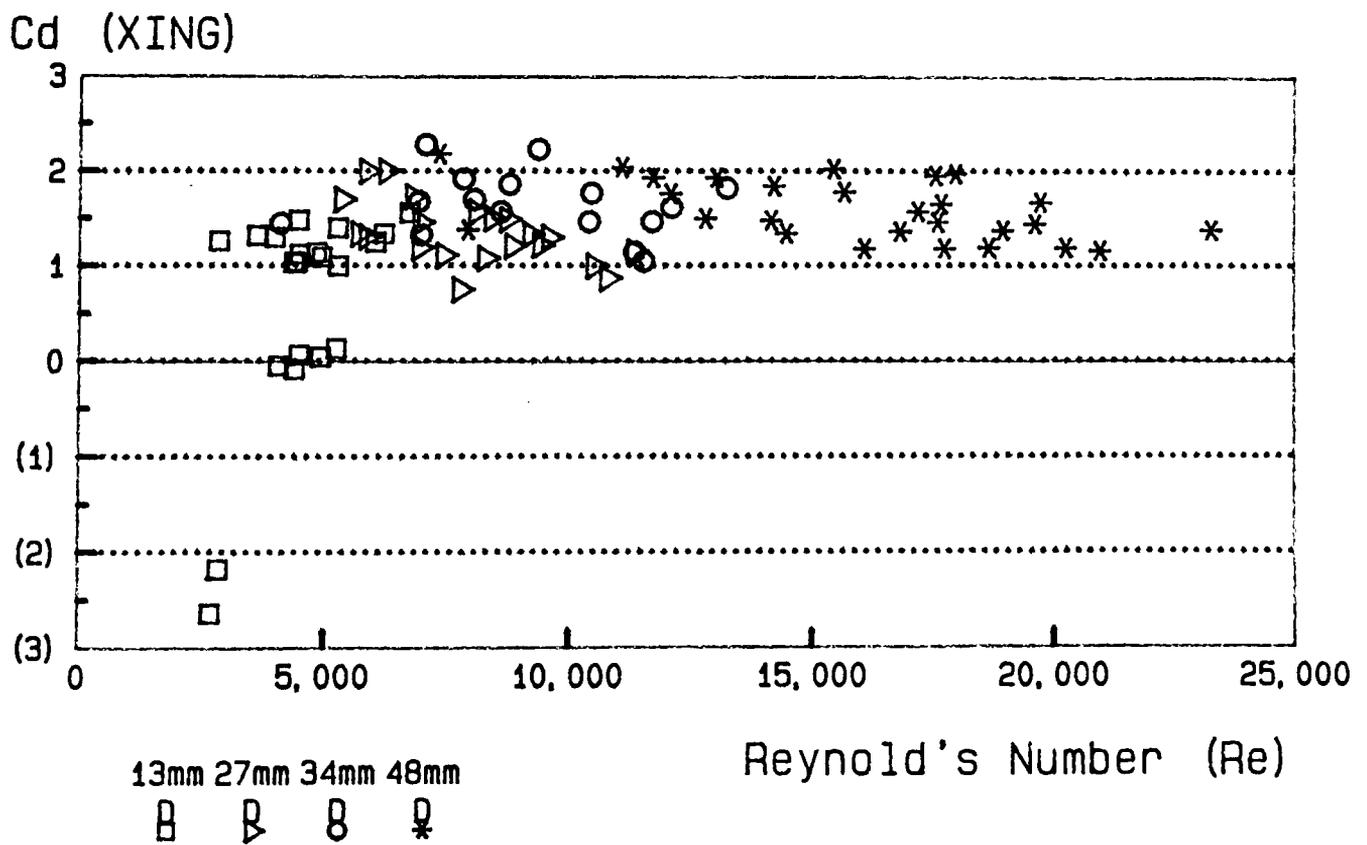
Figure 6.62

6.5.3 Drag Coefficient with Keulegan Carpenter No.

<u>"Least Squares Analysis" (LSA)</u>

Plotting Cd calculated using a LSA with Nkc shows a large scatter in results particularly for Nkc<5. With Nkc increasing from 1.5 to 5, Cd drops from Cd=2 to Cd=1. (figure 6.63)

The results for the 13mm diameter cylinder (6<Nkc<9) are separated from results for larger cylinders.

For results away from the channel bed lie on a smooth curve. The scatter of results for this cylinder nearest the channel bed is high, with Cd negative for all Nkc.

The scatter in the results for Cd at Nkc<5 is to be expected since the fluid/structure interaction is in a region where the forces are inertia dominated.

<u>Crossing Point Method (XING)</u>

Similar trends can be seen for Cd calculated using the crossing point method as with LSA.(figure 6.64),i.e.

- a large scatter in results
- results separated according to D
- Cd decreasing with increasing Nkc

Figure 6.63

Keulegan Carpenter No. (Nkc) versus Cd (LSA)

Cd (LSA)

FITTED LINE

FITTED LINE

13mm   27mm   34mm   48mm

$F_D/F_i < 10\%$

(INERTIA REGIME)

Keulegan Carpenter No. (Nkc)
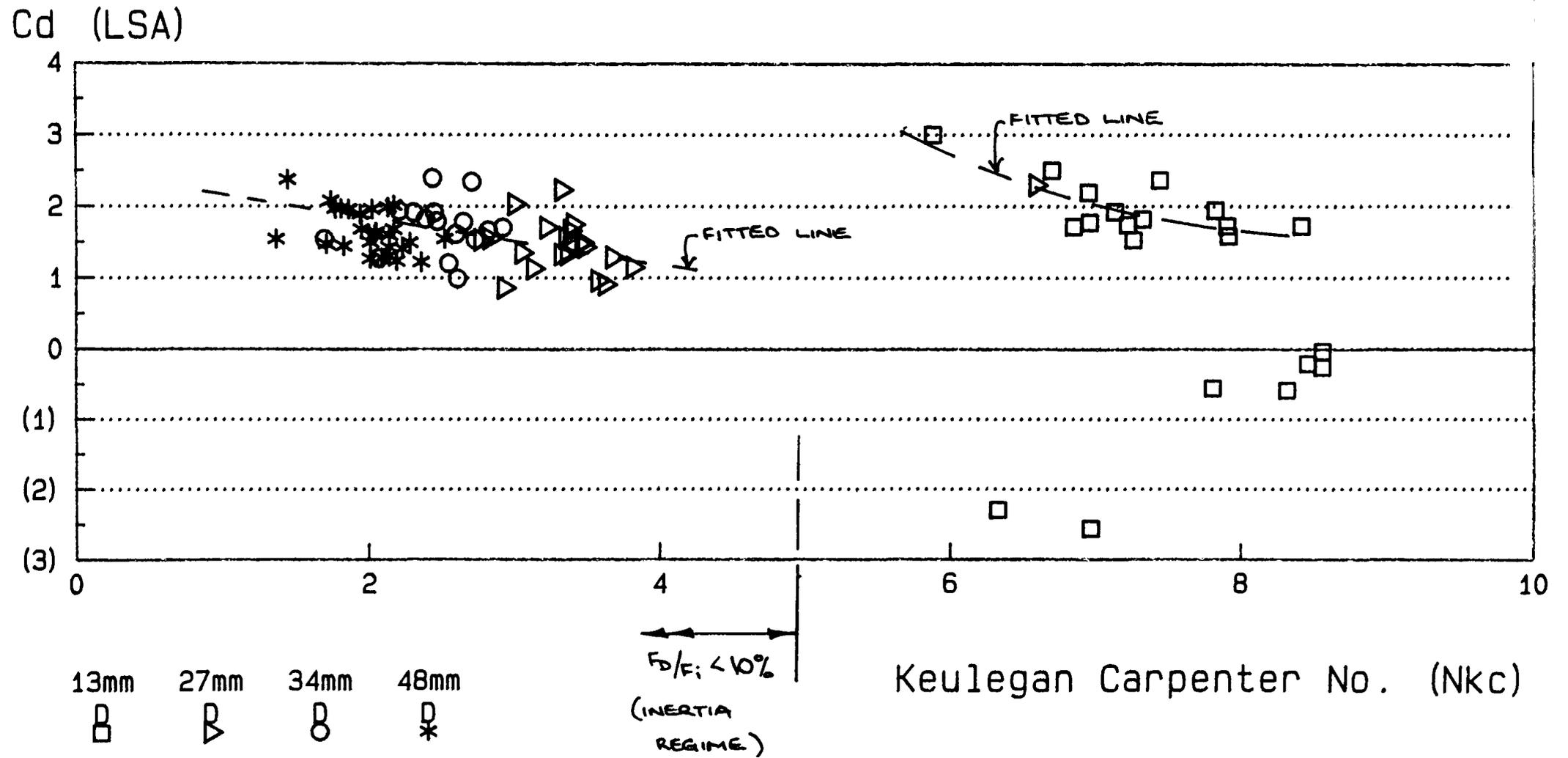
Keulegan Carpenter No. (Nkc) versus Cd (XING)

Figure 6.64

- 239 -
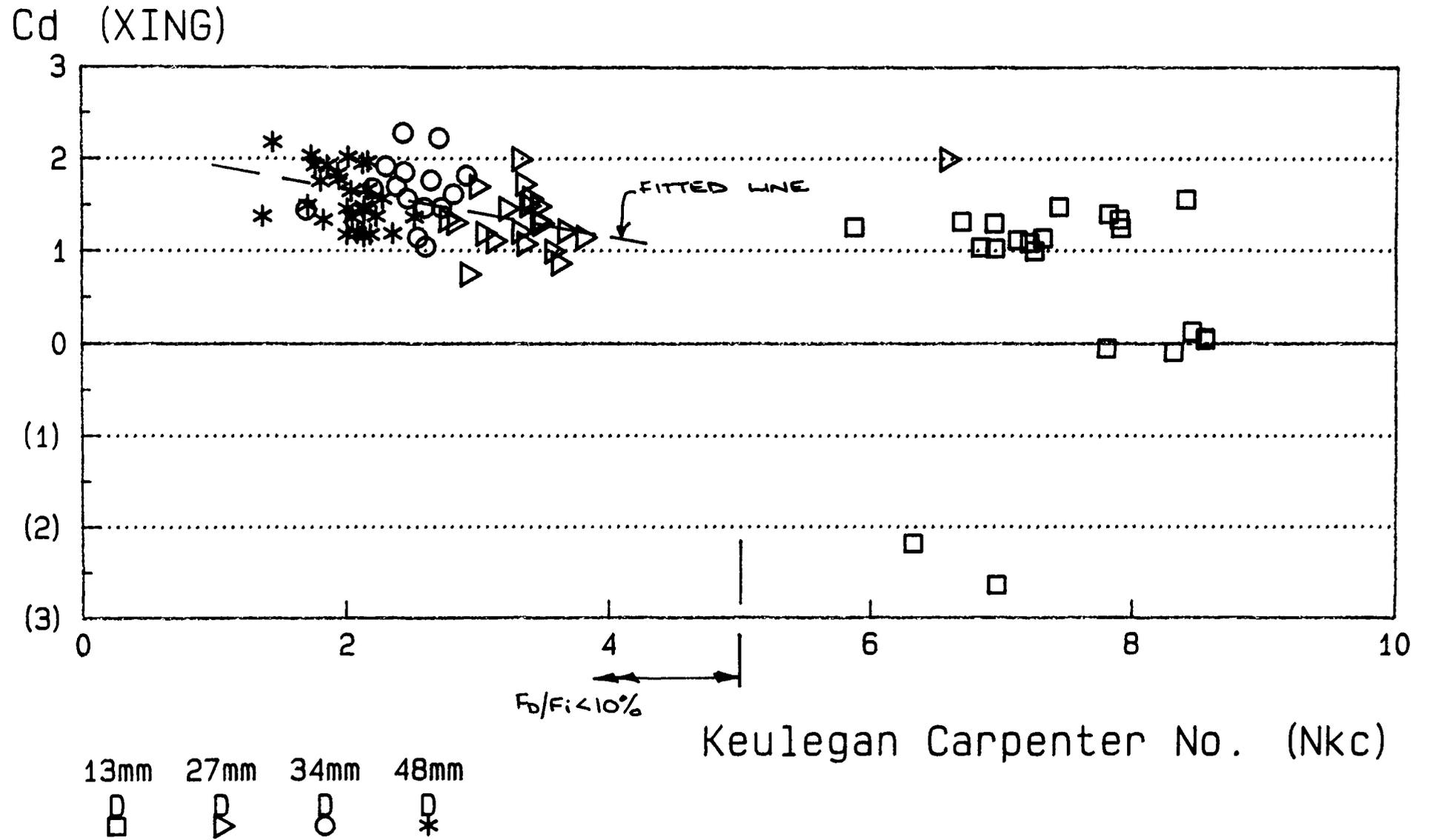
6.5.4 Inertia Coefficient with Reynolds No.

"Least Squares Analysis"

As Re increases from 3,000, Cm drops rapidly from Cm$\approx$11 to Cm$\approx$1.2 as Re=6,000. It remains nearly constant for all Re>6,000.

The results can be viewed as a continuous mechanism as Re increases, hence the results approximate a curve, shown solid.

"Crossing Point Method"

Similar trends of Cm with Re are seen here (figure 6.66), with greater scatter than with LSA. A curve (solid) may be drawn through the results.

Reynold's Number versus Cm (LSA)
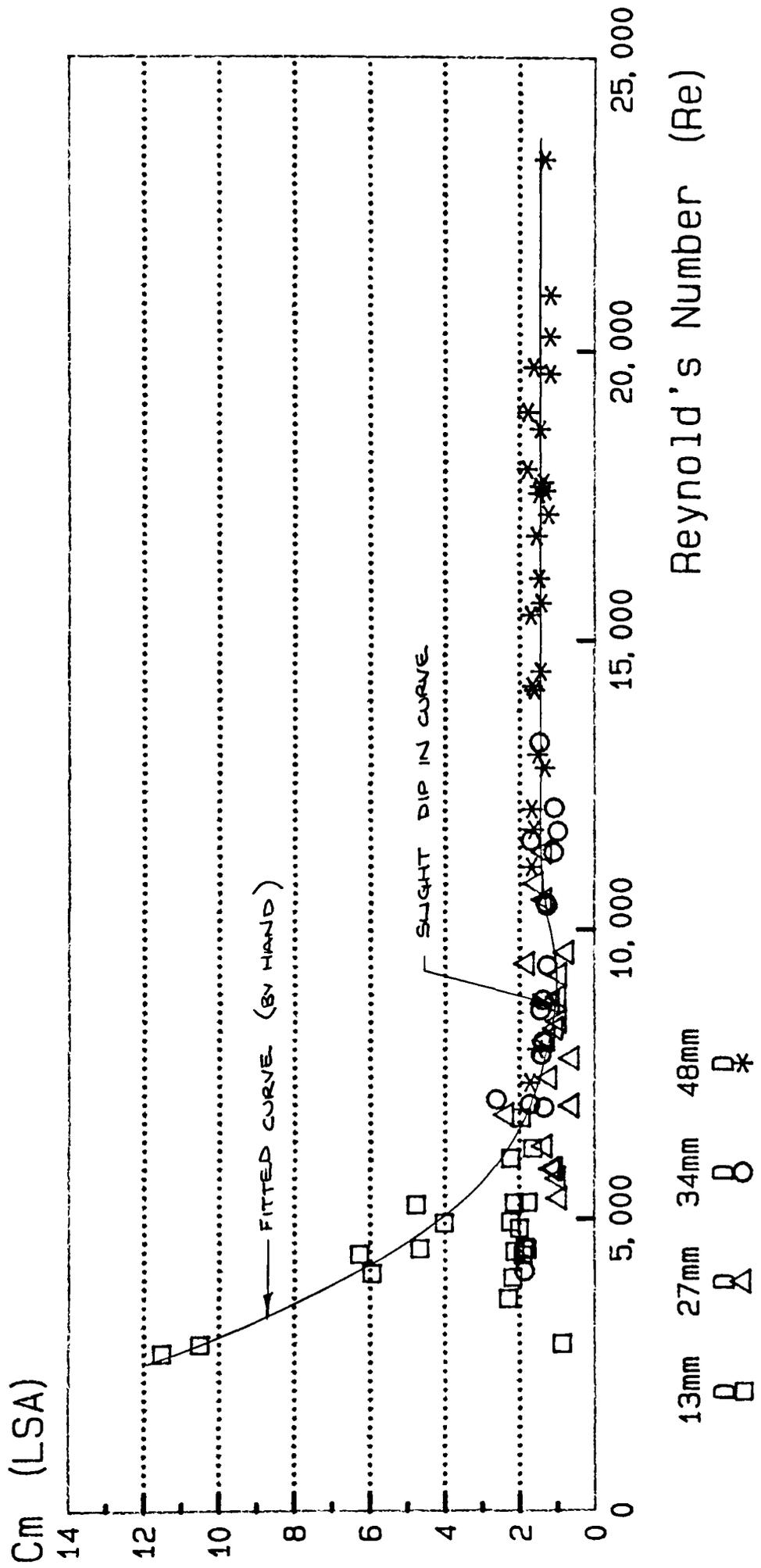
Figure 6.65

Reynold's Number versus Cm (XING)

Figure 6.66

- 242 -

Cm (XING)

FITTED CURVE
(BY HAND)

Reynold's Number (Re)

13mm 27mm 34mm 48mm
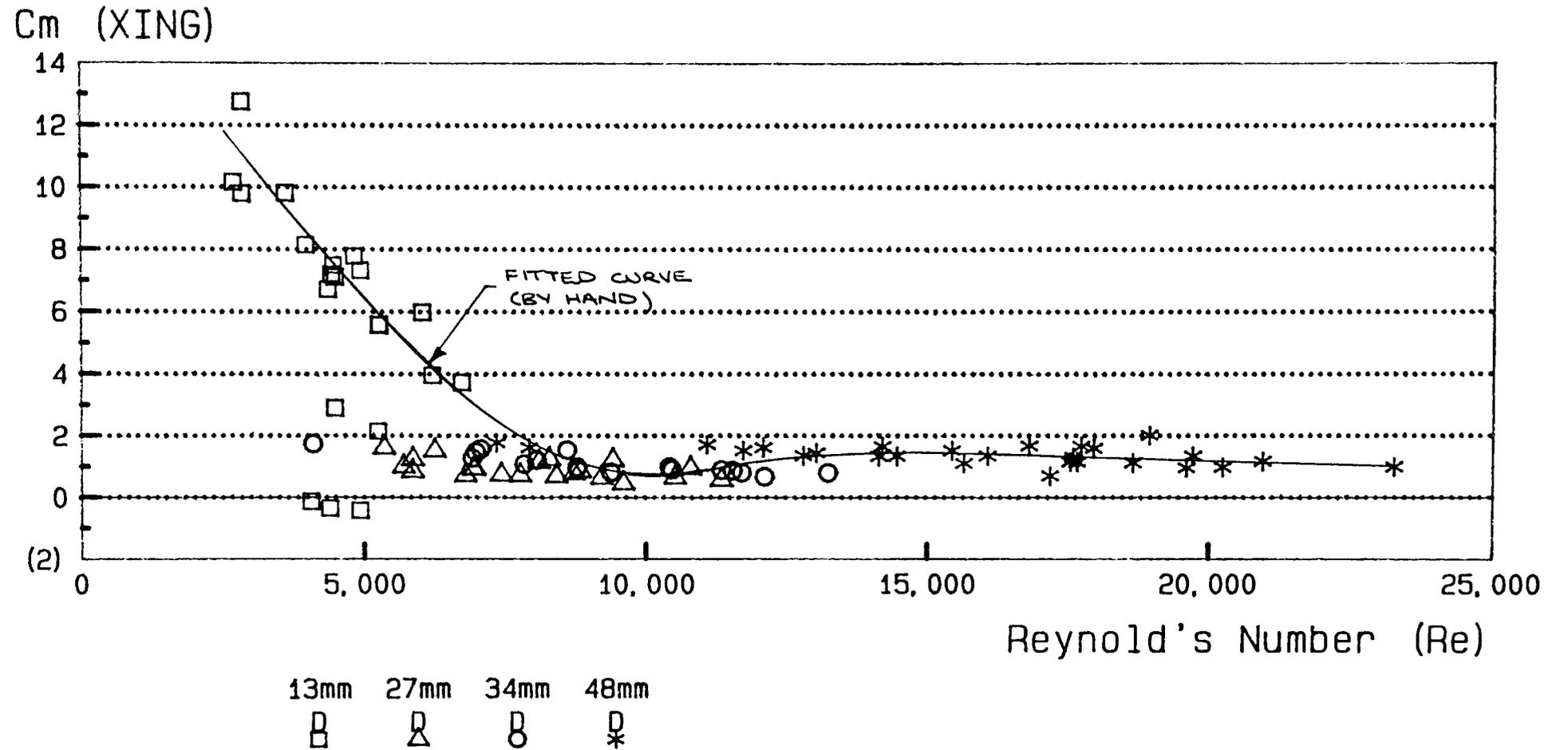
6.5.5 Inertia Coefficient with Keulegan Carpenter No.

"Least Squares Analysis"

The results for Cm in this case lie in two distinct regions. For the 13mm diameter cylinder $(F_d/F_i>10\%)$ no trends can be identified because of scatter of results (figure 6.67).

However for the three larger cylinders though the scatter is much reduced it shows that with $1.2<Nkc<4$, Cm drops from Cm≈1.8 to Cm≈1.0. This is as would be expected since Fd/Fi<10% and therefore in the region where confidence in the values of Cm is high.

"Crossing Point Method"

Similar trends of Cm with Nkc using a LSA are seen in these results (figure 6.68)i.e.

- large scatter of results for smallest cylinder

However results for the largest cylinders show less scatter than with the LSA and can be approximated to a curve as shown. In the range $1.2<Nkc<4$ the value of Cm reduces from 1.8, to between $\frac{1}{2}$ and 1.

6.5.6 Instantaneous Drag Coefficient

With the exception of the 13mm diameter cylinder, instantaneous Cd generally lies between 1.25 and 1.75 as ut/D increases towards the wave crest (figure 6.69a,b,c). Their appears to be

Keulegan Carpenter No. (Nkc) versus Cm (LSA)

Figure 6.67

Cm (LSA)

13mm 27mm 34mm 48mm

FITTED LINE

$F_D/F_i < 10\%$

(INERTIA REGIME)
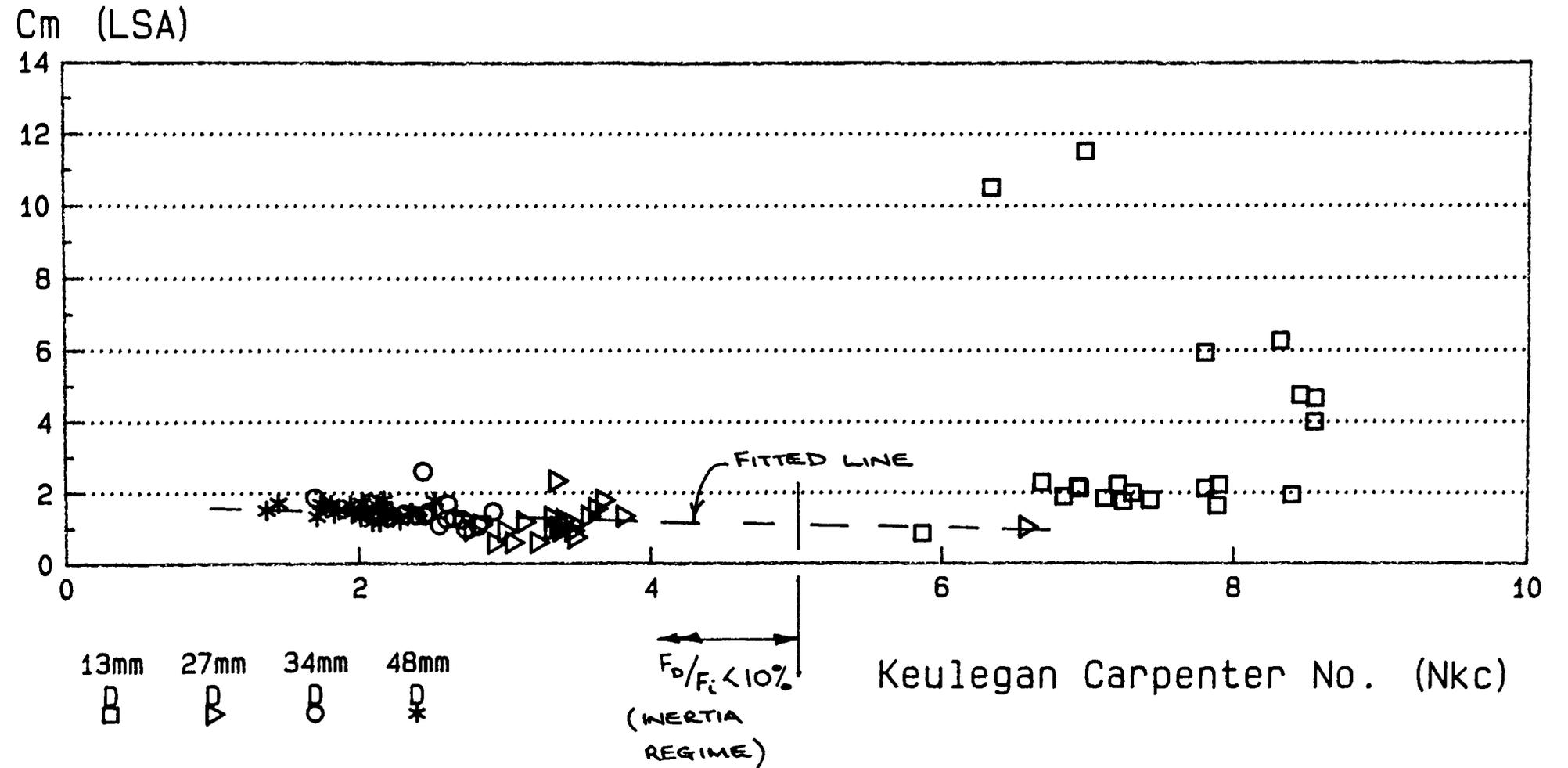
Keulegan Carpenter No. (Nkc)

Cm (XING)
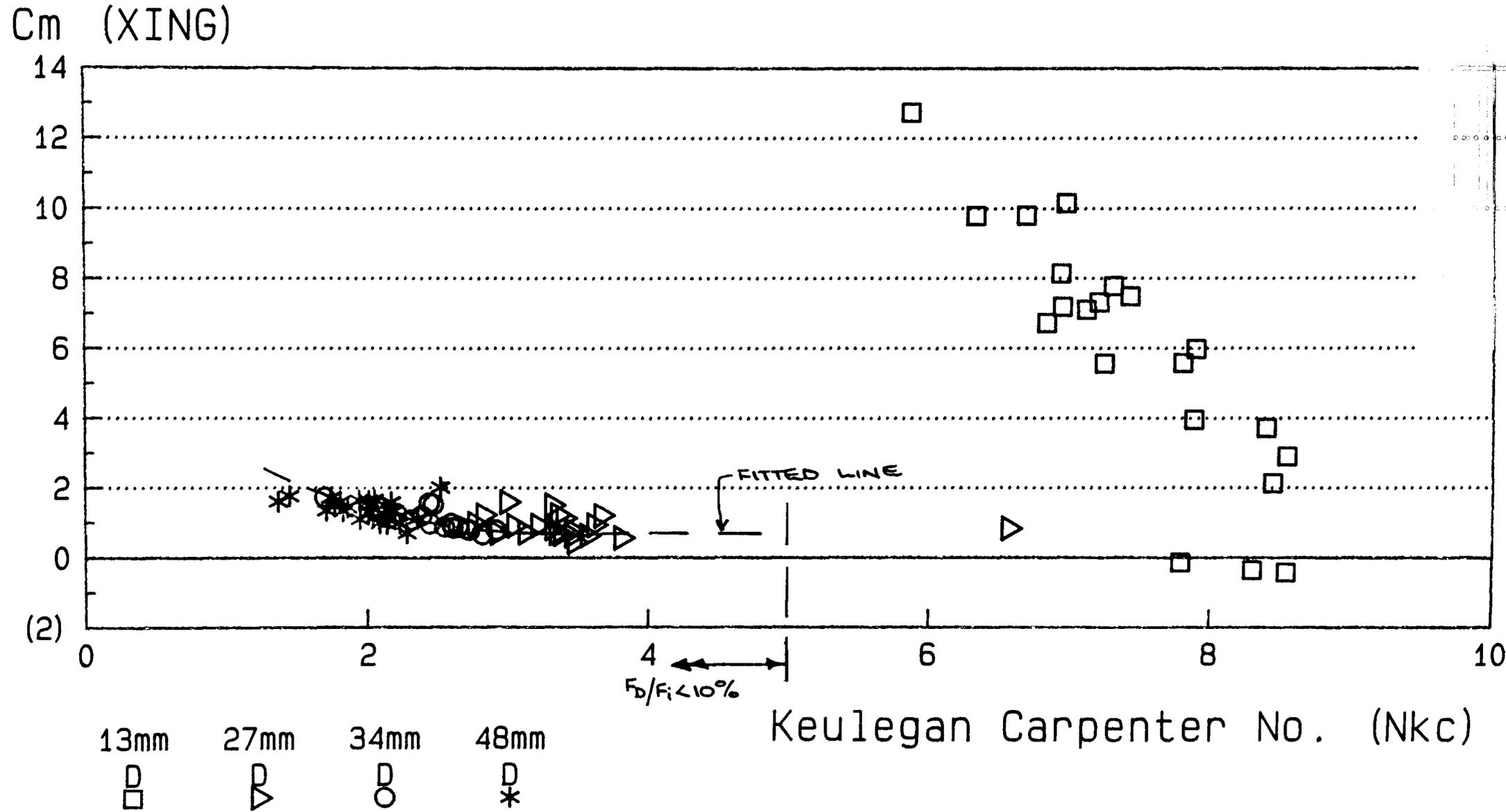
Figure 6.68

Cd (Cd (x) =Cd (-x))
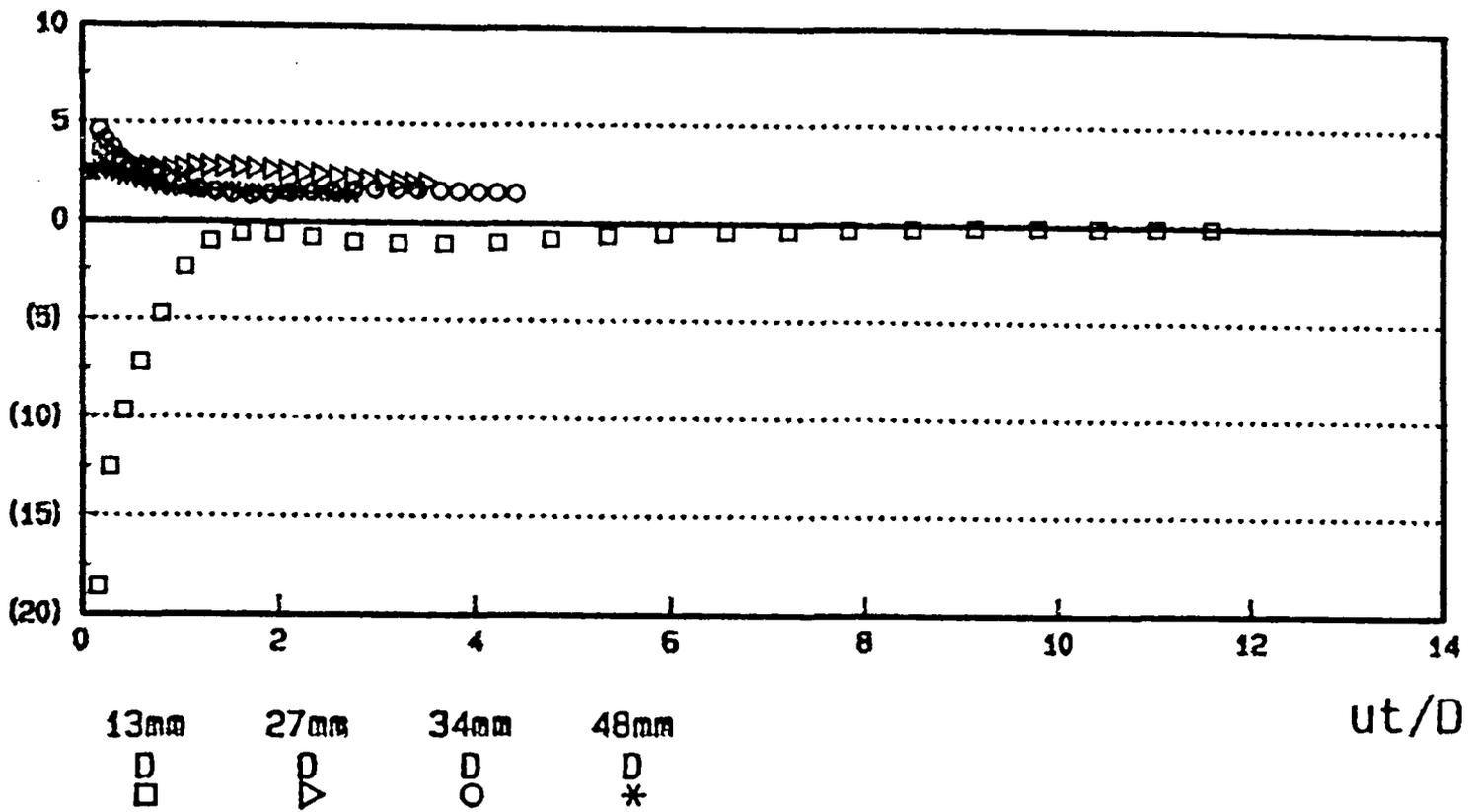
Figure 6.69a - ut/D versus Cd (Zc=0.036)

Cd (Cd (x) =Cd (-x))
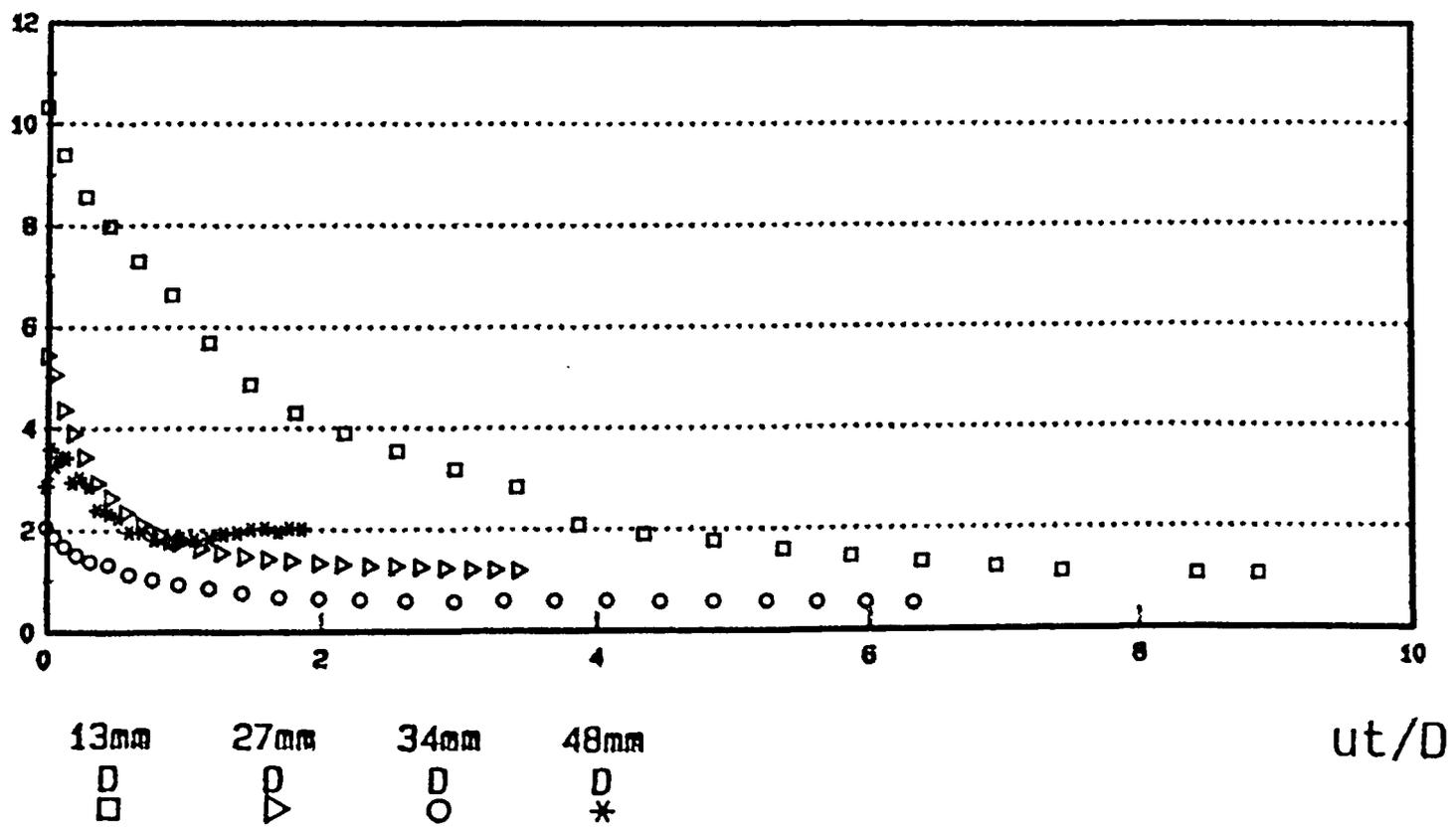
Figure 6.69b - ut/D versus Cd (Zc=0.087)

Cd (Cd (x) = Cd (-x))
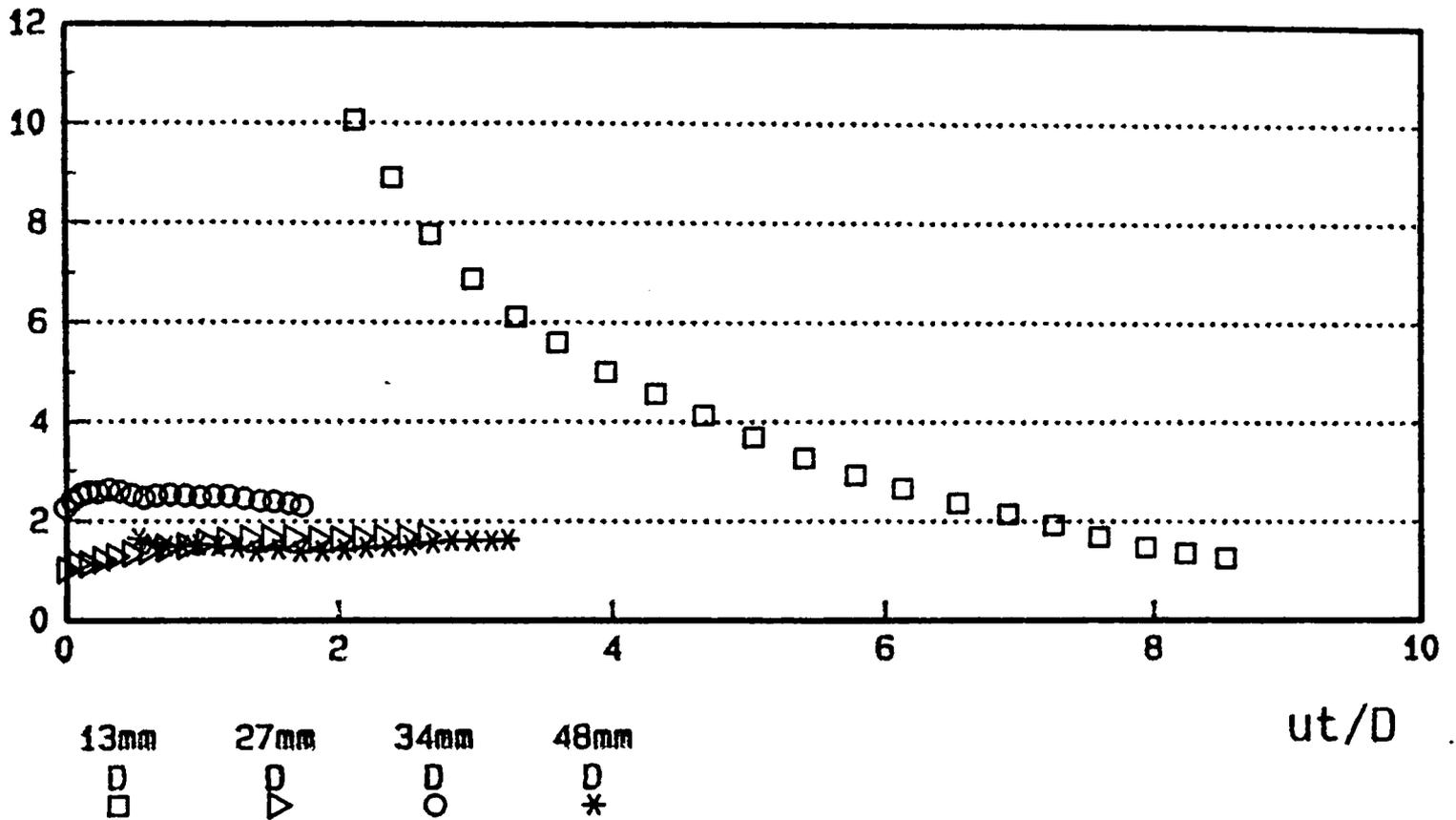
Figure 6.69c - ut/D versus Cd (Zc=0.137)

no specific relationship that describes this tendency, it being unique for each generated wave and does not depend upon wave amplitude, height above the channel bed or diameter of cylinder.

With the 13mm diameter cylinder close to the channel bed Cd remains negative for all ut/D. This is inconsistent with results obtained for all other cylinders and positions.

Plotted against instantaneous Reynolds number no consistent relationship can be identified, though the majority show Cd decreasing with increasing Re which confirms the results of Kulin as in figure 6.61.

6.5.7 Instantaneous inertia coefficient

Results plotted with ut/D show a large scatter, with no
relationships or trends evident (figure 6.70a,b,c).

Cm (Cm (x) =Cm (−x))
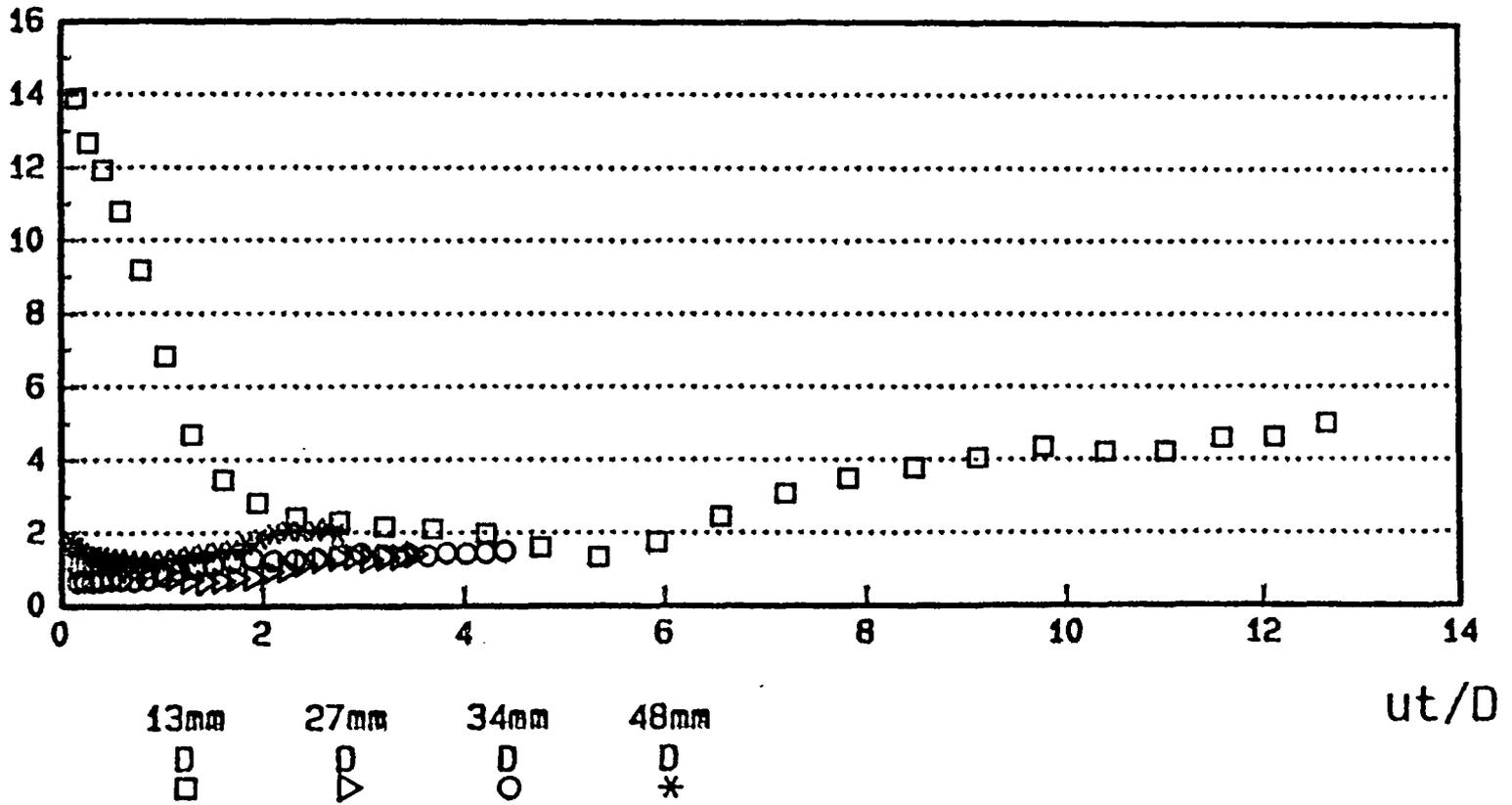
Figure 6.70a — ut/D versus Cm (Zc=0.036)

This is suprising since results for the 27, 34 and 48mm diameter
cylinders are clearly in the inertia regime, where the confidence
in values of Cm is high.
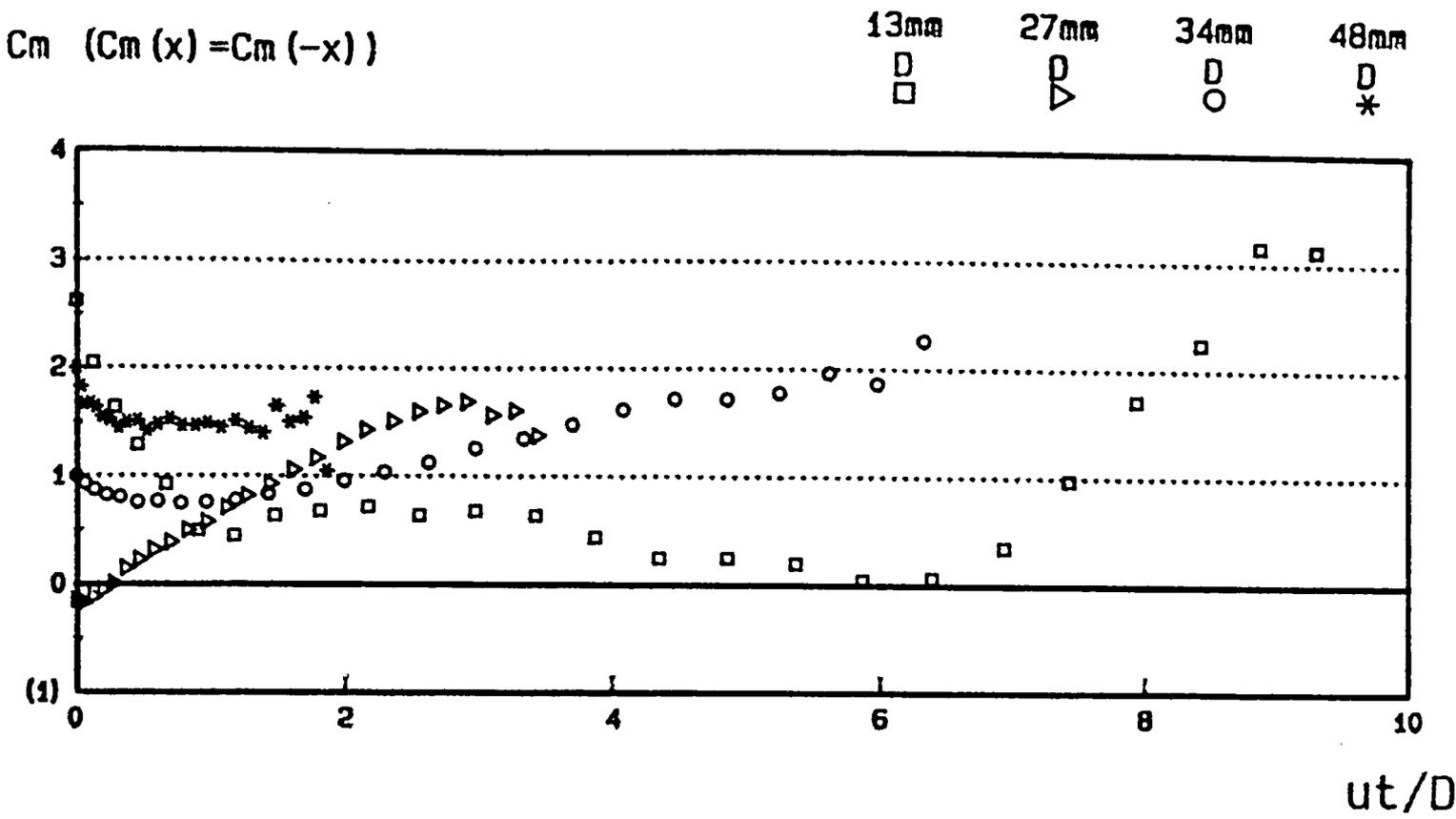
Figure 6.70b — ut/D versus Cm (Zc=0.087)
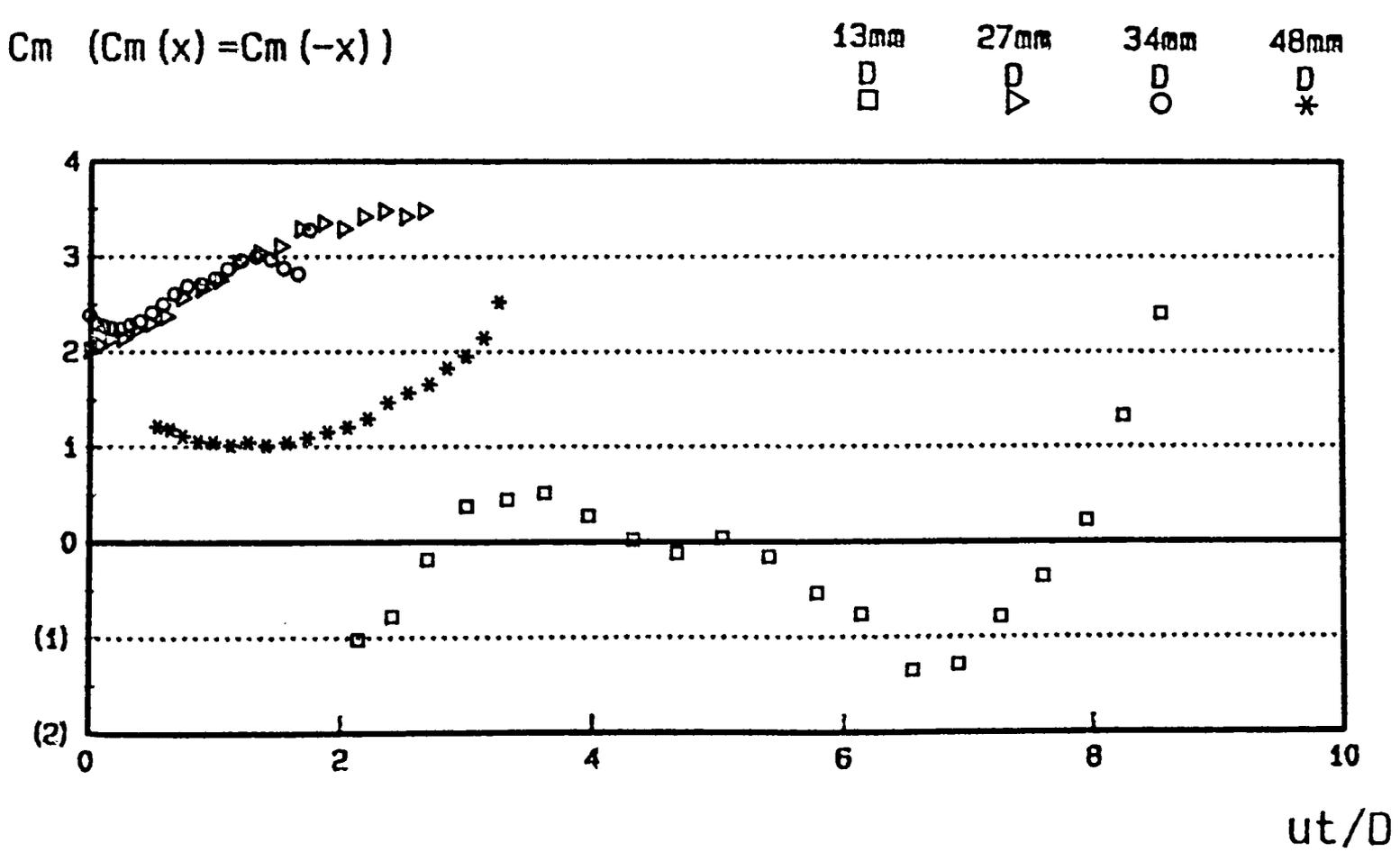
Figure 6.70c — ut/D versus Cm (Zc=0.137)

6.5.8 Instantaneous total force coefficient

The total force coefficient, C_t is given by:

$$C_t = F / (\tfrac{1}{2}\rho u_m{}^2 Dl) \qquad 3.53$$

this can be modified to give instantaneous values by substituting $u_m{}^2$ by u^2, giving

$$C_{ti} = F / (\tfrac{1}{2}\rho u^2 Dl)$$

which can be related to ut/D through the wave.

With the exception of the 13mm diameter cylinder all results show a uniform correlation between C_{ti} and ut/D (figure 6.71). It approximates to the solid curve shown. Though for each cylinder the fitted curve has approximately the same shape, the scatter of results gives a range of C_{ti} for constant ut/D.

At the extremes of the wave ($ut/D \approx 0$), C_{ti} equals approximately 6, dropping quickly to between 2.5 and 3.0 as ut/D nears unity, then slowly dropping further as ut/D reaches the range 4-6.

Results for the 13mm diameter cylinder are mixed but generally follow the trend shown by the other cylinders but with higher values of C_{ti}, except near the channel bed where C_{ti} goes negative.
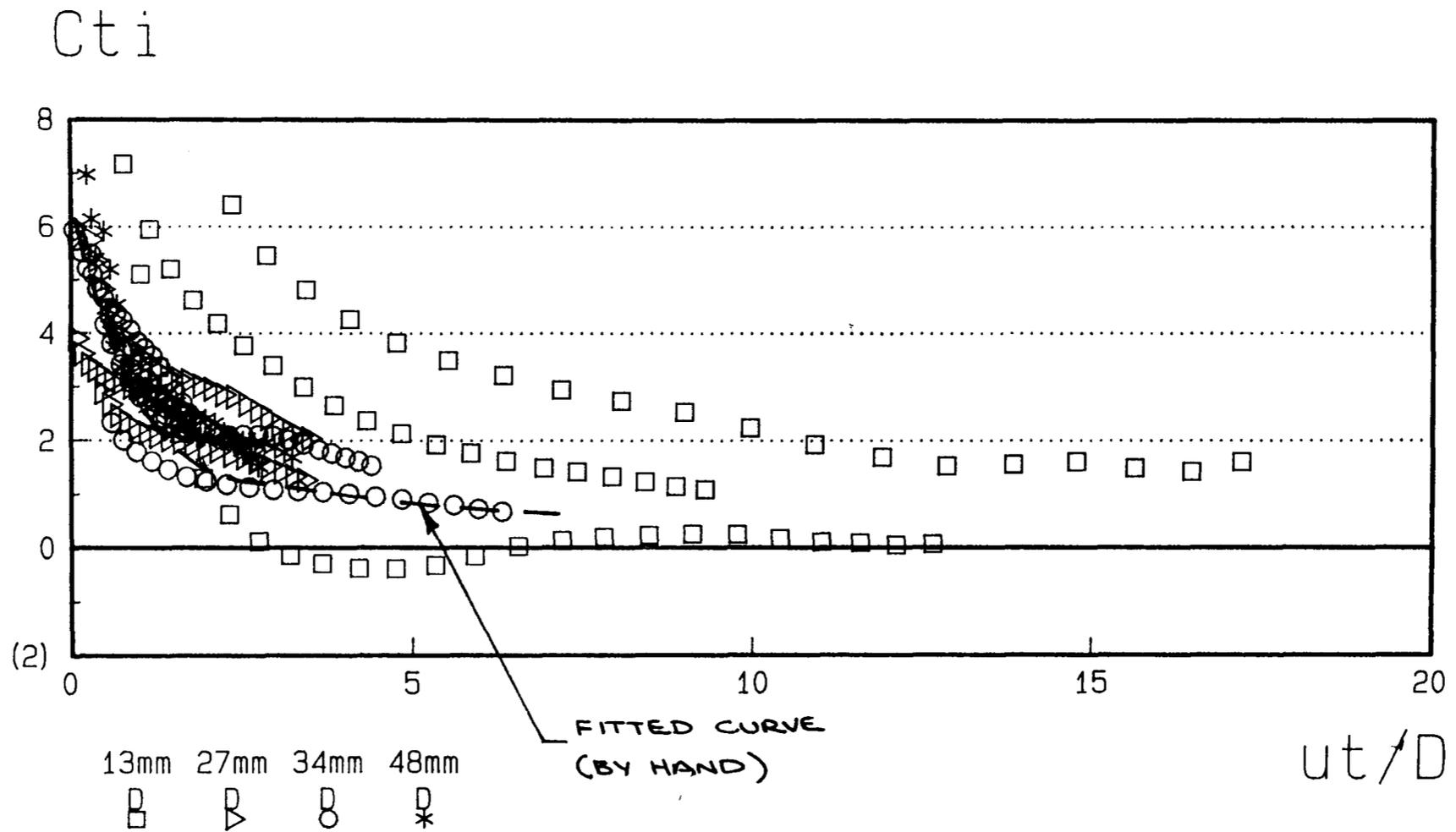
Figure 6.71 - ut/D versus Cti

6.5.9 Confidence level of coefficients

The confidence that can be associated with values of Cd or Cm can be found by calculating the ratio of drag force to inertia force. This characterises the data as being well or poorly-conditioned for calculating Cd or Cm.

This is important since some of the scatter in the results is possibly due to poorly-conditioned data, i.e. data that is determined in a flow regime where errors in that data are likely to be high.

The analysis for the solitary wave is given in section 5.4.6.

The results for the three largest cylinders (27, 34 and 48mm diameter) fall in the inertia regime as given in section 5.4.6. They show limited scatter in results for Cm, when compared with results for the 13mm diameter cylinder, as would be expected.

Results for the smallest cylinder lie in the region where theory suggests neither drag or inertia effects dominate. Consequently the accuracy of values for Cd and Cm are likely to be poor in this region.

Results presented here for the smallest cylinder show a large scatter. This is probably, in part, a consequence of the poor conditioning of both Cd and Cm as described previously.

6.5.10 Summary

With Morison's coefficients, Cd and Cm, calculated using a least squares analysis, at peak velocity and acceleration, and simultaneously either side of the wave crest the following agreement was found:

	Cd	**Cm**
For correlation with Re.		
Least Squares Analysis	Decreasing Cd with increasing Re.	Large scatter on fitted curve.
Crossing Point Method	Large scatter, but generally as LSA.	As LSA
For correlation with Nkc.		
Least Squares Analysis	Large scatter but shows decreasing Cd with increasing Nkc.	Scatter of results. Approx. curve. Decreasing with increasing Nkc.
Crossing Point Method	As LSA	As LSA
For correlation with ut/D.		
Simultaneous either side of wave crest.	Large scatter Cd decreasing with increasing ut/D.	Large scatter

Total instantaneous force coefficient, C_{ti}, shows scatter increasing with decreasing cylinder diameter but decreases with increasing ut/D.

CHAPTER 7   DISCUSSION

7.1 The Solitary Wave

7.1.1 Generation

Longuet-Higgins (1981) postulated that an ideal solitary wave generator would closely follow the particle motion in the wave.

A vertical plate as used here, would not be sufficient because of the difference in particle displacement with depth as the wave progresses. The wavemaker would have to be designed so that the displacement at the surface exceeded that at the bottom by a factor as great as 2.5.

Though in this investigation the motion of the wave generator only roughly matched the motion of fluid particles in a solitary wave, the generated wave for all but the closest observations, approximated a solitary wave.

This was because the solitary wave is a disturbance of minimum energy and intrinsically stable. If it were not so stable the method of generation used here would not be sufficient.

Solitary waves of medium amplitude (a/y_o=0.3) were readily generated in this investigation. These may have been transformed to solitary waves of greater amplitude by allowing them to run into gently shoaling water. This would have gradually steepened the wave which may have been in an almost steady state at the test section.

The main disadvantage in using a non uniform depth of water, is that the initially pure symmetric solitary wave becomes asymmetric. It would have developed a long tail (Kaup & Newell (1978)) or may have produced an additional soliton (Madsen & Mei (1969)).

Boussinesq commented that as a wave propagates in water of gradually decreasing depth, the channel bed must continuously reflect a small part of the movement. The volume and energy of the wave must be divided between the direct and reflected waves for them both to exist. The reflected wave would increase in length and height slowly. Its volume would become finite but without the corresponding energy. The direct wave would conserve nearly all the energy though it would become higher, shorter and consequently less stable. In its final form the wave would lack the base for its increased height and would break. The opposite would occur if the water depth increased.

The limitations of generating high waves in this way may be overcome by using a combination of bed slope, frictional dissipation to disperse some excess energy and a wavemaker that closely follows the particle motion predicted by theory. This is very difficult to achieve in practice and was not attempted here. It was considered sufficient when generating waves of large amplitude, to accept some profile distortions so long as the precise wave characteristics were known.

Tuck (1974) showed that wave amplitude was strongly affected by the size of the gap around the wave generator. He showed that the larger the gap the lower the wave. (figure 2.6). He also demonstrated that a gap varying in size during the generation would create an asymmetric wave, the losses changing as the wave was generated.

As the generator - channel gap was not controlled during the generation cycle it appears this may be the primary influence on the results obtained here.

Despite this the waves showed good agreement with the theory of Boussinesq as previous experimenters have found. The wave characteristics were measured accurately and consistently, consequently they can be considered sufficient for further investigation.

7.1.2 Profile Distortion and Attenuation

Distortion of shallow water waves is inevitable if not only through nonlinear free surface effects. These increase with distance from the wave generator.

Experiments have been performed that show the wave profile varies with the amount of attenuation. An attenuated wave has slightly flatter profile than that of a freshly generated wave of the same amplitude. This would imply that a measured profile would be above theory, the differences being concentrated at the leading and trailing edges of the wave.

This is exactly what was seen in this experimental study. However since the disturbances are in regions of the wave where velocities are low they contribute little to the forces generated. However they may influence the generation and separation of forcing vortices.

The solitary wave profile results obtained in this investigation were affected by disturbances generated with the wave. This was unavoidable in view of previous investigators results. The effects they had on the study were measured.

Results obtained in this study have shown that the solitary wave has a celerity which may be taken as some function of amplitude (figure 6.20). Also the apparent length of a solitary wave is some function of wave amplitude. Thus the wave celerity is a determinate function of the apparent length of the wave. Theory (Lamb §236) shows that energy travels at the group velocity; for deep water this equals half the wave celerity. In deep water, waves outrun their energy and can no longer exist beyond a certain distance.

Though not a long wave as defined by Ursell (1952) the solitary wave is a long wave limit with the group velocity equalling the wave speed. Consequently the solitary wave has permanent form as observed in experiments, the amplitude only altering through the effects of friction.

One consequence of being a "permanent" wave is that the wave is non dispersive, i.e., the wave speed is independent of its height.

This deduction from theory is contrary to the experimental results, where the disturbances generated along with the solitary wave were separated with distance from the generator.

This suggests a small degree of dispersion tending to spread the front of the wave and nonlinear effects tending to steepen the wave as a consequence of increasing wave speed with amplitude.

Typically $\quad \lambda = 1.76 \quad (y_o=0.156 \; : \; a/y_o=0.25)$

$$a\lambda^2/y_o^3 = 0.25*0.156*1.76^2/0.156^3$$

$$=31.8 \quad (\quad =3\% \text{ amplitude})$$

Nonlinear effects predominate

$$a\lambda^2/y_o^3 = 0.25*0.156*1.31^2/0.156^3$$

$$= 17.6 \quad (\quad = 10\% \text{ amplitude})$$

Balance between nonlinear and
dispersion effects

The different definitions for the "wavelength" of the solitary wave confuses its characterisation with the Ursell number. However with a judicious choice for the definition of wavelength for the solitary wave, the Ursell number method of determining the proportion of nonlinear and dispersive effects may be applied.

Calculating the wavelength of the solitary wave as some fixed percentage of its amplitude is simple but not without limitations.

It takes no account of the vertical acceleration of the fluid which ultimately causes dispersion. Furthermore, vertical acceleration of fluid particles is not allowed for in shallow water wave theory.

More accurate estimates of the relative importance of dispersion and nonlinear effects in a solitary wave may be given by a factor including a vertical acceleration term.

It is not common to use the vertical particle acceleration in the determination of characteristics of the solitary wave because it is so small and difficult to measure. This seems to confirm that inconsistency between the measured wave and that predicted by theory are significant. That the waves generated here are not in fact 'solitary', but near 'solitary' and a form of long wave. It does however confirm the need to measure all characteristics accurately.

With the propagation of waves of translation in still water, a major source of energy dissipation is the thin boundary layer of liquid next to the solid boundaries of the channel.

Keulegan (1948) analysed the rate of loss of energy due to viscous shear within these boundary layers. Such an energy loss must be manifested in a decrease in amplitude of the wave.

Keulegan (1948) determined an equation which has been verified by laboratory experiments (Daily & Stephen, 1953; Ippen, Kulin & Raza, 1955) though these indicate slightly lower attenuations than theory, all other factors constant.

$$(a_2/y_0)^{-\frac{1}{4}}-(a_1/y_0)^{-\frac{1}{4}}=1/_{12}(1+2y_0/B)\sqrt{(\nu/(g^{\frac{1}{2}}y_0^{\frac{3}{2}}))}x/y_0 \qquad 7.1$$

Other sources of loss of wave energy include surface contamination, capillary hysteresis, parasitic capillary waves and scattering from bottom roughness.

All but bottom roughness may have a significant effect on laboratory experiments, whereas only the first and the last are likely to be significant in the field. Moreover the boundary layer damping is likely to be laminar in the laboratory but turbulent in the field. Consequently the source of the losses causing the attenuation in small scale experiments as performed here is only of academic interest and only of limited practical use.

Experimental results in this study show that wave profile attenuation between the first two wave probes (i.e. in front of the cylinder) was greater than that calculated using Keulegan's theory. However, changing the constant of proportionality from

1/12 to unity gives close agreement as discussed in section 6.2.5.

It seems that initial instability associated with the generation of the wave produced an observed wave attenuation greater than calculated using Keulegan's expression. This justifies the choice of test section some distance from the generator as proposed by Daily and Stephan (1952).

Not surprisingly the calculated attenuation between wave probes No.2 and No.3 was consistently less than measured. This was because the wave amplitude was affected by the cylinder. It demonstrated the importance of taking readings between stations where the wave profile was stable and not subject to external factors except those of interest.

The scatter in the observed wave attenuations was possibly due to the balance between nonlinear and dispersion forces changing as the wave attenuated as it progressed along the channel. No firm conclusions can be drawn from the experimental results presented here, as this was not the main interest of the thesis.

7.1.3 Wave Probe Calibration

The method used here to fit a 5th. order polynomial to recorded points smooths many of the inconsistent calibration errors. It gave a continuous calibration graph from which to determine the wave profile.

An alternative method of determining wave profiles from the calibrated points, is to linearly interpolate between the measured values. This method relies upon the linearity of response for its accuracy. A commercially produced wave probe amplifier could have been chosen to give a truly linear response, however little

would have been gained in accuracy of the recorded wave above that achieved.

It was very important to determine the dynamic calibration response in this study because of frequency dependent phase shifts introduced into results by signal filtering. These phase shifts were corrected so that the absolute relation with other measured parameters could be seen.

The dynamic calibration also showed a change of recorded amplitude with frequency. Though it was negligible for the calculation of fluid velocities and forces it may have been significant in the comparison of measured and calculated wave attenuations since these were small. Any frequency dependent wave attenuation was corrected in the presentation of the results.

7.1.4. Free Surface Profile

For waves with $a/y_o > 0.3$ the wave profile was consistently higher than theory predicted over the majority of the wave. This was contrary to the findings of Russell. He found that higher waves were more peaked than Boussinesq's relationship indicated and lay beneath Boussinesq's profile close to the wave crest.

Kulin (1958) determined that Boussinesq's equation closely described the measured profile when a/y_o was approximately 0.2; but its shape was too steep for the high waves and too flat for the lower waves, as found in this investigation. (figures 6.6 & 6.15).

These observations have been confirmed by Ippen, Kulin & Raza (1955) and Ippen & Mitchell (1957).

The reason for discrepancies between Russell's results and other experimental studies is unclear.

The method of measuring the wave profile has until recently been using photographic techniques. These were used by Kulin (1958) and Daily & Stephan (1954) and are liable to error as discussed previously.

Modern techniques using conductance wave probes are more accurate, continuous and less liable to systematic error.

Each experimenter used slightly different methods of generating the solitary wave. Kulin (1958) used the horizontal translation of a vertical board in the portion of a sine curve. Russell used two techniques; an impounded volume of water which was suddenly released, also the sudden immersion of a falling weight. Russell found in his experiments that the solitary wave was indifferent to the mode of generation. Thus the wave may have been obtained in numerous ways as long as the method used was single acting.

Daily & Stephan also used two methods; a falling weight into still water, also a more complicated method using a suddenly released reservoir of water to push a moveable wall across the channel and generate the wave. Both methods resembled those of Russell.

Daily & Stephan used the first method to investigate the surface profile and wave celerity; the second method was used to investigate wave amplitude attenuation and fluid velocities. Quite why Daily & Stephan used the two methods is unclear especially since they claimed that both methods gave results for wave profile and celerity that were identical.

These parameters have been shown in this thesis to a poor basis of comparison and may hide discrepancies between the methods.(Section 2.2.1)

In conclusion, it seems that despite the limitations of the method of generation, waves were created which were at the least as good as previous eminent experimenters. That measurements were consistently accurate and confirm work of Ippen, Kulin, Raza and Mitchell. Consequently the wave profile measurements are validated and established as a good base on which to discuss the wave characteristics.

7.1.5. Wave Celerity

This investigation has shown that the errors between the calculated and measured wave celerity were little over 1%, very much as Bazin (1865), Russell (1838) and Daily and Stephan (1952) found earlier.

Measured wave celerities were generally less than those calculated using equation 2.1 (figure 6.19). With $a/y_o < 0.15$ the difference increased (i.e. the change in measured celerity was large relative to that calculated for the same change in wave amplitude).

Work of Longuet-Higgins & Fenton (1974) has confirmed that for $a/y_o < 0.15$ measured celerity is significantly lower than theory predicts. However their results do more closely agree with those of Daily & Stephan (1952) than found here, though the improvement is not significant for waves with $a/y_o < 0.35$ and may be obscured by increasing scatter.

Naheer's results for wave celerity are generally higher than those predicted by Boussinesq's, Laitone's and McCowan's theory. They are consistently higher than those recorded by Daily & Stephan (1952) and French (1970) whereas results presented here closely agree with those of Daily & Stephan and French.

The comparison of results seems to cast doubt on the absolute values obtained by Naheer though the trends in his results are consistent with others. It is interesting to note that Naheer's results below a/y_o=0.1 show the measured celerity drops more rapidly with a/y_o than for larger waves. This exactly mirrors results presented here. The trend identified here for very small waves may indicate a change in the validity of Boussinesq's theory for solitary waves.

As waves decrease in size the problems of measuring celerity increases, since it is more difficult to identify the wave peak. This would possibly lead to a random experimental scatter rather than the systematic error observed here.

Results obtained in this study have shown the celerity of the solitary wave may be taken as some function of the wave amplitude.

A different way of viewing the discrepancy in measured and calculated values of wave celerity is to take the wave amplitude as the basis for comparison i.e. that the results show that there is a systematic tendency for an observed wave height to exceed the theoretical for a given wave speed.

This may be due to the presence of a viscous boundary layer at the bottom, but also may be due to unsteady motions associated with the wave.

In experiments with solitary waves on shoaling beaches, Ippen & Kulin (1955) found maximum amplitudes far in excess of the corresponding amplitude in water of uniform depth, generally by a factor of 2 or 3. They also found that the wave amplitude grew along a beach slower than expected with constant energy. It is possible that in uniform depth, unsteadiness due to energy dissipation may reduce the recorded wave amplitude for a given wave speed.

This suggests that there may be something to be gained from the work that Keulegan carried out on solitary wave attenuation. It may well shed some light on the interrelation found here between wave amplitude and celerity, also to the effect of water depth.

7.1.6 Disturbances generated with the wave

The difference in wave speed between low waves and disturbances generated with them, was small. The exact phase relation between the two wave trains altered as they propagated along the channel. Consequently by the principle of superposition, the wave shape changed as the wave progressed.

The interference by the disturbances generated with the main wave had been observed by several experimenters. (Daily & Stephan (1952), Longuet-Higgins). Most have not studied the solitary waves at heights over which this effect predominates. No limit can be given on the transition point since it depends on several factors, namely

    i)   the distance between the test section and the generator

    ii)   channel characteristics (slope, roughness, etc)

    iii) accuracy of wave generation.

Each experimenter has established a region over which the effects predominate apparently arbitrarily.

This investigation gave results which included all relevant effects making up the wave. This was achieved by measuring wave parameters continuously and accurately for each test. Wave parameters were measured as if at the same position along the channel.

Since the method of generation varied between tests, the effects of the disturbances generated with the main wave varied at the test section. This gave a variability of results for wave profile and wave attenuation particularly for low waves.

To achieve separation at the rear of the wave, a/y_o must be large. With $0.3 \leq a/y_o \leq 0.35$ the measured wave profile was higher than theory over almost all of the wave. The symmetry of the measured wave improved to $a/y_o = 0.45$ (figure 6.15) at which point all minor disturbances had become separated from the wave.

Their was a clear transition in wave profile results as a/y_o increases. The disturbances became separated from the main wave with $a/y_o > 0.35$. By $a/y_o > 0.45$ the main disturbance is separate with only minor surface irregularities primarily at the trailing edge of the wave.

It is worth noting that it is unlikely that the agreement between Boussinesq's theory and measured results remains constant for all a/y_o. Indeed it is likely that Boussinesq's theory is a good "average" of the changes that naturally occur in generated solitary waves. This is implied, not by the expression Boussinesq obtained for the free surface profile but by his expression for the fluid velocities which came from it. This gave no variation of velocity with depth. Clearly this is never

the case in experimental studies because of the differing free
surface and frictional effects that have already been discussed.

Daily & Stephan attributed the success of Boussinesq's equation
for free surface profile to the hyperbolic secant term, and noted
that the differences between measured and calculated results
were not consistent for all a/y_o. (see section 2.2.1). However
no connection was made between his determination of free surface
profile and fluid velocities.

7.1.7 Fluid Velocities

7.1.7.1 Velocity Calibration

The Hot Film Anemometer was successfully calibrated in-situ. Results were in accordance with King's Law for the conduction of heat from a heated sensor. The calibration did not change significantly before velocities were measured beneath a wave.

The literature survey did not find any previous investigation that used a technique of gathering fluid velocities as accurately and "continuously" in a solitary wave as used here.

It was important to measure the fluid velocities, for all practical purposes continuously, to identify the presence and magnitude of disturbance travelling with the wave. These disturbances would obviously have an effect on the formation of eddies and the generation of forces.

Zakanycz (1974) found that an error in measured fluid velocity of up to 30% could result if a Hot Film Sensor was not calibrated in the orientation used in the experiment. He also showed that the data was reproducible over a 2 hour period. Goodman & Sogan (1974) found that calibration of a conical hot film sensor as used here, yields velocities within 2% of the actual so long as the water temperature did not vary by more than 1%. They also showed that such a sensor was not influenced by less than 5% turbulence.

In draw tank calibrations Zakanycz obtained results for 'n' as in this experimental programme. Most experimenters found n=0.5 sufficiently accurate (Fingerson, 1967) though there was some variation since the time taken for the forced boundary layer to become fully established must vary between experiments.

The results of these investigations demonstrate that calibration in-situ was essential to avoid the possible errors. During calibration the velocities were horizontal, there being no vertical component of the motion. In the solitary wave there is a small vertical component which will effect measured values as the probe had a 40 degree angle of acceptance. The effect of this on measured fluid velocities is discussed later.

7.1.7.2 Results

The differences observed between measured and calculated fluid velocities could not have been due to the high acceptance angle of the Hot Film sensor.

This would mean that the sensor did not differentiate between the horizontal and vertical velocities. The sensor output would be the total velocity component of the fluid particles. Figure 7.1 shows the error through the wave that would be introduced. At the wave crest the vertical velocity component, in the absence of any measurable turbulence should be zero.

Consequently there would be no contribution to the value of u/c as measured. As agreement between measured and calculated fluid velocities at wave crest was consistent with the remainder of the wave, the difference cannot be a result of this high acceptance angle of the conical Hot Film Sensor.

The region of forced convection where King's Law is valid is shown in figure 7.1. Analysis of the wave was restricted to within this length and therefore limited the maximum error in measured velocity from this source was 7%. In fact the region of interest was much smaller than this, reducing the error to approximately 3-4%.

The measured fluid velocities compare well with those calculated using the theory of McCowan, despite the theory giving poor

Angle with horiz.
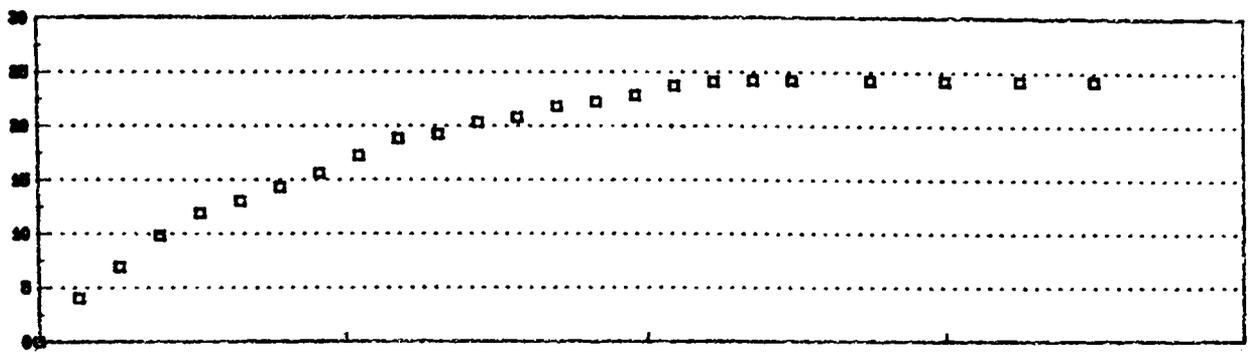
Wave Crest
% Error
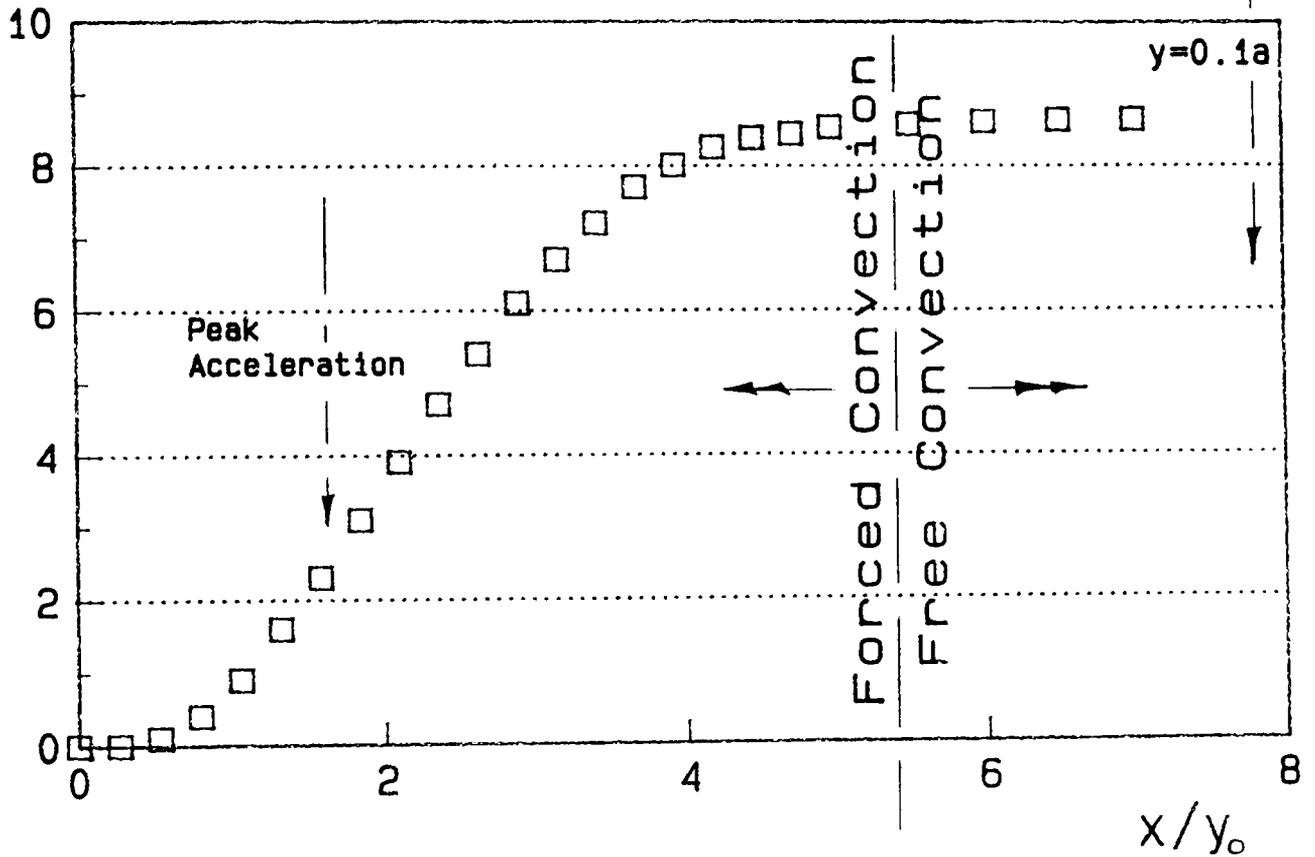
Figure 7.1 - Error from HFA acceptance angle

agreement for wave celerity and wave profiles.

It seems strange that though Boussinesq's theory is widely accepted as giving best agreement with measured wave profile, McCowan's theory gives the best agreement with measured fluid velocities. It can only be concluded that in experiments the initial premise that there is a close correlation between the free surface profile and fluid velocities is flawed. Indeed it may be concluded that either the wave profile or the fluid velocities are

more affected by some factor not included in theory than the other. From the work of Benjamin the vorticity generated with the wave may be that factor and have adversely affected the fluid velocities but had little effect on the wave profile.

It seems unlikely that the differences in the measured and calculated velocities were due to vorticity, because Hot Film Anemometry would respond to turbulence greater than 5% (Goodman & Sogan), and been seen as a disturbance of the fluid velocity trace. No such disturbance was evident.

Fitting a polynomial to measured velocities was essential to the calculation of forces because local variations did not represent changes in fluid flow but merely electrical noise. The polynomial smoothed the measured velocities well over the central portion of the wave. This was where the greatest accuracy was required since the maximum errors in squaring velocities and determining accelerations may be greatest. Indeed where errors between measured and calculated velocities were low, the polynomial accurately smoothed the measured results showing no signs of turbulence and asymmetry except at the rear of moderate and low amplitude waves.

This inconsistency in correlation between measured velocities and theory is unlikely to be due to errors in the calibration from changing environmental conditions and sensor orientation since these were sensibly constant for each test.

The errors in linearising the calibration curve were small (i.e. large regression coefficients) and were unlikely to affect the results to any great extent.

Indeed errors in determining the wave amplitude to be used in the theoretical expressions of McCowan would not account for the discrepancies observed either.

The differences between the measured and calculated fluid velocities are significant to the calculation of forces because the drag component in Morison's equation includes a velocity squared term. Consequently it has been important to show that the differences are not a consequence of experimental error and validity of calibration, but more a result of inadequate theory.

In conclusion, the differences must be from two sources:-

1) Method of generation of the wave

2) The failure of theory to adequately predict the velocity environment beneath the wave.

Investigations which have ignored these factors in their analysis of forces on structures using Morison's equation could well introduce an unacceptably high error and invalidated their findings.

It seems likely that the difference in magnitude between measured and calculated velocities is so fundamental that it must be largely a result of the method of generation.

It may be that as the wave generator was unrestrained at its top and bottom it imparted differing amounts of energy to the water. The difference would only have to be small, since the fluid velocities were small and of short duration, it would create a large difference with water depth. This would create a difference which was apparently random as observed here.

Alternatively it may be due to different or changing gaps between the channel wall and edge of the generator. As Tuck showed, small changes in the gap size would give considerably differing results.

This would also explain the time difference in the peak values since the wave would only have to be minutely asymmetric to give the time differences identified here.

If the orientation of the wave generator was the only thing to affect the comparison of measured and calculated fluid velocities, it may have been identified by plotting difference in the time of the peak against the error in measured fluid velocities.

Should the wave generator top have lagged its base, then the fluid velocities would have been marginally lower and lagged those calculated. The opposite would have been true if the wave generator top had led its base. The wave shape and amplitude would have been unaffected since the displaced mass would remain sensibly constant for both.

Since this combines with the effect of varying gap size which will also have an affect on the measured fluid velocities, no relationship is expected and eliminates this as a useful exercise.

The work presented in this thesis demonstrates how crucial it is to measure the velocity environment accurately for a meaningful comparison and evaluation of forces calculated using Morison's equation. Small differences in wave generation can create a large scatter of results making the use of theoretical velocities invalid.

The changes that occurred between tests within the experimental programme were of no consequence, since the wave parameters were evaluated accurately each time a test was performed.

7.1.8 Fluid/ Structure Interaction

The results for forces on the 27, 34 and 48mm diameter cylinders show a correlation with the formation and separation of eddies, as given below.

> The initial stages of the growth of an eddy would be expected from the upper surface of the cylinder. This was because the fluid had a small vertically upward component, the eddy being weak since velocities were low. "Premature" eddy separation would be induced as the direction of the fluid flow passed the position of maximum vertical component and the flow became more horizontal. Consequently the vertical upward force in the first instance would be generally low. As the second eddy grew the vertical force would became downward but the horizontal force would continue to grow as a continuation of the first eddy and increasing fluid velocities.

> The second eddy would give the maximum horizontal force since velocities peaked during its formation. The second eddy would cause a vertical downward force which is quickly disrupted by a third eddy.

> A third eddy may form at the rear of the wave and like the first eddy would be relatively weak since velocities were once again low. The horizontal force would then drop and become zero.

This fluid/ structure interaction is not confirmed by flow visualisation but seems to explain and be supported by a

number of points:

- the shape of the horizontal force trace,
  as described

- the shape of the vertical force trace, as described

- the trends and scatter of results for Cd and Cm

- differences with the 13mm diameter cylinder

The 27, 34 and 48mm diameter cylinder lie in the inertia regime. The scatter in results for Cm versus Nkc is much lower than for Cd with Nkc as expected. However, since for these cylinders Cd>0, then eddy formation and separation is expected, but not expected to dominate.

The ratio of drag to inertia force shows that the 13mm diameter cylinder is in a flow regime where neither drag nor inertia effects dominate. Consequently the vertical and horizontal force traces are considerably different to those for the larger cylinders, these being more dependent upon the development and separation of eddies.

In summary, the magnitude of the vertical and horizontal forces varied according to the fluid velocities and time available for the formation of the forces. Close inspection of Nkc and Re or similar non-dimensional parameters could possibly be used to describe the forces that are developed both in the horizontal and vertical directions. This very simple method of determining the force characteristic of a wave is somehow flawed as is demonstrated by the scatter of results.

The wake of cylinders within a flow comprise an alternating vortex street, the character of the vortices immediately behind the cylinder and in the wake downstream depends primarily upon Re.

For a cylinder the point at which separation occurs is mobile, and is determined primarily by its shape. The motion of the point at which separation occurs is coupled with the shedding of the vortices as it inevitably affects the distribution of pressure around the body.

Therefore there is a fundamental interaction between the body and the separated flow particularly in the region enclosing the body and its near wake. The dynamics of this interaction is of major importance in determining the time-dependent fluid resistance and characteristics of flow induced vibrations.

For bodies with mobile or fixed separation points undergoing sustained oscillations, the vortex strength is increased. This could be either or both due to increased rate of vorticity flux or due to less destruction of vorticity in the near wake. The growing vortex on a vibrating cylinder seems to "roll-up" more quickly.

Experimental observations do not consider the physical movement of the body, free-stream turbulence and roughness effects. Experience has shown that elastic structures near linear resonance conditions can develop flow induced oscillations by extracting energy from the flow about them. Oscillations of the structure modify the flow and give rise to nonlinear interaction. This is in addition to any nonlinearity which can arise from the restoring force (variable support stiffness) and/or from response dependent structural damping.

If the vortex shedding frequency brackets the natural frequency of an elastic or elastically mounted rigid cylinder, the cylinder

takes control of the shedding. The frequencies of vortex shedding and the body oscillation collapse to a single frequency close to the natural frequency of the body.

When a body is close to its linear resonance conditions it can undergo sustained oscillations at a frequency close to its natural frequency. The phenomenon encompasses a range of +-25% to 30% of its natural vortex shedding frequency, and that the vibration and vortex shedding frequencies lock together and control the shedding process.

The results for natural frequency of vibration of the cylinders used here in water, and indeed the measured results for forces do not show evidence of flow induced resonance.

However the scatter in results does suggest that some cylinder movement may be taking place. This is evidenced by the horizontal force going negative and the scatter in values of Cd and Cm calculated. This is discussed later.

As stated previously, the measured force results for the 13mm diameter cylinder are different in form from that of the larger cylinders. This confirms the results of the analysis which places the smallest cylinder in a mixed drag and inertia regime, whereas the largest cylinders are in the inertia regime. Consequently it seems unlikely that such a simple equation, such as Morison's can adequately represent the forces resulting from this complex fluid/ structure interaction, particularly since these results may be affected by some cylinder movement and a scatter of results as seen here.

7.1.9 Fixed value coefficients

Wiegel showed extensive scatter where Cd and Cm, determined from field tests, were plotted against Re and Nkc. This was due to the irregularity of ocean waves, free surface effects, 3-D flow, inadequacy of the averaged resistance coefficient to represent the actual variation of the non linear force, omission of the some other factor such as effects of ocean currents on separation, vortex formation, etc.. This demonstrates the difficulty of using fixed values of Cd and Cm in an ocean environment, and also graphically illustrates how the coefficients are dependent upon the flow in which the measurements are made.

In this experimental program there was a scatter of results, particularly in values for Cd. This may suggest that some of the scatter of Weigel's data was due to the inability of theory to match the basic fluid/ structure interaction.

Cd and Cm may be determined as Fourier averaged values as Keulegan and Carpenter at low Reynolds number.

They may also be evaluated with least squares, minimising the error between measured and calculated forces, as was performed in this thesis.

Fourier analysis and method of least squares give identical Cm values and Cd differs only slightly.

Close analysis of Keulegan and Carpenter's data shows:-

i) Cd depends on Re and Nkc; Cd decreasing with increasing Nkc

ii) Cm depends on Re and Nkc for Nkc>15; Cm decreasing with increasing Re

Sarpkaya's data gives:-

i) C_m depending on Re and N_{kc};
C_m increasing with increasing Re.

My results show that:-

i) C_d depends on Re and N_{kc}; C_d decreasing with
increasing N_{kc}; $C_d \approx 1.5$ for $2,500 \leq Re \leq 25,000$

ii) C_m depends on Re and N_{kc} for $N_{kc} > 15$; C_m decreasing
with increasing Re.

This investigation has shown general agreement with the results
of Keulegan and Carpenter, and contradicts Sarpkaya's results
for C_m versus Re (figures 6.65, 6.66).

It is worth discussing the affect and physical significance of the
drag and inertia coefficients, also the regime in which they were
measured.

C_d and C_m influenece the relative importance of the drag and
inertia parts of the total force, that expected from fluid
velocities or accelerations. The relative, as well as absolute,
values of the component forces making up the total horizontal
force is important.

C_d and C_m will be affected by a number of different factors,
each of which will be governed by a different theoretical
relationship.

These factors may be ones not directly considered in Morison's
equation, such as cylinder roughness, or alternatively ones
which are not totally satisfied, e.g. the fluid/ structure
interaction.

In some ways Keulegan and Carpenter attempted to allow for these with a remainder function though the method of calculating Cd and Cm is still important.

The Crossing Point Method assumes zero inertia force when drag effects predominate i.e. at maximum fluid velocity. However, because of the overall wave characteristics, the fluid/ structure interaction may imply an inertia dominated force trace. This would suggest that plotted against Nkc, Cd(XING) would have a greater scatter than Cd(LSA) which was essentially Fourier averaged. This was confirmed by results here.

Despite this, the points chosen give maximum definition of Cd and Cm. However, it seems unreasonable that this "instantaneous" value may be applicable to the entire wave.

Morison's coefficients calculated using a least squares analysis, will avoid any "instantaneous" irregularities, since it takes into account the full wave in determining single values of Cd and Cm. So even though coefficients determined using a least squares analysis are more representative and less prone to instantaneous irregularities they still suffer from the limitations of Morison's equation.

By analysing the ratio of the magnitude of the drag and inertia components in the total horizontal force, the confidence in the values of Cd and Cm can be assessed. The majority of results lie in the region where inertia effects dominate. Consequently the accuracy of the inertia coefficient would be expected to be its highest. Results of Cm with Nkc and Re show lowest scatter and best correlation as would be expected.

Summary

It seems that the time invariant Cd and Cm can only give a rough estimate of the in line force on a submerged cylinder, dependent on Nkc and Re. The use of averaged coefficients cannot therefore be expected to represent the time dependent force with equal degree of accuracy for all combinations of Nkc and Re, as was found in this thesis. It was not possible to disregard the drag term for Nkc<5 as inspection of the shape of the horizontal and vertical force traces suggest the presence of a drag force. This needs to be confirmed by flow visualisation.

Keulegan and Carpenter recognised the limitations of Morison's equation and lead them to the calculation of the instantaneous values of Cd and Cm and to the evaluation of a "remainder function". This was to account for the differences between the measured force and the one predicted using the averaged Cd and Cm.

The remainder function has the disadvantage that four coefficients have to be evaluated. Clearly the use of two coefficients is desirable.

Any revision should:-

a)   satisfy the observed fluid dynamics

b)   contain coefficients Cd & Cm determined from the flow characteristics

c)   should reduce to Morison's equation in the drag and inertia dominated regimes.

Further work is required to determine what this revision should be in the case of the solitary wave.

7.1.10 Instantaneous Force coefficients

It was concluded in section 7.1.9 that time invarient Cd and Cm could only give a rough estimate of the inline force on a submerged cylinder, dependent on Nkc and Re. The coefficients were allowed to vary as the wave passed in an attempt to improve the accuracy of predicted forces.

A direct comparison of harmonically oscillating flow with unidirectional flow is not justified. The effect of the flow deceleration is profound in promoting instability and earlier separation.

However, the calculation of instantaneous values of Cd and Cm was repeated here. It showed smooth trends within the confines of one wave, these trends were not repeated to any degree of accuracy on other waves.

The method of evaluating of the instantaneous values of Cd and Cm was not acceptable. It assumes that there is no distinction between accelerating and decelerating flows as long as the absolute values of the corresponding velocities and accelerations are equal.

Since this method does not produce a repeatable pattern of Cd and Cm between different waves it is of little value, since detailed flow characteristics would be needed to calculate forces. As we have seen from previous results, the choice of appropriate theory for fluid velocities would be difficult and be of questionable accuracy. Measurements may also not be possible.

The above results lead to a few conclusions:-

a) instantaneous values of Cd and Cm should not be used.

b) Morison's equation, with Cd and Cm held constant at experimentally verified values, may be used in either the drag and inertia dominated regimes, but seems inadequate for mixed regimes.

In an attempt to remove the drag effects from the total force, a total force coefficient, C_t (equation 3.53) was investigated. It was thought that allowing a time dependency, C_{ti}, whilst removing the drag forces from what is essentially an inertia regime for the 27, 34 and 48mm diameter cylinders would be more likely to give a relationship useful in the calculation of forces.

The results for the total force coefficient, C_{ti} plotted against ut/D (figure 6.71) show a large scatter in results for the 13mm diameter cylinder, the scatter reducing as the cylinder diameter increases. This is as expected since as D increases, the drag force component of the total force reduces.

For the 24, 37 and 48mm diameter cylinders, the results follow a similar curve as the wave passes. This may be expected since the force and velocity profiles for these cylinders are similar.

The scatter may be due to a number of effects

      i)   movement of the cylinder

      ii)   variations in the flow field with cylinder diameter, as evidenced by wave attenuation results (sections 6.2.5 & 7.1.2)

      iii) that the definition of C_{ti} was insufficient to remove drag effects, as described above.

The importance or otherwise of each of these is impossible to assess without further investigation. However it seems that for the cylinders tested beneath the solitary waves generated here, C_{ti} offers a very simple method of roughly approximating the forces generated.

It remains to be seen if this can be applied in practice to any suitable degree of accuracy.

CHAPTER 8   SUMMARY AND CONCLUSIONS

8.1 Summary & Conclusions

The problem of solitary wave interaction with a submerged horizontal cylinder was investigated by experiment. A variety of wave heights and cylinder positions were tested. The objective was to obtain more basic data in a simplified fluid/ structure environment.

The problem of fitting Morison's equation to measured data was solved by investigating the variation of drag and inertia coefficients with various parameters describing the wave characteristics.

The validity of classical theory of the solitary wave was determined for several wave characteristics.

Wave Generation

The horizontal translation of a vertical plate generated waves which approximate a solitary wave. They are shown to be sufficient for use in the experimental investigation so long as the wave characteristics were accurately measured for each test.

Wave Profile

The apparatus, procedures and analysis adopted in this thesis for the gathering and presentation of wave profile data gave consistently accurate results.

The solitary wave profile may be predicted by the theory of Boussinesq. The accuracy depending upon the wave height and distance from the wave generator. The method of generation used here gave waves which exist as a balance between dispersion and nonlinear effects.

This thesis has confirmed that for higher solitary waves the profile was more peaked than the theory of Boussinesq predicts but as Kulin (1958) reported, and contrary to the findings of Russell.

Solitary wave attenuation is shown to be accurately predicted by a modified Keulegan's equation.

Wave celerity

The simple relation of Rayleigh and Boussinesq between wave height and wave celerity has been confirmed as did Bazin, Russell and Daily & Stephan. The discrepancy between the measured and calculated celerities shows a systematic tendency for the observed wave speed to be lower than theory predicted for a given wave height, by 1-2% and was possibly due to channel bed and wall friction.

Fluid velocities

Fluid velocities were accurately measured using the Hot Film Anemometer, calibrated in-situ for each wave. As expected the peak velocity coincided with the wave crest.

McCowan's theory was shown to accurately predict fluid velocities beneath the solitary wave to an accuracy better than 5%. It was concluded that tolerance was a due to limitations in the purity of the solitary wave generated.

It was demonstrated that classical theory was inconsistent over a range of wave characteristics. No total solution for the solitary wave was found. Each theory was found to closely determine only a limited number of solitary wave characteristics.

Wave forces and Coefficients

It was demonstrated that Morison's equation could be used to predict horizontal forces on a submerged horizontal cylinder with reasonable accuracy.

Using Morison's equation with coefficients fixed for the passage of a wave, drag coefficients determined using the crossing point method and least squares analysis showed some scatter with both Nkc and Re; Inertia coefficients showing good agreement with Re and Nkc.

Using Morison's equation with coefficients allowed to vary as the wave passed showed no consistent trend with ut/D.

An instantaneous total force coefficient, C_{ti}, shows good and consistent agreement with ut/D. In inertia dominated regimes the agreement approximates a single curve. In a mixed regime, a family of curves is found.

Lift forces generated during the passage of the wave can for certain fluid velocities exceed the in line forces on the cylinder.

It was demonstrated that the accurate measurement of fluid flow characteristics are an essential prerequisite to the evaluation of theories to calculate forces on structures.

8.2 The Importance of the present study

The importance of this work lies in its broadening and enhancement of understanding in three main areas, namely;

fluid structure interaction, namely the generation of forces on a submerged horizontal cylinder by an accelerated unidirectional flow,

the choice of theory to be used to determine solitary wave characteristics

assessing the validity of Morison's equation in a fluid flow without flow reversal.

Morison's equation can be used to predict forces from a predicted or anticipated wave. Theories have been identified that closely predict wave characteristics, which can then be used to determine drag and inertia coefficients for use in Morison's equation

8.3 Limitations of present study and recommendations for further work

Even though some work is presented here regarding the tolerances that may be excepted in experimental work, these must be rigorously quantified in any future experimental investigation.

Also the level of certainty that may be allocated to the calculation of fluid velocities and Morison's coefficients, C_d and C_m must be determined more rigorously before they may be used in practice for the computation of forces on structures.

It may also be instructive to make a quantitative assessment of the fluid flow environment around the submerged cylinder, since this will

- clearly identify the flow regimes that produce the forces on the structure.

- establish the exact nature of the fluid /structure interaction.

REFERENCES

1. Bazin,   H., "Recherches Experimentales Sur La
                Propagation Des Onde." Memories Dicers
                Savants a l'Academie des Sciences, Vol.19,
                1865, pp 495.

2. Bearman, P.W., Chaplin, J.R., Graham, J.M.R.,
                Kostense, J.K., Hall P.F. and Klopman, G.,
                "The loading on a cylinder in Post-Critical
                flow beneath Periodic and Random Waves".
                Behaviour of Offshore structures, Elsevier
                Science Publishers B.V., Amsterdam, 1985,
                pp 213-225.

3. Benjamin,   T.B., "The Solitary Wave on a stream with
                an arbitrary distribution of vorticity".
                Journal of Fluid Mechanics, 1962, Vol.12
                pt.1, 1962, pp 97-116.

4. Boussinesq, J., "Théorie de L'intumescence Liquide,
                Appelée Onde Solitaire ou de Translation se
                Propageant Dans un Canal Rectangulaire.
                Compte Rendus Acad. Sci., Paris. 1871,
                Vol.72, pp 755-759.

5. Byatt-Smith, J.G.B, "An exact integral equation for
                steady surface waves." Proc. of Royal
                Society of London. A315, 1970, pp 405-418.

6. Byatt-Smith, J.G.B & Longuet Higgins, M.S, "On the
                speed and profile of steep Solitary waves."
                Proc. of Royal Society of London. A350,
                1976, pp 175-189.

7. Chakrabarti, S.K, Wolbert, A.L & Tam, W.A, "Wave forces on vertical circular cylinders." Journal of the Waterways, Harbors and Coastal Engineering Division, ASCE, Vol.102, May 1976, pp 203-221.

8. Chaplin, J.R. "Nonlinear forces on a horizontal cylinder beneath waves". Journal of Fluid Mechanics, 1984, vol.147, pp 449-464.

9. Cokelet, E.D, "Steep gravity waves in water of arbitrary uniform depth." Phil. Trans. Royal Society, A286, 1977, pp 183-230.

10. Daily, J.W & Stephan Jr., J.M, "The Solitary wave - its celerity, profile, internal velocities and amplitude attenuation." Proc. 3rd. Conf. on Coastal Engineering, Cambridge Mass., Oct. 1952, pp 13-30.

11. Daily, J.W & Stephan Jr., J.M, "Characteristics of the Solitary wave." Trans. of American Society of Civil Engineers. Vol. 118, 1953.

12. Fenton, J. "A ninth order solution for the Solitary wave." Journal of Fluid Mechanics, Vol.53, part 2, 1972, pp 257-271.

13. French, F.E. "Wave uplift pressures on horizontal platforms." Ph.D thesis, California Inst. of Technology, 1970.

14. Friedrichs, K.O., "On the Derivation of Shallow Water Theory, Appendix to "The Formation of Breakers and Bores" by J.J. Stoker." Commun. Pure Appl. Math., 1948, Vol.1, pp 81-85.

15. Fingerson, L.M "Practical extensions of anemometer techniques." International Symposium on Hot Wire Anemometry, University of Maryland, March 1967, pp 21-22.

16. Goodman, C.H & Sogin, H.H " Calibration of a Hot Film Anemometer in water over the velocity range 0.5 to 200 cm/s." Flow: Its measurement and control in Science and Industry, Instrument Society of America, 532.51 SYM, pp 589-598.

17. Grimshaw, R. "The Solitary wave in water of variable depth." Journal of Fluid Mechanics, Vol.42, part 3, 1970, pp 639-656.

18. Hogben, N, Miller, B.L, Searle, J.W & Ward, G "Estimation of fluid loading on offshore structures." National Maritime Institute, NMI R11, April 1977.

19. Ippen, A.T & Kulin, G "The shoaling and breaking of the Solitary wave." Proc. of 5th. Conference on Coastal Engineering, Grenoble, France, September 1954.

20. Ippen, A.T, Kulin, G & Raza, M.A., "Daming Characteristics of the Solitary Wave." Technical Report No.16, Hydrodynamics Lab., M.I.T., 1955.

21. Ippen, A.T & Mitchell, M.M., "The Damping of the Solitary Wave from Boundary Shear Measurements." Technical Report No.23, Hydrodynamics Lab., M.I.T., 1957.

22. Kaup, D.J. & Newell, A.C. "Solitons as particles, oscillators and in slowly changing media." Proc. Royal Society A361, 1978, pp 413-446.

23. Keulegan, G.H., "Gradual Damping of Solitary Waves." Journal of Research, National Bureau of Standards, Vol.40, 1948, pp 487.

24. Keulegan, G.H & Carpenter, L.H "Forces on cylinders and plates in an oscillating fluid." Journal of the National Bureau of Standards, Vol.60, No.5, May 1958, paper 2857, pp423-440.

25. Keulegan, G.H & Paterson, G.W "Mathematical theory of Irrotational translation waves." Journal of Research of the National Bureau of Standards, Vol.24, January 1940, pp 47-101.

26. Korteweg, D.J & deVries, G "On the change of form of long waves advancing in a rectangular canal and on a new type of long stationary waves." Philosophical Magazine (5) 38, 1895, pp 422-443.

27. Kulin, G. "Solitary Wave forces on submerged cylinders and plates." National Bureau of Standards Report, No.5876, US Department of Commerce, April 1958.

28. Laitone, E.V "The second approximation to cnoidal and solitary waves." Journal of Fluid Mechanics, Vol.9, 1960, pp 429-444.

29. Lee, J.J, Skjelbreia, J.E & Raichlen, F "Measurements of velocities in solitary waves." Journal of the Waterway, Port, Coastal and Ocean Division, Proc. of the ASCE, Vol. 108, No.WW2, May 1982.

30. Lenau, C.W "The solitary wave of maximum amplitude." Journal of Fluid Mechanics, Vol.26, part 2, 1966, pp 309-320.

31. Levi-Civita, T. "Détermination rigoureuse des ondes permanentes d'ampleur finie." Math. Ann. 93, 1925, pp 264-314.

32. Longuet Higgins, M.S "Breaking waves - in deep or shallow water." 10th. Symposium, Naval Hydrodynamics, Cambridge Mass., 1974.

33. Longuet Higgins, M.S "On the mass, momentum, energy and circulation of a solitary wave." Proc. of Royal Society of London, A337, 1973, pp 1-13.

34. Longuet Higgins, M.S., "Trajectories of particles at the surface of steep solitary waves." Journal of Fluid Mechanics, 1981, Vol.110, pp 239-247.

35. Madsen, O.S & Mei, C.C "The transformation of a solitary wave over an uneven bottom." Journal of Fluid Mechanics, Vol. 39, part 4, 1969, pp 781-791.

36. Morison, J.R, O'Brien, M.P, Johnson, J.W and Schaaf, S.A "The force exerted by surface waves on piles." Journal of Petroleum Technology, AIME, Vol.189, 1950, pp 149-154.

37.Munk, W.H "The solitary wave theory and its application
        to surf problems." Institute of Oceanography
        & Institute of Geophysics, University of
        California, No. 406, 1949, pp 376-424.

38.McCowan, J. "On the solitary wave." London, Edinburgh
        and Dublin Phil. Mag. and Journal of
        Science, Vol.32(5), 1891, pp 45-58.

39.Naheer, E. "Laboratory experiments with solitary
        waves." Journal of Waterway, Port, Coastal
        & Ocean Division. Vol.104, November 1978,
        pp 421-437.

40.Rayleigh, Lord "On waves." The London, Edinburgh
        and Dublin Philosophical Magazine and
        Journal of Science, Vol.1(5), No.4, April
        1876.

41.Rankine, W.J.M. Philosophical Transactions, vol. 153,
        1863, pp 127

42.Sarpkaya, T., "In-line and transverse forces on smooth
        and sand-roughened circular cylinders in
        oscillatory flow at high Reynolds numbers."
        1976, Technical Report No.NPS-695L76062,
        Naval Postgraduate School, Monterey,
        California.

43.Sarpkaya, T. & Garrison, C.J "Vortex formation and
        resistance in unsteady flow." ASME, March
        1963, pp 16-24.

44. Sarpkaya, T. & Shoaff, R.L., "Inviscid Model of 2-Dimensional Vortex shedding by a circular cylinder." 1979a, AIAA Journal Vol.17, No.11, pp 1193-1200.

45. Sarpkaya, T. & Shoaff, R.L., " A Discrete Vortex Analysis of flow about stationary and transversely Oscillating Circular cylinders." 1979b, Naval Postgraduate School Technical Report No. NPS-69SL79011, Monterey, CA.

46. Sasaki, K. & Murakami, T. "Irrotational, progressive surface gravity waves near the limiting height." Journal of the Oceanographic Society of Japan, Vol.29, 1973, pp 94-105.

47. Sawaragi, T., Nakamura, T. & Kila, H. "Characteristics of lift forces on a circular pile in waves." Coastal Engineering in Japan, Vol.19, 1976, pp 59-71.

48. Scott Russell, J., "On Waves." Proc. Royal Society of Edinburgh, 1844, Vol.319.

49. Sibley, P.O. et al. "Particle velocities beneath a solitary wave." Proc. of the Int. Conf. Computational Methods & Exptl. Measurements, Washington DC, July 1982. pp 463-474.

50. Sibley, P.O. et al. " Solitary wave forces on horizontal cylinders." Applied Ocean Research, 1982, Vol 4, No.2 pp 113-115.

51. Starr, V.P. "Momentum and Energy Integrals for Gravity Waves of Finite Height." Journal of Marine Research, Vol.6, No.3, 1947 pp 175.

52. Teng, C.C. & Nath, J.H. "Wave and current forces on a horizontal cylinder". Journal of Waterway, Port, Coastal and Ocean Engineering, Vol. 111, 1985, pp 1022-1040.

53. Toland, J.F "On the existence of a wave of greatest height and Stokes conjecture." Proc. of the Royal Society of London, A363, 1978, pp 469-485.

54. Tuck, E.O "Paddle-Type wavemakers in shallow water." Conference on Marine Vehicles, Paper 15, 1974.

55. Ursell, F. Proc. Royal Society London A, Vol.214, pp 79.

56. Verley, R.L.P "Wave forces on structures - an introduction." The British Hydromechanics Research Association, TN1319, November 1975.

57. Weigel, R. Oceanographical Engineering. 1964, Englewood Cliffs, N.J., Prentice-Hall.

58. Yamada, H. "On the Highest Solitary Wave." Rep.Res.Inst.Appl.Mech., Kyushu University, 1957, Vol.5, pp 53-67.

59. Yamada, H. "Highest waves of permanent type on the surface of deep water." Rep. Res. Inst. Applied Mech., Kyushu University, 1957, pp 37-52.

60. Zakanycz, S., Wright, H.E. & Elrod, W.C. "Velocity measurements in fluids with a constant temperature Anemometer." Flow: Its measurement and control in Science and Industry, Instrument Society of America, 1974, 532.51 SYM, pp 571-577.

APPENDIX A

Least Squares Analysis

Minimising errors according to the theory of least squares, generally

$$\Sigma(Y(x_r)-y_r)^2$$

is minimised.

Morison's equation may be written in the form:

$$F=ACd+BCm$$

Consequently according to the least squares analysis:

$$E=\Sigma(ACd+B-F)^2$$

$$\delta E_{/\delta Cd}=2\Sigma(ACd+BCm-F)A$$

$$\delta E_{/\delta Cm}=2\Sigma(ACd+BCm-F)B$$

$$\Sigma(A^2Cd+ABCm-FA)=0$$

and $\quad \Sigma(ABCd+B^2Cm-FB)=0$

$$\begin{bmatrix} A^2 & AB \\ AB & B^2 \end{bmatrix} \begin{bmatrix} Cd \\ Cm \end{bmatrix} = \begin{bmatrix} AF \\ BF \end{bmatrix}$$

$$[A] \qquad [K] = [F]$$

$$[K]=[A]^{-1}[F]$$

APPENDIX B

Solving Morison's equation simultaneously either side of the wave crest.

$$F_1 = AV_1^2 Cd + BV_1 Cm$$

$$F_2 = AV_2^2 Cd + BV_2 Cm$$

Substituting for Cd

$$F_2 = AV_2^2 (F_1 - BV_1 Cm) + BV_2 Cm$$

$$AV_1^2 F_2 = AV_2^2 F_1 - AV_2^2 BV_1 Cm + BV_2 AV_1^2 Cm$$

Consequently

$$Cm = (V_1^2 F_2 - V_2^2 F_1) / B(V_1^2 V_2 - V_2^2 V_1)$$

$$Cd = (V_1 F_2 - V_2 F_1) / A(V_1 V_2^2 - V_1^2 V_2)$$

MISSING PAGES
REMOVED ON
INSTRUCTION
FROM THE
UNIVERSITY